305

TECHNICAL NOTE

D-608

JUNO II SUMMARY PROJECT REPORT

VOLUME II

THE S-46 SATELLITE

George C. Marshall Space Flight Center
Huntsville, Alabama

A

FOREWORD

The Systems and Instrumentation Branch (Arthur W. Thompson, Chief), Research Projects Division, George C. Marshall Space Flight Center, National Aeronautics and Space Administration, Huntsville, Alabama, obtained and coordinated the contributions for this report.

TABLE OF CONTENTS

Chapter 3

MECHANICAL SYSTEM, DESIGN ENGINEERING AND PACKAGING

Chapter 4

S-46 SATELLITE TELEMETRY

Chapter 5

NETWORKS AND SOLAR POWER SYSTEMS
FOR RADIATION EXPERIMENT SATELLITE S-46

Chapter 6

THERMAL DESIGN OF S-46

Chapter 7

TESTING

LIST OF ILLUSTRATIONS

LIST OF TABLES

NATIONAL AERONAUTICS AND SPACE ADMINISTRATION

Technical Note D-608

JUNO II SUMMARY PROJECT REPORT
VOLUME II
THE S-46 SATELLITE

SUMMARY

Earlier experiments of the State University of Iowa in the investigation of corpuscular radiation indicated the need for additional experiments of a more advanced and discriminating nature. A payload, identified as S-46, was built to carry on the SUI investigations and a Juno II vehicle made available for launching it into orbit.

In this report, the factors preliminary to payload design are considered first. Subjects discussed are (1) selection of the orbital parameters, (2) the most desirable motion of the satellite about its center of mass, (3) useful lifetime of the satellite, (4) the best time to launch, based on such factors as percentage of time in sunlight, initial angle between the satellite axis and the satellite-sun line, temperature requirements, and the effects of orbit perturbations by the sun and moon on the perigee altitude, (5) allowable payload weight, (6) payload instrumentation, (7) data transmission, (8) power supply, (9) best physical configuration, and (10) telemetry reception and tracking.

The program was implemented by construction of three prototype and two flight unit payloads. The structural design and layout, which are described in Chapter 3, produced a payload configuration of a cylindrical housing containing a column of all the instrumentation, the housing partially surrounded by a box structure on which the solar cells were mounted. The complete S-46 weighed only 22 1/2 pounds. A dipole antenna was formed by permanently attaching the payload to, but separated from, the fourth stage rocket motor housing by a fiberglas insulator.

The critical weight limit, imposed by the required highly eccentric orbit, limited the transmission of telemetry and tracking signals to one transmitter. Four of the five output signals from the radiation experiment frequency modulated their subcarrier oscillators directly.

Three possible states in each output, each with a different period, conveyed the type and amount of radiation being reported by the detectors. The fifth output from a detector, together with outputs from the power supply and temperature sensors, was applied to a multiplexer which modulated the fifth subcarrier oscillator. A description, complete with block diagrams, circuit schematics, printed circuit board layouts, and illustrations of modules, is given in Chapter 4 for the subcarrier oscillators, the multiplexer, and the 108 mc transistorized transmitter. The antenna is described and its radiation patterns are shown.

A combined solar cell and rechargeable chemical battery arrangement was selected to provide about 1300 milliwatts of power for the transmitter, subcarrier oscillators, and instrumentation. The analysis and selection of batteries and solar cells are covered in Chapter 5 with the aid of response curves, tables, and performance diagrams. Because the S-46 was to be a non-oriented satellite, it was necessary to evaluate the solar cell placement for the effects of variation in light incidence on the power output as related to (1) aspect of axes with respect to the sun, (2) tumble, (3) rotation or spin, and (4) shadow from protruding parts. Theory, calculations, solar cell performance, and power output versus rotational position are covered in detail and backed up by performance curves and space orientation diagrams. Another extensive study is reported on protective covering material to protect the solar cells from anticipated high intensity electron and proton radiation damage. It was thought that lack of such protection could bring on ruin of the solar cells in a matter of a few days. Solar cell mounting, battery characteristics, and the application of zener diodes and blocking diodes to prevent battery overcharging and discharging and so stabilize the power supply voltage are discussed. The important problem of integrating the various assemblies, sensors, power supplies, timers, etc., into a complete and functional system is treated with the aid of single line diagrams, wiring diagrams, and photographs.

The passive control method of equalizing skin temperatures and thermally insulating the instrument package from the skin was selected from several possibilities. Design of the first prototype payload incorporated the passive control philosophy and the knowledge gained from Explorer VII. The prototype was given one test in which the temperature of the skin was varied in as near a step-function as possible, and another test in which it was subjected to heat fluxes similar to those which would be encountered in space. The tests are described and illustrated in Chapter 7 and the relation of thermal test to design philosophy is discussed in Chapter 6. A qualitative study of the data from the tests indicated that the instrument package maintained a uniform temperature even when high gradients existed around the skin, and further, that this uniform value was near the average value of the skin temperature. Possible errors in the test are considered and suggestions made as to how better

simulation of environmental heat sink conditions could be made and how a radiation source with the intensity and spectral distribution of the sun would be superior to heat blankets.

The test program at the State University of Iowa, for SUI instrumentation, is given in Chapter 7 as it applied to individual components, testing of modules before encapsulation, subassembly testing, and testing in the complete payload. The comparable test program at ABMA is also presented. A detailed report of the thermal tests on prototype PL-1, the electronic tests on prototype PL-2, the environmental tests on prototype PL-3, and the acceptance tests on the PL-4 and PL-5 flight units is included. Test setups are illustrated. One section gives the Test Procedures and Specifications.

The last chapter (Chapter 8) of the report reviews the history of the SUI discovery of the radiation belt and the subsequent experiments to expand the knowledge of it. The design and development of the SUI apparatus in the S-46, with which it was hoped to expand the knowledge, are described. The construction, purpose, location, and functioning of each of the radiation detectors are described. The 700 volt and 160 volt power supplies are explained using supplementing circuit diagrams, performance curves, and illustrations. Pulse shaping circuits, binary scalers, logic circuits and output amplifiers are similarly covered. Fabrication of the SUI equipment is explained and illustrated. Payload calibrations (G-M Counter Plateau Measurement, Apparent versus True Counting Rate, Determination of Absolute Geometric Factor, Determination of Angular Dependence of the Absolute Geometric Factors, and Determination of Absolute Electron Sensitivity) are treated.

The S-46 payload was launched on March 23, 1960, but did not go into orbit because one rocket in Stage II of Juno II failed to fire (Chapter 2). The payload did not go high enough to enter the region of high intensity radiation so the suitability of the cadmium sulfide detectors and the electron spectrometer for investigation of the objectives was not verified. The geometric factors and scaling factors of the G-M counters had been chosen to study the high intensity radiation so little geophysically significant data were obtained during the short flight.

Chapter 1

INTRODUCTION

SECTION I.   OBJECTIVES

The experiments conducted so far in the investigation of corpuscular radiation have produced much information about the charged particles which make up the radiation belts.   As in the case of most major physical discoveries, these simple early experiments indicated the need for further experiments of a progressively more discriminating nature, in order that the new phenomenon can be completely understood.   The ultimate goal of the program of investigation of the corpuscular radiation near the earth is to understand in detail the nature of the radiation (its composition), its origin, how the particles travel to the vicinity of the earth, the trapping mechanism, and the mechanism by which they are lost from the trapping region.   With this understanding it should be possible to gain a greater understanding of a large number of geophysical and heliophysical phenomena such as aurorae, high atmospheric heating, magnetic storms, nuclear processes on the sun, etc.

In November, 1958, NASA received a proposal from Dr. James A. Van Allen that a satellite of the characteristics of S-46 be instrumented by the State University of Iowa (SUI).   A NASA contract was given to SUI in January, 1959, which covered the work on the satellite as well as other aspects of the radiation study program.   In March, 1959, SUI requested a firm scheduling of a Juno II rocket for a satellite of the characteristics of S-46, and in the same month this was done.   The goal of the system design was to arrive at the most valuable experiment possible in terms of its potential yield of new and useful data, within the framework of the imposed limitations.   To gain the desired knowledge, it was recognized by the SUI personnel that an understanding in some detail of at least some of the following aspects was essential:

1.   Identification of the particle types in the various regions

2.   The number-energy spectrum of each of the particle types as a function of position in space

3.   The integrated energy flux as a function of position in space

4. The angular distribution of the various components of the radiation as a function of position along the trapping lines

5. Details of the variations of the whole trapped particle-solar proton complex in time and the relationships between these variations and geo- and heliophysical phenomena

6. The vector magnetic field as a function of position in space and time.

Acquisition of all test data, it was realized, would require a large number of complex instruments. Furthermore, an approximate value for the quantities to be measured would have to be known in advance in order to adjust the scaling factors for the proper range of operation, or the dynamic range of the instruments would have to be very large. Since it was not possible at the time to perform a single "grand experiment" which would accomplish all the listed objectives because of various limitations in rocket and instrumentation capability, it was necessary to continue the investigation on a logical step-by-step basis. After careful consideration of the various factors it was decided (in a personal unpublished communication from J. A. Van Allen to L. H. Meredith, October 20, 1959) that the following program was possible and that it would be the most valuable in terms of its ability to answer the greatest possible number of the most pressing questions about the trapped radiation:

1. "Monitoring of the intensity structure of the two principal zones of geomagnetically trapped radiation over an extended period of time with the broad objective of conclusive establishment of the origins and gross dynamics (i.e., build-up and decay times and mechanisms, local acceleration of particles, long term and short term temporal fluctuations, etc.) of the respective zones and the more specific objective of detailed correlation with solar activity and with geophysical phenomena (aurorae, magnetic storms, heating of the atmosphere, and airglow)

2. "Crude study of the particle composition and the energy spectra of the respective components as a function of position in space and as a function of time

3. "Exploratory study of energy flux of very low energy trapped particles (protons and electrons separately) by use of zero-wall-thickness detectors."

SECTION II.   SYSTEM CONSIDERATIONS

To attain the desired objectives many factors such as orbit, weight, attitude, launching time, lifetime, etc., had to be considered and their priority in the overall system design determined. This was a joint effort of ABMA[1] and SUI personnel. Some of the factors considered, the reasoning, and the solutions reached are as follows:

1.   Orbit Parameters

The weight which can be placed in orbit with a given rocket depends most directly on three of the orbit parameters: perigee height, apogee height, and inclination. The considerations affecting their selection, and the figures decided upon as most desirable for the S-46 orbit were:

a.   Perigee. The basic requirement was that the perigee height should be the lowest value which would insure a one year lifetime for the S-46 satellite. The perigee height is the same as the satellite injection height only if there is no elevation angle error at the time of injection (and, of course, if the injection velocity is sufficiently high). Final injection height depends strongly on first stage vehicle performance. Therefore, the selection of a program injection height had to allow for possible guidance angle errors and variations from standard rocket performance, in order that the perigee would have a high probability of being equal to or greater than the minimum acceptable height.

The perigee height had to be enough below the radiation belts so an approximate calibration of the detectors could be obtained periodically in the relatively stable cosmic ray and albedo flux found between about 50 and 600 km, in order that failure of any part of the instrumentation could be quickly detected. An injection height of 340 km above the earth's surface was established as most desirable for the S-46.

b.   Apogee. Ideally, the apogee height should be sufficiently great so that the detectors would be carried well outside the radiation belts and into interplanetary space, perhaps to a radial distance of 20 earth radii from the center of the earth. Such an orbit would provide frequent passes through the entire radiation belt structure, and would also permit the detection of solar protons and other particles well outside the influence of the magnetic field of the earth. One of the disadvantages of such an orbit was that the period would be so long (48 hours) that important changes might occur within the belt system and be missed entirely while the detectors were outside the system. Another disadvantage was that the satellite weight would have to be so

1.   The Development Operations Division personnel of the Army Ballistic Missile Agency who were engaged in satellite and space activities were transferred to the National Aeronautics and Space Administration on August 1, 1960, and became a part of the George C. Marshall Space Flight Center.

small (due to the limitations in capability of the Juno II vehicle) that the overall value of the experiment in the program adopted would be seriously reduced. It was decided that the S-46 apogee should be high enough so the detectors would pass beyond the peak of the outer belt in the equatorial plane when that peak intensity was at its maximum distance from the earth. Figure 1 shows the counting rate as a function of radial distance as obtained by Pioneers III and IV on December 6, 1958, and March 3, 1959, respectively. The Pioneer IV data were obtained following a period of high solar activity when the peak intensity of the outer belt was at a much greater distance from the earth than at any other recorded time. It was considered likely that the peak intensity would occur at a greater distance only very rarely.

On this basis, a minimum apogee height of six earth radii (38,200 km) from the earth's center was specified, and the flight unit weight was determined accordingly. A final calculation of the trajectory by ABMA, using more accurate rocket performance data and the actual final flight unit weight, indicated a potential apogee height of about 44,000 km.

c. <u>Inclination</u>. To simplify the analysis of the data and to insure the maximum number of sweeps through the central radiation belt structure (rather than in the slot between the belts or outside the outer belt), a minimum inclination orbit was selected. This also produces the greatest apogee height, since the greatest advantage can be taken of the earth's rotational motion. The minimum inclination obtainable from a launching at Cape Canaveral, Florida, is 28.3°, the geographic latitude of the launch site. This requires a launch azimuth of 90° (due east).

d. <u>Summary of orbit parameters</u>. The orbit parameters decided upon, then, were:[1]

(1) Perigee height, 1.0534 r_e from the earth's center (r_e = 6371 km)

(2) Apogee height, 6.906 r_e or greater

(3) Semi-major axis, a = 3.980 r_e

(4) Semi-minor axis, b = 2.699 r_e

(5) Eccentricity, = -.735

(6) Period, P = 40,200 sec = 11.2 hours

---

1. R. J. Davis, F. L. Whipple, and J. B. Zirker, <u>The Orbit of a Small Earth Satellite</u>, Chapter 1 of <u>Scientific Uses of Earth Satellites</u>, (University of Michigan Press, Ann Arbor, 1958), 2nd ed.

8
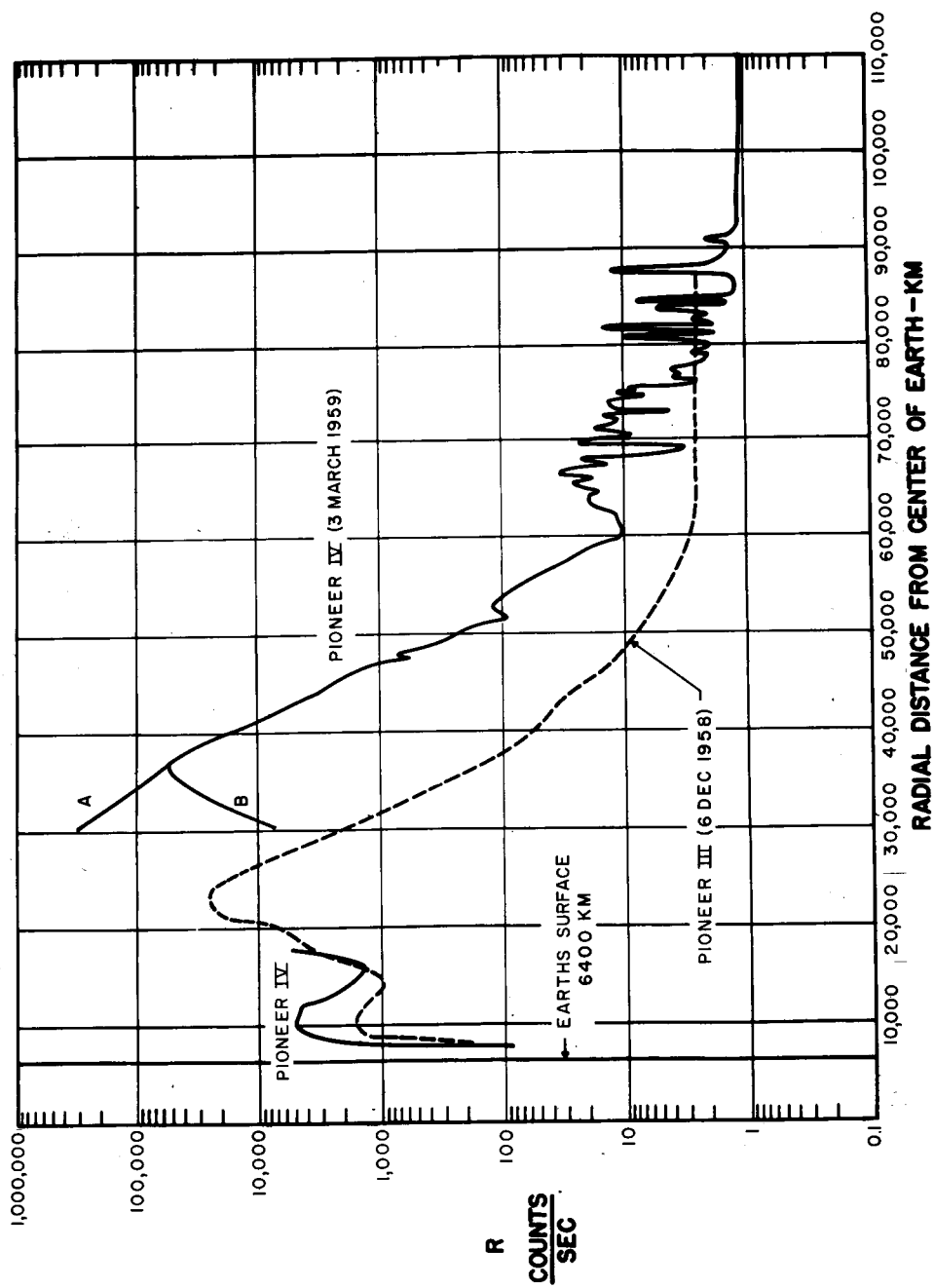
FIGURE 1. INTENSITY DATA FROM PIONEERS III AND IV. The A and B branches of the characteristic curve of apparent counting rate relative to true counting rate for Pioneer IV indicate an ambiguity which is intrinsic to the instrumentation system. Auxiliary data favors A as the correct curve.

(7) Inclination, i = 28.3 degrees

(8) Motion of longitude of ascending node, $\dot{\Omega}$ = -0.51 deg/day

(9) Motion of argument of perigee, $\dot{\omega}$ = +0.47 deg/day.

2. Motion of the Satellite About Its Center of Mass

Several of the radiation detectors to be used with satellite S-46 had defining apertures which made them directional. It was decided that the payload should spin in such a manner that the detectors viewed a wide range of angles, rather than a direction which was fixed in space or changing in a completely unknown way. The superposition of two rotations so that the detectors looked at every point on a full sphere was not considered desirable, since the CdS detectors are light sensitive over the solid angle defined by the aperture, and periodic rotation through the sun and earth would make the measurements very difficult to use. Thus, simple rotation of the detectors about a line perpendicular to the line of detector directivity was decided upon.

One way of obtaining this motion was to spin the satellite initially about its axis of greatest moment of inertia with the detectors directed perpendicularly to the axis, the simple spin then being maintained down to a very low spin rate. Explorer VII was so stabilized, with a spin damping time constant of about two years, and it has kept a very nearly constant direction of its angular momentum vector.[1]

Alternatively, the S-46 could be made to spin initially about its axis of least moment of inertia (its longitudinal axis), with the detector axes directed parallel to the longitudinal axis. Then as the spin rate $\dot{\psi}$ decreased, the satellite would undergo a transition to a complex spin with the longitudinal axis of the payload moving on the surface of a cone of half angle α at an angular rate $\dot{\varphi}$ where α would change from zero to $\frac{\pi}{2}$.[2] Such a transition is illustrated in Figure 2 where (a) shows the relations immediately after injection before tumbling has begun, (b) shows it later as the opening angle α is increasing, and (c) shows α completely opened and the satellite in a flat spin.

---

1. R. J. Naumann, Orientation of Explorer VII (AM 19-A), ABMA Report No. DV-TN-13-60, 20 June 1960.

2. R. J. Naumann, Recent Information Gained from Satellite Orientation Measurement, paper presented at the 4th Symposium on Ballistic Missiles and Space Technology at UCLA, Los Angeles, Calif., 24-27 August 1959.

(a)

(b)

(c)
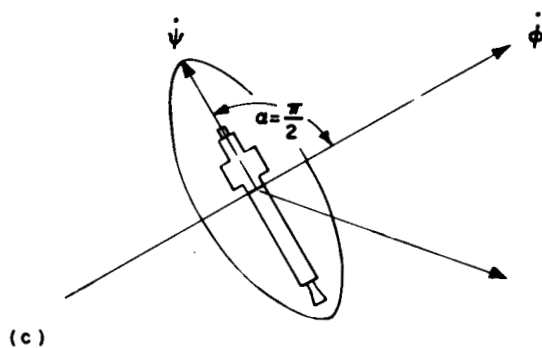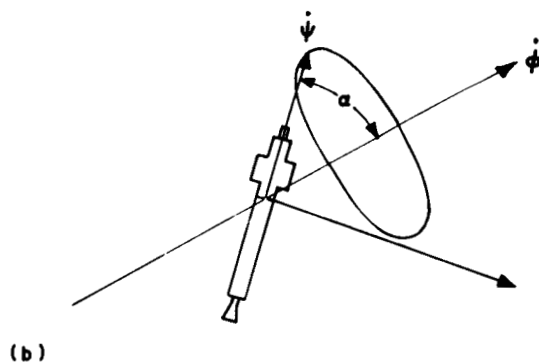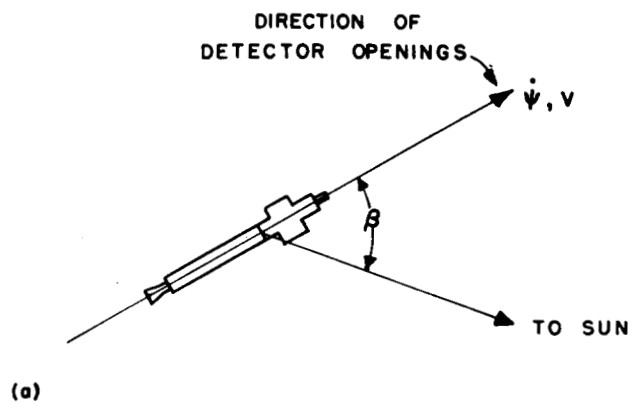
FIG. 2.   SATELLITE MOTION ABOUT ITS CENTER OF MASS

(a) Immediately after injection before tumbling begins
(b) Later, as the opening angle α is increasing
(c) Flat spin with α completely opened

The latter alternative was chosen so that the basic Explorer I, III, and IV configuration could be retained, since it could be fabricated with only slight modification of the previous design. Furthermore, weight limitations would not allow modification of the structure to produce a configuration in which the axis of greatest moment was coincident with the initial spin axis.

Prediction of the opening angle α as a function of time after launch is very difficult and a complete analysis was not performed. It depends on the ratio of the moments about the final and initial spin axes, atmospheric damping, magnetic damping, and energy losses due to flexing of parts of the structure. For the S-46 satellite the ratio of the moments was

$$\frac{I_{trans}}{I_{long}} = 30.$$

3. Lifetime

The satellite was designed to operate for a period of one year to provide a high probability for the occurrence of interesting solar phenomena and to permit the accumulation of a reasonably complete set of data. A timer (described in Chapter 5) was included in the satellite to turn off the instruments at the end of the one year period in conformity with NASA policy, in order that the frequency would become available for later experiments.

4. Launch Time

The launch time was determined after considering:

a. **Percentage of time in sunlight.** This parameter affects both the temperature control problem and the design of the solar battery. It was computed for the one year lifetime for a number of possible launch times. Figure 3 shows the result of the computation for local sun times at the point of injection (H_0) of 0800 and 1000 (1212:57 and 1412:57 UT). The local sun time at the point of actual injection was 0922:24.

b. **Initial angle between the satellite axis and the satellite-sun line.** This parameter affects the temperature control problem and the design of the solar battery, and had to be chosen to minimize the lengths of the periods of time during which the light sensitive particle detectors would sweep across the sun or earth.

c. **Temperature requirements.** It was desired that the temperature remain within the limits 0°C to +50°C. Minus 20°C and +75°C were established as absolute limits.

12
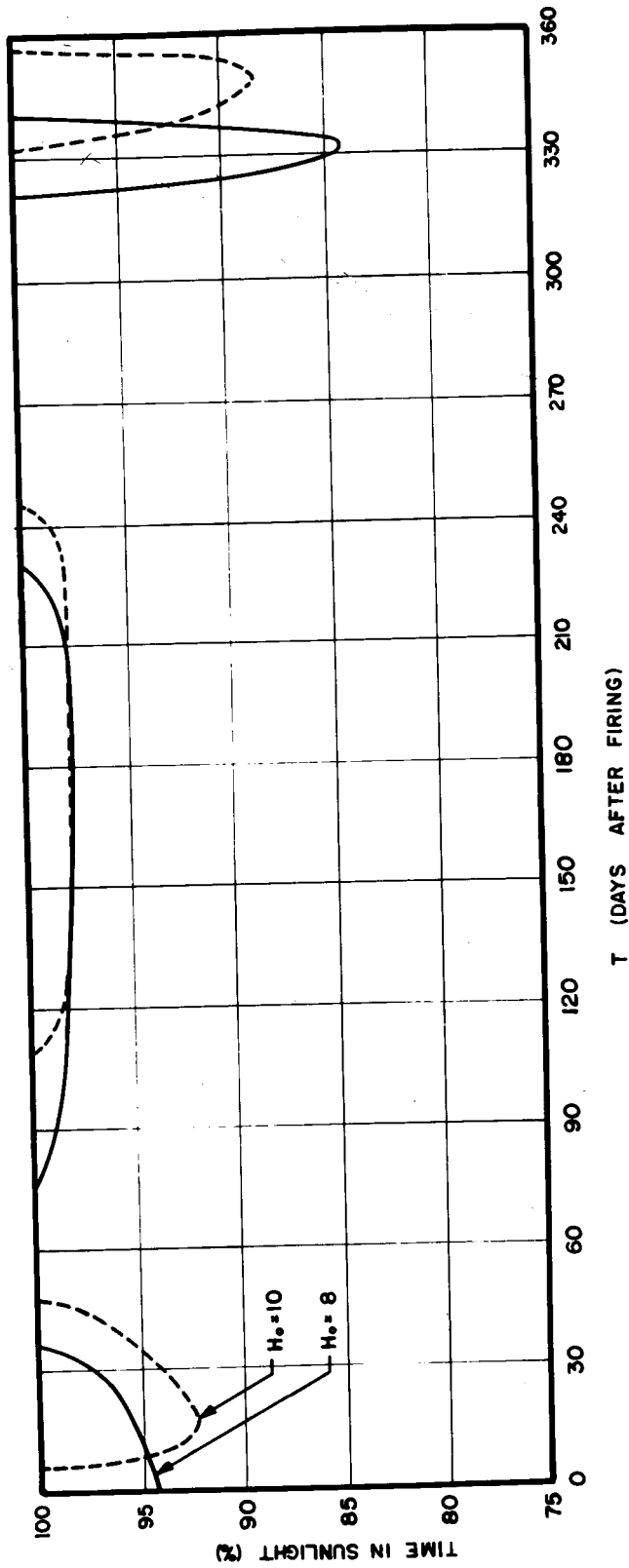
FIG. 3.   PREDICTED PERCENTAGE OF TIME IN SUNLIGHT FOR THE S-46 PAYLOAD

        d. Effects of orbit perturbations by the sun and moon on the
perigee altitude.[1] In cases where all conditions could not be met
simultaneously for the entire one year period, emphasis was placed on
the first two months of operation, since the probability of successful
operation of the instrumentation diminishes with time. Less weight was
attached to those considerations which might have resulted in temporary
cessation of proper operation (such as those which lead to an abnormal
but not damaging temperature) than to those which could have resulted in
premature permanent failure (such as those which cause the perigee height
to be markedly reduced).

        Consideration of items a, c, and d indicated a launching time between
0800 and 1200 for the epoch beginning March 23, 1960. Consideration of
item b placed a more severe limitation on the launch time because of the
necessity that the detectors not point toward the sun either initially,
or after conversion of the satellite motion to a flat spin. The factors
bearing on the selection of the exact time interval were:

        (1) The detectors were somewhat light sensitive within a
cone of half angle 20°, with the cone axis coincident with the longitudi-
nal axis of the payload.

        (2) An initial angle error of 10° between the detector
axes and the intended direction of injection was considered possible
because of possible misalignment of rocket thrust with respect to the
longitudinal axis, and guidance angle errors at the time of final stage
ignition.

        (3) The detectors should not "see" the sun for a minimum
initial period of twenty hours to permit the collection of meaningful
data from at least several orbits very early in the satellite's lifetime.

        Figure 4 shows a projection of the initial satellite motion onto the
plane of the ecliptic. The arrow at the position of injection points in
the initial direction of the spin axis. The initial angle to the sun
from the payload (β) is indicated in Figure 2 as well as in Figure 4.
The launching time (March 23, 1960) was chosen so that β would be between
50° (0834 EST) and 59° (0907 EST). Figure 5 shows how the angle β
changes during the one year period for local sun times at injection of
0800 and 1000. Assuming that the direction of the angular momentum
vector remains fixed in space and that $\beta = 50°$ initially, the satellite
alignment would follow the following pattern: During the first few

---

1. R. J. Naumann, The Effect of Lunar and Solar Perturbations on the
    Perigee Height of a High Eccentricity Satellite (AM-19C), ABMA Report
    No. DV-TN-5-60, 4 March 1960.
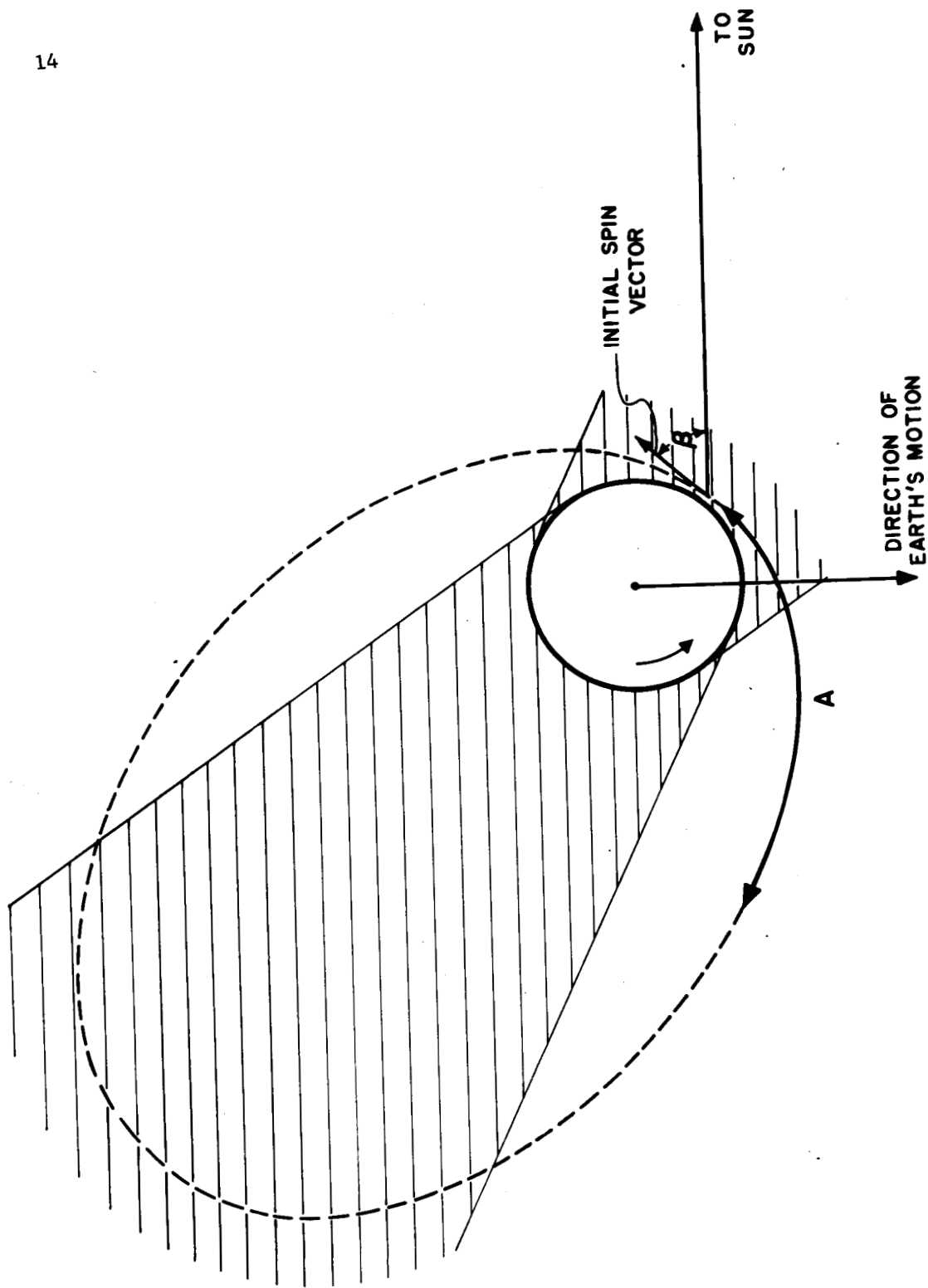
FIG. 4. APPROXIMATE PROJECTION OF THE INITIAL S-46 ORBIT
ONTO THE PLANE OF THE ECLIPTIC
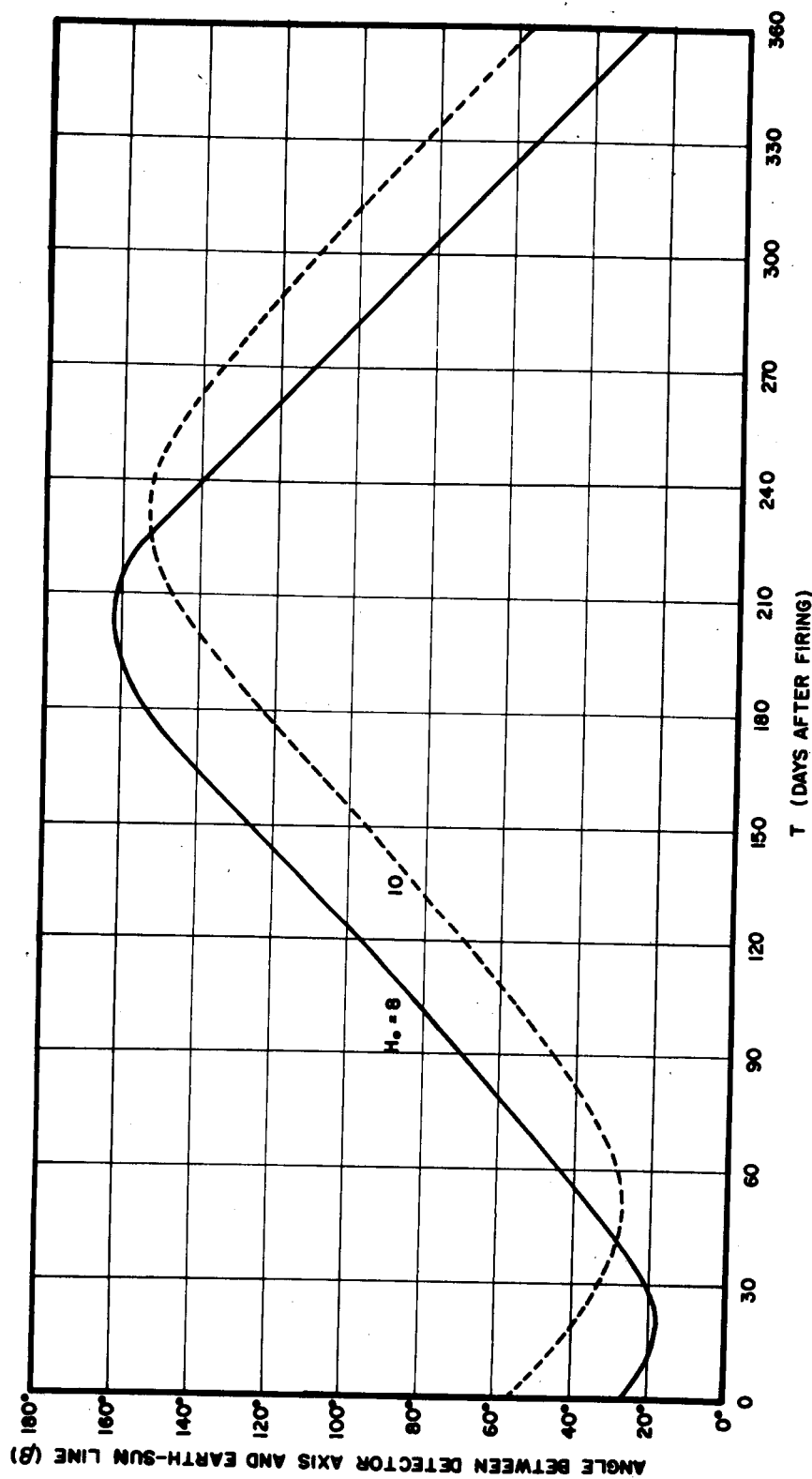
FIG. 5. PREDICTED ANGLE BETWEEN SPIN AXIS AND EARTH-SUN LINE

15

orbits the sun would remain outside the cone of detector light sensitivity. The earth would fall within this cone on the portion of the orbit marked A in Figure 4. As the satellite transformed from a simple spin to a flat spin, the sun would fall within the cone while α was in the approximate range 30° to 65°. The angle β would change at the rate of about one degree per day due to the earth's rotation about the sun. After α became equal to 90°, the sun would fall within the cone of sensitivity again about 110 days after launch, and would continue to do so for about 50 days. The earth would fall within this cone whenever the satellite is within the shaded regions in Figure 4.

The launch time interval agreed upon was 0834 to 0907 EST on March 23, 1960. A postponement of the firing date of as many as three days would have required no change in the launch time. The vehicle was actually launched at 0835:11 on March 23, 1960. Details of the flight are reported in Chapter 2.

5. Payload Weight

The permissible payload weight based on the above considerations was computed by ABMA to be 10.19 kg. The final payload weight for the unit launched on March 23, 1960, was 10.22 kg. Itemization of the weight is given in Chapter 3.

6. Payload Instrumentation

It was decided to incorporate five radiation detectors in the payload. Two of the detectors, A and B, were to be cadmium sulfide semiconductor crystals capable of measuring the energy loss of electrons and protons having energies of less than 100 electron volts. The two detectors were identical except that detector A employed a magnet to curve the paths of all electrons having energies below about 500 kev away from the crystal so that it would act almost exclusively as a proton detector. Thus, the two detectors would accomplish the simultaneous separate determination of low energy electron and proton fluxes. The currents through the crystals would be produced by a regulated power supply and converted into pulse rates by charging capacitor-neon bulb relaxation oscillator circuits. The pulses would be counted by binary scalers.

A third detector, detector C, would be an electron energy spectrometer having an energy "window" of approximately 45 kev to 55 kev. It would consist of defining apertures, a magnetic field, another aperture, and a thin window Geiger-Mueller (G-M) counter. Only those electrons having energies within the desired range would be deflected through the proper angle by the magnetic field and so be counted by the counter. The G-M counter would be surrounded by a lead and stainless steel absorber to reduce the counting rate contribution from high energy

particles which pass through the structure and from X-rays (bremsstrahlung) produced by the inelastic scattering of particles in the structure.

Detector D was planned to be identical to the G-M counter assembly in detector C except that no entrance opening would be provided in the absorber. Thus, it would count only the radiation which penetrated the absorber. Its use would allow subtraction of the component counted by detector C which did not enter through its opening. It would also be useful in conjunction with detector E to obtain information about the radiation absorption spectrum.

Detector E was to be a G-M counter surrounded by a moderately thin absorber and located outside the shell in order to obtain as clean an environment as possible.

Binary scalers would be used to count the pulses from the G-M counters in detectors C, D, and E, the same as for A and B.

Since the detectors would be penetrating regions in which the pulse rates would be extremely low, as well as the centers of the belts, the need for a large dynamic range was recognized. This was provided by telemetering of three different scaling factors for each detector. The outputs of three stages in each binary scaler would be combined in logic circuits to provide a completely unambiguous eight level code for each channel. This combining would be done in such a manner that the required information bandwidth would be minimized. In addition, RC integrating circuits with time constants of five seconds were planned for inclusion to further reduce the information bandwidth. Passing the outputs of the logic circuits through amplifiers would provide low output impedances.

The plan was for the outputs of the five detector channels to frequency modulate individual voltage controlled subcarrier oscillators, directly, in the case of all except the detector D channel, and through an electronic commutator in that channel. Using a commutator would permit the sampling of several slowly changing temperature and voltage measurements with a sufficiently low sampling duty cycle so that the value of the data from the primary experiment would not be significantly reduced. The analog auxiliary measurements to be sampled by the commutator were:

a. The detector assembly temperature, to be made by a thermistor located on the electron spectrometer housing and in thermal contact with all radiation detectors

b. The temperature of a thermally isolated disk ("Tabor" sensor) which would be used to obtain information about the spin rate and attitude of the satellite, to check theoretical thermal design calculations, and to ascertain the effects of spatial environment on the special coating ("Tabor" coating) which is applied to the disk. This special type of coating has a

high solar absorptivity and a low infrared emissivity, and would be very useful in the thermal design of satellites if it can be determined how well it can maintain its surface characteristics in spatial environment.

     c. The voltage of one of the solar power supplies

     d. Two channel calibration voltages.

The plan was that the commutator would first sample the radiation detector output for about 649 seconds, then the auxiliary measurements for eleven seconds each. Thus, the duty cycle for the detector D radiation measurement would be 649 seconds on and 55 seconds off.

The outputs of the five subcarrier oscillators were to be combined in a simple arithmetic summing circuit.

7. Data Transmission

A transmitter frequency of 108.03 mc/sec was selected to permit the use of the extensive network of tracking and receiving stations which are equipped for that frequency.

The transmitter power requirement was determined by a conventional signal-to-noise ratio computation.[1,2] The signal power received at the input to a receiver (P_r) for a transmission path through free space is

$$P_r = P_t \frac{G_t G_r \lambda^2}{(4\pi r)^2}$$

where P_t is the radiated power,

    G_t is the transmitting antenna gain referred to isotropic radiation,

    G_r is the receiving antenna gain, with the same reference,

    λ is the wavelength, and

    r is the distance from transmitter to receiver antenna.

Total noise power (P_n) is the sum of the sky noise (P_{ns}), which is a function of the receiving antenna beam width, the region of the sky to which the receiving antenna is directed, and the receiver generated noise (P_{nr}). A value of +10 db (referred to ideal-receiver noise) was used to represent the sky noise (cosmic, solar, atmospheric, and man-made noise) in all computations. Atmospheric and man-made noise was considered negligible at 108.03 mc/sec at the isolated receiver locations.

---

1. Reference Data for Radio Engineers edited by H. P. Westman (American Book Stratford Press, Inc., New York, 1956) 4th ed., pp. 750-769.

2. H. J. Peake, Some Basic Considerations of Telemetry System Design, NASA Technical Note D-355, June 1960.

P_{nj} = kTB was the equation used to get the ideal-receiver input circuit Johnson noise power. k is Boltzmanns constant, T is the absolute temperature, and B is the receiver bandwidth in cps. The value of kTB for T = 290°K and B = 1 cps, is -204 dbw or -174 dbm. The receiver total noise power (P_{nr}) is given by

$$P_{nr} = P_{nj}F$$

where F is the noise figure of the receiver. Total noise power (P_n) thus was established by:

$$P_n = kTBFP_{ns}$$

and the signal-to-noise ratio established by:

$$\left(\frac{S}{N}\right)_P = \frac{P_r}{P_n} = \frac{P_t G_t G_r \lambda^2}{(4\pi r)^2 kTBFP_{ns}}$$

Values of some of the parameters for the S-46 system were:

G_t = -7.8 db above isotropic (10 db below that at the lobe peak and for parallel transmitting and receiving antenna polarization vectors).

G_r = 23 db for the Minitrack antenna.

λ = 2.78 meters (λ^2 = 8.9 db (meter)).

$(4\pi)^2$ = 158 (= 22 db).

r = 44,000 km (r^2 = 153 db (meter)).

kTB = -174 dbm.

F = 4 db (with reference to ideal-receiver noise).

N_s = 10 db (with reference to ideal-receiver noise).

Thus the S-46 signal-to-noise power ratio in db was given as

$$\left(\frac{S}{N}\right)_P = P_t(dbm) - B\ (db) + 9\ db.$$

Figure 6 is a plot of the calculated signal-to-noise power ratio as a function of transmitter power (P_t), with the receiver bandwidth (B) as a parameter, for the S-46 system under the most unfavorable
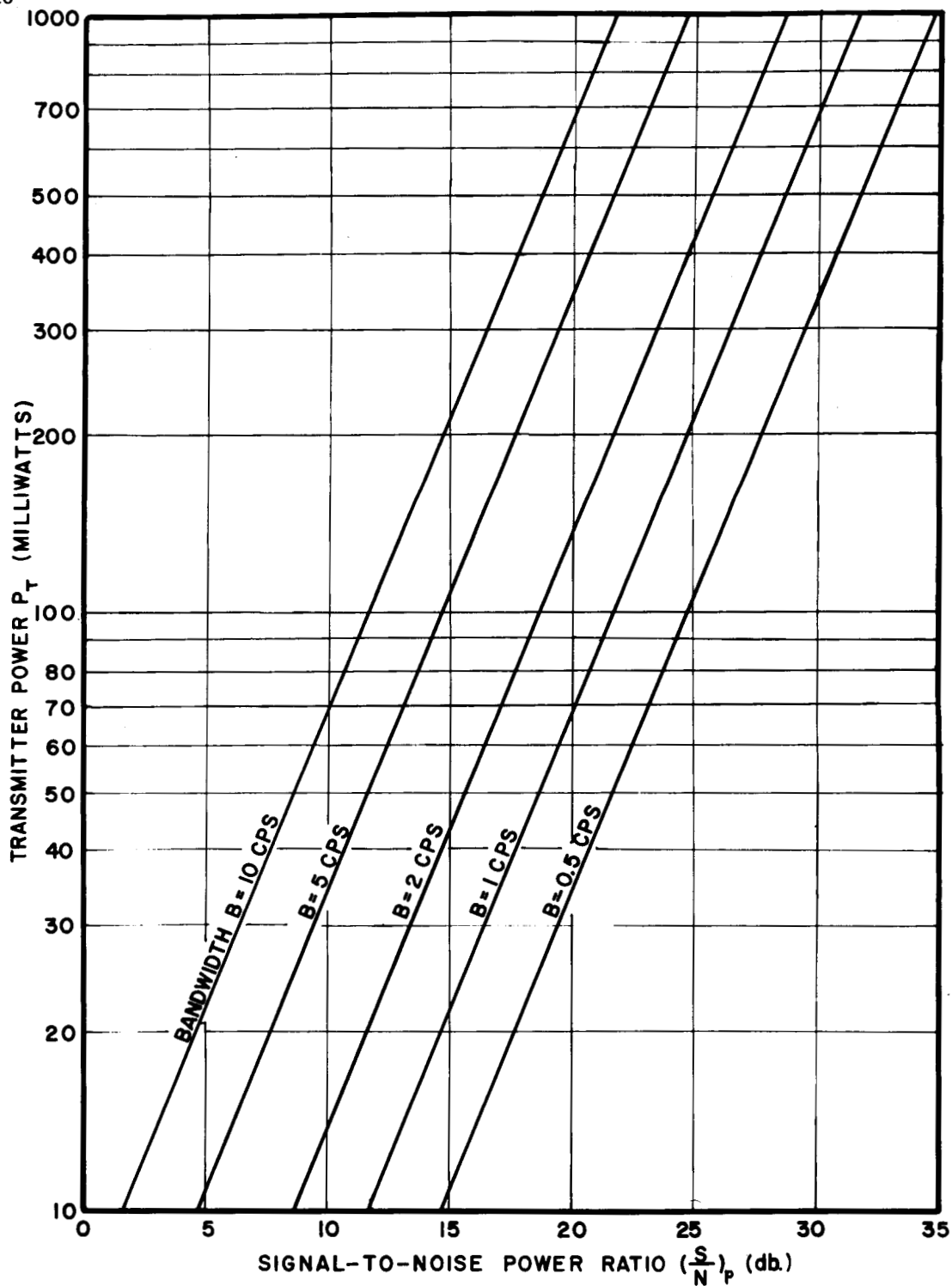
FIG. 6. SIGNAL-TO-NOISE POWER RATIO FOR THE S-46 SYSTEM

conditions. It was decided that the minimum signal-to-noise voltage ratio should be 4:1, that is, $\left(\frac{S}{N}\right)_P$ = 12 db. An additional 8 db was allowed for system degradation. This indicated, for B = 2 cps, a transmitter power output of 200 mw, requiring, on the basis of the transmitter in existence at the time of the computation, a transmitter input power of 800 mw. Subsequent improvements in transmitter and power supply designs resulted in about 300 mw more output, which should have resulted, under the worst conditions, in $(S/N)_P$ = 23 db.

The computations were experimentally checked by using a payload and a receiver with a variable attenuator at its input. This test showed that the telemetry threshold power (received signal power for S/N = 1) with B = 20 cps, was -140 dbm, in good agreement with the predicted result.

The transmitter was phase modulated by the composite signal with a maximum phase deviation of ±1.5 radians. It drove an antenna in which the active elements of an asymmetrical dipole were the payload shell and the fourth stage rocket motor. The elements were insulated at the driving point by a fiberglass gap. Antenna impedance was matched to the transmitter output impedance.

Details of the transmitter design and construction are provided in Chapter 4.

8. The Power Supply

The S-46 system concept included a solar cell-secondary battery electrical power system to supply all circuits. To guard against a possible hazard of radiation damage to the solar cells over a period of weeks or months of cell exposure, it was decided to cement thin (0.15 mm) plates of radiation resistant glass over the individual cells.

Six separate solar cell groups - one on each side of the mounting structure - would provide adequate power under all possible satellite orientations. Excess capacity of solar cells was decided upon to allow for:

    a. 25 percent battery losses

    b. Operation 20 percent of the time in the earth's shadow

    c. 12 percent solar energy transmission loss in the glass covers

    d. 24 percent for additional and unknown and unforeseen losses.

The computed solar battery power capacity and requirements for the S-46 satellite were as shown in Table 1.

Table 1

S-46 SOLAR BATTERY POWER CAPACITY

Supply System	Payload Reqts (mw)	Side Plate Capacity (each)(mw)	End Plate Capacity (each)(mw)
Transmitter, 15.6 volts	967	1750	1750
Commutator and Subcarrier Oscillators, 10.4 volts	107	245	500
SUI Instruments, 6.5 volts	192	517	7.35

Nickel-cadmium batteries were specified to regulate the voltage furnished to the instruments, as the solar power voltage flucuated, and to furnish power during periods when the satellite would be in the earth's shadow. Sufficient battery capacity was to be used so the batteries would be cycled over only the top 10 percent of their charge-discharge curves, this being considered necessary to insure long cycle lifetime of the batteries. It would also permit operation of the satellite for eight to ten hours from the batteries alone in the event of solar cell power failure.

A detailed description of the S-46 satellite power system design and construction is given in Chapter 5.

9. Physical Configuration

The determination of a payload physical configuration for S-46 was an evolutionary process accomplished jointly by SUI and ABMA personnel.

The payload was generally similar to that of Explorers I, III, and IV,[1,2] the most obvious difference being the addition of a box-like

1. G. H. Ludwig, Cosmic Ray Instrumentation in the First U. S. Earth Satellite, Rev. Sci. Instr. 30, 223 (1959).

2. G. H. Ludwig, The Instrumentation in Earth Satellite 1958 Gamma, M.S. Thesis, State University of Iowa research report 59-3, (February 1959).

structure to support the solar cells. The 1.067 meter long fourth stage rocket was attached to the payload assembly by a fiberglas antenna insulator ring. The payload was 0.587 meter long and consisted of a 15.88 cm diameter thinwall cylinder on which the solar cell frame was attached, and within which the instrument column was located. The radiation detectors were located at the top of the payload, with all directional detectors pointing upward. The channel E G-M counter was located in a detector assembly thimble protruding from the top of the payload.

Located below the detector assembly, in order, were the SUI scaling and encoding circuitry and the ABMA transmitter, commutator, subcarrier oscillators, and chemical battery pack. The SUI instrumentation and the ABMA telemetry system were contained in separate assemblies, connected by several screws and a single electrical cable, thus simplifying fabrication, testing, and definition of areas of responsibility.

10. Telemetry Reception and Tracking

Arrangements were made for telemetry data acquisition and satellite tracking facilities to be provided by NASA in the event of a successful launching. Satellite tracking was to have been done by the established network of Minitrack stations located primarily along the west 75th meridian for the lifetime of the satellite. A satellite ephemeris based on their observations was to have been provided by the NASA Space Computing Center located in Washington, D. C.

Most of these Minitrack stations did not, however, possess the necessary equipment for the recovery of the telemetered data. For this purpose, several networks of stations were evaluated with regard to the percentage of time the satellite would have been within range of at least one of the stations. The stations considered, with a brief description of the equipment and station availability at the time of the S-46 launching, are:

a. Fort Monmouth, New Jersey; U. S. Army. 15 and 18 meter diameter parabolic antennae, necessary receivers and recording equipment were available. A time code generator was to be furnished by NASA. All equipment was operational except the time code generator.

b. Singapore, BCC; Space Technology Labs (STL). A quadhelix antenna with 18 db gain and all necessary equipment was being installed. Readiness for the first week or two of the satellite flight was somewhat questionable.

c. South Point, Hawaii. Equipment and availability same as for b.

d. Jodrell Bank, England. Equipment same as for b but **early** availability even more questionable.

e. Goldstone, California; Jet Propulsion Laboratory (JPL). A 26 meter diameter parabolic antenna and all necessary equipment were on hand. Availability, however, was contingent on schedule and success of several other projects.

f. Monterey, California; D. S. Kennedy and Co. An 18 meter diameter dish antenna was available. All receiving, recording, and timing equipment was to be provided by NASA.

g. Blossom Point, Maryland; NASA. A 16 Yagi antenna array with 23 db gain was available. Equipment was being installed but had not been tested for reception of phase modulation. It was expected to be available shortly after scheduled launch date.

h. Johannesburg, South Africa. Same as g.

i. Woomera, Australia. Same as g.

It was proposed that a network consisting of stations a, b, c, and d be used initially, until the network consisting of stations g, h, and i was completed and operating properly, at which time the latter would become the primary network. Either of these networks was capable of providing more than 90 percent horizon to horizon data acquisition of which more than 70 percent was above a 10 degree elevation angle for the satellite S-46 orbit. The other stations listed above were considered alternate stations.

All stations were to have recorded the demodulated signal on one of two tracks of a $\frac{1}{4}$-inch magnetic recording tape. The other track was to have either a direct recording of a suitable standard time station such as WWV, or an accurate pulse coded time signal. The tapes were to have been sent to NASA for editing and rerecording, and these recordings were to have been forwarded to SUI for data reduction and analysis.

SECTION III. IMPLEMENTATION

By March 25, 1959, much of the system design had been completed and detailed block diagrams for the experiment were in existence. The SUI experiment was the only one to be carried in the satellite, which was designated S-46 for identification purposes. Five S-46 payloads were fabricated in this program, three prototype test units, and two flight units. Table 2 indicates the payload designations and the manner in which each payload was employed.

Table 2

SATELLITE S-46 PAYLOADS

ABMA Payload Number	SUI Package Number	Name	Function in Program
PL-1	PT-3	Thermal Test	Measurement of thermal characteristics; antenna impedance measurements and matching; vibration and spin on cluster.
PL-2	PT-2	Electrical Test	Payload electrical tests; temperature-vacuum soak; RF radiation tests; flight acceptance vibration tests.
PL-3	PT-1	Environmental Test	Shock; vibration; spin; acceleration with spin; RF radiation tests; temperature calibration.
PL-4	FU-2	Flight Unit	Primary flight unit. PL-4 with SUI FU-1 was given all flight acceptance tests. PL-4 and FU-2 mated on March 18 and launched March 23, 1960. Note: 213 G-M counter in detector E.
PL-5	FU-1	Flight Unit	Spare flight unit. PL-5 with SUI FU-2 was given all flight acceptance tests. PL-5 and FU-1 mated on March 18, 1960. Note: 302 G-M counter in detector E.

For differences between payloads see Table 7, Chapter 8.

The first prototype SUI instrument package was delivered to the Development Operations Division, Army Ballistic Missile Agency (ABMA) on October 21, 1959. The ABMA prototype testing program began soon after that and is reported in Chapter 7. The first SUI flight unit instrument package was delivered to ABMA on January 25, 1960.

The attempt to launch the satellite payload S-46 into orbit on March 23, 1960, (slightly more than one year after the beginning of the project) was not successful. The failure was due to the improper functioning of the high-speed rocket stages of the Juno II vehicle and is explained in Chapter 2. The description of the Juno II vehicle is in the Appendix of Volume I of this report series.

Chapter 2

THE S-46 FLIGHT

SECTION I. THE VEHICLE

The vehicle used in the attempt to orbit the S-46 satellite was the sixth Juno II to be launched and was designated as Juno II vehicle AM-19C. This vehicle was basically the same as the Juno II vehicle AM-19A used for the Explorer VII mission (Volume I of this report). With the exception of the difference in payloads, the main difference between the two vehicles was that the shroud of AM-19C was insulated with resin, since the rocket was programmed along a low trajectory which would subject the satellite to greater aerodynamic heating and loading stresses than AM-19A underwent.

SECTION II. PAYLOAD PACKAGE

The payload or flight unit of Juno II AM-19C was a 22.6 pound package, designated S-46, which was to orbit as an artificial earth satellite. It was instrumented to carry out the following missions:

1. Monitor the intensity and structure of the Van Allen radiation belts over an extended period of time

2. Study the energetic charged particle composition and energy spectrum as a function of position in space and/or a function of time

3. Establish the origins of the radiation belts, investigate their buildup and decay times, their long and short term fluctuations, and the possible local acceleration of particles in the belts

4. Study the total amount of energy carried by very low evergy charged particles in the radiation belts

5. Correlate changes in the radiation belts with solar activity, aurorae, magnetic storms, air glow, and the heating of the atmosphere

6. Study spin and tumble motions of the satellite.

The payload package, not including the Stage IV motor case, was a 6.25-inch (15.88 cm) diameter cylinder 23.1 inches (58.7 cm) long. About one third of the length of the cylinder was encased in a box 9.5 inches high by $13\frac{1}{2}$ by $13\frac{1}{2}$ inches. The outside surface of the box was covered with 380 square inches

of shielded solar cells to produce power for the telemetry. The cylindrical part of the payload contained the instrument column. The upper half of the cylinder housed the Van Allen (State University of Iowa) experimental equipment. Immediately below was the telemetry transmitter, followed by the subcarrier oscillator and a nickel-cadmium battery pack of about three pounds. Gaps were provided in the lower end of the aluminum shell for the asymmetric axial dipole antenna.

One transmitter was carried in the S-46 package to provide continous telemetry transmission with five subcarrier channels. About 200 milliwatts output on an rf carrier frequency of 108.03 mc/s was expected to give satisfactory telemetry transmission.

To provide 200 milliwatts output the transmitter required an input of 900 milliwatts at 15.6 volts. An additional 100 mw at 10.4 volts and 300 mw at 6.5 volts were needed to power the subcarrier oscillators and SUI experiment equipment. Since solar cells can provide about 7.5 milliwatts per square centimeter, the 1310 milliwatts of power required a minimum of about 150 square centimeters of solar cells. To take care of tumble, spin, and satellite attitude effects on the solar cell power output, the solar cell area was increased to 380 square inches.

SECTION III. FLIGHT DATA

1. General

The mission of injecting the 22.6 pound payload into orbit was not accomplished. Booster performance was near predicted, but deviations during upper stage flight caused the payload to impact about 1600 km east southeast of Bermuda. The upper stage deviations began in the second stage where an effective thrust loss of 10-15 percent was observed in addition to angle errors. Stages III and IV burned normally, but with increasing effective attitude deviations due to the second stage disturbance. The most probable cause of the failure was non-ignition of one of the eleven second stage rockets.

Juno II AM-19C (S-46 Satellite payload) was launched from the Atlantic Missile Range at 0835:11 EST, March 23, 1960. The launch azimuth was 90.0 degrees. One telemeter link served for transmission of data for 73 measurements on Stage I (booster) performance.

Range instrumentation at the Atlantic Missile Range provided the following tracking coverage at launch:

```
Fixed Camera:   0.158  -   21.380  sec
UDOP        :  15.0    -  154.8·   sec
Theodolite  :   1.25   -  126.0    sec
1.16 Radar  :  19.0    -  330.1    sec
3.16 Radar  : 178.0    -  479.6    sec
```

The maximum wind velocity at firing was determined by rawinsonde to be 23.1 meters per second from 256 degrees azimuth at 14.24 km altitude. The ceiling was 29.23 km.

2. First Stage Flight Performance

Some of the more important engine parameters and their deviations from the corresponding predicted values are given below. The total flow rate has been adjusted for the one percent error usually observed in the telemetered liquid oxygen flow rate. All three of the parameters given have been determined from the telemetered measurements.

	Measured	% Deviation from Predicted
Sea Level Thrust (1b)	148,649	-0.83
Sea Level Specific Impulse (sec)	245.07	-1.03
Total Flow Rate (1b/sec)	606.55	+0.21

The cutoff signal for the first stage was given by the guidance velocity computer 2.7 seconds earlier than predicted. The telemetered engine parameters above are inconsistent with this earlier cutoff time. The earlier cutoff required either a higher thrust, higher flow rate, or a lower liftoff weight than nominal. A two percent uncertainty in the measurements of flows and chamber pressure is considered to account for the major part of the discrepancy. Both cutoff velocity and time are known to a much higher degree of accuracy than any of the telemetered engine parameters.

The AM-19C first stage trajectory agreed quite well with the predicted trajectory in range and altitude. The actual range at cutoff was about 2.5 km less than the precalculated value. Actual altitude at cutoff exceeded the precalculated value by 5 km.

3. Cluster Flight Performance

Eight stations, located at Atlantic Missile Range, Florida, Redstone Arsenal, Alabama, Fort Monmouth, New Jersey, Aberdeen, Maryland, Blossom Point, Maryland, Atlantic, North Carolina, Bermuda, and Mayaguez, Puerto Rico, tracked the payload by one-way doppler shift of the 108.03 mc/sec frequency of the payload transmitter during the coasting and cluster periods of the flight of Stage II. Due to poor signal, interference, and low elevation angle, all the stations did not maintain lock during the complete flight. However, the Aeroballistics Division, ABMA was able to analyze the doppler data from these stations to obtain a partial conclusion as to cluster performance.[1] The station at Redstone Arsenal picked up the payload signal at 162.8 seconds of flight time and held lock until the end of the second stage burning at 487.8 seconds of flight time at which time the signal level dropped abruptly about 25 db. Contact was not reacquired thereafter because the payload had passed below the horizon. Two 16.9 db gain ground antennae were used at Redstone Arsenal for tracking; one antenna was vertically polarized and one was polarized horizontally. The antennae were connected to a hybrid ring which led, in turn, to two separate receivers. The signal level as measured at the Redstone receiver input terminals varied from 117 dbm to 136 dbm. Good telemetry was recorded during the entire tracking period.

Aeroballistics Division employed the observed doppler data in a least squares solution for the mean acceleration, direction and magnitude during second stage burning. Although some ambiguity was encountered due to observational error, a large loss of effective thrust was established. The magnitude of the thrust loss indicated a failure to fire one rocket in the second stage cluster of eleven. The angle deviations also present require the collision of the second stage and rotational launcher during the separation process, as would be expected with one motor not burning.

Six of the eight tracking stations lost lock at third stage ignition when an abrupt drop of received signal strength occurred. All indications are that Stages III and IV burned normally but with increasing attitude deviations. The increasing deviations and additional disturbances may have arisen as a result of collision between Stages II and III and Stages III and IV during separation actions. Although these disturbances contributed to the ultimate failure of the AM-19C vehicle to place the S-46 payload package in orbit, the primary cause was the failure of one Stage II rocket to fire.

1. C. R. Fulmer, H. F. Kurtz, and J. P. Lindberg, Preliminary Aeroballistics Evaluation of Jupiter Test Flight AM-19C, ABMA Report DA-TM-33-60, 2 May 1960.

4. Cluster Spin Rate

The spin rate of the rotational launcher as determined from telemetry (Figure 7) dropped from 600 rpm to 527 rpm shortly before second stage ignition. A similar drop of lesser magnitude was observed previously on vehicle AM-19A, as seen in the figure.

At ignition of Stage IV, the spin rate derived from signal strength records was still 8.8 cps (527 rpm). The spin dropped shortly after ignition of Stage IV to about 7.7 cps (462 rpm). This last 10 percent drop corresponds to similar spin decreases observed near the same time in previous Juno vehicles, although the magnitude of the drop was previously nearer 25 percent.[1]

5. Cluster Attitude

The payload telemetry data received by the Space Technology Laboratories' 60-foot dish at Cape Canaveral and by the Blossom Point minitrack station have been reduced by the State University of Iowa. The two cadmium sulfide detectors carried in the S-46 payload were sensitive to light as well as cosmic radiation, and, hence, their response (on telemetry channels 1 and 2) during the flight could be indicative of the vehicle attitude.

At about 1338:48 UT (217 seconds flight time) the count rate increased sharply from less than 0.005 cps to about 0.5 cps and 2 cps in the respective channels (Fig. 8). At 1339:25 UT (254 seconds flight time) a further increase to 40 cps was seen in both channels, after which both count rates decayed gradually to about 1 cps, in a manner characteristic of the cells after removal of a source.

The time of the first rise at 217 seconds flight time corresponds closely to the ignition time of the lateral kick rocket mounted in the shroud. This rocket was programmed to ignite three seconds after shroud separation, which occurred at 214 seconds flight time. At the time of ignition of the kick rocket the shroud should have been about five meters in front of the cadmium sulfide cells and about 2.4 degrees off the longitudinal axis (detector direction) due to the spatial tilt program of the instrument compartment.

---

1. F. Kurtz, Summary of Cluster Deviations, ABMA Report No. DA-TN-36-59, 15 April 1959.
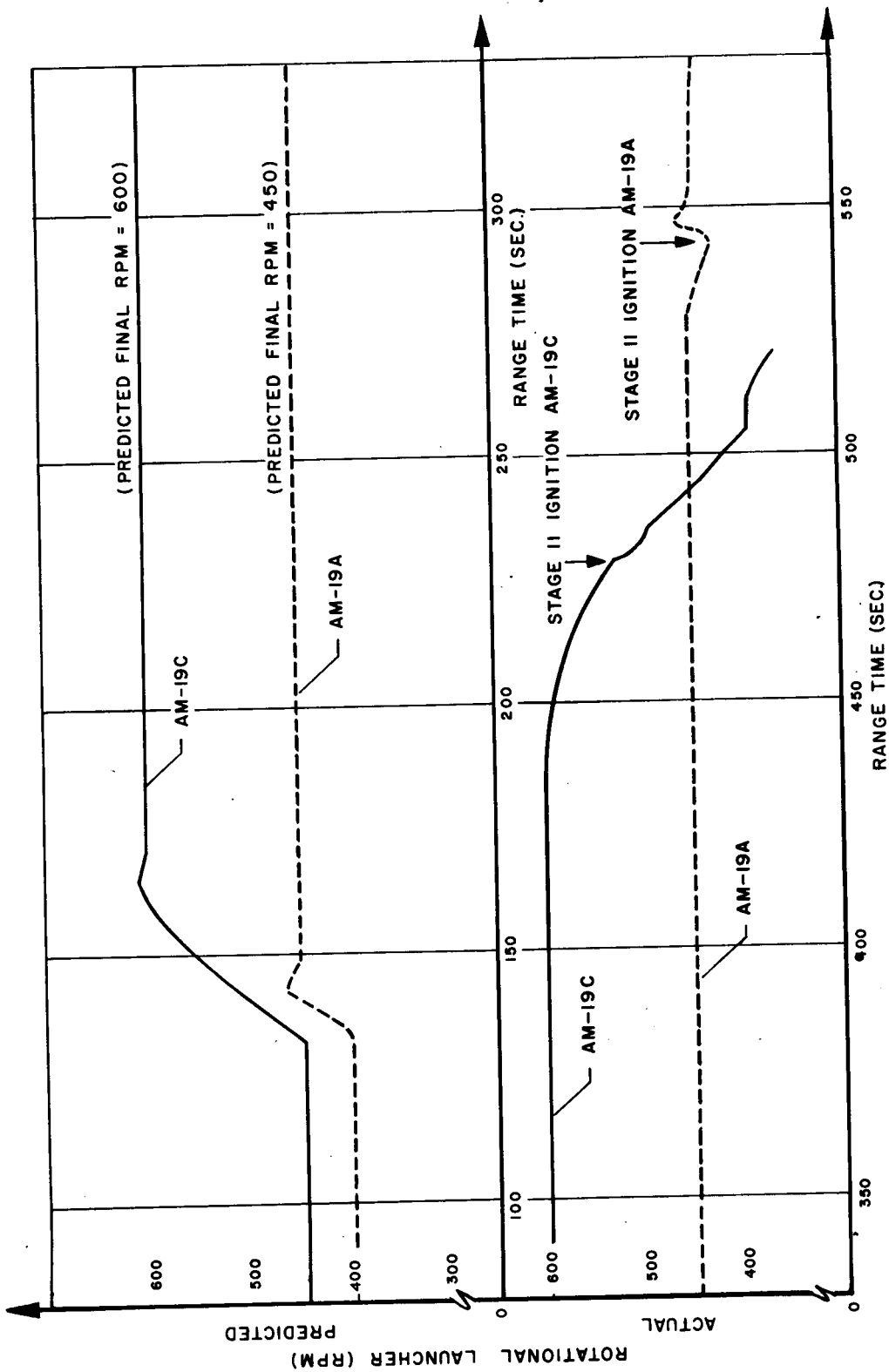
FIG. 7. ROTATIONAL LAUNCHER RPM COMPARISON FOR AM-19C AND AM-19A
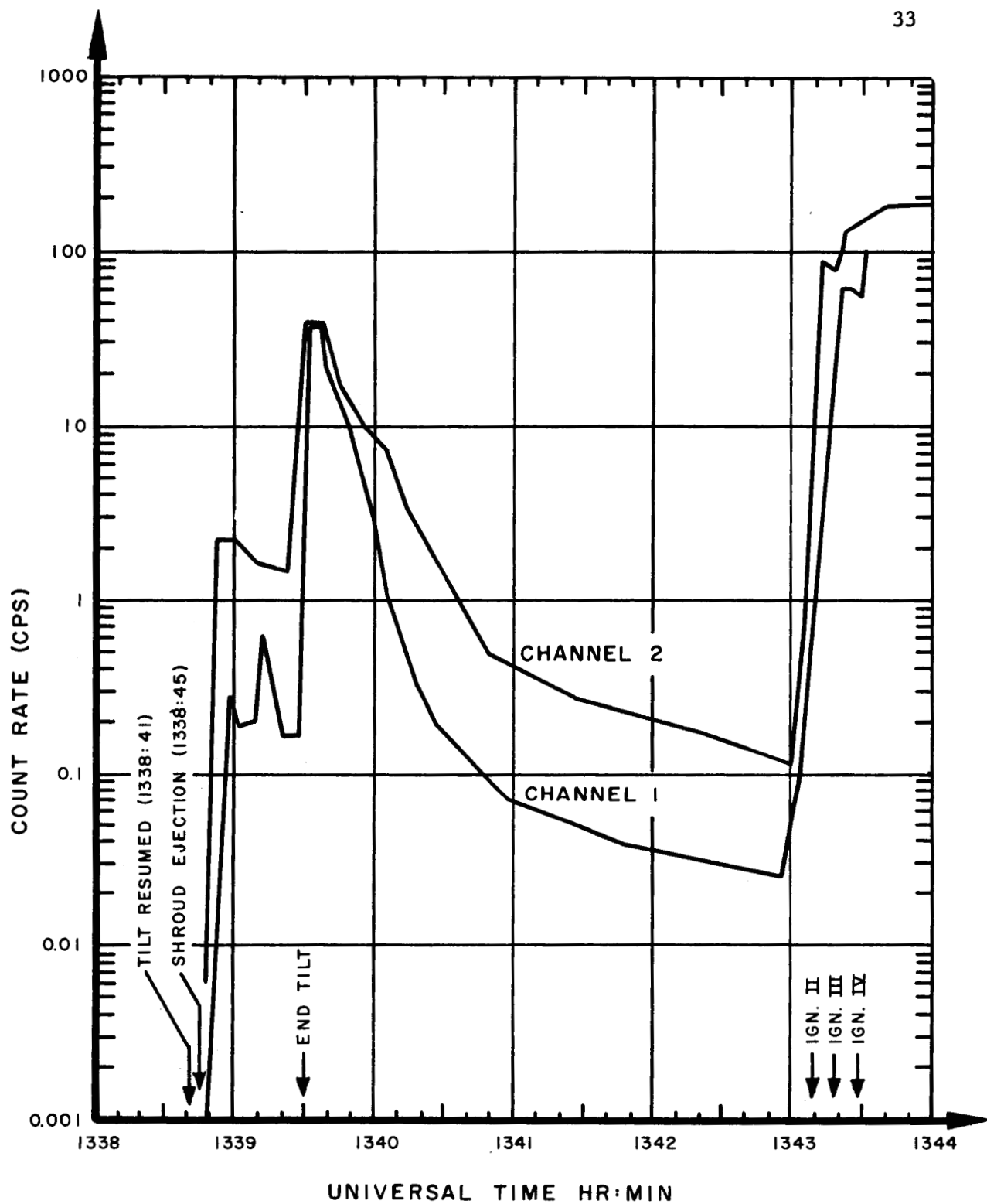
FIG. 8. CADMIUM SULFIDE DETECTOR COUNT RATE - AM-19C

The second rise in CdS cell count rate occurs at 254 seconds flight time, about five seconds before completion of the spatial tilt program. At that time there were no vehicle events which might provide a light source. Figure 9 shows the sun direction and the vehicle longitudinal axis direction, at the time of interest, projected on the celestial sphere.

From cutoff until beginning of the spatial tilt program at 210 seconds flight time, the longitudinal axis was at an angle of 11 degrees with the sun. The tilt program tilted the vehicle along the line shown at a rate of 0.8 degree per second for a total of 39 degrees, increasing the angle with the sun to 44 degrees at the end of the tilt program at 259 seconds flight time. The State University of Iowa advised that, at an angle of 15 degrees, the sun should produce a count rate in either detector of less than 0.1 cps. Direct sunlight would not appear to provide an explanation for the observed 40 cps rate. The shroud should also have been outside the stated cone of response of the CdS cells and unable to act as a reflector.

Just prior to 1343:00 UT (469 seconds flight time) the CdS cells again shows a steep increase in count rate, larger than previously. The count rates show some fine structure during and after the rise but essentially leveled off at over 100 cps until loss of telemetry at 1344:16 UT.

Second stage ignition occurred at 478 seconds flight time, about nine seconds after the rise in count rate began. Hence, large attitude motion of the cluster during burning is not a complete explanation. At cluster ignition the angle of the horizontal axis with the sun was 44 degrees, and with the nearest horizon point about 17 degrees.

SECTION IV. FREE FLIGHT PERFORMANCE

Following cluster flight, one-way doppler data were received, during varying periods of time, from stations at Atlantic Missile Range, Florida, Fort Monmouth, New Jersey, Puerto Rico, and Bermuda.

The data obtained were insufficient to permit a solution for both position and velocity vectors at injection (burnout of Stage IV). However, approximate injection conditions were obtained by application of differential corrections to the velocity vector and using an assumed position at injection obtained by crude adjustment of the predicted position to allow for the cluster deviations. The injection conditions, thus established, were approximately 1600 km range, 355 km altitude, and 6400 meters per second earth-fixed velocity. Based on these results, it is concluded that the apex of the free flight occurred at the

35
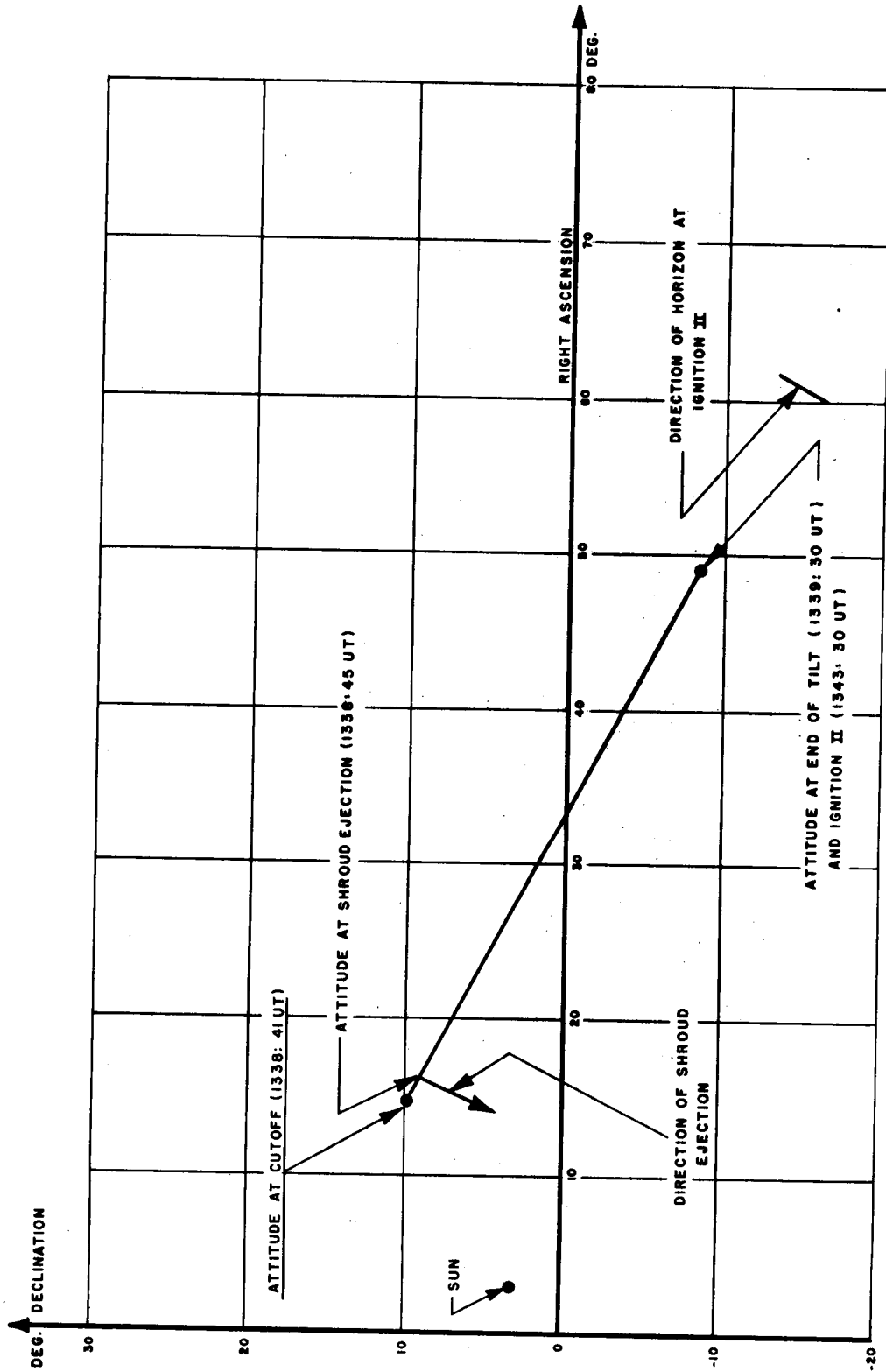
FIG. 9. ATTITUDE OF CADMIUM SULFIDE DETECTORS - AM-19C

injection point and that the ballistic impact of S-46 occurred about 788 seconds after injection (1348:19 UT) at a point in the Atlantic Ocean roughly 1600 km east southeast of Bermuda.

The residual difference between the observed doppler and that predicted for a free flight from the above injection conditions is shown in Figure 10. The data fit, particularly in the case of the Atlantic Missile Range data, shows some systematic error; at least some of the error is due to position error remaining in the injection error conditions obtained. However, the standard deviation of the overall fit was only 6 cps and the predicted signal loss times (at zero degrees elevation angle) for the four microlock stations agreed quite well with the observed times.
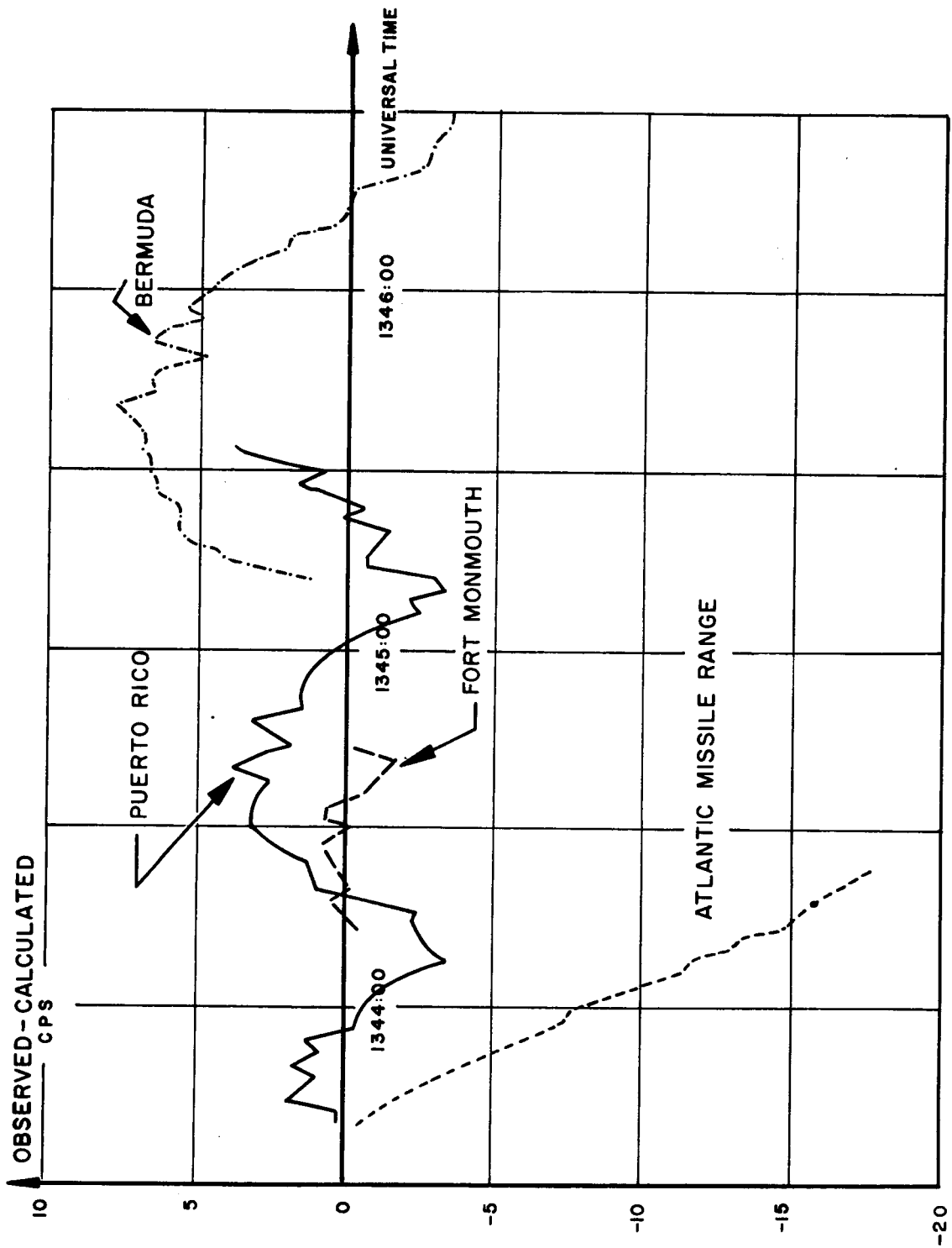
FIG. 10. FIT OF DOPPLER DATA TO FREE FLIGHT SOLUTION FOR AM-19C

Chapter 3

MECHANICAL SYSTEM, DESIGN ENGINEERING AND PACKAGING

Helmut M. Pfaff
Chief, Mechanical Systems Section
Electro-Mechanical Engineering Branch
Guidance and Control Division
Marshall Space Flight Center
National Aeronautics and Space Administration
Huntsville, Alabama

SECTION I. INTRODUCTION

The mission of S-46 satellite (to detect and measure electron, proton, and X-ray radiation in the zones of the great radiation belts) would be best accomplished by injecting it into a highly eccentric orbit. By the means described in this and succeeding chapters, the final weight of the launched flight unit was only 22.58 pounds, including adapter ring, SUI test cover and strip-off plastic coating. With the Juno II propulsion capability, it was anticipated that a 22.58 pound satellite could be orbited to an apogee of 44,000 km.

SECTION II. BASIC DESIGN CONSIDERATIONS

The antenna design, described more fully in the next chapter, required that the flight unit remain attached to and stay with the 4th stage. This arrangement eliminated the need for a special separation device as used in the predecessor satellite, Explorer VII. Furthermore, since no restrictions were placed on the attitude of the orbiting body, a rod-shaped configuration (dynamically speaking) was chosen for the payload-antenna-stage IV combination (Fig. 11). The telemetry and SUI equipment was powered by solar-cell-charged chemical batteries described in Chapter 5. To keep the batteries charged under the most unfavorable conditions during the lifetime of the satellite required both a large number and a large area of solar cells. This meant that design-wise a large area had to be provided on the outside of the flight unit to support the solar cells. This problem was solved by adding a solar cell base to the main structure of the flight unit. After considering the similarity of missions, an outside configuration of the 'Explorer I type' with the additional solar cell base was selected.
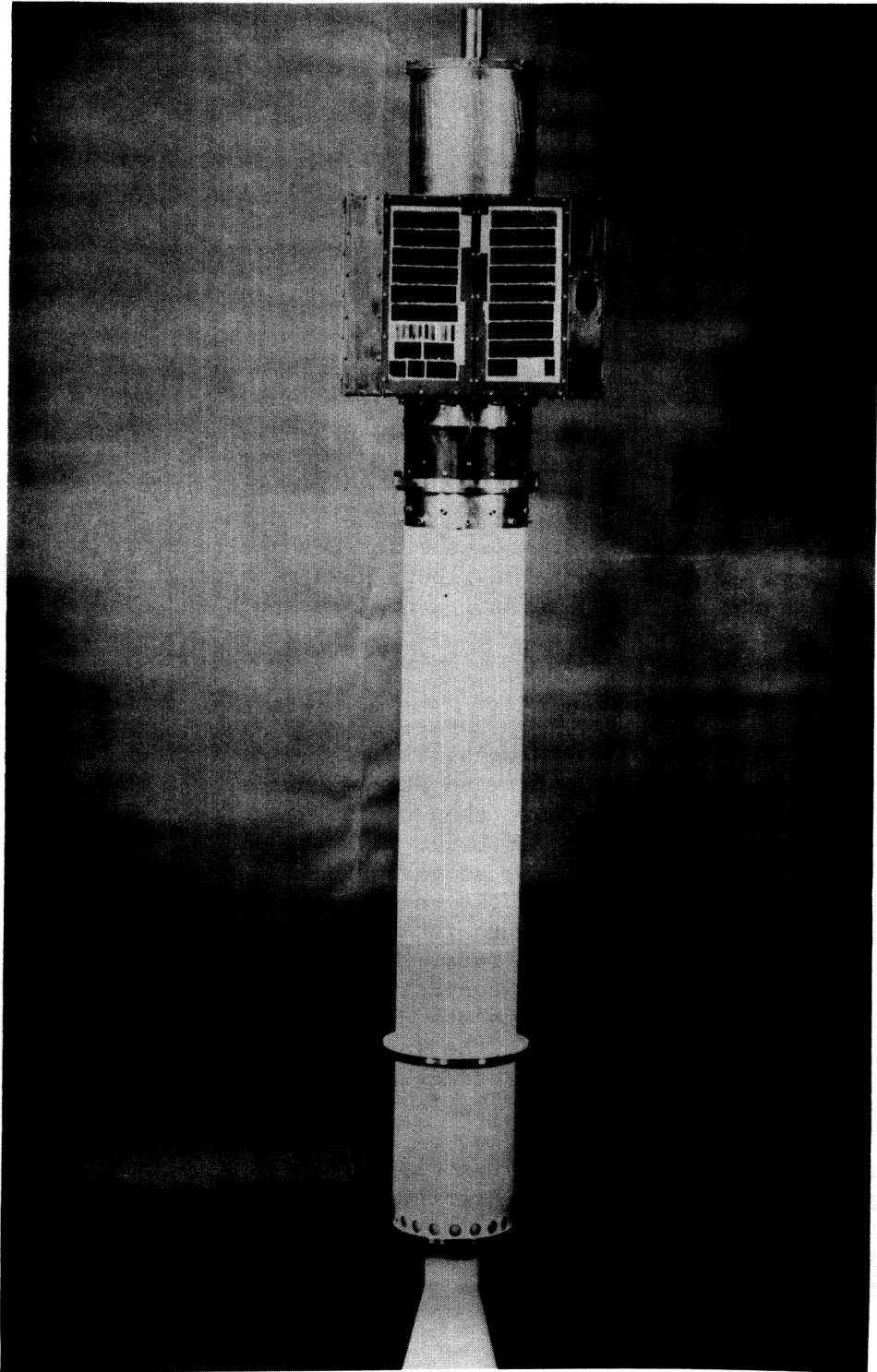
FIG. 11. S-46 PAYLOAD, ANTENNA, AND STAGE IV ROCKET

SECTION III. LAYOUT AND DESIGN

The major structural assemblies comprising the flight unit were the instrument housing, instrument column, and the solar cell base.

1. Instrument Housing

The instrument housing was a cylindrical shell machined from 6061-J6 aluminum alloy. The wall thickness was 0.76 mm and the inside diameter was 15.71 cm. The cylinder was lightened by boring a large number of holes in the section which was located inside the solar cell framework (Fig. 82). The lower end of the housing was attached to an antenna gap which may be seen in Figures 83 and 86. This antenna gap was made of laminated fiberglas cloth and 91LD phenolic resin. Strength was obtained by careful molding of the basic shape to avoid the necessity for cutting through the fibers when machining the corners. This material was used because of its high strength and electrical and thermal insulating properties.

2. Instrument Column

The instrument column consisted mainly of the SUI radiation detector package (Geiger counter and Van Allen apparatus described in Chapter 8) at the top, a spacer, then the telemetry (described in Chapter 4) and the battery-distributor part of the low voltage main power supply section (Chapter 5) at the bottom (Fig. 88). These major groups were made up of single decks which had a standardized cylindrical shape and overlapped each other to form a neat well knit stack which was held firmly together by two rods. The major group could be separated by removing a single electrical connector and six screws. This easy disassembly into major components was highly advantageous in simplifying the working arrangements between the various responsible laboratories. The major units were completely assembled in the various laboratories and then brought together for a simple final assembly.

The complete instrument column fit smoothly into the instrument housing assembly where it was supported by the antenna gap at the bottom, a central ring, and another ring at the top. The entire column could be removed from the housing by removing the upper end plate and the mounting screws and connector plugs at the bottom, and sliding it out of the top of the housing.

3. <u>Solar Cell Base</u>

Several layouts were tried for the solar cell box which surrounded the lower two thirds of the instrument housing. The configuration finally selected reflected a design that ensured maximum exposure of the solar cells under any orientation in orbit. The basic structure of the solar cell base is shown in Figure 85. Solar cells were cemented, with Armstrong C cement impregnated with TiO_2, to cover plates which were machined and webbed internally for strength. The cover plates with solar cells attached were then screwed to the basic structure. The assembled solar cell base was then attached to matching flanges on the instrument tube to form the flight unit configuration. The flight unit was attached to the 4th stage motor by means of a magnesium ring adapter (Fig. 12). The adapter ring was match-machined on one side to the payload flange and on the opposite side to the flange of the 4th stage motor. By this new method only the adapter ring had to be sent to JPL for match-machining to the Stage IV Sergeant rocket case instead of sending the entire flight unit as was necessary in the past.

In order to stay within the strict weight limitations, the entire solar cell base structure was fabricated from magnesium alloy, type AZ-31B. Furthermore, the solar cell carrying plates were made from magnesium anodized by the Dow No. 17 process.

The distribution of weight throughout Satellite S-46 is shown in Table 3 of actual weights of the components and major assemblies comprising the Flight Units No. 1 and 2.

SECTION IV. THERMAL DESIGN

Details concerning thermal design philosophy and thermal tests are given in Chapters 6 and 7. In order to fulfill the special requirements with respect to the proper heat balance of the orbiting satellite, the following steps were taken:

1. The surface of the internal structure of the solar cell base was painted with TiO_2.

2. The external surface of the instrument housing tube, covered by the solar cell base, was painted with TiO_2.

Table 3

MEASURED WEIGHTS OF SATELLITE S-46 FLIGHT UNITS

Item	Flight Unit No. 1 (PL-4)		Flight Unit No. 2 (PL-5)	
	Compo-nent Weight (lb)	Major Assy Weight (lb)	Compo-nent Weight (lb)	Major Assy Weight (lb)
INSTRUMENT HOUSING ASSEMBLY		2.47		2.53
FLIGHT UNIT ADAPTER LOWER RING (Spacer between flight unit and Stage IV Sergeant rocket)		.10		.10
SOLAR CELL BOX ASSEMBLY		7.14		7.13
Heat Balance Strip with Sensor	.13		.13	
Solar Cell Top Plate	.84		.84	
Solar Cell Bottom Plate	.86		.86	
Solar Cell Left Hand Plate (4)	1.12		1.12	
Solar Cell Right Hand Plate (4)	1.08		1.08	
Heat Balance Strips (3)	.22		.22	
Structure Assembly	2.11		2.11	
Wiring and Cement	.31		.30	
Screws	.47		.47	
INSTRUMENT PACK ASSEMBLY		12.17		12.18
Cosmic Detector Package (See Table 9)	6.38		6.39	
Instrument Pack Spacer	.13		.13	
Transmitter Assembly	1.07		1.07	
Multiplexer Assembly	.34		.34	
Subcarrier Oscillator Deck "A"	.52		.52	
Subcarrier Oscillator Deck "B"	.48		.48	
Battery Distributor Assembly	3.07		3.07	
Instrument Pack Rod Assembly	.04		.04	
Instrument Pack Ring Assembly	.06		.06	
Screws	.08		.08	
INSTRUMENT SHELL COVER MOUNTING RING		.08		.08
Mounting Ring	.05		.05	
Screws	.03		.03	
INSTRUMENT SHELL COVER ASSEMBLY		.36		.27
Instrument Shell Cover	.20		.20	
Cosmic Detector Probe Cover	.13		.04	
Screws	.03		.03	
RING AND SPACER ASSEMBLY		.15		.15
LIQUID ENVELOPE (Strippable transparent blue)		.03		.03
BALANCE WEIGHT		.10		.08
TOTAL WEIGHT		22.60		22.55
FLIGHT WEIGHT (Total weight minus liquid envelope)		22.57		22.52

GEIGER COUNTER

VAN ALLEN PACKAGE

DIPOLE ANTENNA

SOLAR CELL BOX

INSTRUMENT PACKAGE

108 m.c. transmitter
time division multiplexer
sub-carrier oscillator
battery pack

ANTENNA GAP

ALIGNMENT SPACER

4th STAGE MOTOR
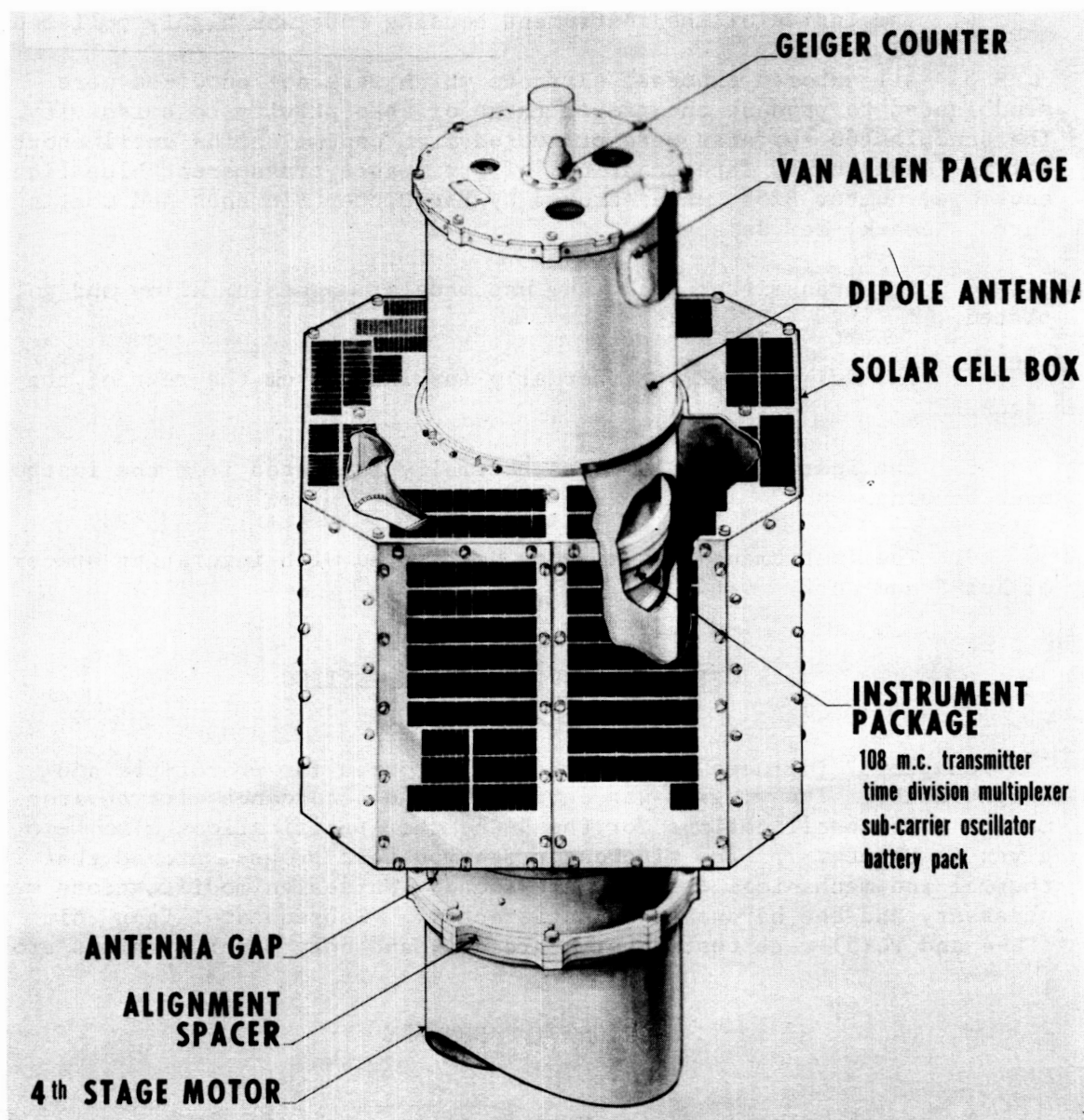
FIG. 12. LOCATION OF UNITS IN S-46 SATELLITE

3. The holes within the same part of the instrument housing tube were covered from the inside with aluminum foil.

4. The inside of the instrument housing tube was highly polished.

5. All exposed external surfaces which were not anodized were sandblasted to produce the proper ratio of absorptivity to emissivity. The sandblasted surfaces were protected from contamination until shortly before launching by three coatings of strippable transparent blue liquid envelope, number 3253, manufactured by the Better Finishes and Coatings Corp., Newark, New Jersey.

6. The transmitter deck ring was made of magnesium alloy and gold plated.

7. The SUI package was thermally insulated from the rest of the stack.

8. The instrument column was thermally insulated from the instrument housing.

9. The instrument housing tube was capped with insulating spacers of Kel-F and cork.

SECTION V. ENVIRONMENTAL TESTING

Chapter 7 includes data on the test program for prototypes and flight units. The program was carried out in accordance with environmental test specifications for the S-46, the specifications also being given in Chapter 7. The rigorous prototype test program proved that the thermal and mechanical designs were sound. No design modifications were necessary and the hardware was satisfactory. Subsequent flight units (PL-4 and PL-5) were tested very carefully and only minor problems arose.

SECTION VI. SUMMARY

Due to the mission of the S-46 satellite, the main structural design problems were to develop an ultra-light structure and to provide the necessary space for the solar cell pads. The design was developed on an Explorer I type configuration with an additional solar cell base.

Since satellite S-46 did not go into orbit, no final statements can be made as to the effectiveness of the design. However, the results of a very thorough and comprehensive test program provide a basis for believing that the chances were very good that, from the mechanical standpoint, S-46 would have fulfilled its anticipated mission.

Chapter 4

S-46 SATELLITE TELEMETRY

O. A. Hoberg
Chief, Instrumentation Development Branch
and
H. W. Kampmeier
Chief, Special Projects Office
Guidance and Control Division
Marshall Space Flight Center
National Aeronautics and Space Administration
Huntsville, Alabama

SECTION I. INTRODUCTION

The purpose of the S-46 satellite telemetry was to monitor and
telemeter the intensity structure of the radiation zones over an
extended period of time, with the broad objectives of conclusive estab-
lishment of the origins and gross dynamics, that is, the buildup and
decay times of the respective zones, and with the more specific
objectives of correlation with solar activity and with geophysical
phenomena. In addition, instrumentation was to provide means for a
crude study of the composition of the radiation in the respective zones,
with particular emphasis on the nature of the penetrating component and
on the energy spectrum of the less penetrating component.

Because of the critical weight problem that existed for the highly
eccentric orbit anticipated, the telemetry scheme for the radiation
experiment developed by the State University of Iowa (SUI) was the
subject of several meetings between SUI, NASA, and ABMA personnel. Of
the two transmitters originally planned — one for tracking and one for
telemetry — the tracking transmitter had to be eliminated due to
weight and space restrictions for the solar power supply. Certain
payload internal parameters, such as temperatures and voltages, were
to be telemetered, but an additional subcarrier oscillator could not
be provided for these measurements without degrading the scientific
information at apogee. Time sharing of one SUI channel with the internal
measurements was the solution agreed upon. The final form of the S-46
telemetry is described in this chapter. The test program and test
specifications are discussed in Chapter 7. The radiation experiment
instrumentation by SUI is covered in Chapter 8.

SECTION II. GENERAL DESCRIPTION

The telemetry instrumentation was designed and developed to monitor and telemeter the radiation information. The radiation experiment was developed by the State University of Iowa, and the telemetering system by the Army Ballistic Missile Agency. The radiation experiment had five output signals (Fig. 13). Each output signal had three possible states, with each state having a different period. The particular state and the period of that state depended on the amount and type of radiation received by the detectors. Each radiation output, except one, directly frequency modulated an individual subcarrier oscillator. The remaining output was applied to a multiplexer or electronic commutator, as it is sometimes called. Outputs from the power supply and temperature sensors were also applied to the multiplexer. The multiplexer sequentially sampled the various inputs and fed the result to the output, which modulated the remaining subcarrier oscillator. The composite signal from the subcarrier oscillator phase modulated the rf transmitter. The radio frequency signal was passed to an antenna for transmission to receiving stations.

SECTION III. SUBCARRIER OSCILLATOR

The subcarrier oscillator package was made up of two decks, A and B. The package included five subcarrier oscillators tuned to Inter-Range Instrumentation Group (IRIG) bands 1 through 5, a voltage regulator, and a mixer amplifier. The schematic diagram is shown in Figure 14.

The subcarrier oscillators were conventional multivibrator type voltage controlled oscillators (VCO). The high harmonic content of the multivibrator output waveform was removed in an LC low pass filter. The VCO's were all tuned so that high band edge would indicate an input of 0 volts and low band edge would indicate an input of +6 volts. All but the channel 4 voltage controlled oscillator had normal input circuits and displayed the standard IRIG frequency responses. The channel 4 VCO had an RC network in its input which gave it an extremely slow response. Its time constant was such that it reached 95 percent of a step function in approximately 5 seconds.

The five voltage controlled oscillator outputs were mixed in a ladder type linear adding network and fed into a high input impedance amplifier which provided a high degree of isolation between the terminating resistor of the mixing network and the output terminal. It consisted of an emitter follower using two Darlington connected transistors

48
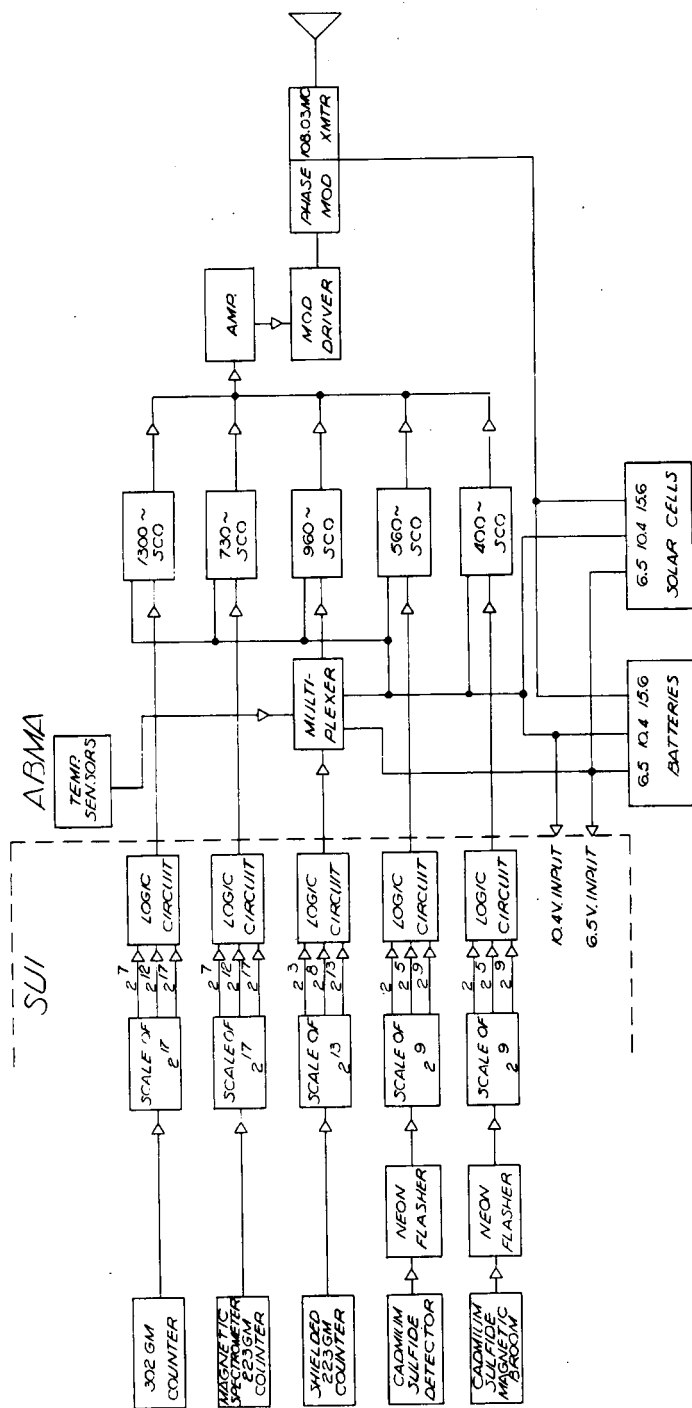
FIG. 13. BLOCK DIAGRAM OF INSTRUMENTATION FOR SATELLITE S-46

FIGURE 14. SCHEMATIC DIAGRAM OF SUBCARR

NOTES:
1. SELECT VALUE FOR 88K INPUT INPEDENCE

ER OSCILLATOR ASSEMBLY FOR S-46 SATELLITE

and bootstrapping techniques to obtain a high input impedance, a low output impedance, and near unity gain. The amplifier operated from the unregulated 10.4 volt source.

Since a multivibrator type voltage controlled oscillator is sensitive to variations in supply voltage, a voltage regulator was used to provide a nearly constant 6 volts for the VCO's over a wide range of supply voltage. The regulator was a conventional series type, using a zener diode as the reference generator and a single transistor as the series regulating device.

Location of the components on the printed circuit board subassemblies for the decks A and B are shown in Figures 15 and 16, respectively. Figures 17 and 18 show the assembly for the corresponding decks.

SECTION IV. MULTIPLEXER

The multiplexer was included in the S-46 satellite to enable transmission of a small number of low bandwidth vehicle parameters without the loss of significant data from the primary experiment. The very low anticipated received signal strength from S-46 at apogee made it undesirable to add another subcarrier oscillator for this purpose. This would require a reduction of peak transmitter deviation for the other subcarrier oscillators and would not be tolerable. As an alternative, one of the primary experiment data channels might be interrupted briefly at wide internals and the auxiliary information inserted. This is the function of the multiplexer. The multiplexer was a six channel device with the primary data connected to the first channel. This channel was connected for eleven to twelve minutes. At the end of this period, channels two through six were sampled sequentially for approximately eleven seconds each. At the conclusion of this fifty-five seconds the multiplexer returned to channel one. As the auxiliary data are in pure analog format, as opposed to the quantized nature of all other data, some form of calibration was desired to correct for system drifts during the satellite's lifetime. This was accomplished by applying fixed levels to channels 2 and 3. Channels 4, 5, and 6 are available for the temperature and voltage measurements.

The multiplexer consisted of six analog gates controlled by a ring counter. The basic timing for the system was furnished by a multi-vibrator with an eleven second period. The long period, during which channel one was transmitted, was determined by dividing the oscillator output frequency by 64 with a binary divider. The schematic diagram, Figure 19, is included to aid in further study of the multiplexer operation. Location of the components on the printed circuit board
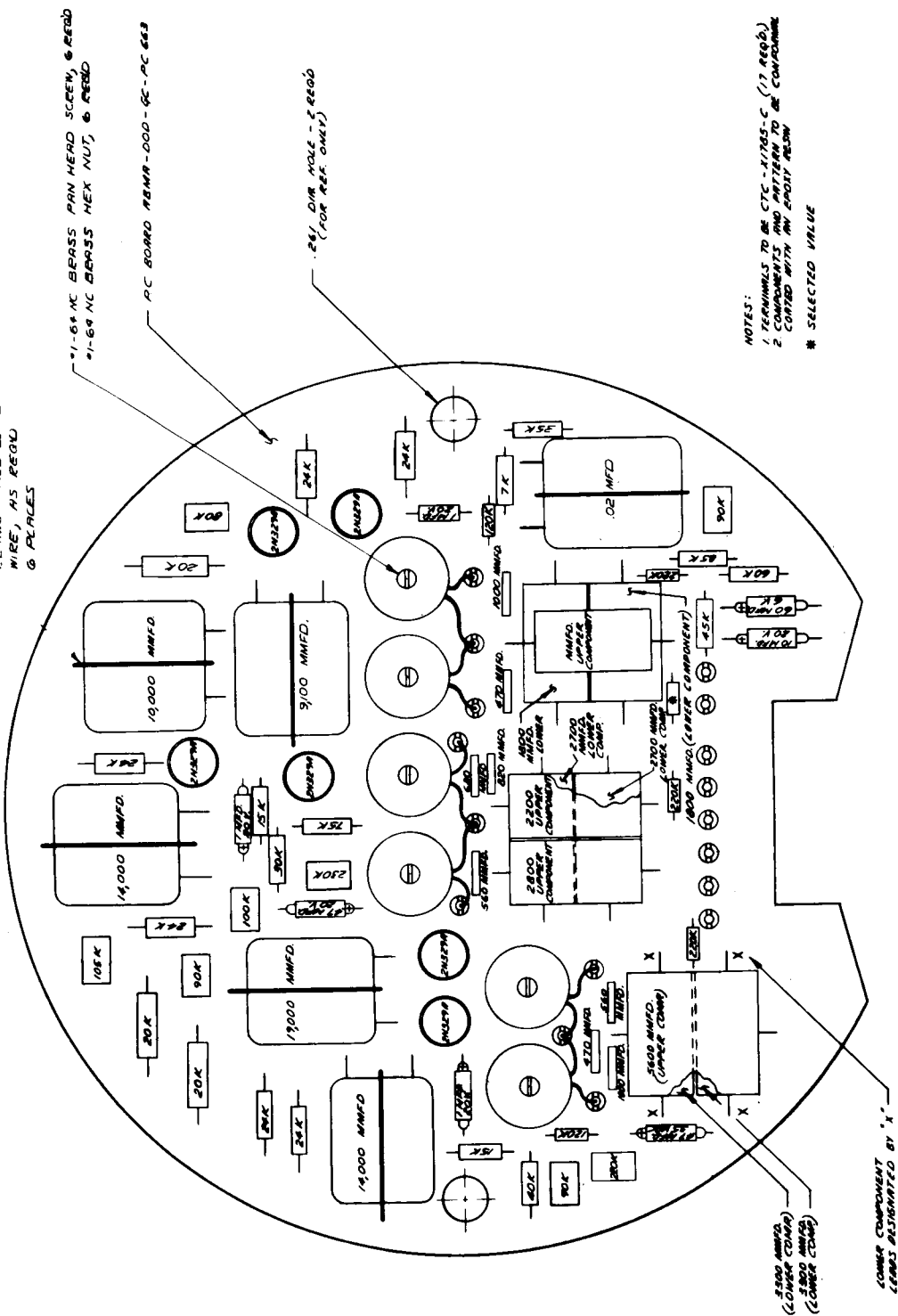
51

FIG. 15. PRINTED CIRCUIT BOARD SUBASSEMBLY FOR SUBCARRIER OSCILLATOR DECK "A"
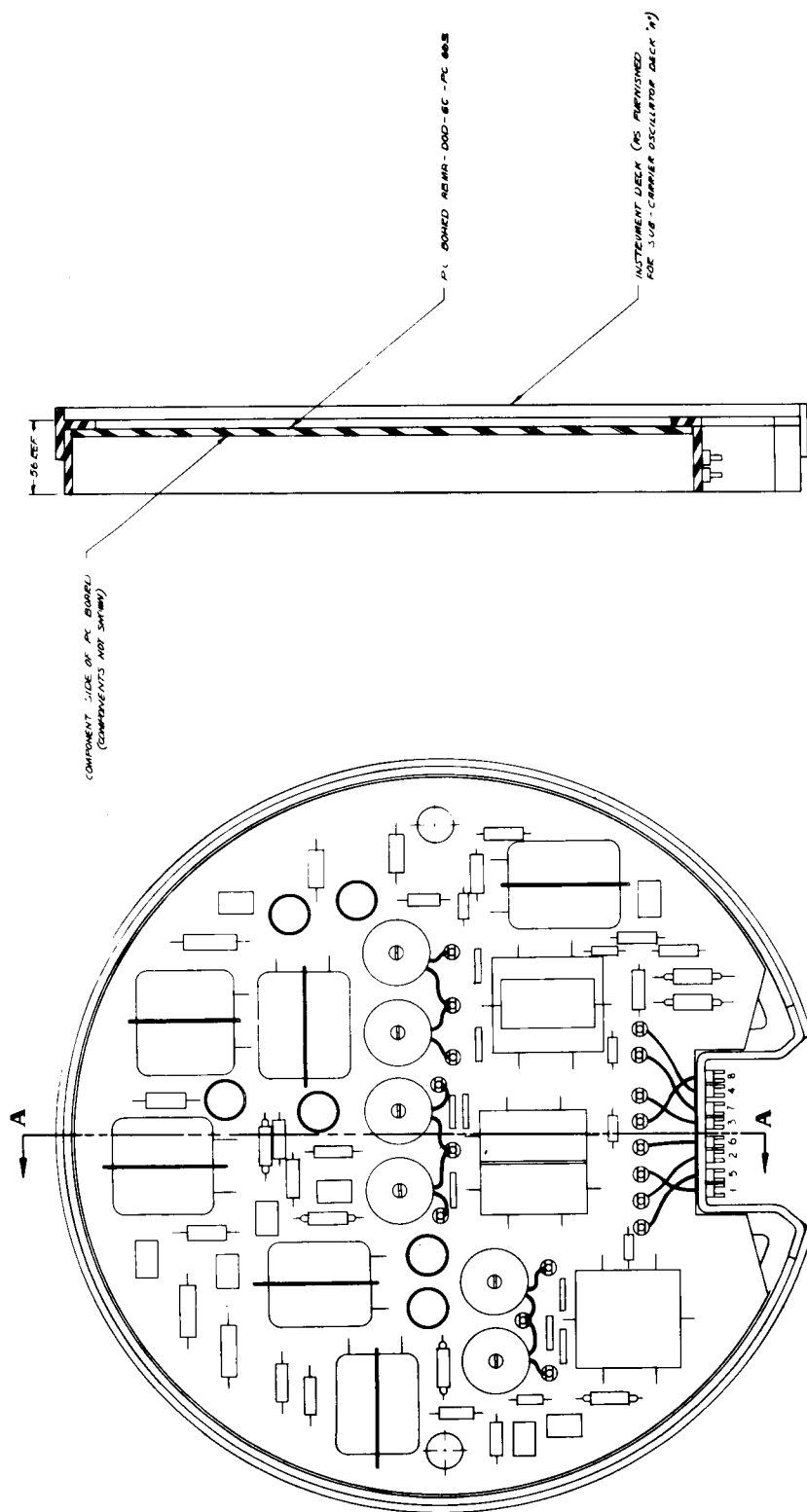
FIG. 16. PRINTED CIRCUIT BOARD SUBASSEMBLY FOR SUBCARRIER OSCILLATOR DECK "B".

53
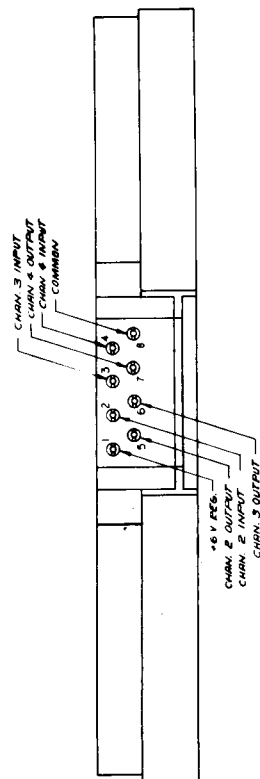
FIG. 17. SUBCARRIER OSCILLATOR DECK "A" ASSEMBLY
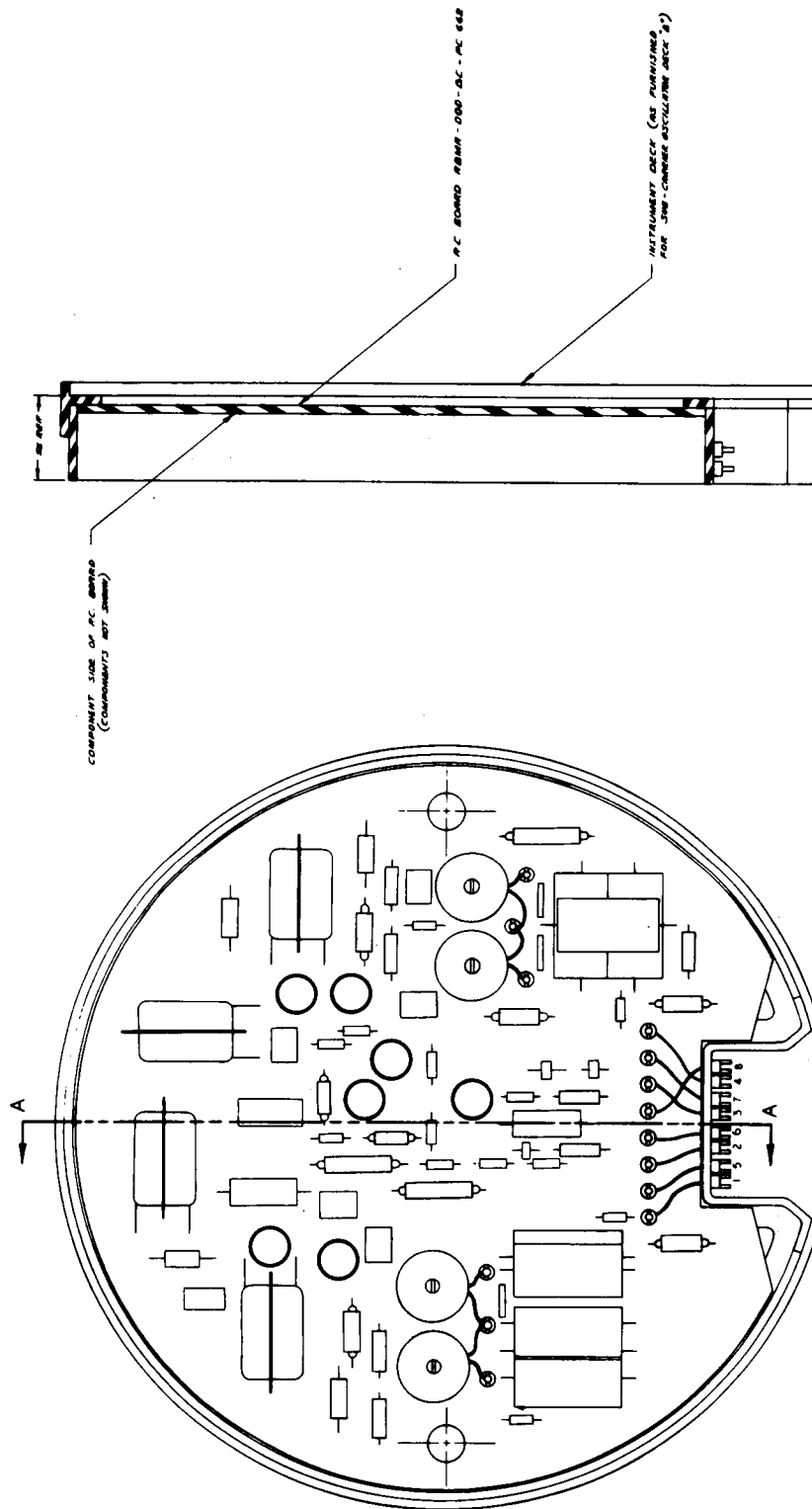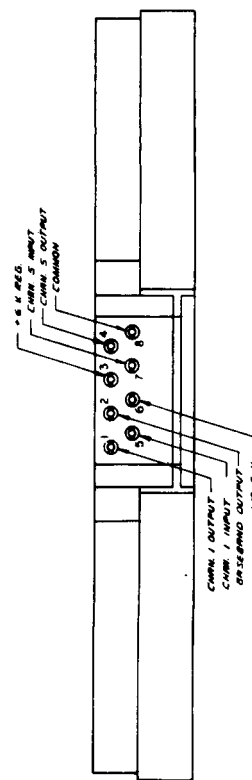
FIG. 18. SUBCARRIER OSCILLATOR DECK "B" ASSEMBLY
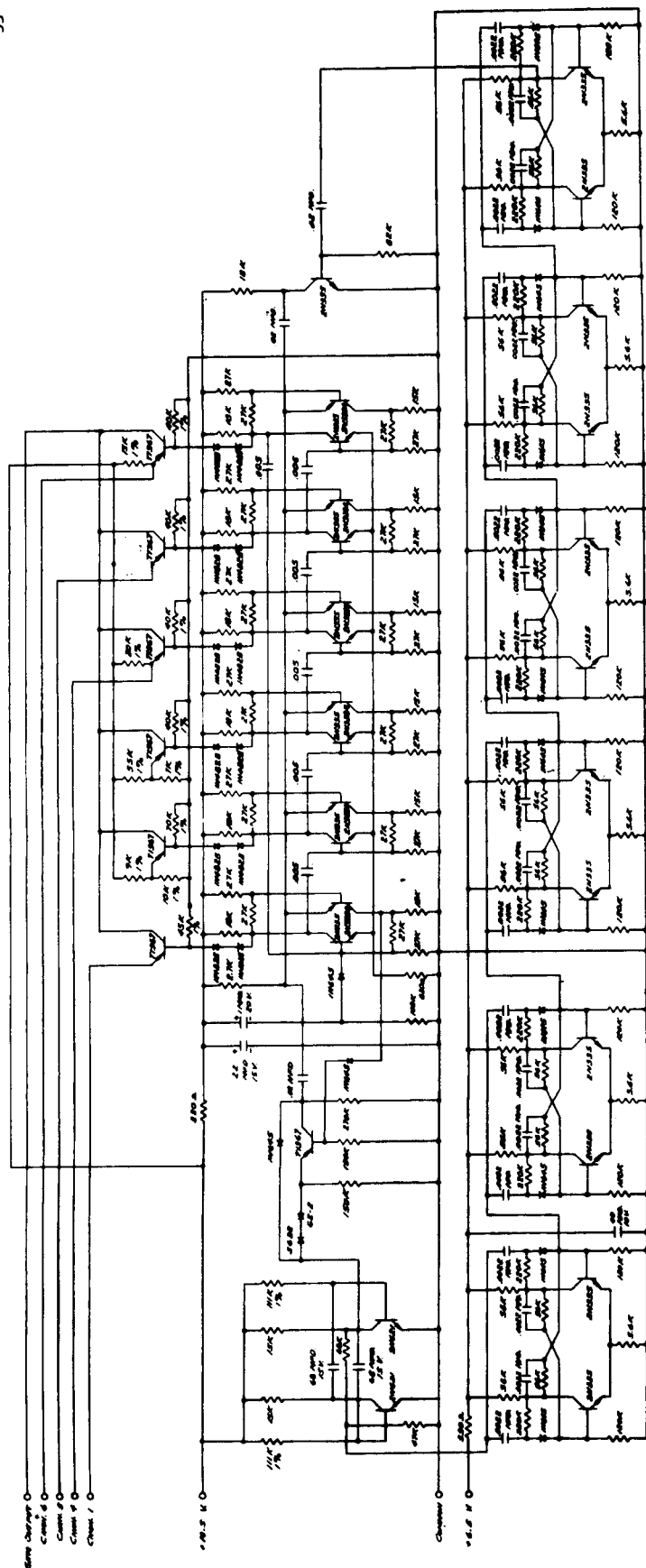
CHANNEL ALLOCATION CHART

CHAN. 1 - SUI RADIATION DATA
CHAN. 2 - HIGH CALIBRATION
CHAN. 3 - LOW CALIBRATION
CHAN. 4 - TEMPERATURE OF SKIN
CHAN. 5 - SOLAR CELL VOLTAGE.((10.4 VOLTS)
CHAN. 6 - TEMPERATURE OF SUI PACKAGE

FIGURE 19.   SCHEMATIC DIAGRAM OF THE S-46 MULTIPLEXER

subassembly for the multiplexer is shown in Figure 20. The assembly drawing for the S-46 multiplexer is Figure 21.

SECTION V. TRANSMITTER

1. General

The specifications for the transmitter for the S-46 satellite were firmly established on April 2, 1959, when NASA requested ABMA to supply an amplitude modulated, 200 milliwatt, 108.03 mc telemetering transmitter for the S-46. Approximately 800 milliwatts of primary power were allotted to power the transmitter and the five subcarrier signals to modulate it. The schematic diagram of the transmitter is shown in Figure 22.

An initial study of the signal strength to be expected from the intended orbit indicated that 200 milliwatts of radiated power would be marginal. For this reason tests were made to determine where improvements could be made in the system. It was concluded that a phase modulated (PM) signal provided as much as 4 db advantage over amplitude modulation (AM) for this application. Another 1.5 db advantage occurred in the fixed input transmitter for PM so that a system advantage for PM versus AM amounted to as much as 5.5 db. This information was reported to NASA and an approval to change from AM to 1.5 radian peak PM was received. This transmitter would also be used for tracking the satellite.

The disk or "pancake" type of instrument was required in this satellite. It was decided to build the transmitter disk of pie-slice shaped modules as shown in Figures 23 and 24 to facilitate the locating and servicing of any troubles which might occur while testing the transmitter. Each module was potted separately in foam with no overall potting; a single module could be easily tested or replaced if necessary. The signal terminals on each module were located near the outside of the disk for isolation, and dc power was supplied each module in the center of the disk. Wherever possible, the rf input and output of each module were at a 50 ohm impedance level to simplify module testing and evaluation.

2. Modular Assemblies

a. Power amplifier. The W.E. type GF-40022 PNP GE Transistor was selected for this application. This transistor was found to operate at 15 volts with 55 to 60 percent efficiency and 9 to 10 db gain while delivering 300 to 500 milliwatts output at 108 mc. This supply voltage allowed a sufficient margin of safety from the unit's breakdown voltage and thus permitted the supply voltage for the entire transmitter to be chosen as 15.6 volts. The transistor was operated with the collector
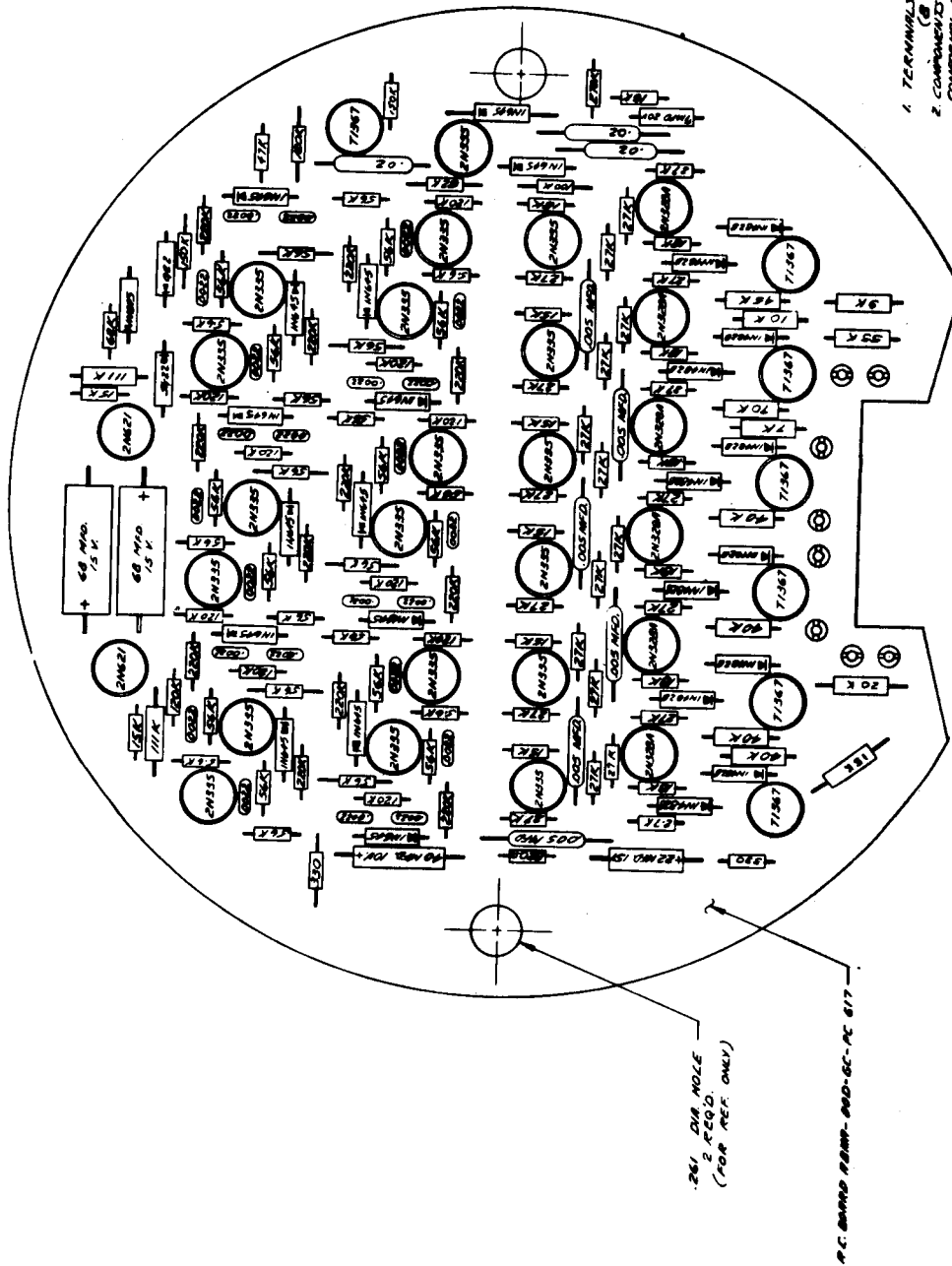
FIG. 20. PRINTED CIRCUIT BOARD SUBASSEMBLY FOR S-46 MULTIPLEXER
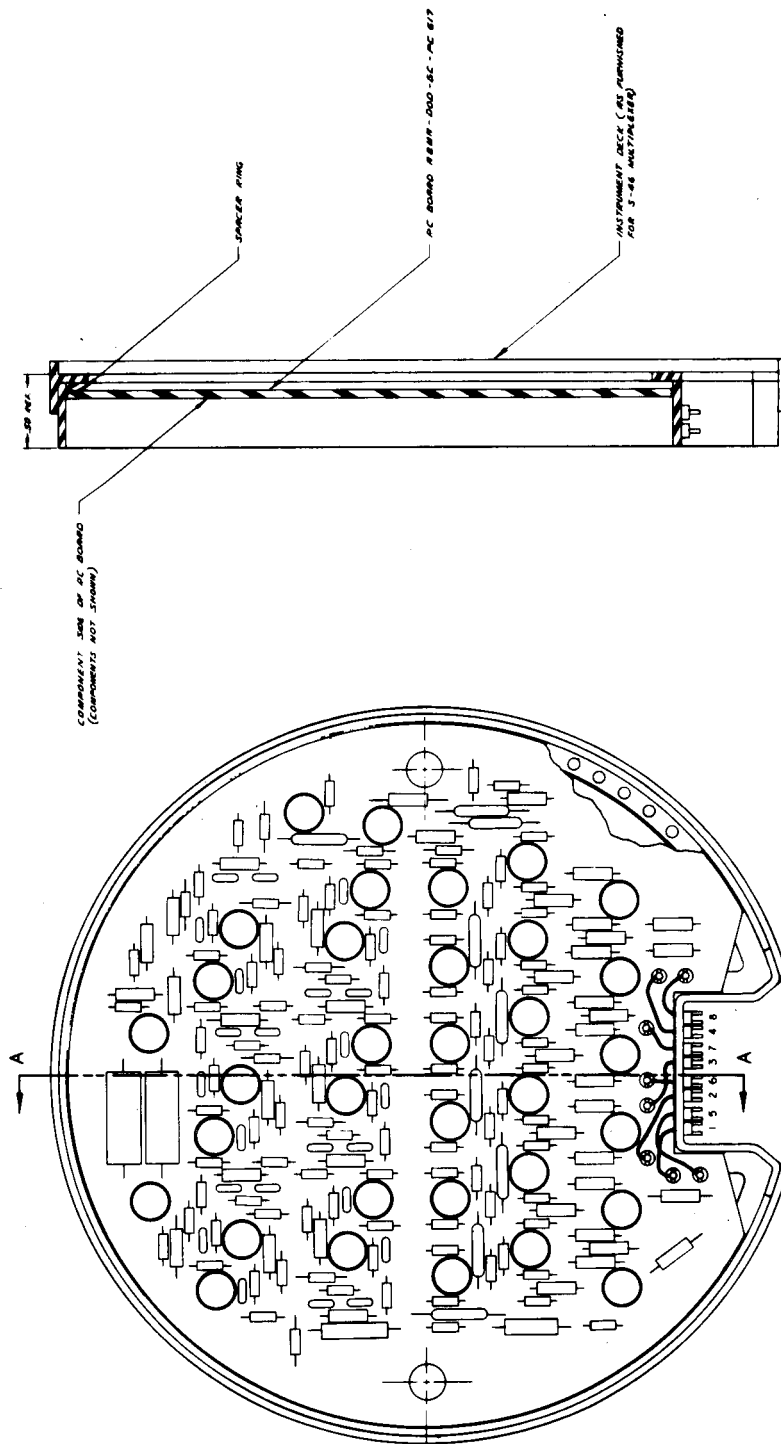
58
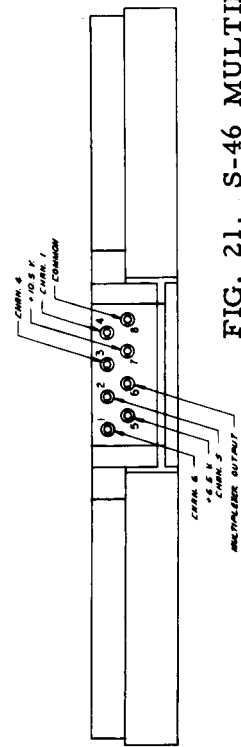
FIG. 21. S-46 MULTIPLEXER ASSEMBLY
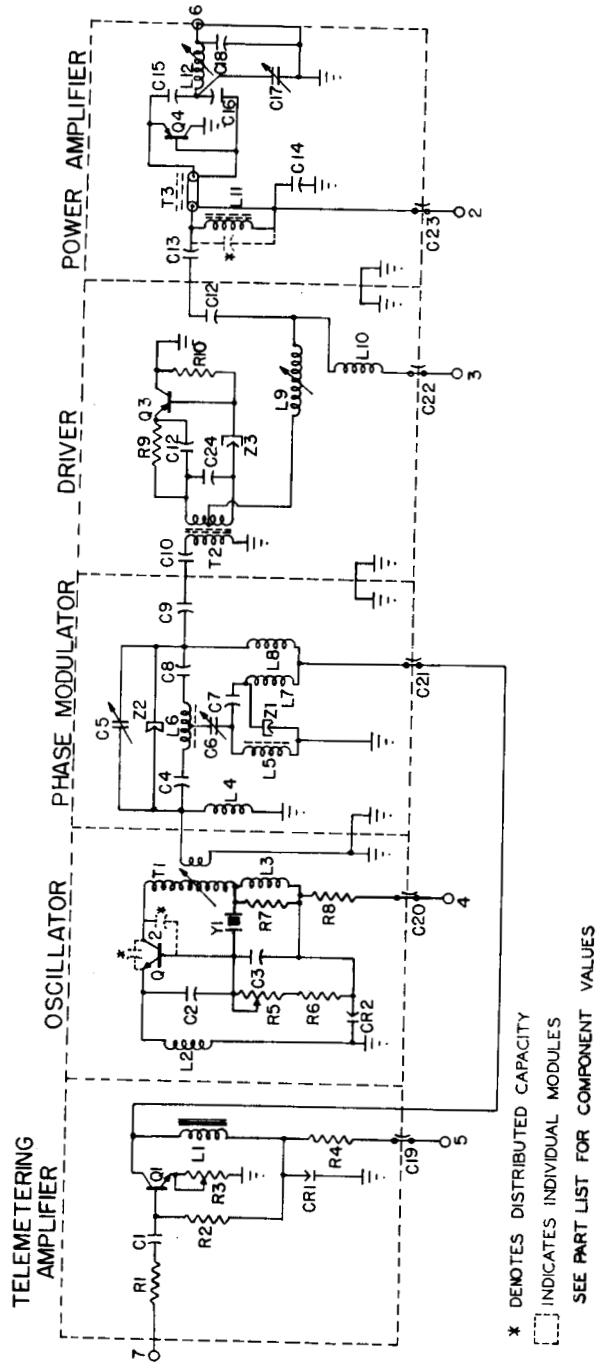
FIG. 22. CIRCUIT DIAGRAM FOR 108 MC TRANSISTORIZED TRANSMITTER
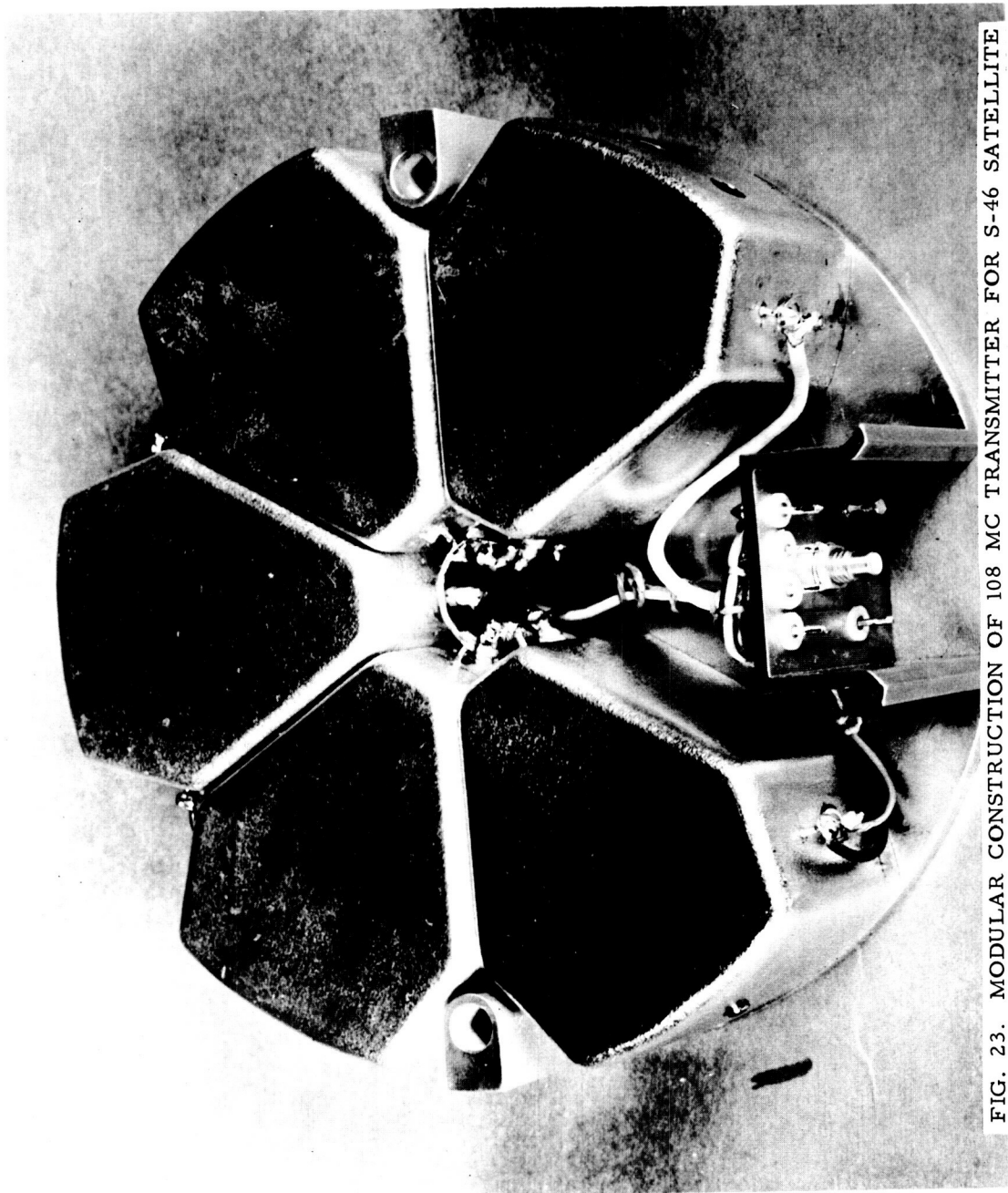
FIG. 23. MODULAR CONSTRUCTION OF 108 MC TRANSMITTER FOR S-46 SATELLITE

Phase Modulator

Oscillator

Telemetering
Amplifier

Driver

Power
Amplifier
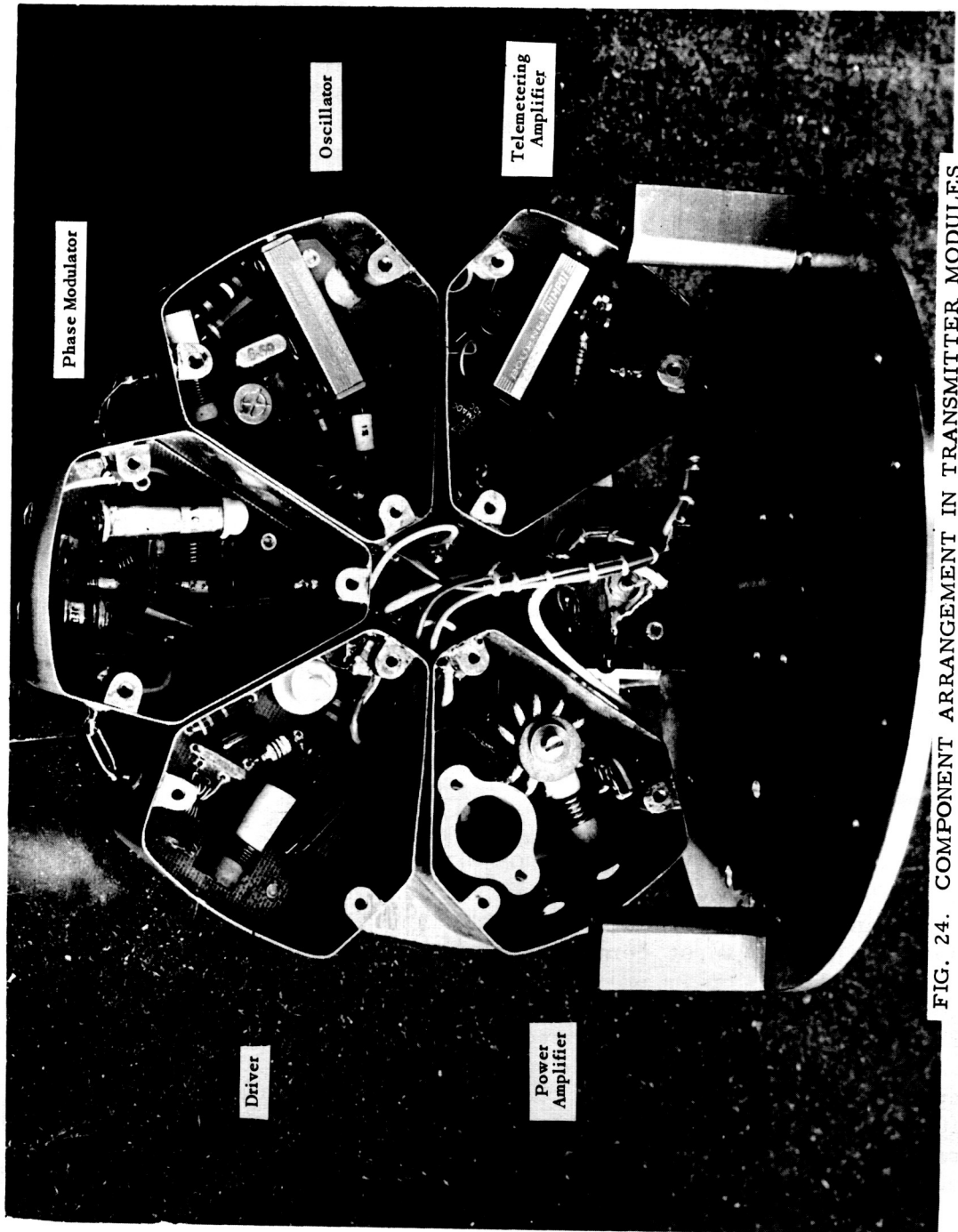
FIG. 24. COMPONENT ARRANGEMENT IN TRANSMITTER MODULES

(case) at rf and dc ground potential to permit simple removal of collector dissipated heat. An aluminum heat conducting cylinder between the flange of the transistor case and the base plate of the transmitter provided the heat exit path. A PNP transistor in this arrangement required a positive supply voltage. Thus a positive 15.6 volt supply was used for the entire transmitter. It may be noticed from the schematic wiring diagram, Figure 22, that the circuit was rather unusual in several other respects. The output was taken from the junction of C15 and C16. C17 plus collector capacity, L12, and C18 form a pi-matching network to transform the transistor output impedance to 50 ohms. This network also suppressed the harmonic output. C15 and C16, together with the transistor base and the time average emitter resistance, formed legs of a null bridge to cancel all passive coupling between input and output. The emitter and base terminals of the transistor have 1 mmf capacity each to the case (collector) and these capacities formed a third pair of legs to the bridge which were approximately nulled by the ratio of the rest of the bridge. The transistor drive was applied across the emitter to base diagonal of the bridge. Both of these terminals were above ground by approximately the transistor output potential. In order that one side of the driving source be grounded, an isolation transformer was necessary. This transformer (T3) consisted of several turns of sub-miniature 50 ohm coaxial cable wound on a ferrite ring. The driving currents were coaxial in the transformer so they were not coupled into the high permeability ferrite. Any transistor output current that tended to flow to ground through the transformer was not coaxial and, therefore, encountered a very high impedance because of the ferrite. Thus the drive terminals were transposed from a grounded source to "hot" terminals without disturbing or coupling to the output circuit. The choke L11 provided a dc short between emitter and base so the only input bias was the $^1/_2$-volt contact potential within the transistor emitter-base diode. At the drive level of 38 milliwatts this caused the angle of current flow to be slightly less than 180°, thus providing efficient operation and with no bias power loss. The length of coaxial cable on the trans-former and the components L11 and C13 were chosen to provide 50 ohms impedance at the input terminals of the module.

     b. _Driver._ In most respects the driver was a low power version of the power amplifier. It used a W.E. SCL 7002/7 or a 2N1195 PNP GE Transistor. The output matching network used the collector-to-base capacity and L9 to transform to the 50 ohm module output terminals. L10 was only for dc feed. The input used a more conventional isolation transformer with windings on opposite sides of a ferrite ring. The secondary was center tapped so the two halves served as the null bridge legs balanced against the base and time average emitter resistance. The bias circuit was typical except that it used a silicon diode (Z3) to provide a controlled voltage of about 0.7 volts to limit the emitter current through R9. A large silicon junction was required in the diode for good voltage control with low current and, thus, small loss of power

for bias. The large junction had several hundred mmf capacity so no additional by-pass was required. The 0.7 volt across the silicon diode was controlled by the barrier potential of the diode. This voltage overcame the barrier potential of the transistor emitter-base diode. Therefore, since temperature variations changed the barrier potentials of both together, the temperature effect on bias was canceled. This bias arrangement kept the transistor operating at uniform gain and current over the temperature range. The bias provided class AB operation for high gain and reasonable efficiency. The primary of the isolation transformer and C10 were chosen to provide 50 ohms impedance at the module input terminals.

     c. <u>Phase modulator</u>. This circuit was a bridged "T" network evolved from a lattice network. It is best to explain the operation of the lattice network first and then show the evolution of the bridged "T". Figure 25a shows the basic lattice network. If the legs were reactive and reciprocal with respect to the characteristic impedance, then the network had zero attenuation to all frequencies and a phase shift that changed with frequency. For a phase modulator it was desired rather, that the phase shift at the constant input frequency be variable. This was done by varying the two reactive legs together so that the reciprocal relationship was maintained. One pair of reactive legs could be capacitive diodes but then, to be reciprocal, the other pair of legs had to be inductances which may be varied electronically in a very special way. This problem was solved by quarter-wave networks which had the same characteristic impedance as the lattice, since, when a quarter-wave network is terminated with reactance, the reciprocal to this reactance always appears at the other end of the quarter-wave network. Therefore, the circuit evolution to Figure 25b allowed the exclusive use of identical capacity diodes as the jX reactances. To reduce the number of diodes required to two, the hybrid version shown in Figure 25c or the bridged transformer "T" of Figure 25d may be used. Either is classically equivalent to Figure 25b but the "T" was chosen because it gives a common input and output terminal with the simplest transformer. The variable reactance, j2X, of Figure 25d may be a capacity diode alone, or it may be a diode combined with other reactances. The tangent function of the basic phase formula, Figure 25a, and the capacity-voltage characteristic of the capacity diode are two non-linear items to be considered when trying to obtain a linear relation between diode control voltage and phase shift in the molulator. By forming the basic reactance, jX, from a capacity diode and linear inductance in series or shunt, it is possible to find combinations where the two non-linear items compensate. The shunt combination was chosen since it results in less signal voltage on the diode. Most capacity diodes follow the law:

$C = C_n / \sqrt{E_n}$, where C is the capacity, C_n is the normalized capacity at

$$\alpha = 0$$
$$\beta = 2 \ \tan^{-1}\left(\frac{X}{Z_0}\right)$$
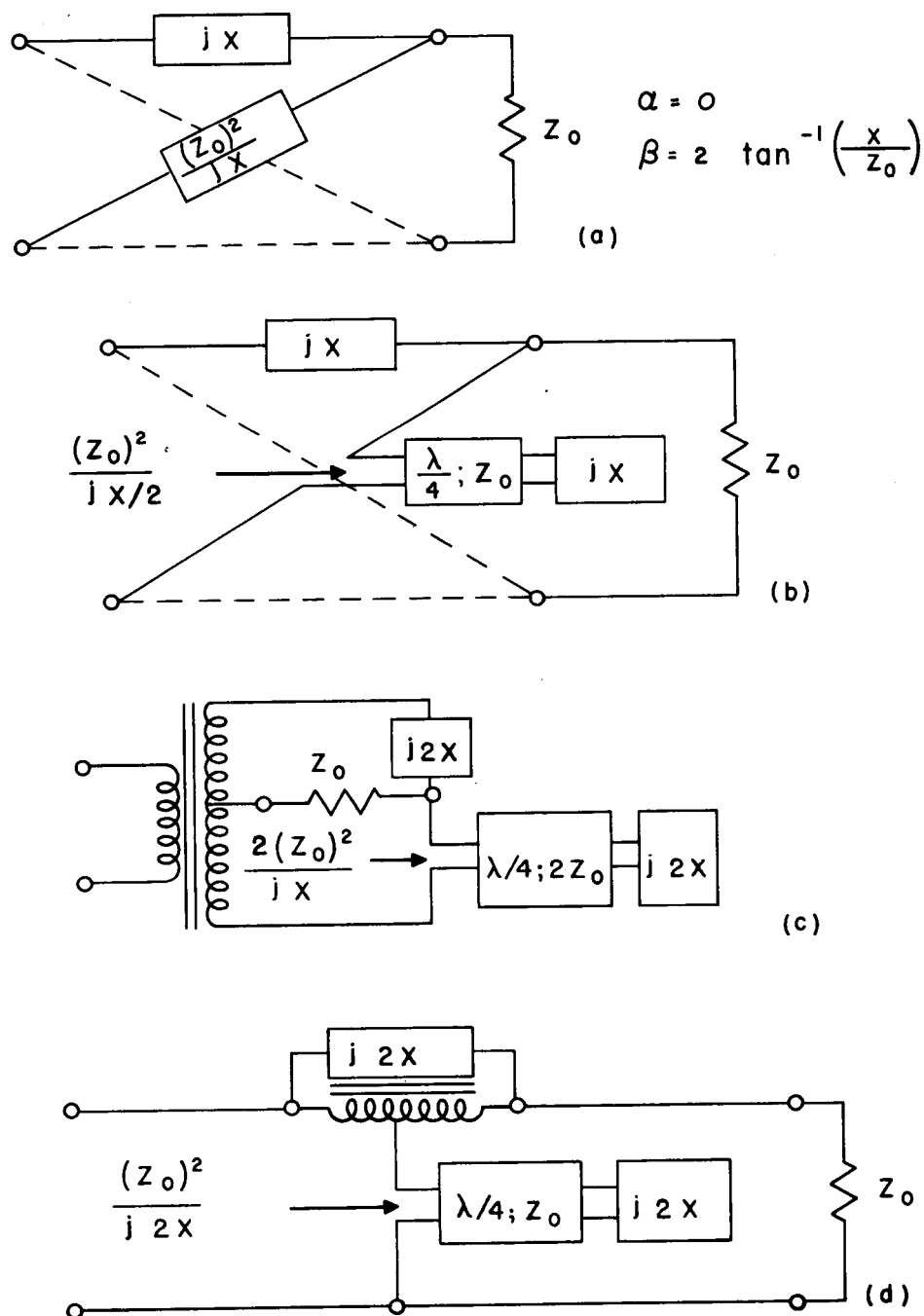
FIG. 25. PHASE MODULATOR CIRCUITS

The basic lattice network shown in (a) is modified in (b) to use identical capacity diodes as the jX reactances and is further modified in (c) to reduce the number of diodes to two. A bridged "T" network is shown in (d).

the fixed bias, and E_n is the instantaneous voltage normalized with respect to the fixed bias. With diode and inductance in parallel:

$$\frac{1}{jX} = \omega C - \frac{1}{\omega L} = \frac{\omega C_n}{\sqrt{E_n}} - \frac{1}{\omega L}$$

Let $\omega^2 = \dfrac{1}{L\, C_n}$; so

$$\frac{1}{jX} = \omega C_n \left(\frac{1}{\sqrt{E_n}} - 1 \right) = \frac{1}{X_{C_n}} \left(\frac{1}{\sqrt{E_n}} - 1 \right)$$

and

$$\beta = 2 \tan^{-1} \frac{X_C}{Z_O \left(\dfrac{1}{\sqrt{E_n}} - 1 \right)}$$

By plotting this last equation it was determined that by making $\dfrac{X_C}{Z_O} = \frac{1}{4}$, a quite linear phase versus diode control voltage characteristic could be obtained over a ±1.5 radian shift in phase. A characteristic impedance of 100 ohms was chosen since at 50 ohms the diode capacity required was quite large and stray inductances were troublesome. The circuit on the schematic diagram, Figure 19, may be seen to be similar to that in Figure 25d. The upper j2X basic reactance is composed of Z2 and L6. The quarter-wave network is composed of C6, L5, and C7. The second diode, Z1, has no inductance shunting it because a series capacity at the input of a quarter-wave network is equivalent to a shunt inductance at the network output and, therefore, C6 may be slightly reduced in capacity to duplicate the action of an inductance shunting Z1. The mutual inductance of L6 also provides the transformer action required in the circuit in Figure 25d, and C5 allows for slight differences in diodes and coils. C4 and C8 are blocking capacitors so that bias may be applied to Z2 without upsetting the L6 transformer symmetry L4, L7, and L8 are for application of bias and modulating signal to the diodes. C9 and L8 form a network to match the 100 ohms characteristic impedance to the 50 ohm module output terminals.

d. <u>Crystal oscillator.</u> Since the transmitter was to be used for tracking as well as telemetering, it was necessary to provide maximum frequency stability in the oscillator. At 108 mc a fifth mode crystal was necessary; this high mode provided a very high crystal L/C ratio to resist frequency pulling. A voltage control diode (CR2 in Fig. 22) was used to minimize pulling caused by supply voltage variations changing

the collector-base transistor capacity. A Fairchild silicon NPN tran-
sistor was used instead of a GE unit to minimize changes in the transistor
phase shift caused by temperature changes. The crystal was kept out of
the feed-back network to prevent the "oscillation drop-out" effect with
tuning. The feed-back was achieved by C2 and distributed collector-to-
emitter capacity. The crystal was placed in series with the collector-
to-base inductance (T1). L3 and R7 fed the direct current and canceled
and damped the crystal static capacity to prevent non-crystal-controlled
oscillations. With this circuit it was possible to intentionally pull
the crystal from its natural frequency by ± 1 kc without changing the
amplitude of oscillation appreciably. It was most convenient to be able
to do this since the crystal cannot be ground to absolutely correct
frequency.

e. _Telemetering amplifier._ This module was required for gain
and for pre-emphasizing the subcarrier signals. The iron core choke L1,
Figure 22, emphasized the high frequencies and also fed the diode
(CL1) controlled bias to the phase modulator. A great range of gain could
be had by adjusting the non-bypassed emitter resistance R3. R1 simply
provided the 10K ohms input impedance required by the modulating equip-
ment and made the source appear to the transistor as a constant current
signal generator. Constant dc base current biasing was permitted because
the silicon transistor was used at relatively low temperatures for silicon.

SECTION VI. ANTENNA

The antenna used on the S-46 satellite was the familiar "gap" or
dipole, formed by the fourth stage Sergeant rocket motor (Fig. 34)
which did not separate from the payload, and the payload itself. The
payload was insulated from the fourth stage by a fiberglas "gap". The
maximum power lobe of this nonsymmetrical antenna was inclined slightly
to the rear of the satellite. Figures 26 through 29 show the antenna
radiation pattern.

Electrical connection was made between the two dipole elements and
two straps inside the insulator by screws that went through the insulator.
These straps formed the tie points for connecting the antenna to the
transmitter.

The dc control lines that crossed the antenna gap had rf chokes in
them to isolate the lines fron the antenna (Fig. 30b).

The impedance of the antenna at the strap tie points was transformed
to 50 ohms by an impedance matching device whose schematic is shown in
Figure 30a. The components of this device were mounted on a fiberglas
block on the gap.

ANTENNA RADIATION PATTERN
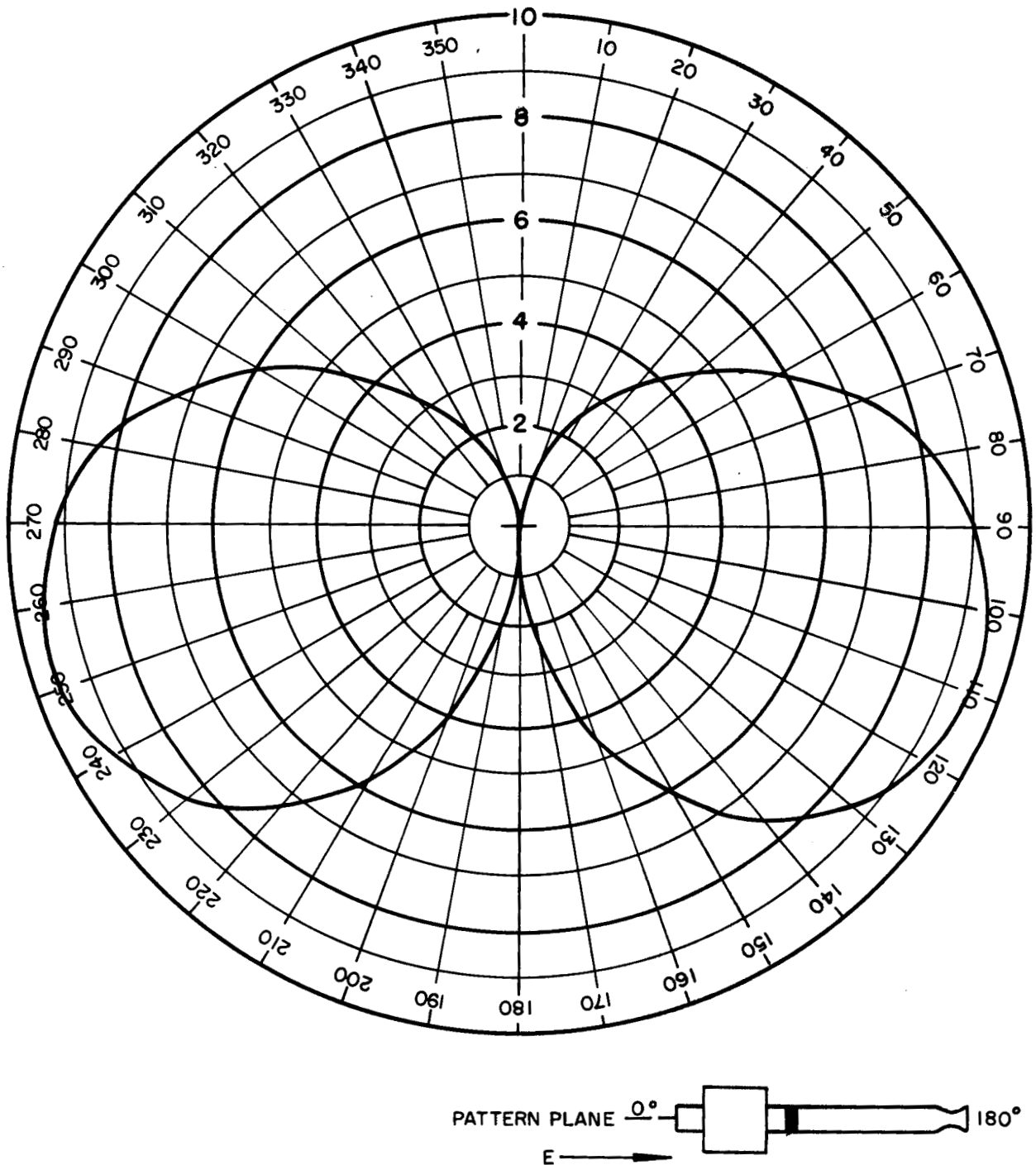
FIG. 26. VOLTAGE PATTERN FOR 108 MC S-46 ANTENNA

ANTENNA RADIATION PATTERN

PATTERN PLANE

E
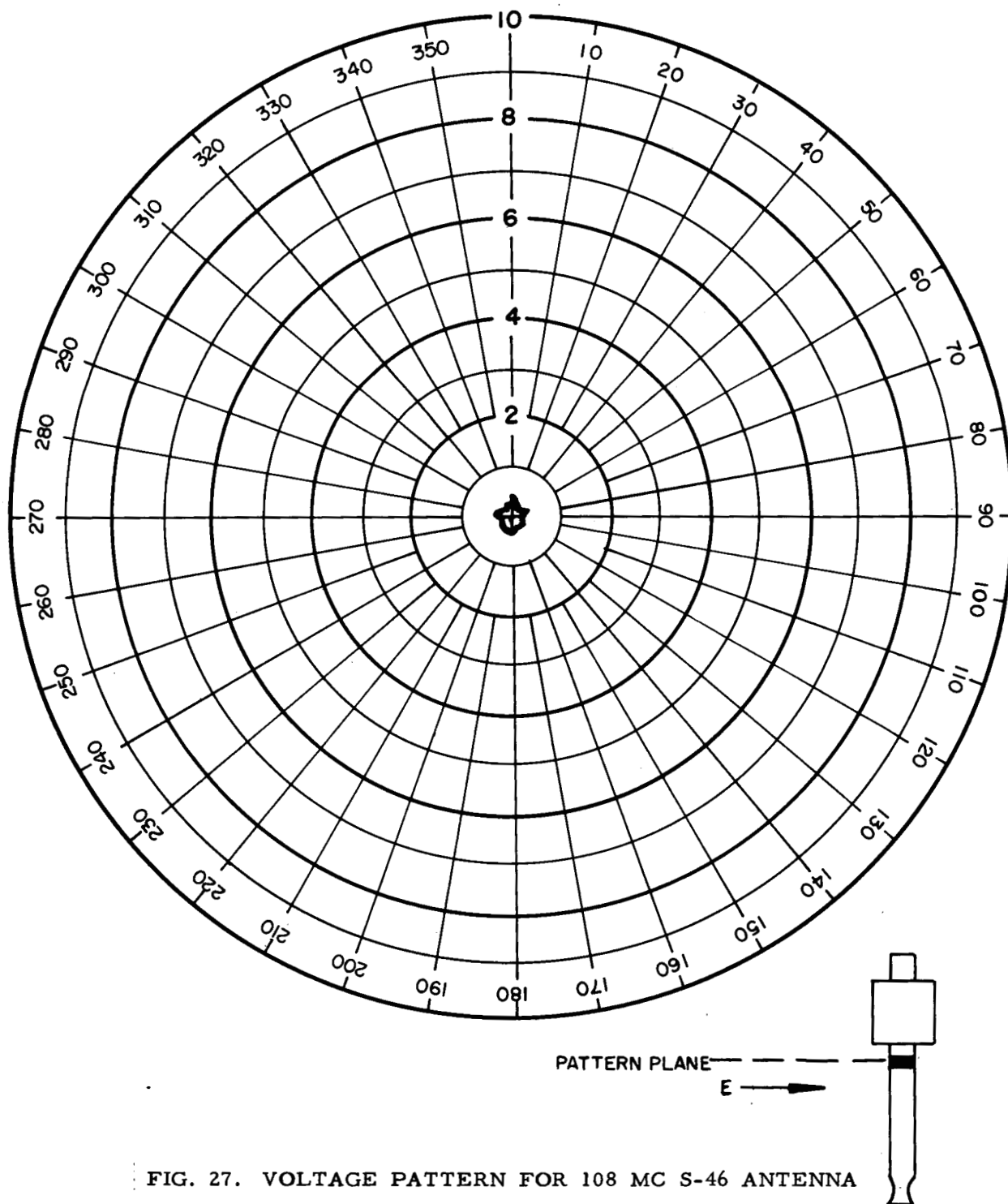
FIG. 27. VOLTAGE PATTERN FOR 108 MC S-46 ANTENNA
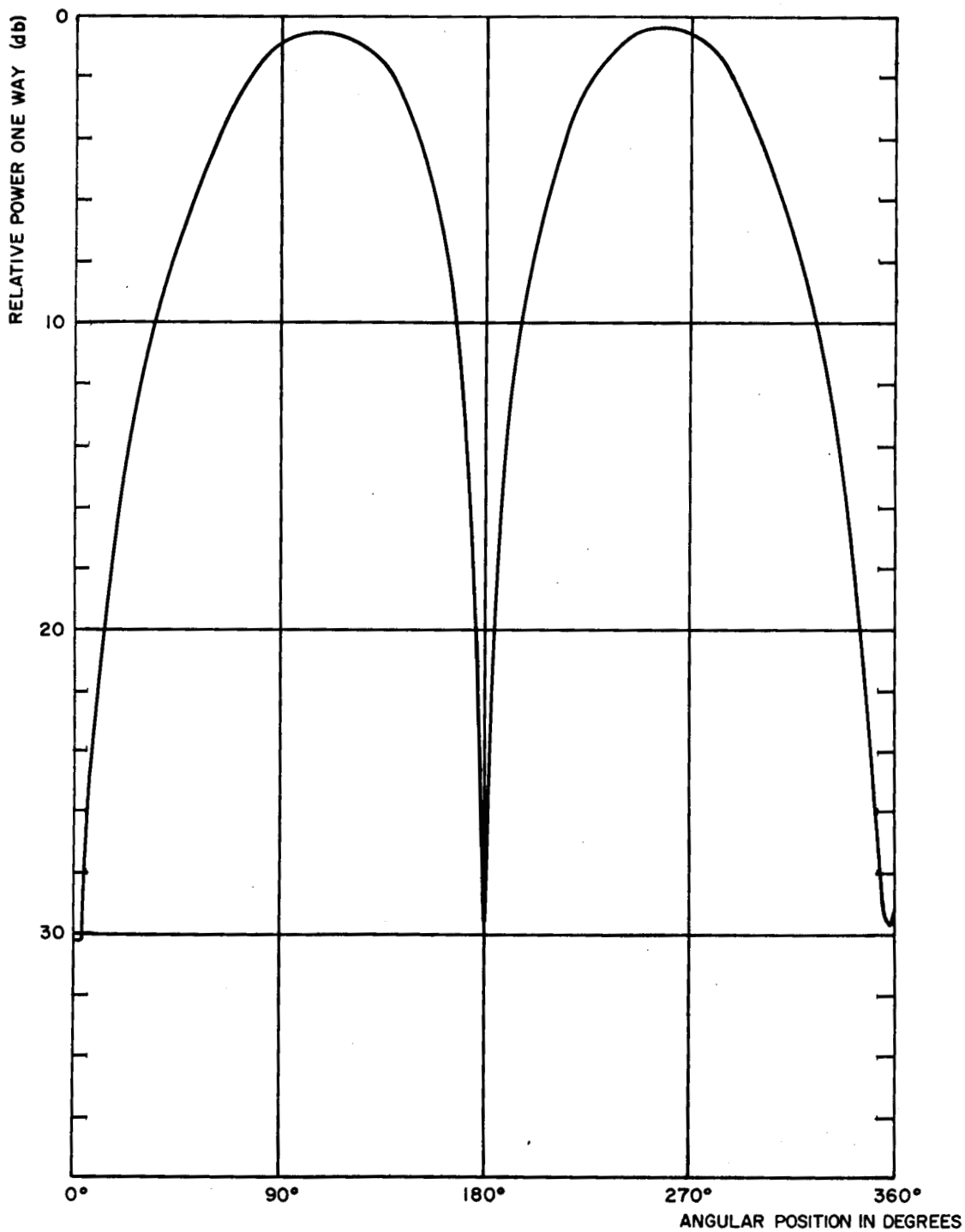
FIG. 28. DECIBEL PLOT FOR 108 MC S-46 SATELLITE ANTENNA

(For Pattern Plane of Figure 26)
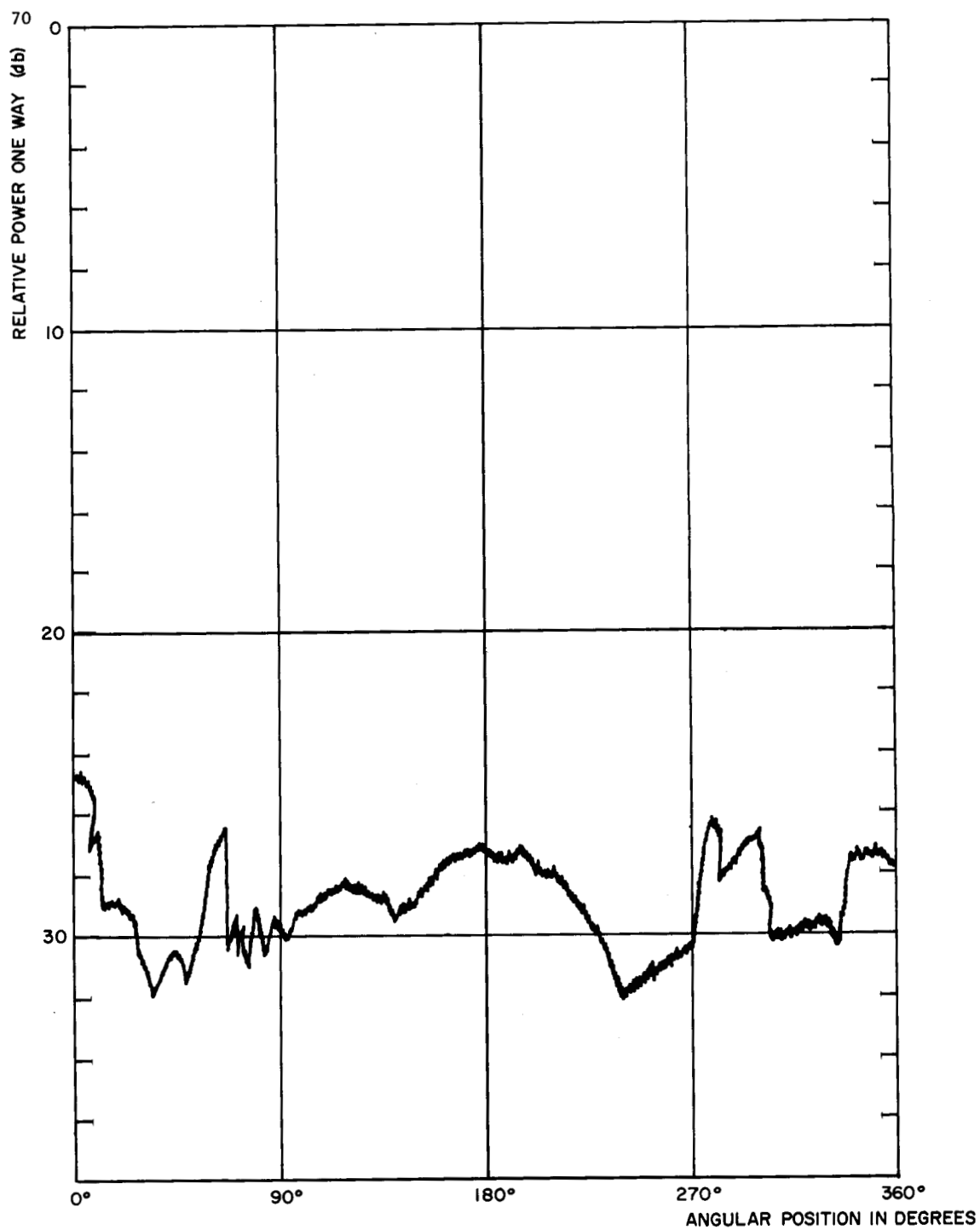
FIG. 29.   DECIBEL PLOT FOR 108 MC S-46 SATELLITE ANTENNA

(For Pattern Plane of Figure 27)

TO TRANSMITTER

0.08 μhy
APPROX.

TO SERGEANT

0.47 μhy

2 $\mu\mu$fd
APPROX.

TO PAYLOAD SHELL
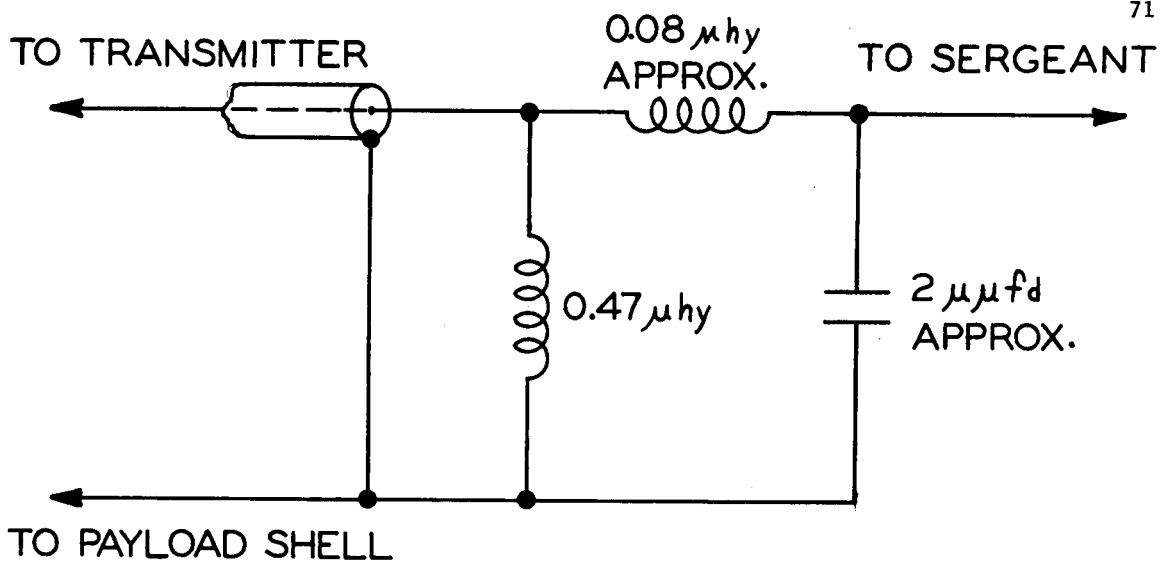
(a) ANTENNA MATCHING DEVICE

CORE –GENERAL CERAMIC Q-2

x 7

H_1 H_2 H_3 H_4

x 7

H_1 H_2 H_3 H_4
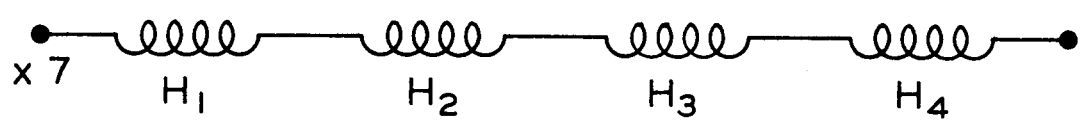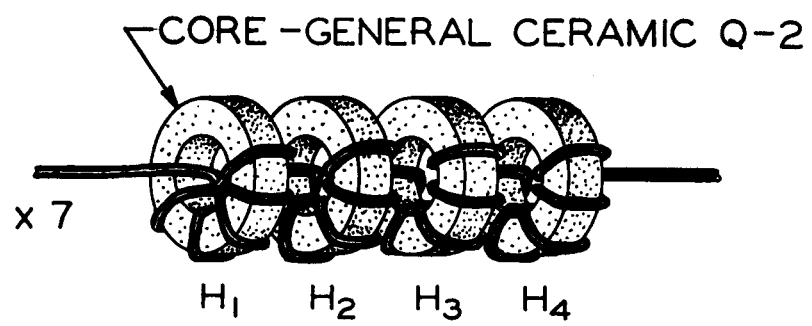
(b) RF CHOKE ASSY

FIG. 30. ANTENNA MATCHING AND RF CHOKE DEVICES

The transmitter was connected to the antenna by a short length of Micro-dot cable. The cable had an Amphenol series 27 right angle connector on the transmitter end and terminated in a Micro-dot connector on the other end.

SECTION VII. POWER SUPPLY

The internal batteries and the solar cells used to supply the 15.6, 10.4, and 6.5 volts for the complete instrumentation are discussed in detail in Chapter 5, "Networks and Solar Power Systems for Radiation Experiment Satellite S-46."

Chapter 5

NETWORKS AND SOLAR POWER SYSTEMS
FOR RADIATION EXPERIMENT SATELLITE S-46

Eugene H. Cagle, Phil Youngblood, and Richard Boehme
Electrical Systems Integration Branch, Guidance and Control Division
George C. Marshall Space Flight Center
National Aeronautics and Space Administration
Huntsville, Alabama

SECTION I.   PRELIMINARY DESIGN CONSIDERATIONS

1. Introduction

The preliminary proposal of the State University of Iowa (SUI) for an instrumented satellite to measure radiation intensities at altitudes of 300 and 38,000 kilometers established a continuous power requirement of 1125 milliwatts and a total payload weight of 22 pounds. Since solar cells were to be used to recharge the batteries, it was necessary to protect the cells from micrometeorite hazards with some type of glass cover. These covers, along with the bonding used, accounted for 121 grams of the weight specified for the power supply.

2. Satellite Configuration

Because of the requirement for the satellite to tumble end over end, it was desirable to leave the empty fourth stage shell attached to the payload and to keep the payload as nearly cylindrical as possible. A cylindrical body with a diameter of six inches provides area for mounting solar cells only along the sides. In the event that the satellite tumbled in such a way that an end of the cylinder pointed directly toward the sun, the output of solar cells on the sides of the cylinder would become zero twice per revolution. Such a condition could cause a power supply voltage fluctuation of as much as 20%, since the nickel-cadmium batteries deliver power for two short intervals during the revolution and receive a continuously varying charge current during the remainder of the revolution. Furthermore, adequate cell area would have to be provided on the sides to insure that the average power output would be sufficient to supply the load and charge the batteries. On the other

hand, this same solar cell area would produce an excess of power when the plane of rotation of the satellite was perpendicular to the sun's rays. This excess power would have to be dissipated to prevent overcharging the batteries. Thus, it becomes apparent that for a non-oriented satellite, it is advantageous to maintain a projected solar cell area that is as nearly constant as possible. This can best be done by equally spacing a large number of parallel connected groups of cells on a spherical body. Mounting and assembly considerations made this arrangement impractical.

Various other configurations were considered, including three and four-finned cylinders. However, preliminary calculations showed that the requirements of a light weight, constant power output system could be met by placing an equal group of cells on each of the six sides of a rectangular body. This application required that the rectangular body be placed around the cylindrical instrument housing.

A group of cells on the dark side of a satellite connected in parallel with a group on the light side presents a load to the illuminated group. Reverse current flow through the inactive cells can be prevented by inserting diodes in series with each group of cells. However, most silicon diodes have a forward voltage drop of from .7 to .9 volt and this can cause an appreciable loss in the circuit. Diodes with a forward voltage drop of about .7 volt were selected from a group of type 1N697 for this application.

3. Power Requirements

During the preliminary design stages, plans were made to provide three different voltages for the transmitter, sub-carrier oscillator and multiplexer, and the State University of Iowa instrumentation package. There were several changes in the voltage level and power level during the design phase, but the final total power level was only about 12% above the initial estimated level.

An input power of 800 milliwatts to the transmitter was estimated to be the minimum that would provide an acceptable signal level at apogee. The requirement was that additional transmitter power be provided, if possible without exceeding the weight limitation.

The final design was based on the following power requirements:

Transmitter	57.7 ma at 15.6 volts =	900 milliwatts
Sub-carrier Oscillator	11.6 ma at 10.4 volts =	121 milliwatts
Instrumentation	47.2 ma at 6.5 volts =	307 milliwatts
	Total	1328 milliwatts

The approximate voltage of each power supply was determined by the requirements of the equipment which consumed the power. The exact voltage, however, was determined by the average voltage of a nickel-cadmium battery. During discharge, the nominal voltage of a nickel-cadmium cell is 1.2 volts; during charge, the average voltage is 1.4 volts. Since the batteries were connected to the system continuously, whether receiving a charge or delivering power, the average system voltage was considered to be 1.3 volts per nickel-cadmium cell. The maximum voltage during charging was limited by zener diodes to 1.45 volts per cell and it was expected that, after some deterioration of the nickel-cadmium cell, the voltage would drop to 1.15 volts per cell during discharge. This gave a voltage variation of $\pm$ 11.5% about the nominal value.

Using the 1.3 volts per cell as the average system voltage, the transmitter supply of 15.6 volts required 12 nickel-cadmium cells connected in series. The 10.4 volts sub-carrier oscillator supply required eight cells in series and the instrumentation supply of 6.5 volts required five cells in series.

4. Orbit and Temperature Requirements

Preliminary calculations indicated that the orbit period would be about 10 hours and that the satellite would be in the earth's shadow a maximum of two hours. There would also be periods when the satellite would be in a 100% sunlight orbit, which would give maximum solar cell temperatures of 80°C. Subsequent studies indicated that the period might be more than 10 hours and that the firing time would have to be carefully selected to prevent the time in the shadow exceeding two hours.

The maximum solar cell temperature of 80°C, upon which the power supply design was based, appeared to be completely adequate; in fact, temperatures were expected to be somewhat lower.

5. Battery Selection

To obtain extremely long cycle life (over 5000 cycles) from sealed nickel-cadmium batteries, it is necessary to limit the discharge to about 10% of total battery capacity. Tests have shown that increasing the depth of the charge-discharge cycle causes a corresponding decrease in the number of cycles from a battery. It would seem advisable to select a large cell that is not discharged more than 10% of total capacity before it is recharged for an application where long battery life is desirable. However, a large cell requires a comparatively high trickle charge to maintain it in a charged condition. In this particular application where solar cell area and, therefore, battery charging current is limited, it is important to avoid selection of a cell that requires a high trickle charge.

76

It was expected that this satellite would complete about 860 orbits in a period of one year, of which 50% or more would be in sunlight during the complete orbit. This meant that the batteries were to be cycled about 400 to 450 times during the life of the satellite. It was determined that a cell of a size that delivered approximately 20% of its capacity during a two-hour discharge would have a cycle life in excess of 2000 cycles and could be recharged during the ensuing eight-hour charge period with a relatively low charging current from the solar cells.

At very low charging rates, about 150% of the ampere-hours delivered on discharge must be returned to the battery during charge.

The average charging current required to return the battery to the fully charged condition is given by

$$I_c = \frac{I_1 \times T_1}{T_c \times \eta_{AH}}$$

where

I_c = average battery charging current required from solar cells

I_1 = average electronic load current

T_1 = maximum time per orbit that the battery is under load

T_c = minimum time per orbit that the battery is receiving charge

η_{AH} = ratio of ampere-hours delivered from battery under load to ampere-hours required to return the battery to fully charged condition.

Based on a T_1 of two hours, and a T_c of eight hours, η_{AH} of 0.67 and I_1 as given in paragraph 3, the I_c for each of the three supplies was determined. This information and other pertinent battery data are tabulated on the following page.

Table 4

BATTERY DATA

Supply	Transmitter	Sub-Carrier Oscillator	Instrumentation
V_1 (volts)	15.6	10.4	6.5
I_1 (milliamperes)	57.7	11.6	47.2
Max. Battery Drain (milliampere-hours)	115.4	23.2	94.4
I_c (milliamperes)	21.6	4.4	17.7
*Cell Type	VO.500	VO.180	VO.500
Cell Capacity (milliampere-hours)	500	180	500
Discharge Depth in % of Rated Capacity	23.1	12.9	18.9
Cells in Series	12	8	5
Battery Weight (grams)	488.0	117.5	194.1

* The cell type designations are those of the manufacturer, Gulton Industries, Inc.

6. Solar Cells

The incident solar radiation outside the earth's atmosphere is approximately 140 milliwatts per square centimeter. This value can vary by ± 3.4% as the earth moves from perihelion to aphelion. The spectral distribution of the solar radiation approximates that of a 5900°K black body. A plot of the distribution of this radiation is shown in Figure 31 together with the spectral response plot of a silicon solar cell. It can be seen that the solar cell responds to the wave lengths between approximately 0.4 and 1.2 microns. Integration of the solar energy distribution curve has shown that this wave length band contains approximately 55% of the total solar energy available. Other factors, such as reflection losses, internal resistance losses, and junction property restrictions, limit the maximum theoretical conversion efficiency of silicon solar cells. Various estimates have indicated that the maximum efficiency lies between 18% and 22%. One manufacturer claimed to have produced a few cells of 16% efficiency.

Solar cells with a minimum conversion efficiency of 9% at 30°C are readily available now at a cost of approximately $4.00 each for 1 x 2 cm cells. Cells with a 10% conversion efficiency are becoming available now at about 50% higher cost, but at the time the solar cell order was placed for the S-46 Satellite, the supply of 10% cells was limited. For reasons of availability and economy, it was decided to use two sizes of the 9%
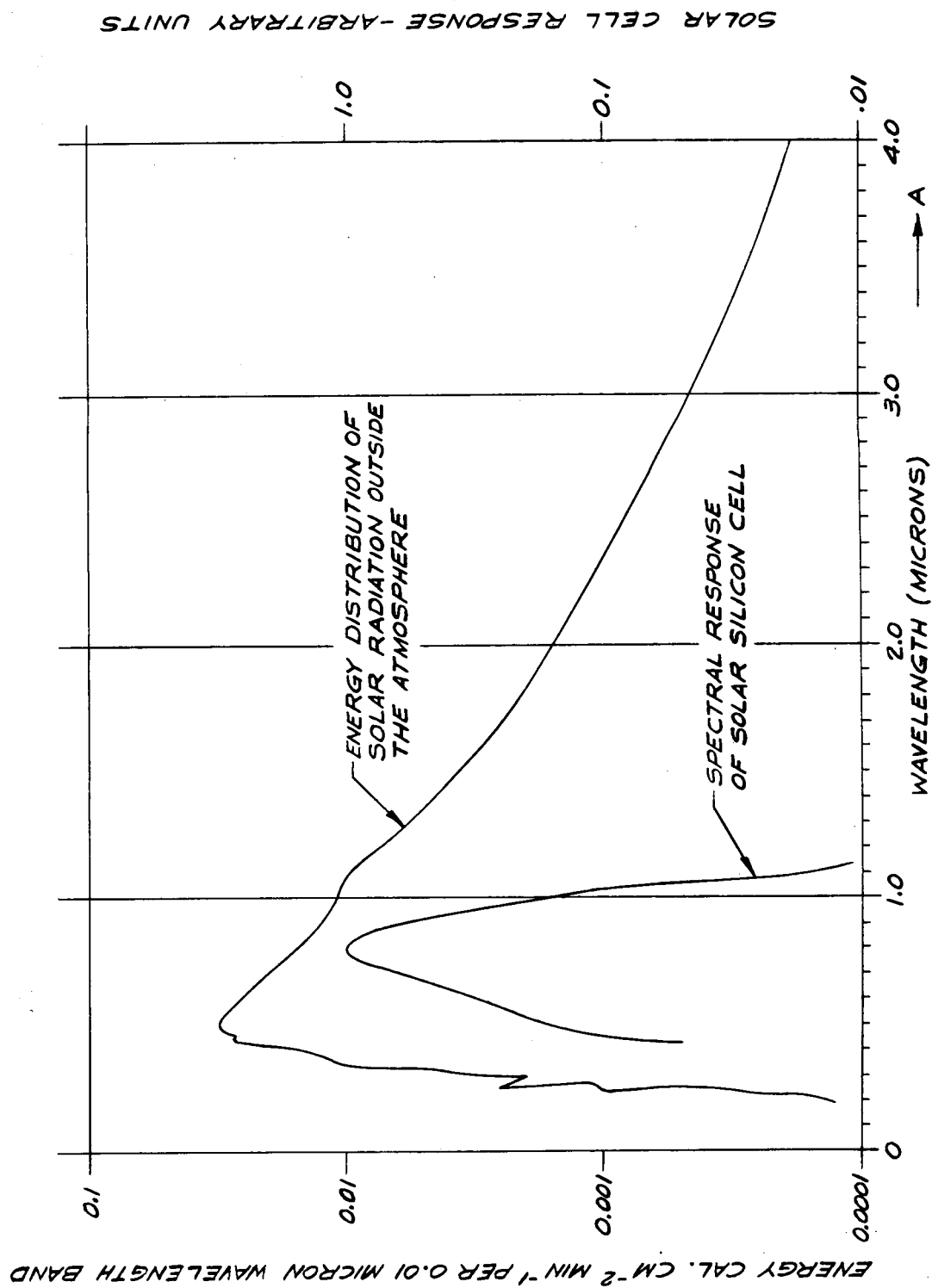
FIG. 31. SPECTRAL DISTRIBUTION OF SOLAR ENERGY AND SPECTRAL RESPONSE OF SILICON SOLAR CELL

cells. The solar cells employed on Satellite S-46 were procured from the International Rectifier Corporation.

In connecting solar cells in series, mismatch in the voltage-current characteristics plus the small effect of connection resistance reduces the overall efficiency of a group of cells. By carefully checking the output characteristics and matching cells with similar characteristics in a series group, these losses can be minimized. However, tests have shown that in connecting 9% cells in series to produce 16 to 18 volts or less, the group efficiency is reduced to about 8%.

A further loss in conversion efficiency is incurred when the cell temperature is raised above 30°C. Conversely, the efficiency increases with a reduction in temperature. Figure 32 shows the current-voltage characteristics for a typical 1x2 cm solar cell at three different temperatures with an incident light intensity of 140 mw per square centimeter. From the curves in Figure 32 it can be determined that at a cell temperature of 80°C, the efficiency of the cell is 71% of its value at 30°C. Therefore, series connected cells with a group efficiency of 8% would be reduced to 5.68% efficiency at 80°C.

The maximum power output is obtained with the load adjusted to give .40 volts with the cell at 30°C and .324 volt with the cell at 80°C. This optimum power point varies among cells even of the same efficiency and accounts for the major part of the loss in group efficiency when using a number of cells in series.

The curve in Figure 33 is included only for comparison and shows the current-voltage characteristics for a similar 1 x 2 cm cell with a light intensity of 70 milliwatts per square centimeter.

The thermal design studies performed by the Research Projects Division indicated that the maximum solar cell temperature would be 80°C. Since solar cell efficiency is an inverse function of temperature, the 80°C temperature was used as the basis of this design.

In paragraph 3 the transmitter power requirement was given as 57.7 ma at 15.6 volts. In addition to this, the average battery charging current was given in paragraph 5 as 21.6 ma. The solar cells must deliver the sum of these currents at a voltage equal to the system voltage plus the voltage drop in the blocking diode.

The required power output of the solar cells is given by

$$P_o = I_o V_o$$

where P_o = power output of solar cells in milliwatts

CURRENT IN
MILLIAMPERES
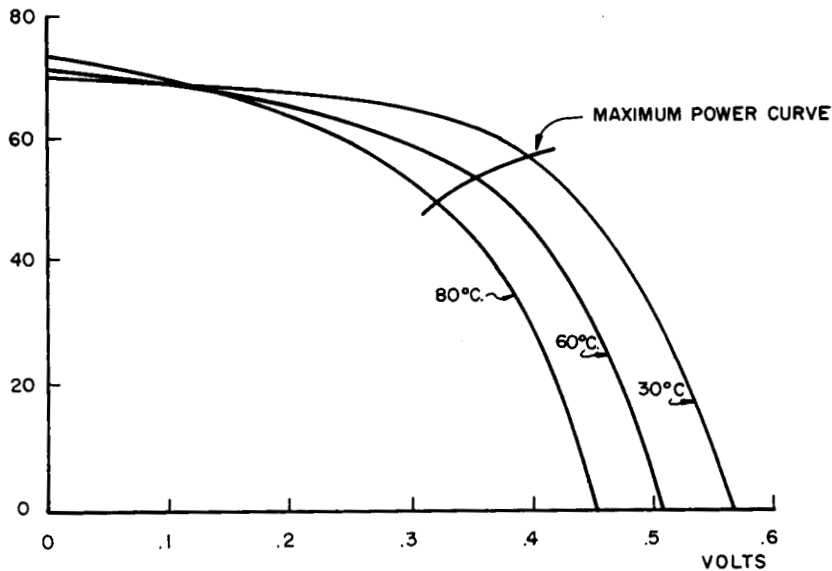
FIG. 32. CURRENT-VOLTAGE CHARACTERISTICS AT DIFFERENT CELL
TEMPERATURES FOR A TYPICAL 1 x 2 CM SOLAR CELL
WITH CONVERSION EFFICIENCY OF 9%.
(Light Intensity: 140 mw/cm^2)

CURRENT
MA
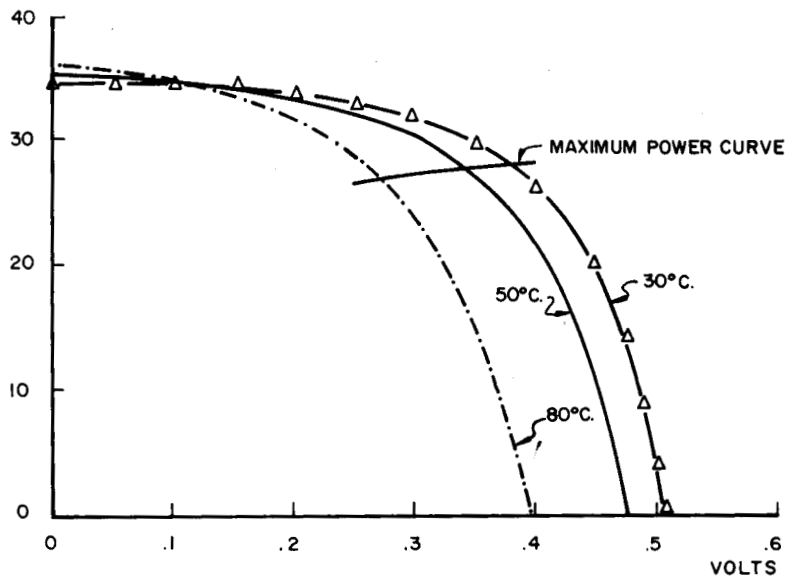
FIG. 33. OUTPUT CURRENT-VOLTAGE CHARACTERISTICS AT DIFFERENT CELL
TEMPERATURES FOR A TYPE 1020C SOLAR CELL WITH CONVERSION
EFFICIENCY OF 8.5%. (Light Intensity: 70 mw/cm^2)

I_o = sum of electronic load current and battery charging current in milliamperes, and

V_O = sum of average system voltage and voltage drop across blocking diode.

The number of series connected cells required for each voltage was determined by dividing V_O by the optimum cell voltage at the maximum expected temperature (.324 volt at 80°C from Figure 32).

With the solar cell surface perpendicular to the sunlight, the total solar cell area needed to produce the required power is given by the equations

$$A = \frac{P_O}{\eta K}$$

where A = active solar cell area in square centimeters

η = group solar cell efficiency at the design temperature

K = solar constant in milliwatts per square centimeter

The dimensions of the type S-1020C solar cell are 1 x 2 cm and it has an active area of 1.8 square centimeters since the top electrical contact covers a strip 0.1 cm wide along the 2 cm dimension. The dimensions of the type S-0520C cell are 0.5 x 2 cm and it has an active area of 0.8 square centimeter since the top contact on this cell is also along the 2 cm dimension. The required solar cell area for each supply was obtained by the use of these two cell sizes.

From the above equations, the number and type of cells for each power supply were determined and the results placed in tabular form as follows:

Table 5

SOLAR CELL SUPPLY DATA

Supply	Transmitter	Sub-Carrier Oscillator	Instrumentation
Average System Voltage	15.6	10.4	6.5
Diode Drop	.7	.7	.7
V_O (volts)	16.3	11.1	7.2
Required Series Cells	51	34	22
I_o (milliamperes)	79.3	16.0	64.9

Table 5 (cont.) Supply	Transmitter	Sub-Carrier Oscillator	Instrumentation
P_o (milliwatts)	1292	177.5	467
A (square centimeters)	162.5	22.4	58.7
Cell Arrangement and Type	2 x 51(S-1020C)	1 x 34(S-0520C)	1 x 22(S-1020C) 1 x 22(S-0520C)
Group Cell Area (cm^2)	183.6	27.2	57.2
Percent of Required Area	113.	121.4	97.5

Note that the required area is exceeded by the actual solar cell area in every case except for the instrumentation power supply. In this case, the actual cell area is 2.5 percent less than the calculated required area, but due to the limitations on the available area, it was not considered justified to increase the cell mounting area enough to accomodate two paralleled groups of the 1 x 2 square centimeter cells.

SECTION II.   SOLAR CELL LAYOUT AND ASSEMBLY

1. Effect of Rotational Position

To completely analyze a solar cell system layout for a non-oriented satellite, it is necessary to evaluate the design for the effects of variation in light incidence on the power output that results from the following:

    a. Aspect of axes with respect to the sun
    b. Tumble
    c. Rotation or Spin
    d. Shadow from protruding parts

The instrumentation requirements in conjunction with imposed weight and size limitations required that the S-46 payload have the configuration shown in Figure 34. The cylindrical body diameter was that of the last stage rocket and the rectangular box was required to provide adequate solar cell mounting area for the mission.

When the power requirements became firm, a preliminary system design was made. This design was based on unconfirmed orbital and temperature information. Once the battery capacity was established, the solar cell groups were designed and a preliminary layout was made so that the cells could be distributed properly on each of the six sides of the structure. Special care was taken in cell placement on the top and bottom plates to avoid undue shadowing of any group by the instrument

MULTIPLEXER

SUB-CARRIER OSCILLATOR

BATTERY PACKS

ANTENNA GAP

FOURTH STAGE

TRANSMITTER

S.U.I. PACKAGE

42.0

23.1

6.85

SOLAR CELLS

SOLAR CELLS

12.6
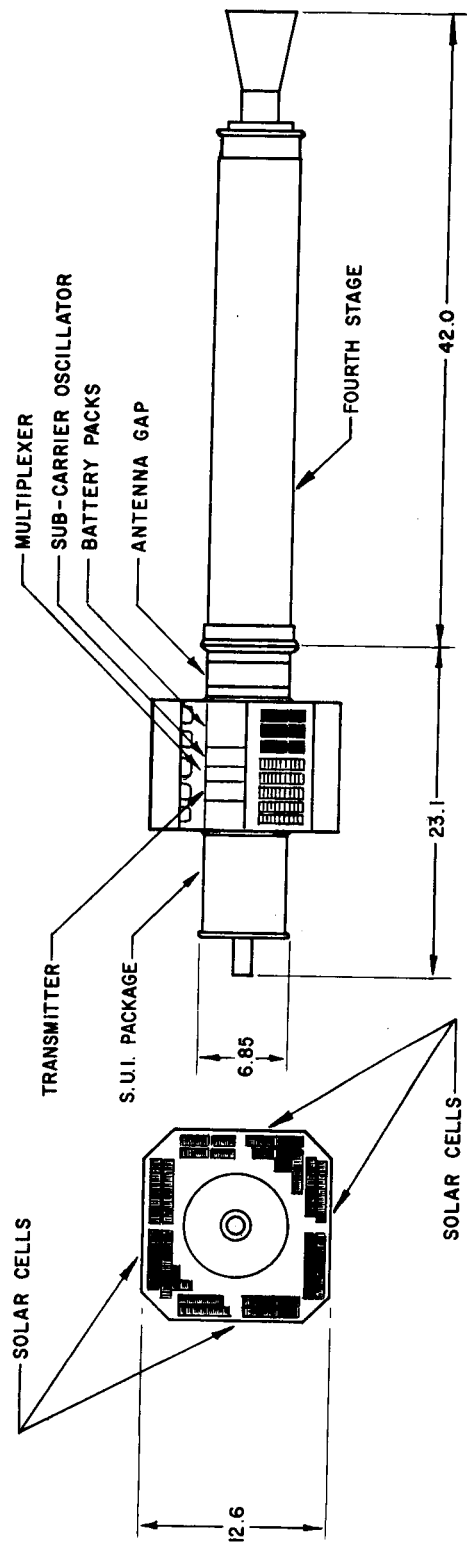
FIG. 34. CONFIGURATION OF S-46 RADIATION MEASUREMENT SATELLITE

housing or the fourth stage rocket protruding through the solar cell box
assembly. Complete shadowing of any single cell effectively cuts off the
power output of an entire series string of cells. This was particularly
true of the transmitter supply which required about 70% of the total
power and which had the greatest number of cells in series.

The preliminary cell layout was used to graphically determine angu-
lar positions where a cell became completely shadowed. This was done for
various assumed attitudes of the satellite with respect to the sun. At
this time, an attempt was made to arrange the cells to keep each group
active for as much of the tumble cycle as possible. Rough calculations
of average power per cycle were made for the conditions which appeared
to provide the smallest average projected cell area per cycle. This
information was later used for the final design and cell arrangement.

2. Calculation of Rotational Influence on Solar Cell System
   Power Output

The general equation for analyzing the effect of satellite rota-
tional positions on the solar cell system output was first based on the
assumption that the power generated varies directly with the cosine of
the angle between a line normal to the cell surface and the incident
light vector. The curves shown in Figure 35 relate the power output of
a typical silicon solar cell to the angle of incidence of light for a
fixed load. Although the curve for optimum power (not shown) would
closely follow the true cosine curve, the fixed load curve must be used
for this type of analysis. This is not reflected in the general equa-
tion to be derived, but corrections for deviations from the true cosine
function were later made when the problem was fed to the computer.

Figure 36 shows the S-46 satellite at an arbitrary position in space.
The fixed X-Y-Z coordinates were established so that the origin was a
point on the spin (longitudinal) axis of the satellite and placed so the
"Z" axis represents the axis about which the body tumbles. The positions
of the coordinates were located by letting the plane established by Y and
Z intersect the sun and the satellite so that the light vector L always
lay in the Y-Z plane. The angle ϕ , therefore, is defined as the angle
which the light makes with the plane of tumble rotation defined by the
X-Y plane. The degree of tumble rotation is shown as the angle β
between the spin axis S and the plane of the light vector (Y-Z plane).
The degree of spin rotation about the S axis is given by the angle θ,
shown in Figure 36 as the angle between the reference X-Y plane and the
vector P_1.

The vector P_1 has been constructed normal to the plane of side 1 of
the solar cell box assembly. This side was arbitrarily designated as
the reference plane of the satellite for the purpose of relating rotation
about the S axis with the fixed coordinate system. The length of P_1 is
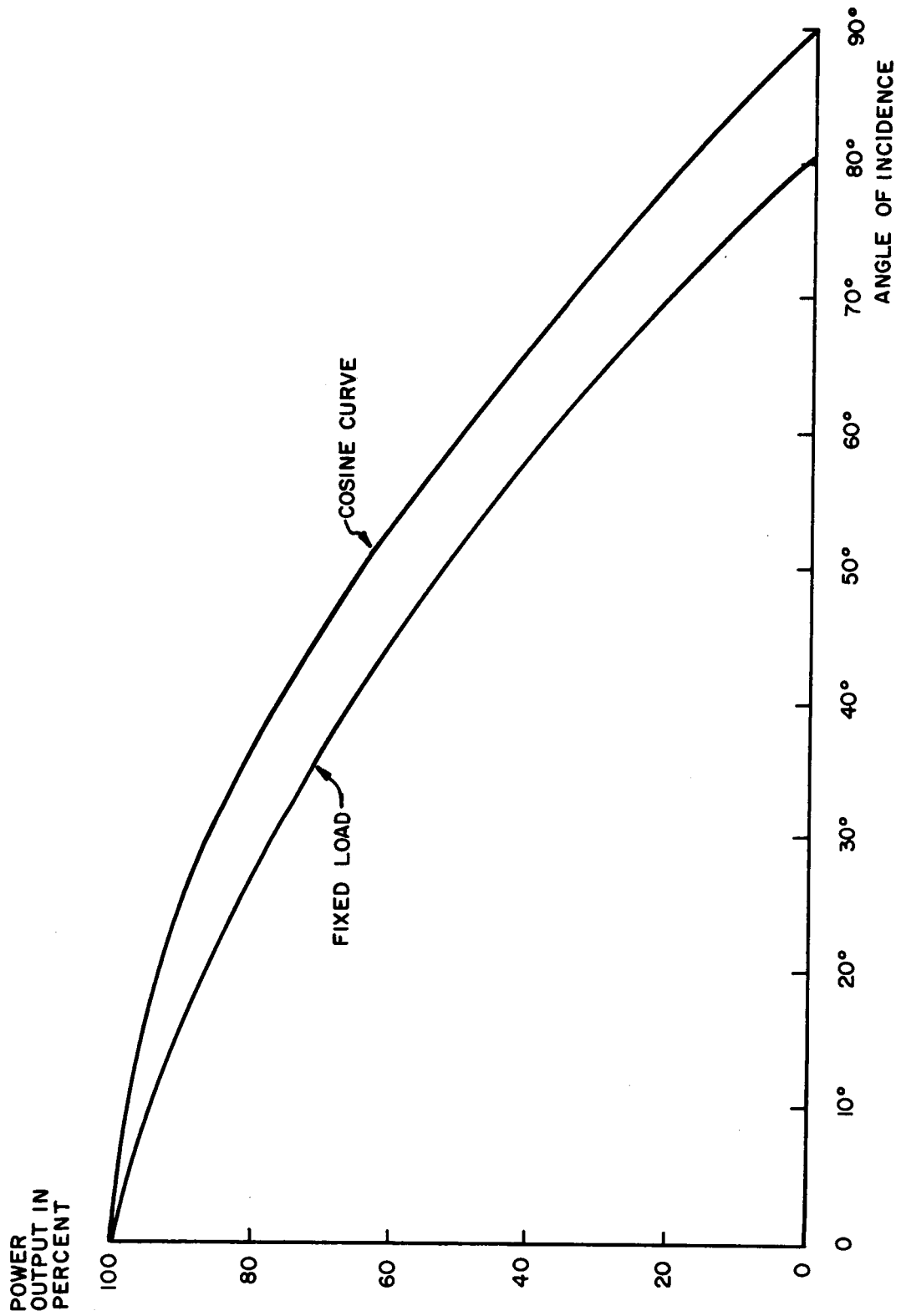
FIG. 35.   SILICON SOLAR CELL OUTPUT VERSUS LIGHT INCIDENCE

(a)

(b)

Satellite Position
Shown: β = +30°
θ = +45°

(c)

Transmitter
Cells Area

Satellite
Position:
β = 0°
θ = +45°
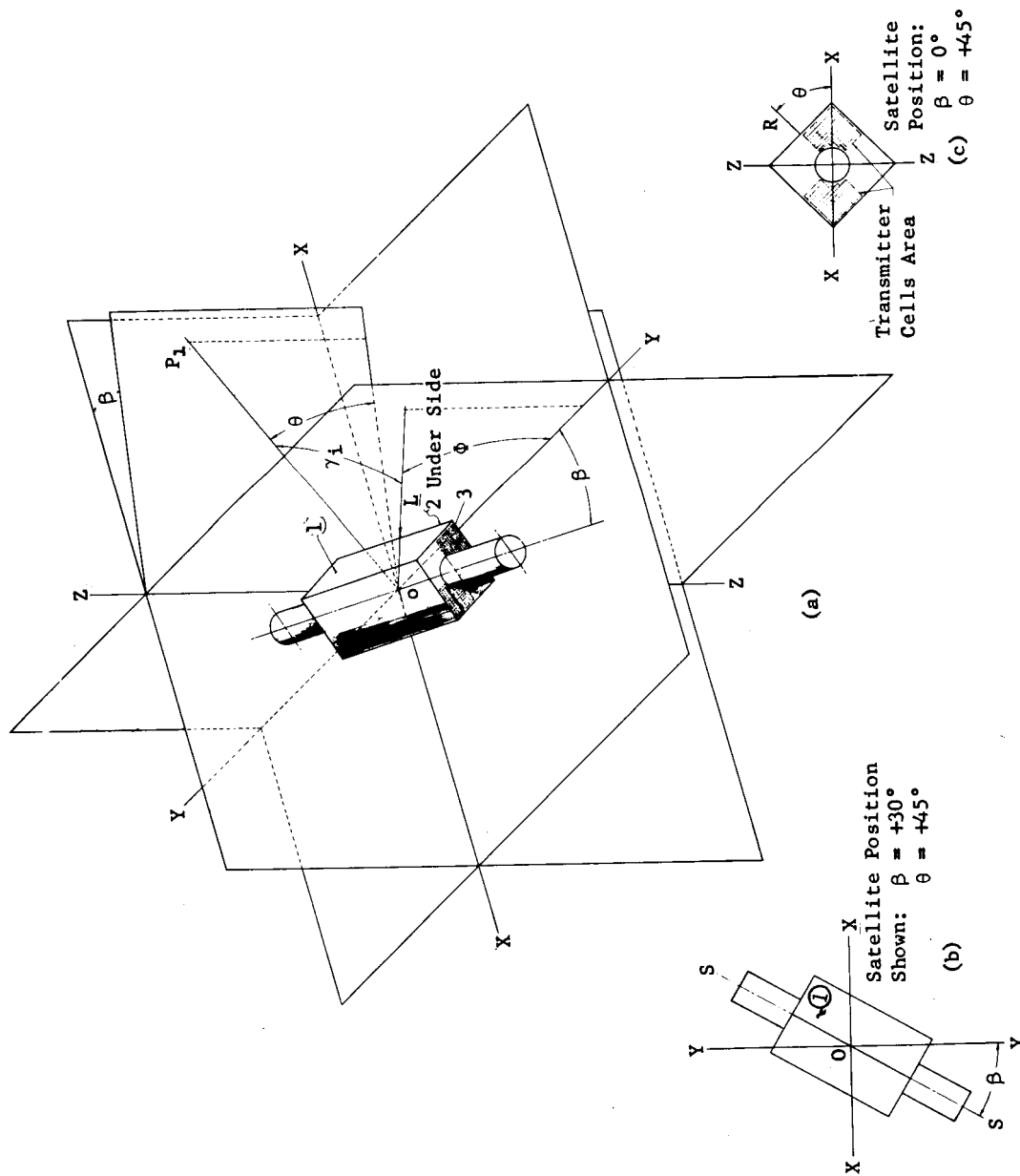
FIG. 36. ARBITRARY SPACE POSITION OF SATELLITE S-46

the component of the light vector L that is perpendicular to side 1 of the satellite. The angle between L and P_1 represents the true angle of incidence of light on that side, that is:

$$P_1 = L \cos \gamma_1 \tag{1}$$

P_1 can be determined in terms of L and known angles with respect to the coordinates by relating the trigonometric functions shown on Figure 37. The projection of vector L on a plane which is perpendicular to the X-Y plane and contains the line P_1 is L_1 as shown. The component of L_1 that is normal to the solar cells has already been designated as P_1. Then,

$$L \cos \delta = L \cos \phi \cos (90° - \beta) = L \cos \phi \sin \beta \tag{2}$$

Also,

$$P_1 = \cos (\theta-\delta) = L(\cos \theta \cos \delta + \sin \theta \sin \delta) \tag{3}$$

Substituting Equation 2 into 3

$$P_1 = L(\cos \phi \sin \beta)(\cos \theta + \sin \theta \tan \delta) \tag{4}$$

However,

$$\tan \delta = \frac{L \sin \phi}{L \cos \phi \sin \beta} \tag{5}$$

Substituting Equation 5 into 4,

$$P_1 = L(\cos \phi \sin \beta \cos \theta + \sin\phi \sin \theta) \tag{6}$$

Therefore,

$$\cos \gamma_1 = (\cos \phi \sin \beta \cos \theta + \sin \phi \sin \theta) \tag{7}$$

In a similar manner, the cosine of the angle of incidence for side 2 of the solar cell box can be derived, which is:

$$\cos \gamma_2 = \cos \phi \sin \beta (\theta-90°) + \sin \phi \sin(\theta-90°) \tag{8}$$

For side 3 of the solar cell assembly, which is an end through which the cylinder protrudes, the function is:

$$\cos \gamma_3 = \cos \beta \cos \phi \tag{9}$$

FIG. 37. TRIGONOMETRIC RELATIONSHIPS FOR SATELLITE S-46 IN AN ARBITRARY SPACE POSITION

For simplicity, it was specified that the solar cell area of side 1 generate 100% output power when the light is normal to its surface. Since all four sides were identical and because both ends were symmetrical and contained the same number of solar cells as the sides (for the transmitter supply, only), it was necessary only to establish functions for two sides and one end plate. Because of the geometry only three solar cell areas can be illuminated at any one time. Proper selection of the starting position of the reference side of the configuration with respect to the coordinate planes allowed complete investigation of all the possible conditions for angular variations of 90°. Variations of angles beyond 90° would result in repetition of output conditions.

In general, therefore, prior to correction for deviation of the power output curve from a cosine function of the angle of incidence, the total relative output power for the solar cell assembly of S-46 satellite can be expressed as:

$$W = W_1 + W_2 + W_3$$

$$W = W_o \ (\cos\gamma_1 + \cos\gamma_2 + \cos\gamma_3) \tag{10}$$

where, $W_o = W_1 \cos 0° = 100\%$ for a given light intensity L. Correcting for the deviation from a true cosine function, Equation 10 becomes:

$$W = W_o \left[f(\gamma_1)(\cos\gamma_1) + f(\gamma_2)(\cos\gamma_2) + f(\gamma_3)(\cos\gamma_3) \right] \tag{11}$$

where the functions, $f(\gamma)$, can be obtained from Figure 35 as the ratio of the fixed load curve to the cosine curve. The above equations were further modified to correct for loss of output from the end plates due to shadowing by the protruding cylinder. This effect was essentially a step function which occurred at various positions when any one cell became completely shadowed, cutting off an entire series string. For the transmitter supply, such a decrease amounted to 50% of the cells on one end panel. It was graphically determined from the cell layout that this condition occurred when the following two conditions existed simultaneously:

a. When the angular rotation about the S axis (defined as θ) was less than 125° or greater than 145° (also when θ was not between -35° and -55°).

b. When the angular rotation about the axis Z (defined as β) was more than 2-1/2°.

The sharp decrease in power output due to shadowing may be seen, for example, on Figure 39, where the curve changes abruptly at $\beta = 2$-1/2°.

The ABMA Computation Laboratory, using an analog computer, simulated the problem as shown in Figure 38. The curves, Figures 39 to 52, were
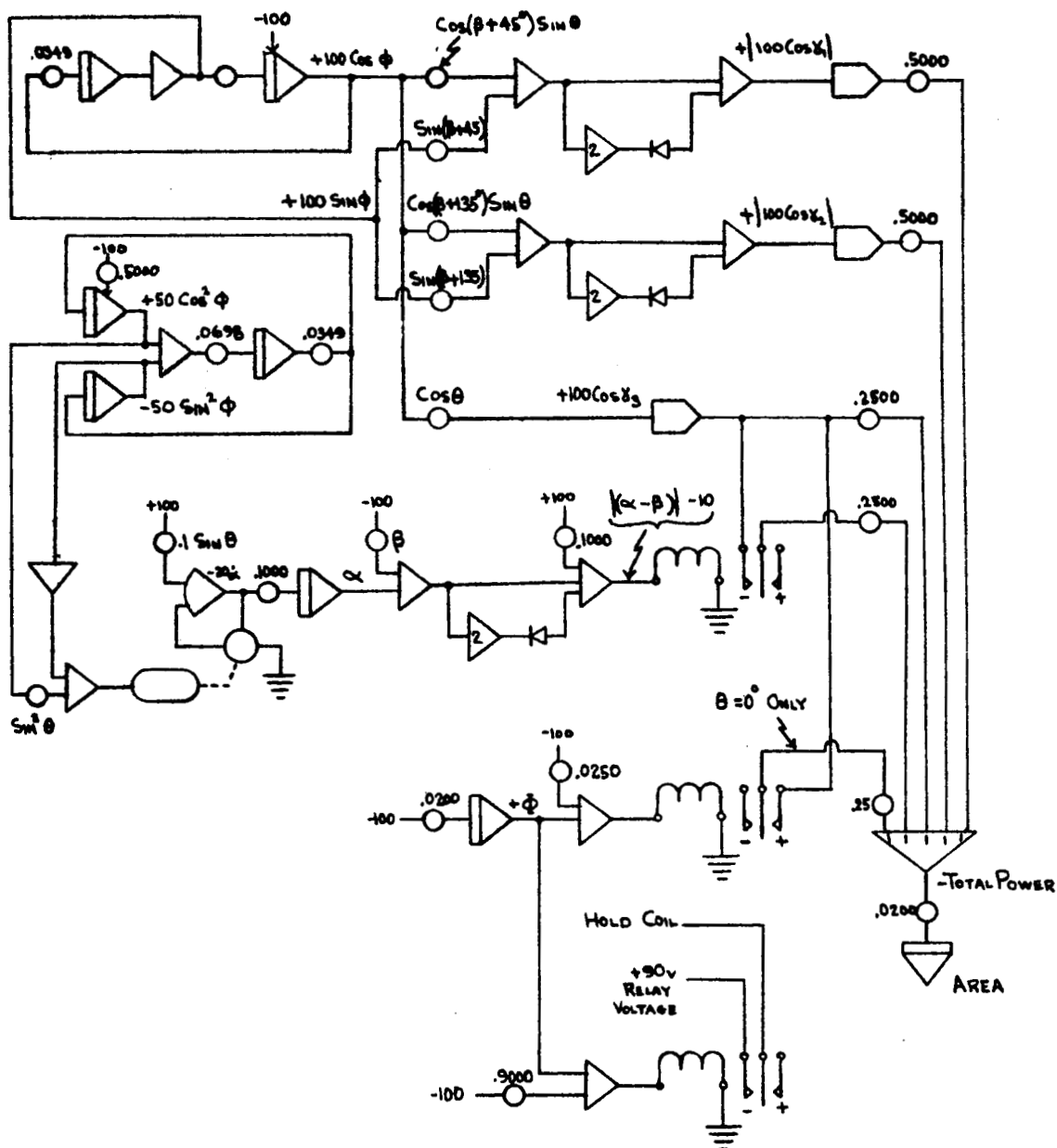
FIG. 38. SIMULATION DIAGRAM FOR S-46 SATELLITE
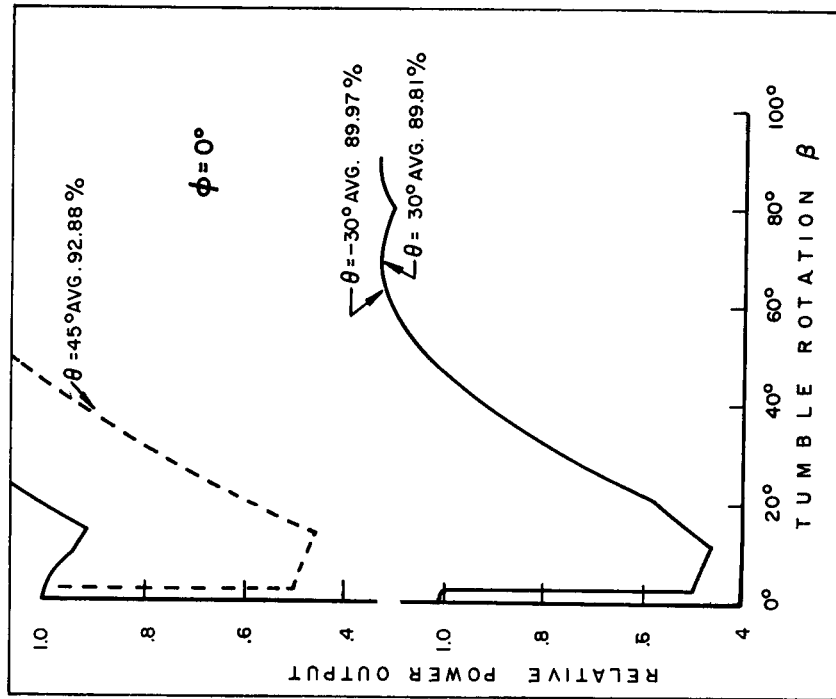
FIG. 40. POWER OUTPUT VERSUS ROTATIONAL
POSITION. $\phi = 0°$; $\theta = -30°$, $+30°$, and $+45°$.
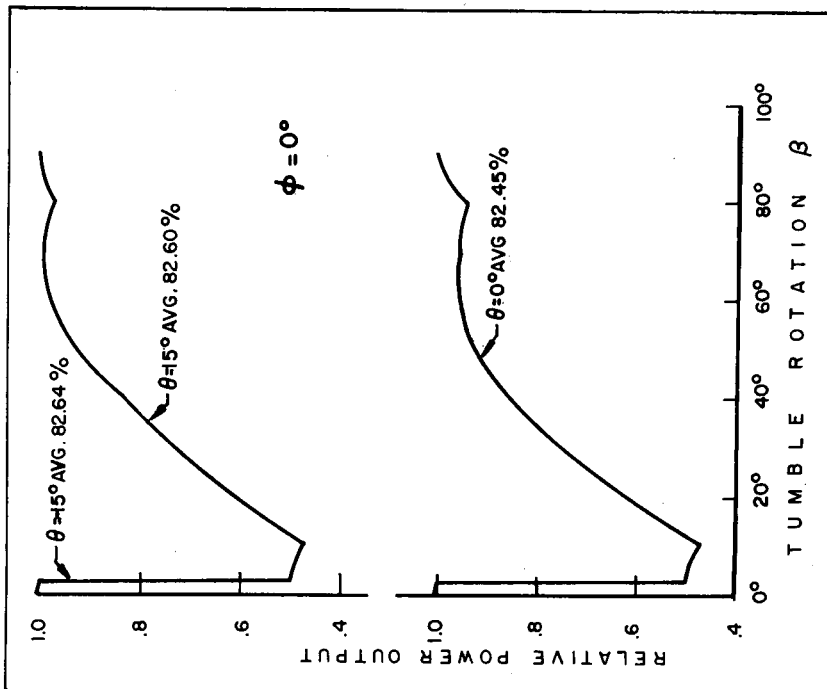
FIG. 39. POWER OUTPUT VERSUS ROTATIONAL
POSITION. $\phi = 0°$; $\theta = -15°$, $0°$, and $+15°$.
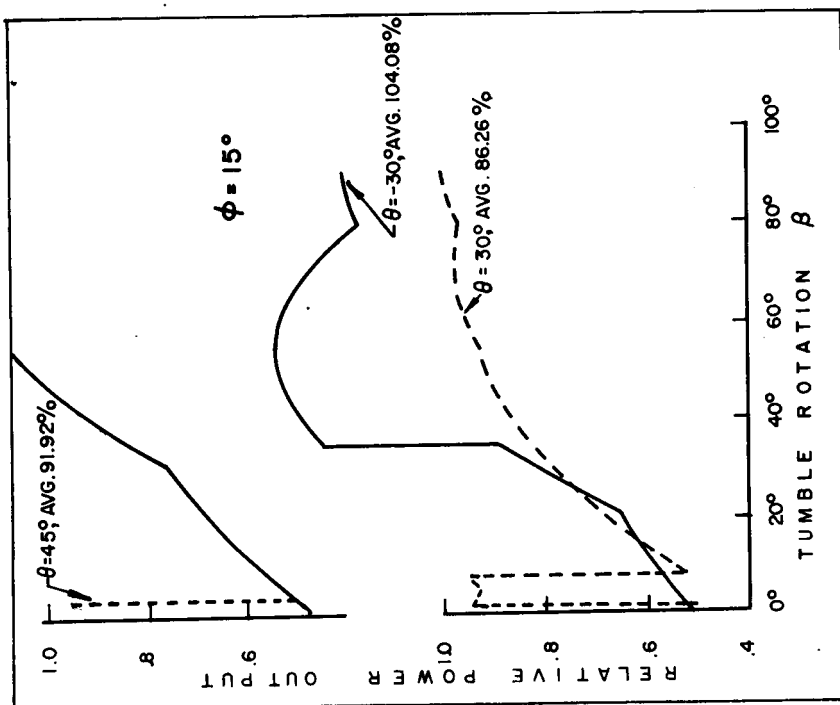
FIG. 42. POWER OUTPUT VERSUS ROTATIONAL
POSITION. $\phi = 15°$; $\theta = -30°$, $+30°$, and $+45°$
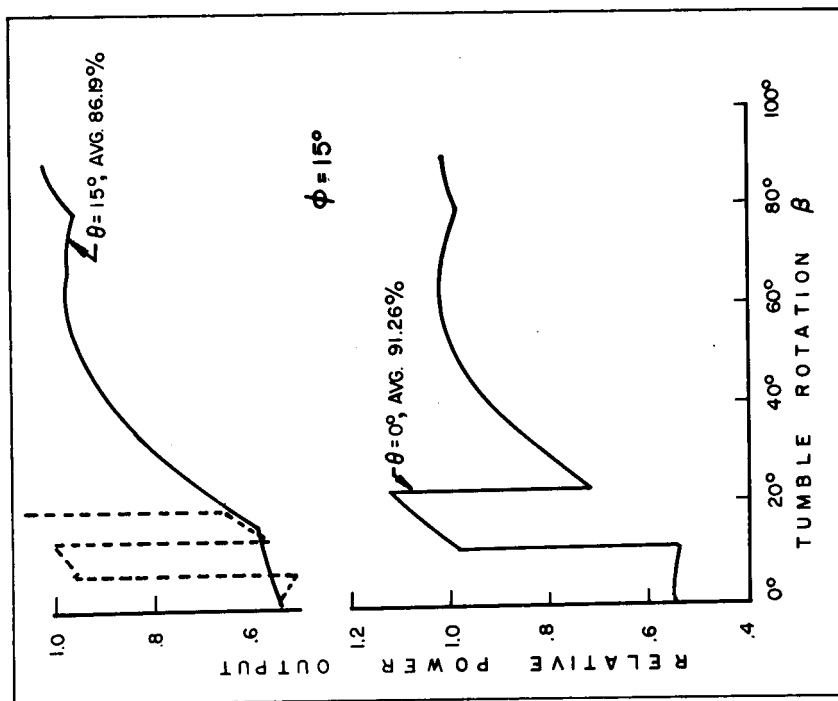
FIG. 41. POWER OUTPUT VERSUS ROTATIONAL
POSITION. $\phi = 15°$; $\theta = 0°$, and $+15°$.

FIG. 44. POWER OUTPUT VERSUS ROTATIONAL POSITION. $\phi = 30°$; $\theta = -45°$, $-30°$, $+30°$, and $+45°$.

FIG. 43. POWER OUTPUT VERSUS ROTATIONAL POSITION. $\phi = 30°$; $\theta = -15°$, $0°$, and $+15°$

FIG. 46. POWER OUTPUT VERSUS ROTATIONAL POSITION. $\phi = 45°$; $\theta = -45°$, $-30°$, $+30°$, and $+45°$.
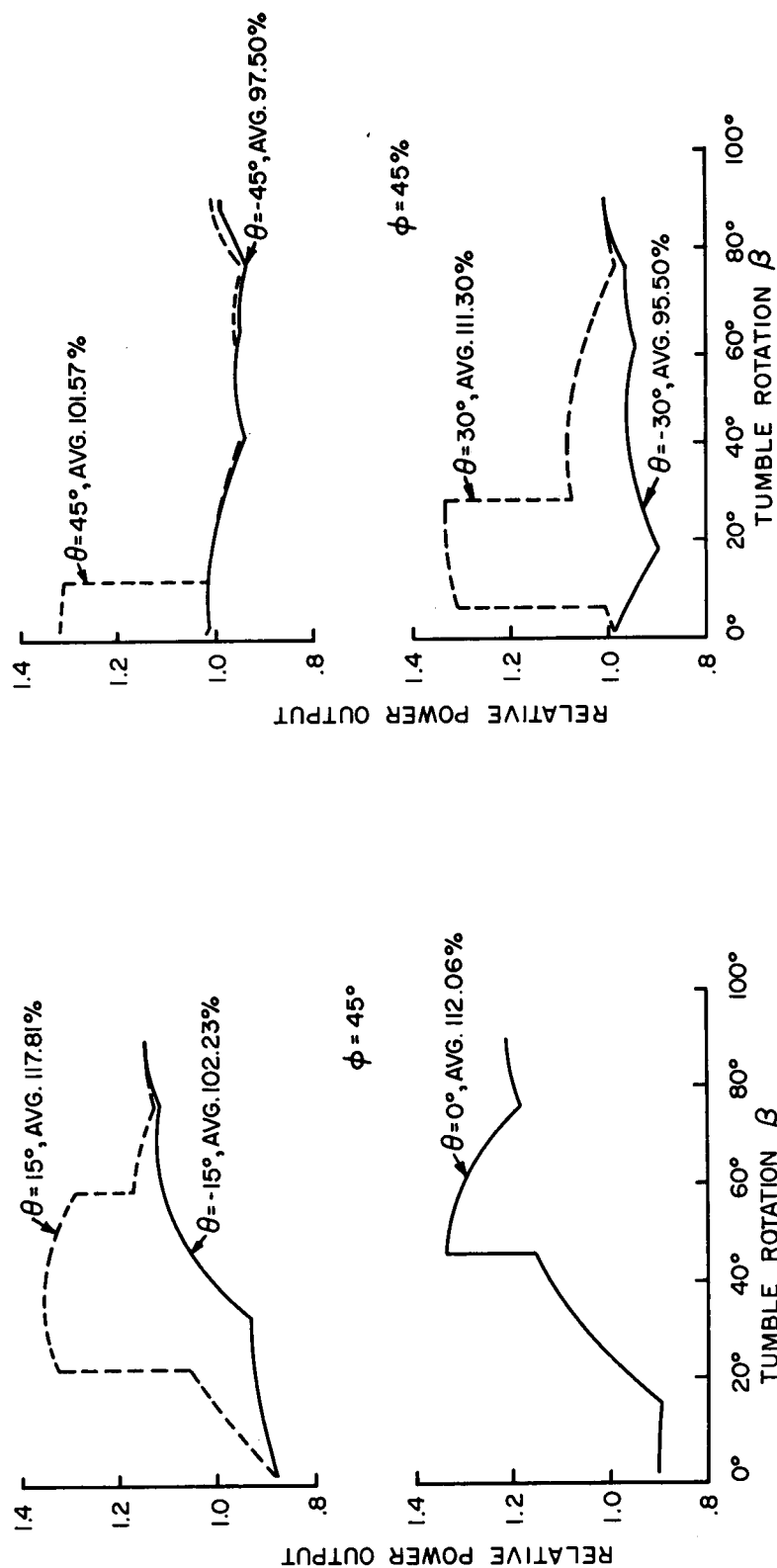
FIG. 45. POWER OUTPUT VERSUS ROTATIONAL POSITION. $\phi = 45°$; $\theta = -15°$, $0°$, and $+15°$.

FIG. 48. POWER OUTPUT VERSUS ROTATIONAL POSITION. $\phi = 60°$; $\theta = -45°$, $-30°$, $+30°$, and $+45°$.
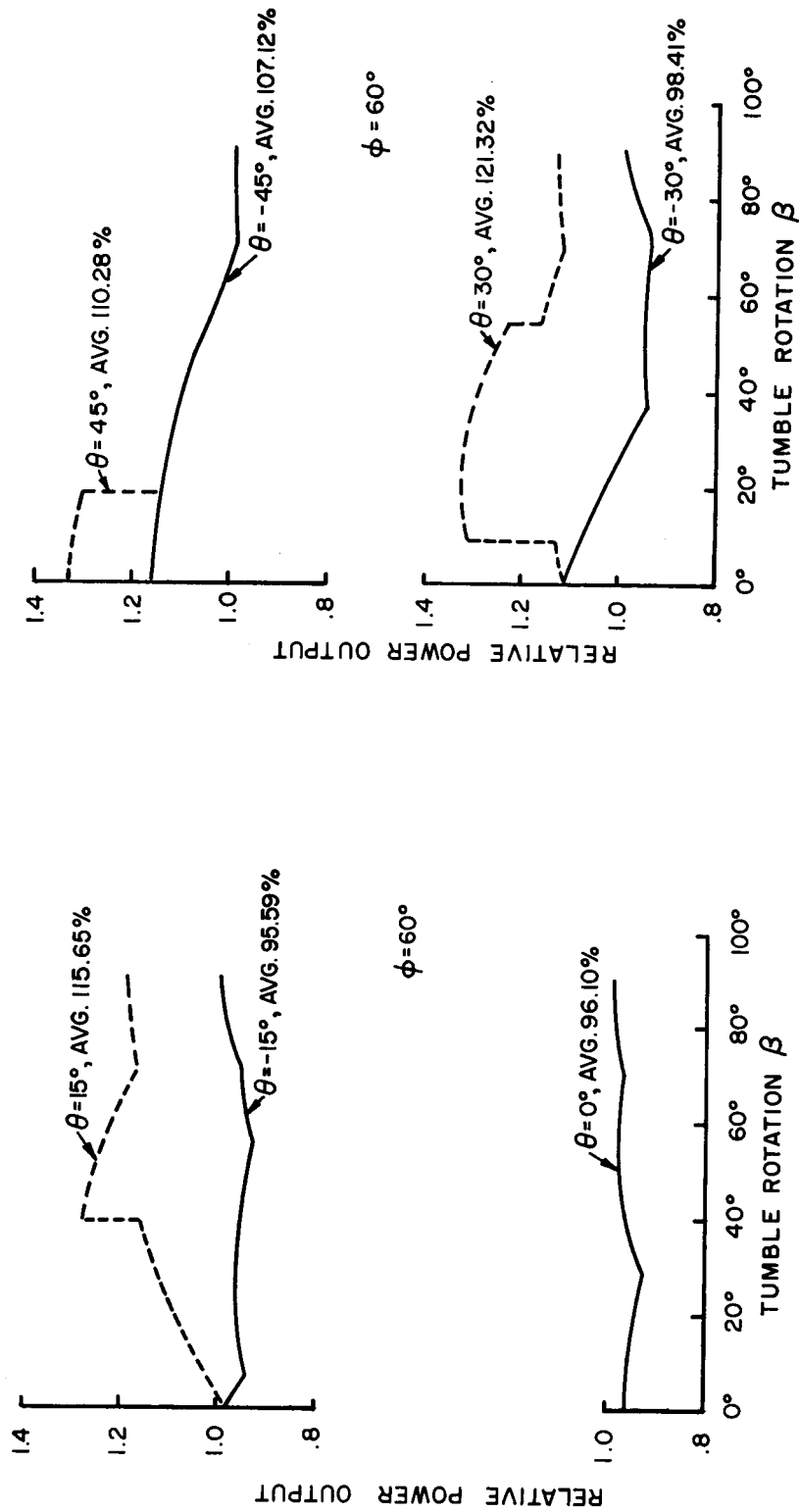
FIG. 47. POWER OUTPUT VERSUS ROTATIONAL POSITION. $\phi = 60°$; $\theta = -15°$, $0°$, and $+15°$.

96

$\phi = 75°$

$\theta = 45°$, AVG. 116.37%

$\theta = -45°$, AVG. 115.23%

RELATIVE POWER OUTPUT

$\phi = 75°$

$\theta = 30°$, AVG. 116.70%

$\theta = -30°$, AVG. 103.81%

RELATIVE POWER OUTPUT

TUMBLE ROTATION β

FIG. 50. POWER OUTPUT VERSUS ROTATIONAL POSITION. $\phi = 75°$; $\theta = -45°$, $-30°$, $+30°$, and $+45°$.

$\phi = 75°$

$\theta = 15°$, AVG. 107.61%

$\theta = -15°$, AVG. 95.03%

RELATIVE POWER OUTPUT

$\phi = 75°$

$\theta = 0°$, AVG. 94.97%

RELATIVE POWER OUTPUT

TUMBLE ROTATION β

FIG. 49. POWER OUTPUT VERSUS ROTATIONAL POSITION. $\phi = 75°$; $\theta = -15°$, $0°$, and $+15°$

FIG. 52. POWER OUTPUT VERSUS ROTATIONAL POSITION. $\phi = 90°$; $\theta = -45°$, $-30°$, $+30°$, and $+45°$

FIG. 51. POWER OUTPUT VERSUS ROTATIONAL POSITION. $\phi = 90°$; $\theta = -15°$, $0°$, and $+15°$

plotted by the computer to an accuracy of about 1%. These curves show only the investigation of the transmitter portion of the power system. Since the structural design provided mass-inertia ratios that would cause the body to tumble shortly after injection, the tumble rotation angle β was selected as the continuous variable for plotting the information. The percent average output per cycle of rotation is given, also, with each curve.

It may be noted, for the conditions selected, that the minimum average was 82.5% (Figure 39) and the maximum average was 121.3%, shown on Figure 48.

The average relative power per cycle of tumble rotation, obtained from the foregoing curves, was plotted against the spin rotation angle θ in Figures 53 and 54 to demonstrate the effect of spin superimposed on tumble for fixed values of φ (the angle of the sun with respect to the plane of tumble rotation). By integrating the curves for φ = 0° and φ = 90°, the minimum and maximum average relative power for the system was obtained for simultaneous spin and tumble. These values, expressed in percent of optimum output power from the cells on one side of the box, were 89% and 108%, respectively.

3. Design Modifications

In compliance with the original request that additional transmitter power be provided if possible, three additional solar cells were added in series with each group of the transmitter supply. It was readily seen on the preliminary layout that to add a parallel group of 51 series cells would have required a considerable increase in area and weight. Since three cells could be added without an additional area requirement, it was decided to include that number to obtain an increase in capacity of approximately 6%.

The slight disadvantages that result from obtaining additional area with series cells are:

      a. Increase in average voltage of overall system
      b. Reduction in voltage per cell from the optimum design conditions

Since only three cells were to be added the above effects were not considered serious, because the system average voltage was increased only 3% and the operating cell voltage was reduced to .312 volt per cell.

The transmitter supply design became, for each side and each end plate, two parallel strings of 54 cells in series having a total active area of 194.4 square centimeters.
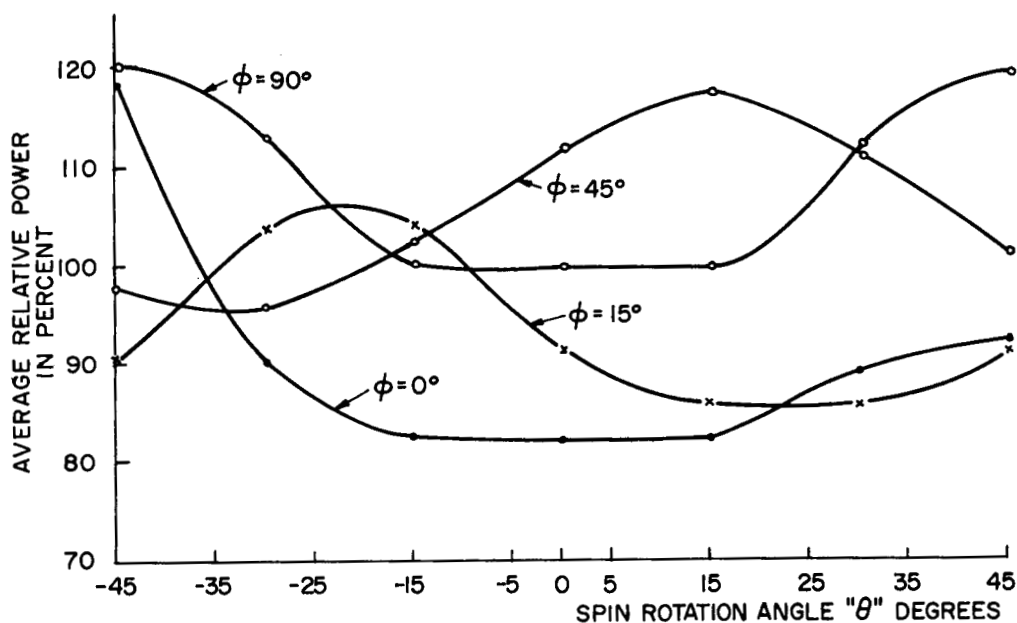
FIG. 53. RELATIVE AVERAGE POWER PER TUMBLE CYCLE AS A FUNCTION OF SPIN ROTATION. $\emptyset$ = 0°, 15°, 45°, and 90°.
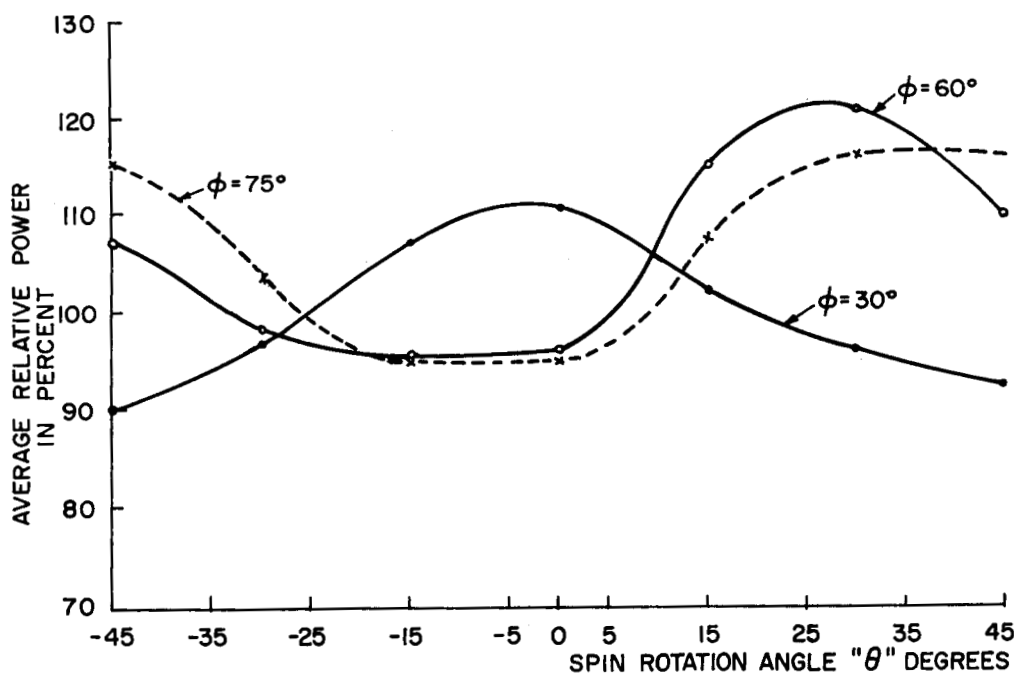
FIG. 54. RELATIVE AVERAGE POWER PER TUMBLE CYCLE AS A FUNCTION OF SPIN ROTATION. $\emptyset$ = 30°, 60°, and 75°.

Accounting for the effect of rotation and shadowing, (para. 2 and Fig. 53), the smallest effective projected area became 173.2 square centimeters (89% of 194.4 sq cm). Therefore, the effective projected cell area exceeded the minimum requirement of 162.5 sq cm (Sec. I, para.6) by 6.6%.

The instrumentation supply design (Section I, para. 6) was marginal due to limited space allowed on the side panels. However, the area of the end plates was greater than that of the sides, which made it possible to use two parallel groups of 22 series-connected, 1 x 2 cm cells instead of the one group of 1 x 2 cm cells paralleled with a group of 0.5 x 2 cm cells required by Section I, para. 6. The effective area of cells on each end plate then became 138% of that on a side.

Considering the entire solar box assembly, the added cells increased the average area of the instrumentation system to 113% of the initial design area. This increase was sufficient to overcome the 2.5% initial deficit and to compensate for the 11% power reduction, due to angular rotation as computed in paragraph 2, for a system having equal active cell area on each side and each end plate.

The reduction factor 0.89, as used for the transmitter supply, does not exactly apply to the instrumentation supply because of the unequal distribution. However, it was conservative to employ this factor since the larger area groups were placed in parallel on the end plates of the solar box assembly. Close observation of the results of the analysis made in paragraph 2 will show that the shadow from the protruding cylinder on the end plates is the cause for the effective projected area being smaller than that of one side. For rotational positions where shadowing does not occur, the projected area will be 100%, or larger than the side panel area. When shadowing comes into effect on the instrumentation supply, it essentially cuts the active cell area of the end plate in half, as was the case for the transmitter supply. However, the remaining active area on the end represents 69.3% of the area on a side panel, whereas, in the transmitter supply case the remaining active area was only 50%. Therefore, reduction in power, resulting from conditions giving the smallest projected area, will be less than for the transmitter supply. It was expected that this factor would be about 95%.

The only major change in power requirements that occurred after the solar cell design had been completed was the reduction of the demand on the instrumentation supply (6.5V) by SUI. The reduction was from 300 milliwatts to 195 milliwatts. Since both the structural and electrical design had been completed, and most of the prototype hardware fabricated, it was not feasible to redesign.

Design refinement for the sub-carrier oscillator (10.4V) supply followed the same procedure and reasoning that was applied to the instrumentation supply. Because this supply required only one series string

of 34 of the 0.5 x 2 cm cells, it was possible to include two of such groups in parallel on the end plates of the solar box assembly. Without these additional cells, it would be possible to have no output for certain angular positions.

For the sub-carrier oscillator supply the final arrangement included one group of 34 series-connected cells on each side, and two identical groups on each of the end panels. The lowest average projected effective area was computed to be 124% of the area per side, which gave 32.6 square centimeters. The above area exceeded the design requirement by 45%.

4. Assembly Considerations

a. Cell Selection and Fabrication. The first step taken in assembly considerations was the selection of cells in regard to efficiency. Each of the silicon solar cells was individually tested under a 500 watt tungsten filament photoflood bulb. The spectral range of this bulb was nearer that of sunlight in the response range of a solar cell than any other bulb tested. The light intensity was controlled by the use of a variable voltage supply. The light was filtered through 2.54 cm of water to reduce heating of the cell. Several cells were calibrated in sunlight and then were used as standards to adjust the intensity of the artifical illumination. The cells were checked at the computed optimum load point and the load resistance was maintained constant throughout the sorting process to assure good series matching. Only the cells with an efficiency of 9% or better were used for flight model payloads. The lower efficiency cells were used on the prototype payloads.

After the solar cells were tested for efficiency, the cells were soldered into various size shingles. This was performed by placing the cells in a specially designed jig made of fiberglas and beryllium copper. Silver Q flux was used to improve bonding during the soldering process. A 450 Induction Heater was used to solder the cells. The shingled strips were checked again for efficiency before being cemented on the solar cell plates. Because of the difference in the voltage-current characteristics and resistance of the soldered connection, the efficiency is usually reduced to about 8.0%.

The number of cells per side (2 panels) was:
    IRC Type S-1020C (1 x 2 cm) 130
    IRC Type S-0520C (0.5 x 2 cm) 56

The number of cells per end plate was:
    IRC Type S-1020C (1 x 2 cm) 152
    IRC Type S-0520C (0.5 x 2 cm) 68

The total number of cells used per payload was 824 cells of the type S-1020C and 360 cells of the type S-0520C.

An epoxy cement was used to attach the cells onto the plates. The analysis of the mixture was as follows:

Armstrong C-1	100%
Armstrong Flex	40% by weight
Armstrong Activator E	10% by weight
TiO_2	51.5% by weight
Cellosolvent	10% by weight

This cement was selected for use because of its excellent bonding qualities and its ability to dry in a relatively short time (approximately 2 hours). It will withstand ultraviolet rays, and temperatures ranging from -120°F to 250°F, without appreciable deterioration. The TiO_2 was added to the mixture to prevent damage from ultraviolet rays and to improve thermal balance conditions.

b. <u>Plate Selection and Fabrication</u>. Because of the critical weight limitations, magnesium was selected as the material for the solar cell plates. Dow 17 Anodize was used for an insulation coating on the plates. For additional insulation, a thin coating of Armstrong C-1 cement was used on the plates in the cell area.

Because of the shadow projected by the cylinder housing and the fourth stage, correct placement of the cells on the end plates was very important. There were two groups of cells in parallel on each end and side plate for the 15.6-volt power supply. Each group consisted of 54 series-connected, International Rectifier Corporation type S-1020C cells. To minimize the effect of shadowing, the cells on the end plates were placed as far as possible from the cylinder. The two groups of cells for the 15.6-volt supply were placed on diagonally opposite corners of the end plates to prevent the cylinder shadow from blocking both groups at any time. The same precaution was followed in locating the 10.4-volt and 6.5-volt power supplies on the end plates.

The final solar cell arrangement is shown on Figure 55, where the solar cell box is shown prior to assembly and wiring.

The average weight of the side panel plates was 73.45 grams each before the cells were put on. After the cells and glass slides were cemented on the plates, the average weight was 124.7 grams each, giving an increase of 51.25 grams. The cells and cement covered approximately 196 square centimeters on each of the side plates, which was an average increase in weight of 0.26 gram per square centimeter. The average weight of the end plates was 278 grams before the solar cells and the glass
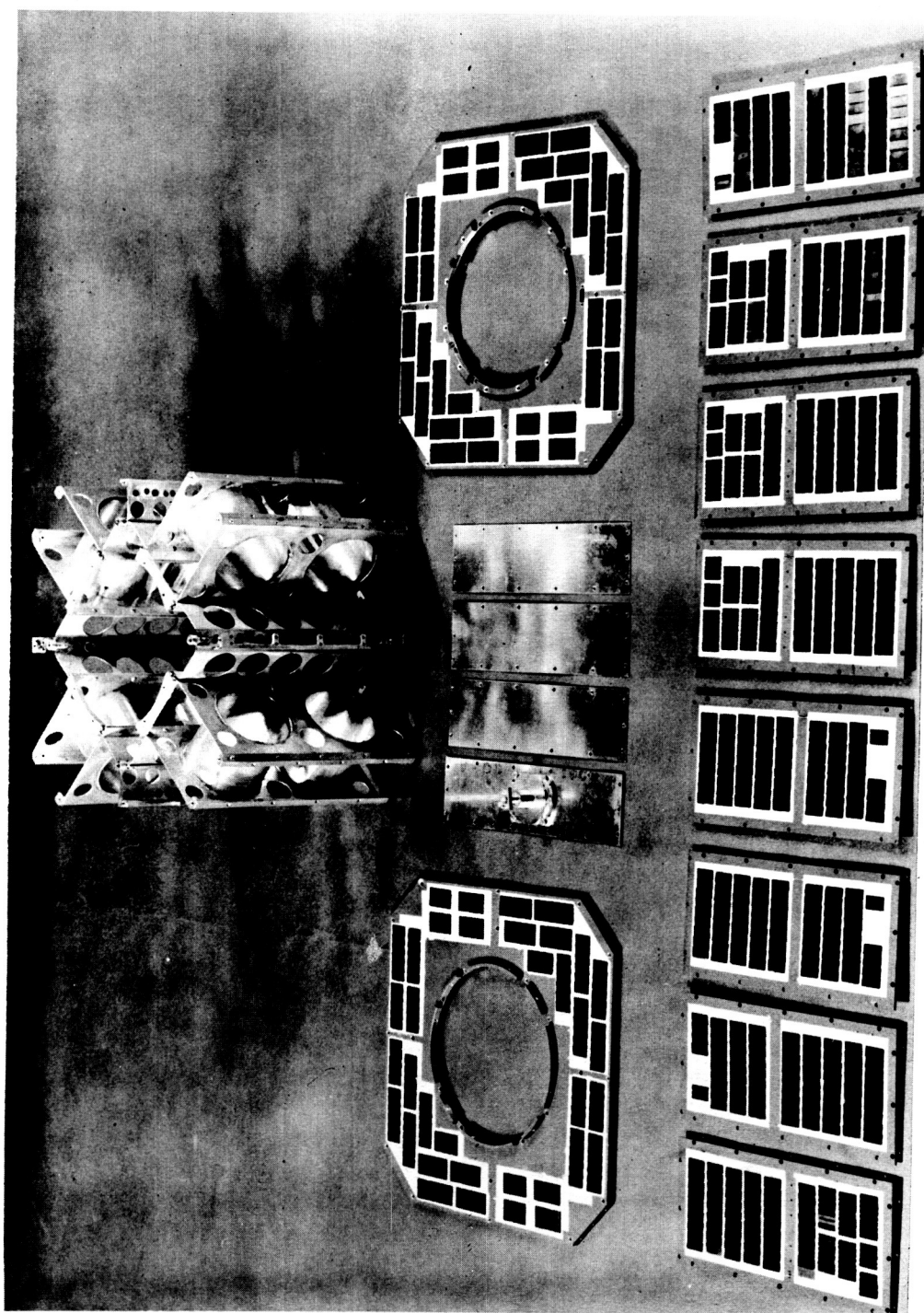
FIG. 55. SOLAR CELL BOX PARTS

slides were attached. After the solar cells and glass slides were cemented on, the average weight of the end plates was 389 grams. The total weight of all of the solar cell plates for flight model number 1 was 1668 grams.

The sides of the solar cell box assembly consisted of two separate panels to insure ease of handling and wiring, and to reduce vibration effects in the center of the plates.

To improve thermal balance of the solar cell box, Lepage's liquid solder was applied to the structure where the side plates make contact. Also, a thin coat of Fe_2O_3 was applied to the cemented area around the solar cells to reduce heat radiation losses.

SECTION III. PROTECTIVE COVERING INVESTIGATION

1. Reasons for Study

The National Aeronautics and Space Administration and the State University of Iowa presented information which indicated that there was a high probability of excessive radiation damage to the solar cells and consequent failure of the satellite in a time period of one day to one week. Because of the extremely high orbit, it was expected that the satellite would pass through areas of high intensity electron and proton radiation. High intensity particle radiation would damage the solar cells. For protection against this radiation, it was considered necessary to put some type of protective cover over the cells.

An investigation was made at State University of Iowa and ABMA Research Projects Division to determine the amount of damage to the solar cells at different electron and proton energy levels. Most of the information concerning the radiation belt came from an emulsion pack carried in a missile nose cone, and from the experiments of Dr. Van Allen. To penetrate the 6 gm/cm^2 of material surrounding the emulsion pack, the electrons and protons, respectively, must have had energies greater than 12 mev and 55 mev. In this investigation no pertinent data on the radiation energy levels at this high apogee orbit were known; therefore, most of the conclusions on the expected solar cell damage were taken from theoretical calculations. By such calculations with unprotected solar cells, the expected life time could be as low as one day of operation.

This investigation showed that some protective shield would have to be used to increase the life time of the satellite. Adding about 25 mg/cm^2 to 50 mg/cm^2 of shield protection would increase the operational life time of the satellite to several weeks.

2. Limitations Imposed by Design

By the time a final decision was reached on the requirement for a protective covering on the solar cells, attachment of the solar cells to the box assembly had been completed. Fused silica glass 1/16-inch thick, like that used on Explorer VII and Vanguard I, was the best protection known to this division. To use this type of covering would require complete redesign of the payload. Also, to obtain the high apogee type of orbit required by State University of Iowa, the weight penalty of glass was too great. In selection of the covering, consideration had to be given to the critical weight limitation and to a method of attaching the covering without redesign of the solar cell assembly.

Mica was suggested as a cover by State University of Iowa. It was also suggested that the mica should be at least .005-inch thick to give the protection required. After testing the mica for power loss and adhesive qualities, it was not considered practicable for use as a protective covering.

Glass slides, 0.006-inch thick, with magnesium floride coating on top and an ultraviolet coating on the bottom were selected. The effects of outer space environments upon cement used to bond the glass slide directly to the solar cell were not known; therefore some other means of attaching the glass slides had to be considered. By making the glass slide length greater than the solar cell length, epoxy cement could be used to cement the protruding glass directly to the material of the base. This method increased the reliability of the solar cell power system because the glass slides protected their own cement bond. If the outer space environment caused a deterioration of the cement, there would be no change in the solar cell output.

Glass slides were placed on the environmental model and subjected to all mechanical test requirements without any damage. Solar cell plate samples with glass slides were run in a vacuum of 10^{-9} millimeters of Hg and temperature range of -40°C to 80°C for 72 hours with no damage to the solar cells or glass slides. Additional samples were subjected to an ultraviolet light with no apparent damage.

3. Materials Evaluated

To provide protection of the solar cells from the radiation, as described in paragraph 1, the following materials were selected for consideration for a protective covering of the cells:

1. Mylar   .002-inch thick
2. Mylar   .003-inch thick
3. Mylar   .005-inch thick

4.	Mylar	.0075-inch thick
5.	Mica, ruby	.0017-inch thick
6.	Mica, ruby	.006-inch thick
7.	Mica, muscovite	.006-inch thick
8.	Mica, muscovite	.0048-inch thick
9.	Teflon	.002-inch thick
10.	Glass, clear (Corning Glass)	.006-inch thick
11.	Glass, coated (Optical Coating Lab., Inc.)	.006-inch thick

Such materials were selected for their light weight, and absorption characteristics.

Tests were conducted with the above materials to determine which, when used as a solar cell protective covering, would result in the minimum decrease of the solar cell power system efficiency and still provide the required protection.

These tests consisted of measuring the output power or voltage of an unprotected solar cell or cells at various angles of incidence with the illuminating intensity being held at a constant level. The same solar cell or cells were then covered with one of the selected protective materials and the tests repeated. The results of the tests were put into graphical form for comparison. Figure 56 shows the per cent loss in solar cell output for the various materials with the angle of incidence equal to zero degrees. Figures 57 and 58 show the effect of mica, clear glass slides, and coated glass slides, as the angle of incidence was varied to between 0 and 90 degrees. Figures 59 and 60 show the decrease in the solar cell output and percentage loss in output when .0017-inch ruby mica, .006-inch ruby mica, and .003-inch Mylar were used as protective covers.

To simulate the effects of spin conditions on the output of the solar cell power system with and without protective covering, a miniature model of the solar cell assembly was constructed. Solar cell strings consisting of eight cells in series were mounted on each of the four sides of the model. The model was rotated under the light source to simulate spin rotation of the satellite.

Identical tests were performed with and without mica covering. The output was recorded from side 1 (referenced perpendicular to source), then with sides 1 and 2 connected in parallel.

Figures 61, 62, and 63 compare the output voltage, power, and per cent change in power from side 1 in sunlight with and without a .0048-inch
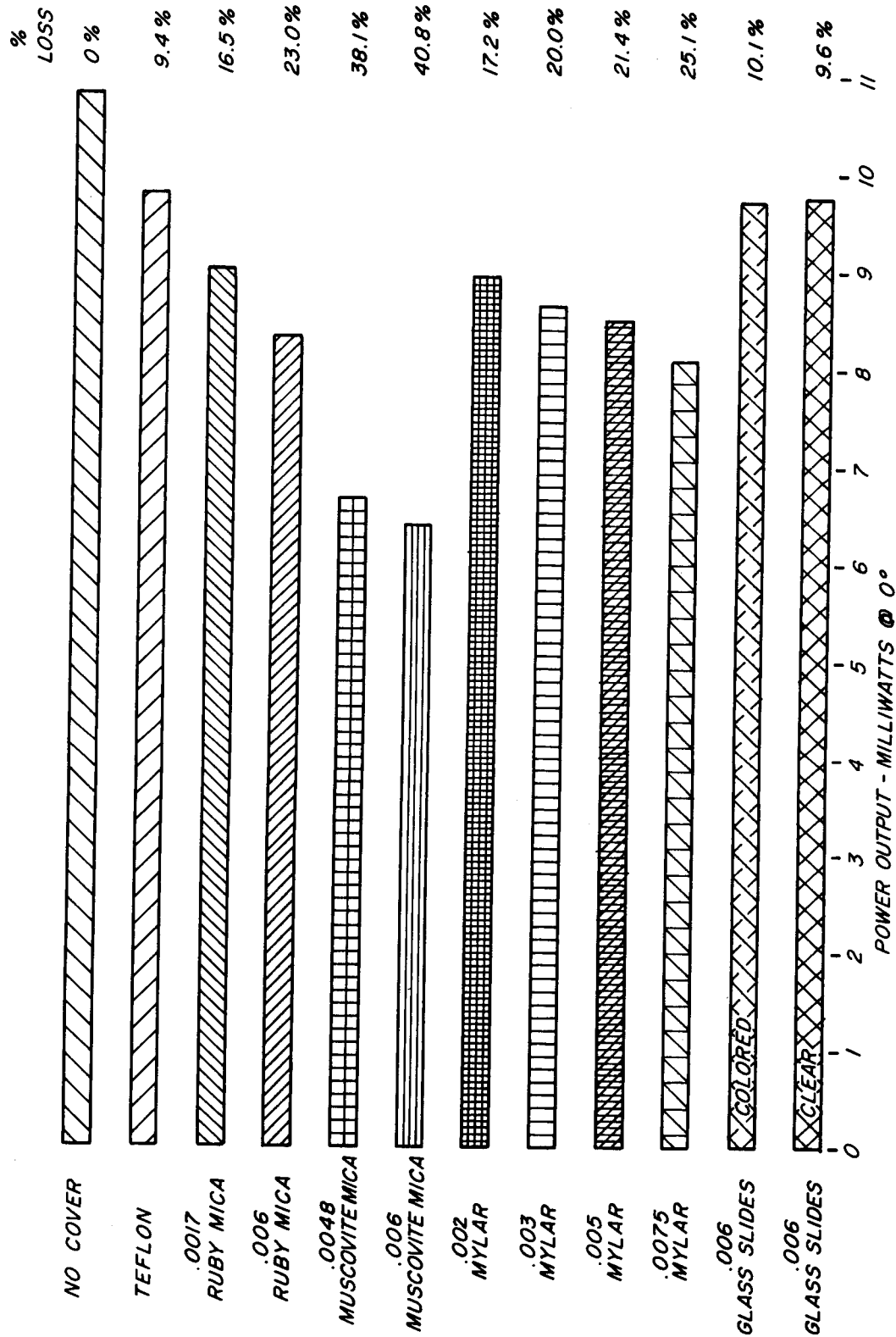
FIG. 56. AVERAGE POWER LOSS OF MATERIALS INVESTIGATED

108

1. Solar cell unprotected
2. Muscovite mica .0048 inch thick over solar cell

FIG. 57. SOLAR CELL POWER OUTPUT VERSUS ANGLE OF INCIDENCE

1. Solar cell unprotected
2. Solar cell covered with coated glass slide
3. Solar cell covered with clear glass slide
4. Muscovite mica .006 thick over solar cell
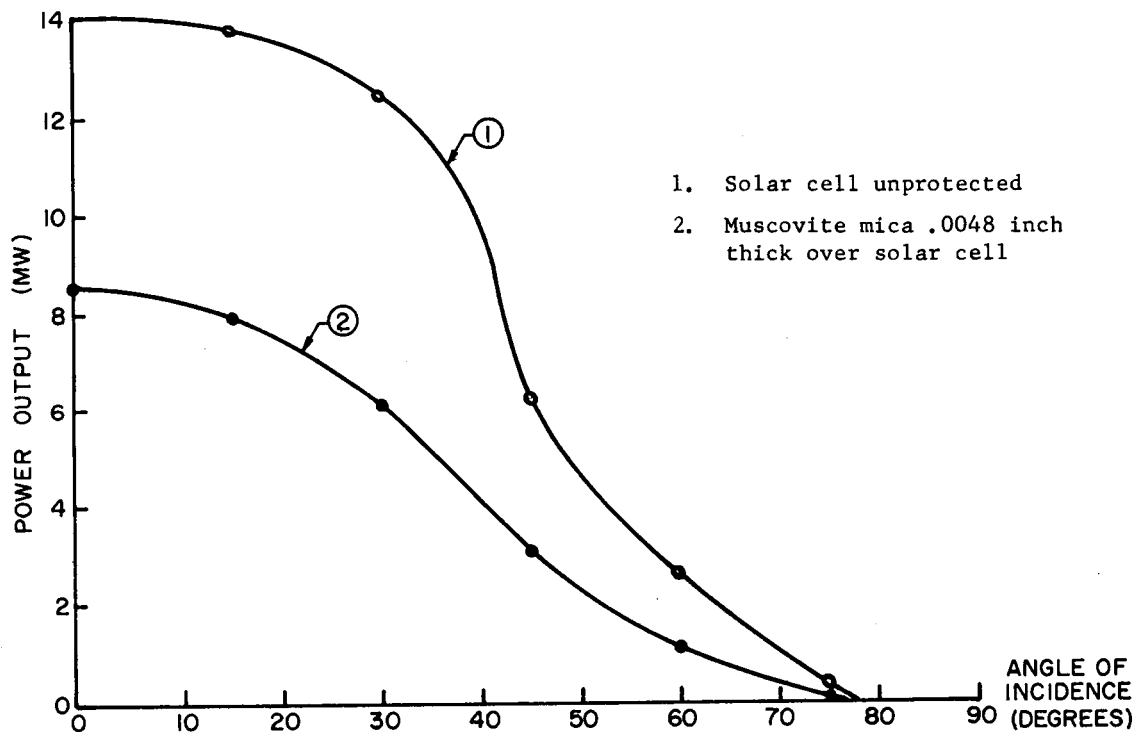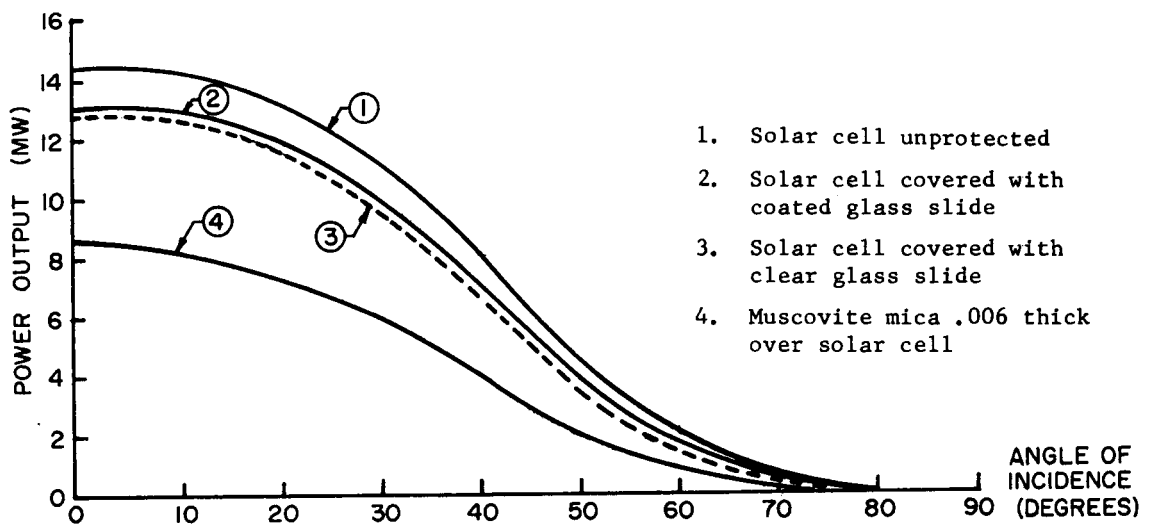
FIG. 58. SOLAR CELL POWER OUTPUT VERSUS ANGLE OF INCIDENCE
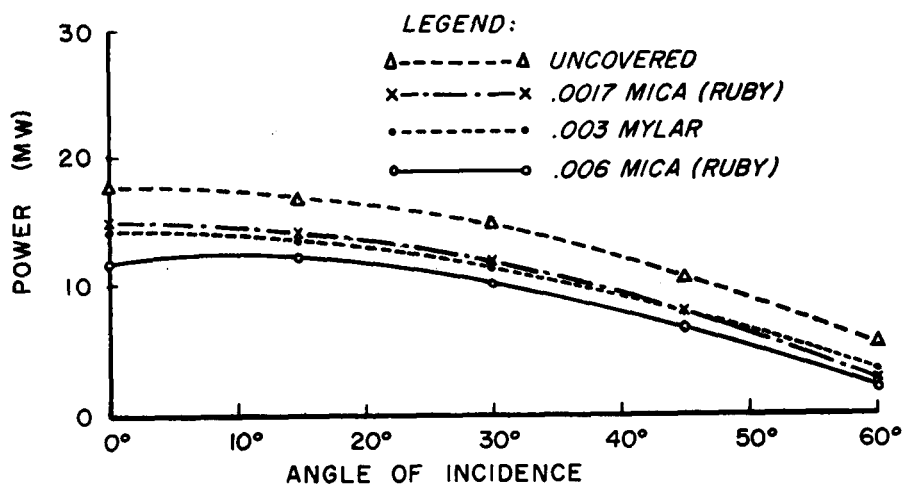
FIG. 59. SOLAR CELL PROTECTIVE COVER TEST (Power in milliwatts)
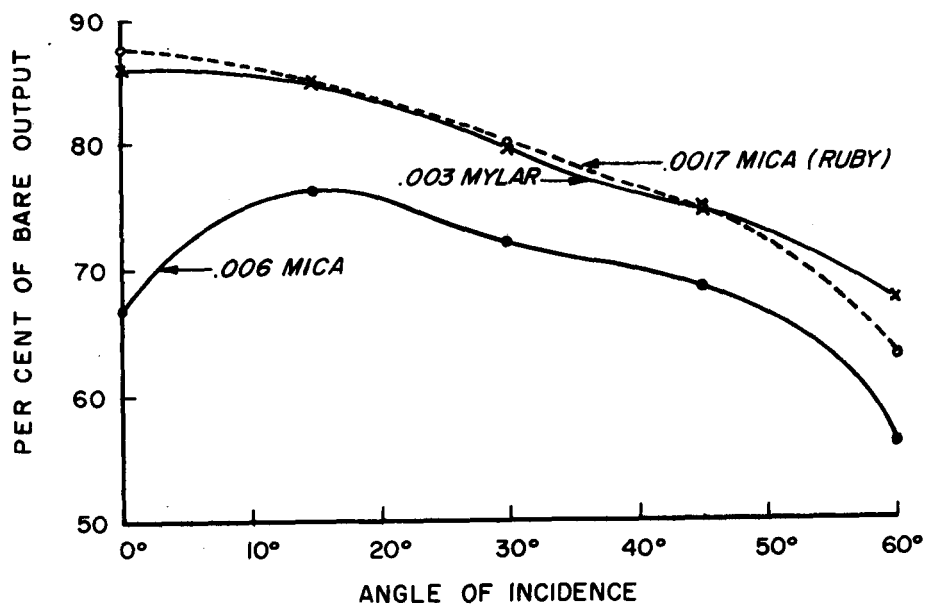
FIG. 60. SOLAR CELL PROTECTIVE COVER TEST (Output)

110
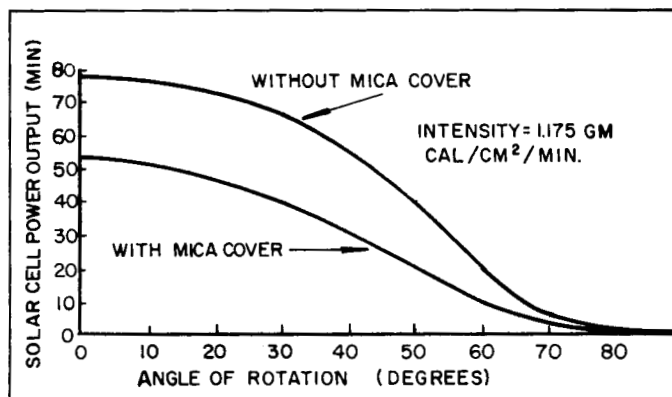
FIG. 61. SOLAR CELL POWER OUTPUT VERSUS ANGLE OF ROTATION
(Cell in sunlight with and without .0048 inch thick mica cover)
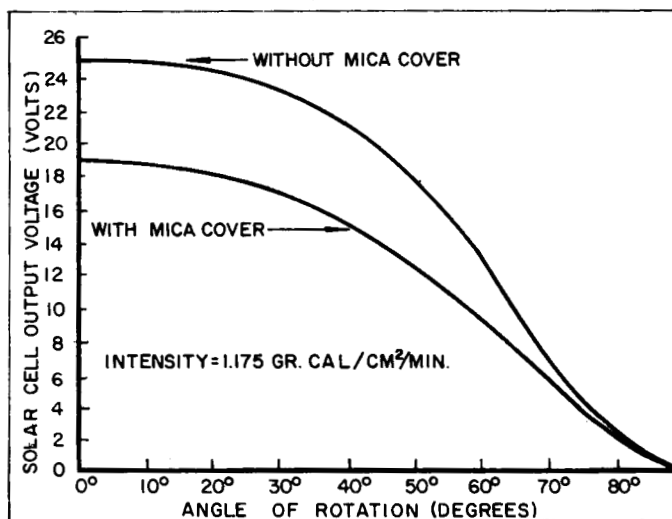
FIG. 62. SOLAR CELL VOLTAGE OUTPUT VERSUS ANGLE OF ROTATION
(Cell in sunlight with and without .0048 inch thick mica cover)
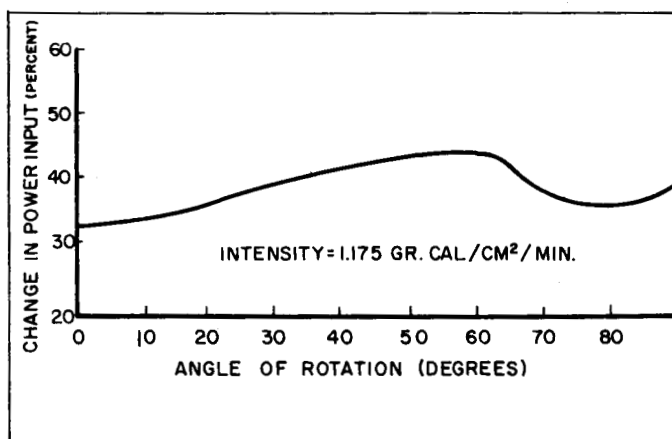
FIG. 63. RELATION OF POWER OUTPUT OF .0048 INCH THICK MICA
COVERED SOLAR CELL TO ANGLE OF ROTATION

muscovite mica cover. Figure 63 shows that an average 38.1 per cent decrease resulted due to the use of the mica cover.

Figures 64, 65, and 66 show the voltage drop, power loss, and per cent change in power when sides 1 and 2 were connected in parallel. An average of 33 percent in power output was lost due to the mica cover.

In Figure 67 similar results were indicated when the same test as above was conducted with artificial illumination. In Figures 67 and 68 the output voltage decreased an average of 30% when the solar cell was covered with the mica protector as compared with the unprotected cell results.

From the results, as shown in Figures 62 through 68, an approximate one-third increase in the total number of solar cells would be required to obtain sufficient output power with the use of a mica protective cover.

To further substantiate the results as obtained above, tests were conducted with a Perkin-Elmer spectrophotometer (Model 13/U No. 97) to determine the amount of light transmitted through mica and a coated glass slide as the wave length of the transmitting source was varied. These tests were conducted in the wave length portion of the spectrum to which the solar cell is sensitive (reference Fig. 31). In Figures 69 and 70, the coated glass slide possessed much better light transmission properties than that of the mica cover.

Mechanical tests were also conducted with mica, Mylar, and glass slides, to determine how each would adhere to the solar cell mounting surface when Armstrong X-91 epoxy resin compound was used as the adhesive. Glass proved to be the best for bonding to mounting surfaces. The mica proved very unsatisfactory due to flaking of the material where the surfaces were in direct contact with the bonding agent.

Finally, all materials were subjected to temperature and moisture tests. Once again, mica was the only material to give unsatisfactory results due to its physical property of high moisture absorbency.

4.   Protective Cover Selection and Application

In selection of the type of material which would finally be used as a protective covering for the solar cells, careful consideration was given to each material to determine which had the best combinational characteristics of: (1) radiation non-deterioration, (2) minimum decrease in solar cell power system efficiency, (3) good bonding adhesion, (4) low moisture absorption, and (5) minimum discoloration under ultraviolet exposure.
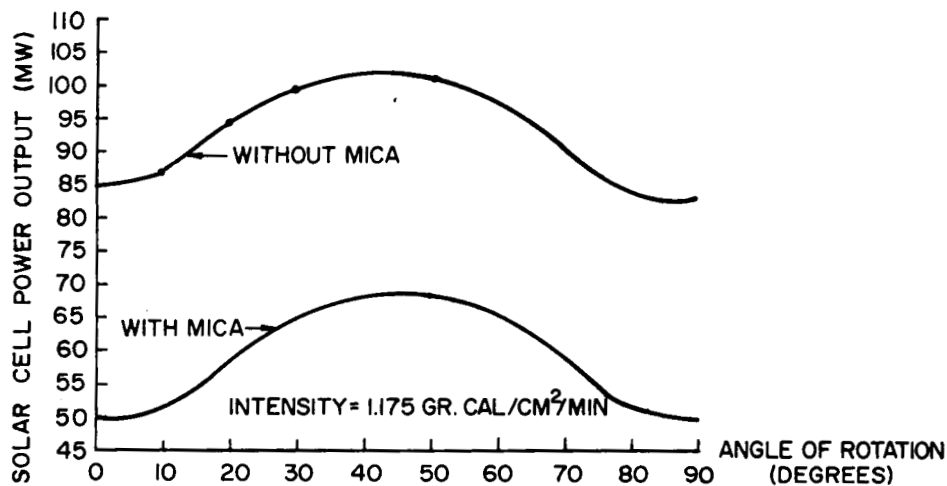
FIG. 64. SOLAR CELL POWER OUTPUT WITH AND WITHOUT MICA COVER
VERSUS ANGLE OF ROTATION (Taken in sunlight, two sides)
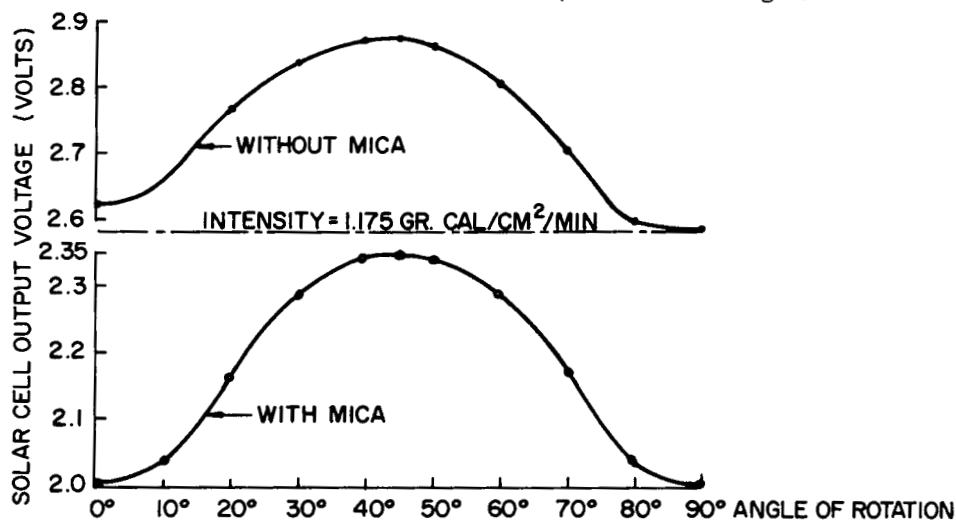
FIG. 65. SOLAR CELL OUTPUT VOLTAGE WITH AND WITHOUT MICA
COVER VERSUS ANGLE OF ROTATION (Taken in sunlight, two
sides in parallel)
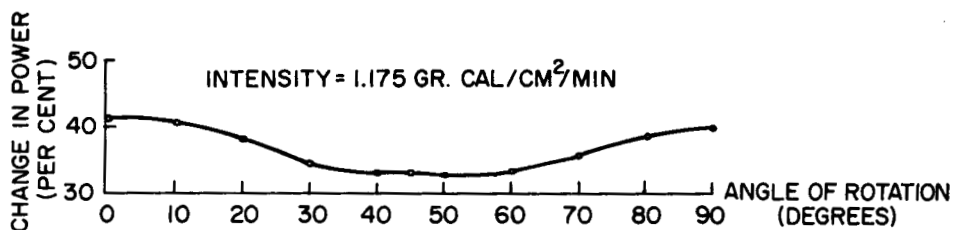
FIG. 66. RELATION OF POWER OUTPUT OF MICA COVERED SOLAR CELL TO ANGLE
OF ROTATION. (Taken in sunlight. Two strings of eight cells each, the strings
mounted at right angles to each other and connected in parallel.
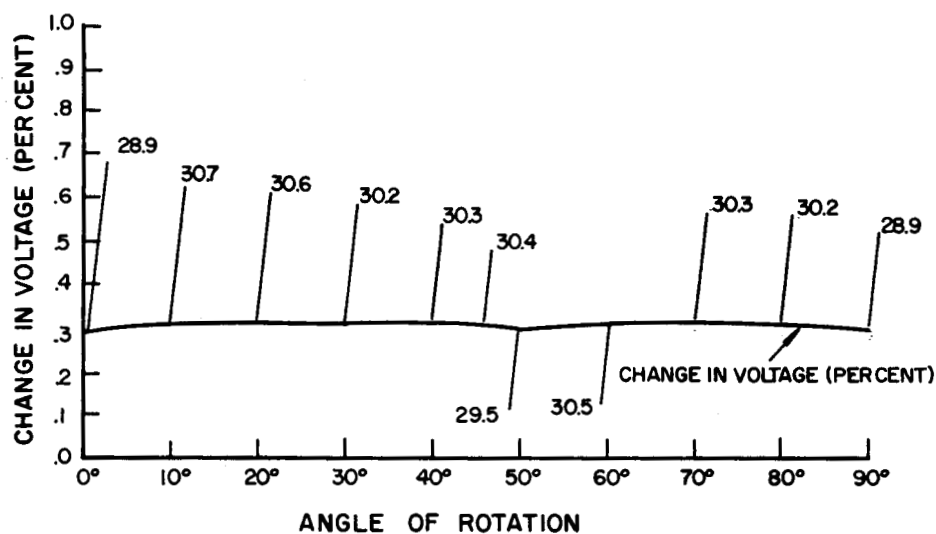
FIG. 67. OUTPUT VOLTAGE CHANGE OF A MICA COVERED SOLAR CELL VERSUS
ANGLE OF ROTATION. (Artificial illumination. Intensity = 0.541 gm Cal/cm^2/min.)
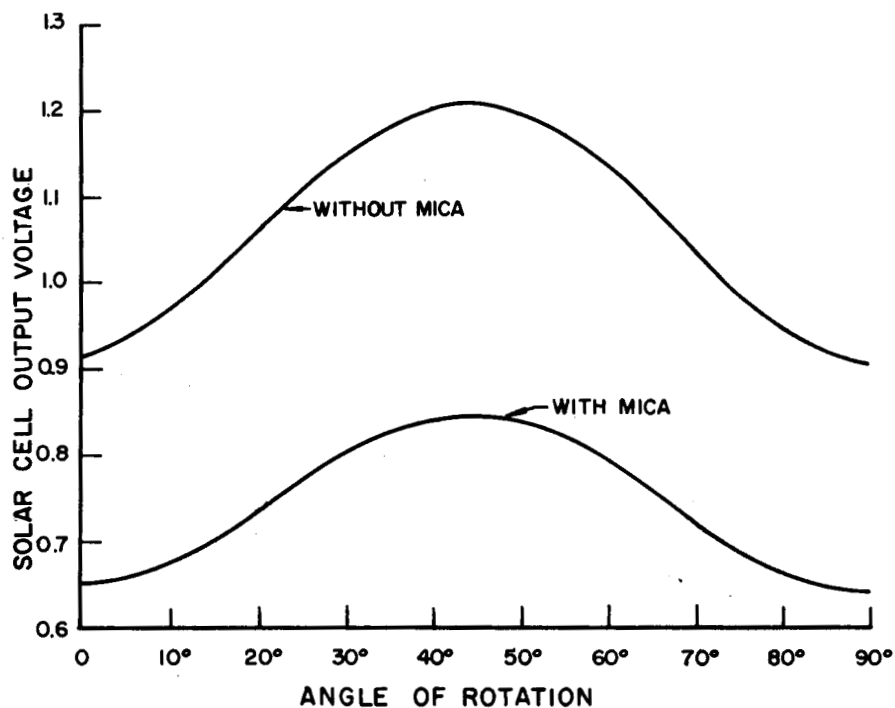
FIG. 68. OUTPUT VOLTAGE OF SOLAR CELL WITH AND WITHOUT MICA COVER
VERSUS ANGLE OF ROTATION. (Artificial illumination)

CURVE A : 100% LINEARITY RUN
CURVE B : SAMPLE NO. 1, .006 IN. THICK
CURVE C : SAMPLE NO. 2, (IRRADIATED) , .00575 IN. THICK

PERKIN ELMER SPECTROPHOTOMETER, MODEL 13/U
FUSED SILICA PRISM, PbS DETECTOR FROM 0.70μ TO 1.2μ
FUSED SILICA PRISM, 1P28 DETECTOR FROM 0.4μ TO 0.7μ
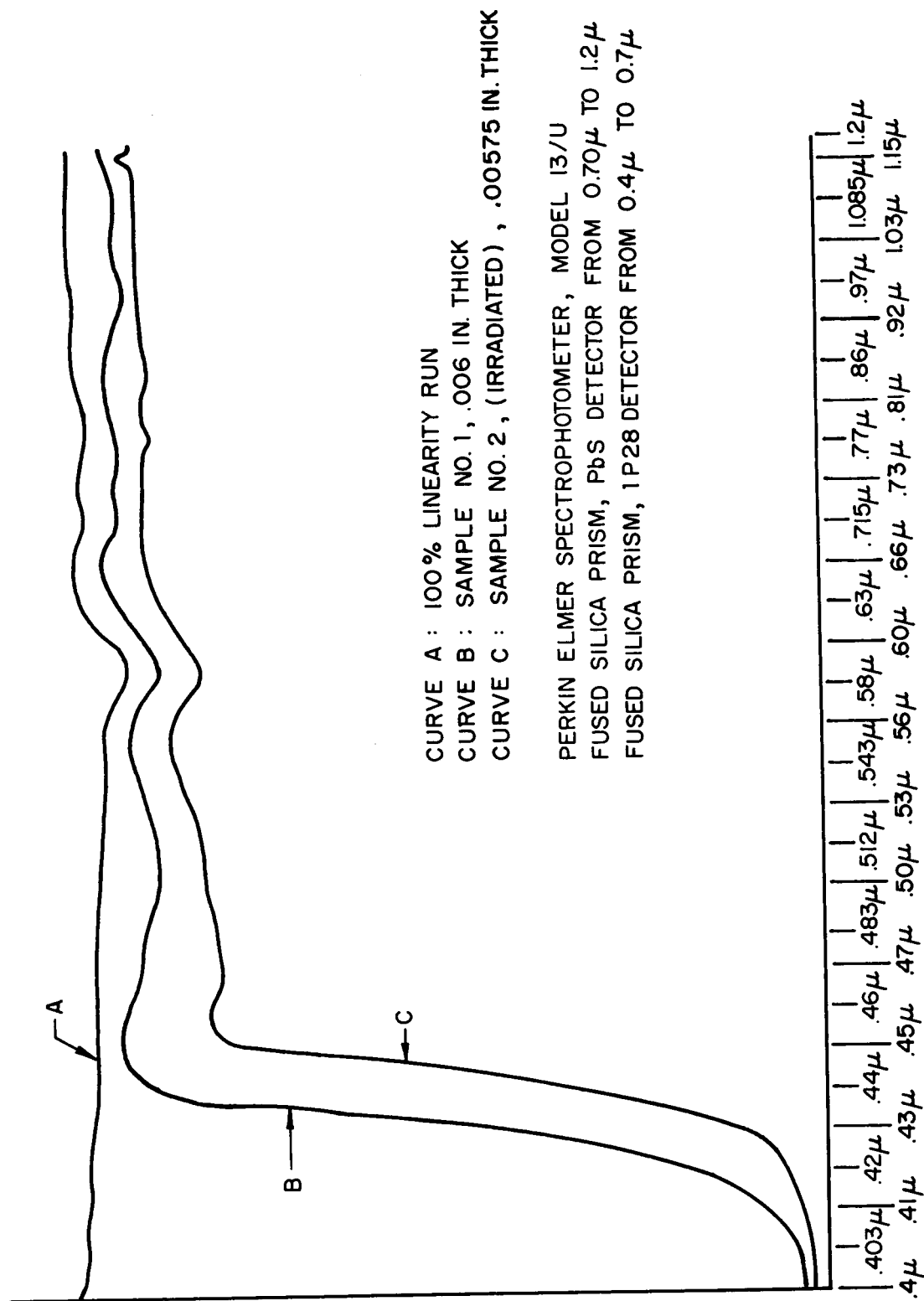
FIG. 69. LIGHT TRANSMISSION VERSUS WAVE LENGTH FOR TWO COATED GLASS
SLIDE SAMPLES
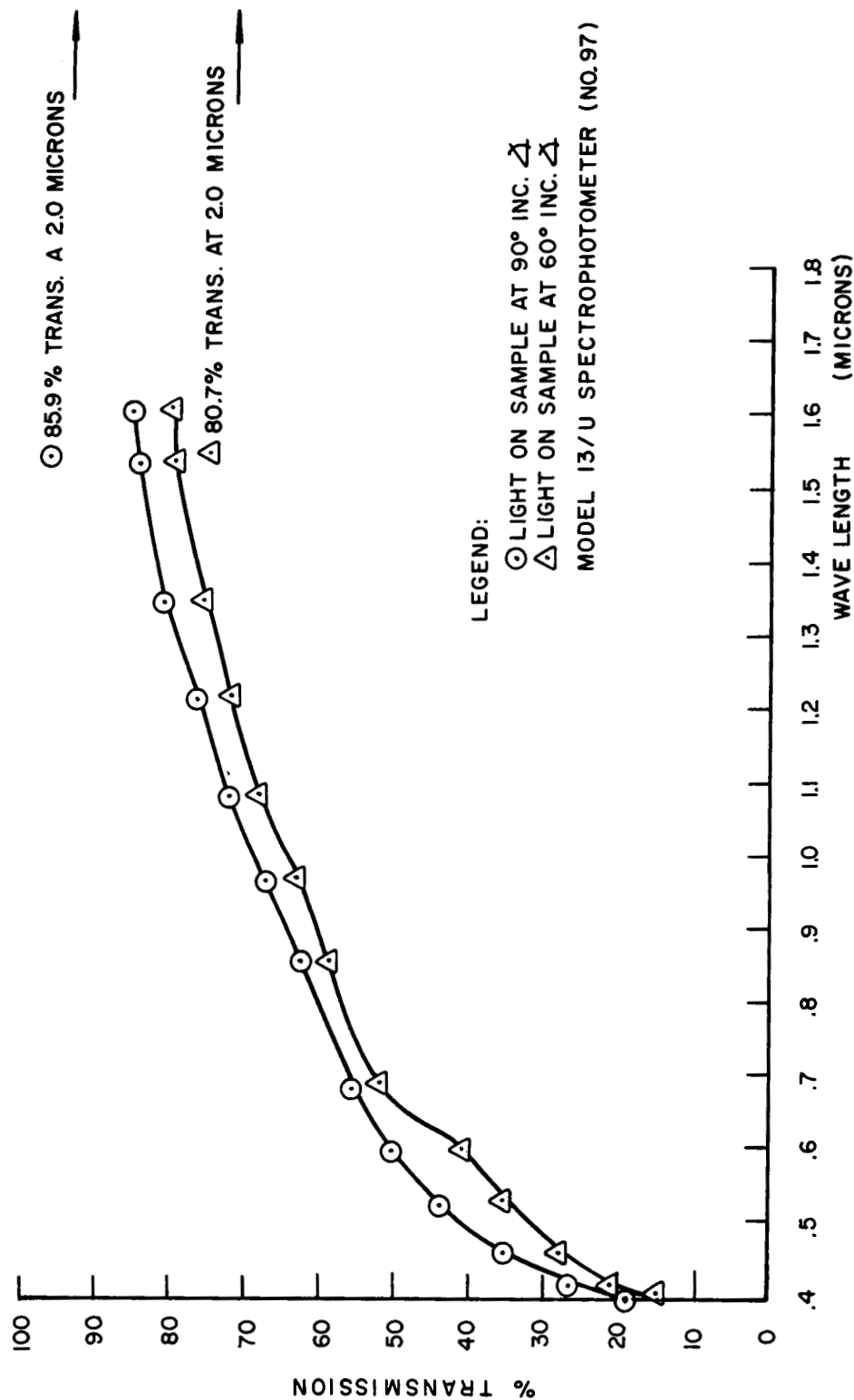
MICA SAMPLE .0075 INCHES THICK

FIG. 70. LIGHT TRANSMISSION VERSUS WAVE LENGTH FOR .0075 INCH THICK MICA SAMPLE AT 60° AND 90° ANGLES OF INCIDENCE

All materials over .004-inch thick that were tested provided suf-
ficient protection against radiation deterioration. From results as
shown in paragraph 3, a protective covering of Teflon resulted in the
minimum decrease in solar cell power output, with near equal results
being obtained from glass slides. Due to possible decomposition of
Teflon by outer-space environment, a decision was made against its use
as the protective covering. A covering of mica or Mylar would result in
major redesign of the solar cell box assembly. Such redesign would be
required to increase the outside area of the assembly for mounting 30%
more solar cells and for mounting hardware. This redesign would have
resulted in a schedule delay. Furthermore, mica was not satisfactory
due to excessive moisture absorption and poor bonding characteristics.
Therefore, glass slides were selected as the protective covering material.
Satisfactory results were obtained in all tests conducted when glass
slides were used. This selection did not require redesign of the box
assembly, and application could be achieved without schedule delay.

Although coated glass slides produced slightly larger power losses,
these offered the advantage of protecting the cement against ultraviolet
deterioration. The coated slides were also superior for thermal control
of the assembly. Therefore, coated glass slides were chosen for the S-46
satellite. Application of the glass slide protective covering over the
solar cells was a delicate operation. Each of the 1128 solar cells had
to be covered individually with a slide which was 3 millimeters greater
in length than the solar cell. This allowed 1-1/2 millimeters overlap
on either edge of the glass slide for cementing to the Armstrong C-1
compound, which was used to mount the solar cells on the box assembly.
Armstrong X-81 epoxy resin, with a mixture of TiO_2 was employed as the
adhesive. The compound was mixed and allowed to harden to the point
where it became very sticky. Then, a very narrow strip of the X-81 was
spread near the edge of the solar cell. Extreme care was necessary to
avoid contamination of the P-surface of the solar cell. Time was allowed
for the X-81 to become almost stiff, then the glass slide was placed over
the cell to be covered. Slight pressure was applied to the edges to as-
sure good contact with the adhesive. The thin strip of X-81 compound
supported the glass slides at the edges. (see Fig. 71). The plate was
cured at room temperature and allowed to harden at least 12 hours.

Weight increase, due to addition of the protective glass slide covers,
was 68 grams average for the side plates and 53 grams average for the end
plates. The increase in total payload weight was 121 grams. Because of
the delicate operation of cementing the glass slides in place, a total
of 238 man hours per payload was required. It was required that instru-
ments be used for handling to avoid damaging or contaminating the delicate
slide coating.

GLASS SLIDE

AIR SPACE

SOLAR CELL

ARMSTRONG X-81,
FOR ADHESIVE SLIDE

ADHESIVE LAYER OF ARMSTRONG C-1

INSULATING LAYER OF ARMSTRONG C-1

SOLAR CELL BOX ASSEMBLY
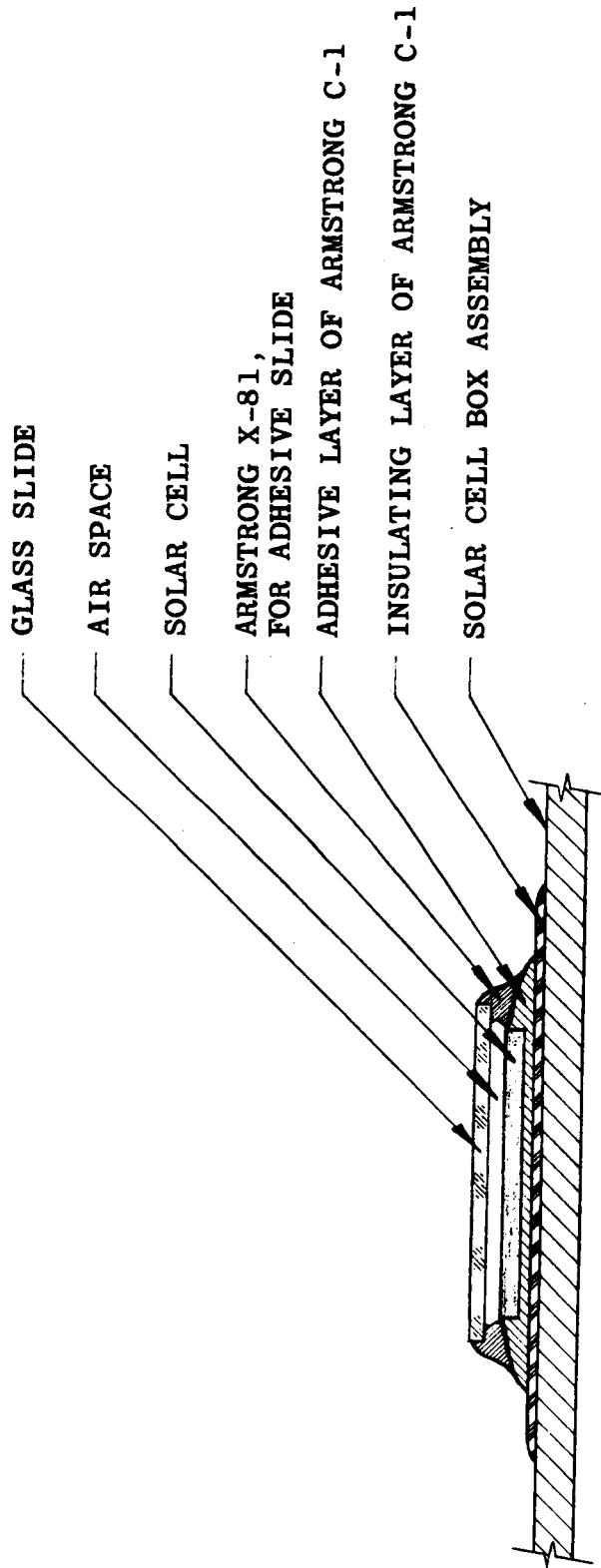
FIG. 71. CROSS SECTION OF SOLAR CELL AND PROTECTIVE COVER MOUNTING

5. <u>Solar Cell System Design Review</u>

As established in paragraphs 3 and 4, the coated glass slides selected for protective covers effectively reduced the output power by 10.9%. A review of the solar cell system design (Sec. I, para. 6 and Sec. II, para. 3) revealed that the 15.6 volt transmitter supply was the least conservative, with a capacity of only 6.6% greater than the requirement. Imposing a 10.9% loss from the protective covers would have reduced capacity to 3.5% less than the design requirement. It was fortunate, however, upon re-evaluation of the thermal control design with the added glass slides, that the thermal designers concluded that the maximum temperature would not exceed 65°C. Therefore, an untimely redesign of the payload was avoided because this decrease in maximum temperature would raise the cell efficiencies more than enough to compensate for an output deficit of 3.5%.

<div align="center">SECTION IV. POWER SYSTEM PERFORMANCE</div>

1. <u>Solar Cell Assemblies</u>

Tests were conducted for the power output of the solar cells after the plates were fabricated and wired. Each plate was individually tested under tungsten filament photoflood lamps before the cells were covered with glass slides. The plates were also tested under sunlight for power output. The light intensity of the sun was measured with an Epply pyrheliometer, model 50. The calibration of the pyrheliometer was 8.85 mv/calorie/cm^2/minute. The output was read with a differential voltmeter. A typical output from the pyrheliometer for normal sunlight was 9.5 millivolts.

Following the assembly of glass slides to the plates, the performance of the solar cell groups was checked again in the sunlight and in artificial light to determine the percentage loss caused by the glass slides. As predicted, this loss amounted to about 10 percent of the total power output.

After the plates were assembled into a complete unit, the power output was checked again. To check the output of a single side, all the other sides were covered since they were wired in parallel. Tests were run on each of the six sides in this manner for each of the three separate power supplies.

The solar cell assembly was also checked in the sunlight with the 9 o'clock side perpendicular to the sun rays and leaving all the other sides exposed. A typical value for the 15.6 volt supply under this

condition at optimum load was 17.15 volts at 80.0 ma or 1372 mw. For this test a resistive load of 210 ohms simulated the transmitter and battery. The 10.4 volt supply for the sub-carrier oscillators had an output of 11.1 volts at 21.6 ma load or 240 mw. The 6.5 volt supply for the instrumentation had an output of 7.25 volts at 50 ma load or 362 mw. The nickel-cadmium batteries were not in the circuit, but the zener diodes were across the output of the solar cells during the measurements. All measurements were performed at a solar input of 85 mw/cm^2 and a cell temperature of approximately 40°C.

The output of the solar cell supply was also tested with the sun rays making an angle of 45° with respect to the normal on the 6 and 9 o'clock sides. Under this condition, there was an increase in power output of about 1.2 times the output obtained when the light was normal to a side.

Using a complete payload solar cell power system under artificial illumination, the battery charging characteristics were determined as shown on Figure 72. Because of the extreme heating conditions, there was a gradual decrease in the total output power of the solar cell supply; this caused the battery charging current to drop somewhat faster than normal. Due to heating and non-uniformity of intensity over a large area, measurements of an assembly were extremely difficult when artificial illumination was employed.

2. Blocking Diodes

To prevent inactive portions of the solar cell power supply system from becoming an additional load on the active portions of the power system, a blocking diode was placed in series with each string of cells before making the parallel connections.

Careful consideration was given to the forward resistance of various types of diodes. Because of size and temperature limitations, only miniature silicon diodes were considered. Tests were conducted to select diodes which would result in minimum voltage drop in the forward direction. A 1N697 type diode proved to have the lowest obtainable forward resistance, giving a drop of 0.7 volt at calculated load. With this selection, the power loss of the system was minimized.

3. Zener Diodes

Reference to Sections I and II will show that large fluctuations of voltage and power can result from variations in temperature and in position of the satellite with respect to the sun. To prevent excessive battery charging, the system was voltage limited by silicon zener diode voltage regulators placed across each of the three solar cell power supplies. The zener diodes were selected so as to limit the battery charging

120
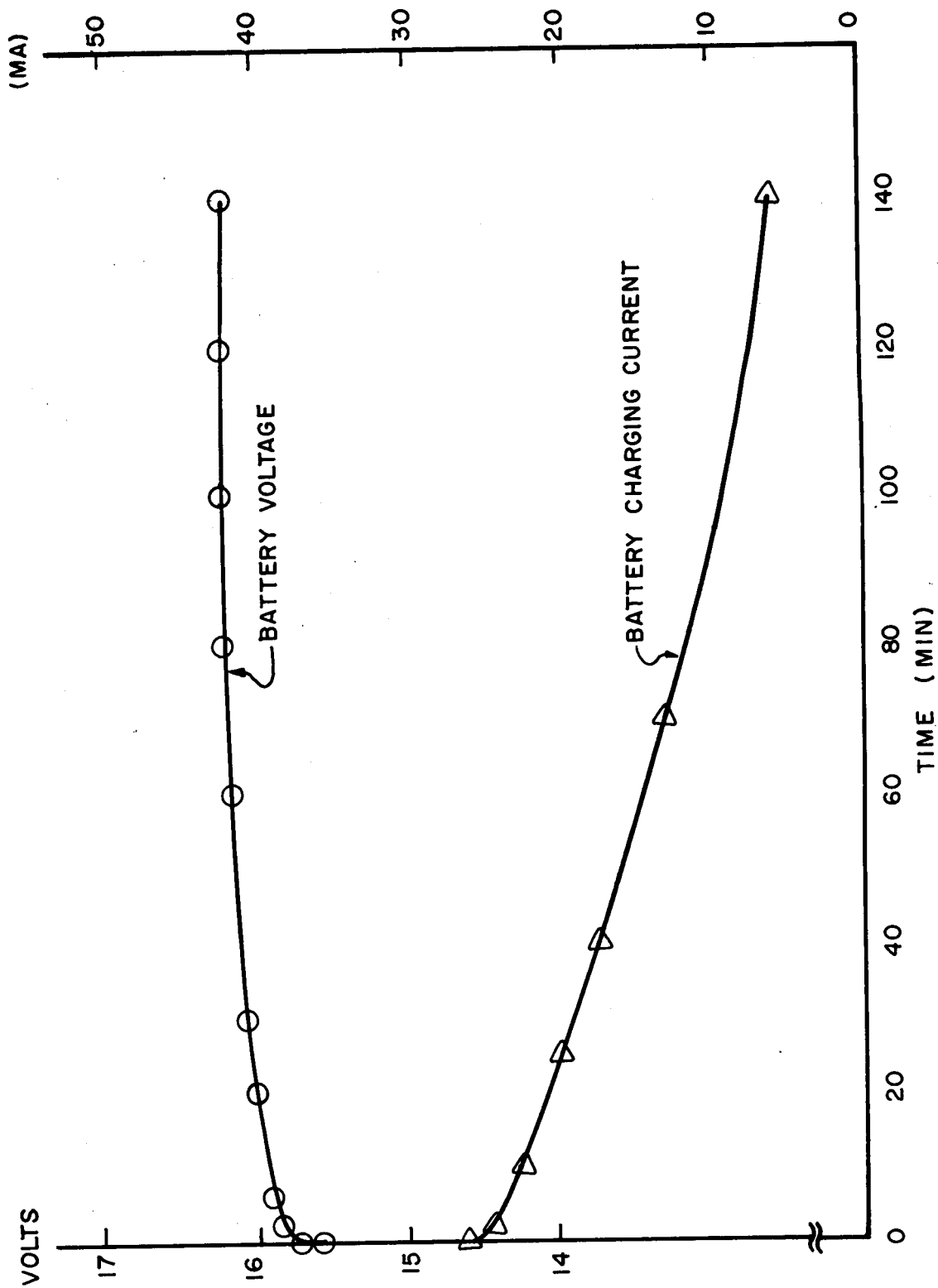
FIG. 72. BATTERY CHARGING CHARACTERISTICS OF COMPLETE SOLAR CELL POWER SYSTEM WITH ARTIFICIAL LIGHT SOURCE OF APPROXIMATELY 100 mw/cm²

voltage to 1.45 volts per cell. It was desirable that these diodes have a breaking current-voltage characteristic and that their dynamic resistance be as low as possible. Also, it was necessary to select diodes having very low temperature coefficients. A zener diode, Transitron type SV908, 10 watts, was selected for the 6.5 volt supply. The breaking point for this diode began at 6.9 volts and completely limited the system to 7.45 volts. The actual characteristic curve for this zener diode is given in Figure 73. In the 10.4 volt supply, a zener diode, Transitron type SV1016, 750 milliwatts, was used for the regulator. This diode had a breaking point starting at 10.65 volts, and was capable of passing 30 milliamperes at battery charging voltage of 11.6 volts. For the 15.6-volt supply, two zener diodes, types SV906 and SV2016, 10 watts each, were connected in series to avoid exceeding the diode wattage rating at elevated temperature and to obtain a low temperature coefficient. This combination began breaking at 16.3 volts and was capable of passing 60 milliamperes of current at battery charging voltage, that is, 17.5 volts.

4. Battery Characteristics

Three Gulton 4VO-.500, 500 milliampere-hour wafer cell batteries were connected in series to give the required +15.6 volt supply. One Gulton 8VO-.180, 180 milliampere-hour wafer cell battery was used for the +10.4-volt supply. One Gulton 5VO-.500 milliampere-hour wafer cell battery was used for the +6.5 volt supply. Upon receipt of these batteries, each battery was charged at 50% of rated capacity for two hours and 15% of rated capacity for the following four hours. A close observation of the terminal voltage was maintained to prevent over-charging the battery for if the terminal voltage exceeds 1.5 volts per cell during charge, there is an excess of oxygen liberated from the chemical reaction in the cell. Each cell has an absorption type of material to take care of a small amount of oxygen, but it cannot absorb excessive oxygen. The excess oxygen will create a pressure in the cell that can easily cause swelling, or rupture the sealed battery casing.

After the batteries had been charged, they were discharged at 50% of rated capacity until the terminal voltage read 1.0 volt per cell. Two more complete charge and discharge cycles were made on each battery. Further assurance that a battery would be acceptable for satellite application, was provided by a 60-minute charge and a 40-minute discharge cycle which was repeated 12 times on each battery. The depth of discharge for this process was 20% of rated capacity. Any battery that displayed abnormal voltages or currents, either under charge or discharge, was replaced by another battery. A typical charge and discharge curve is shown in Figure 74.
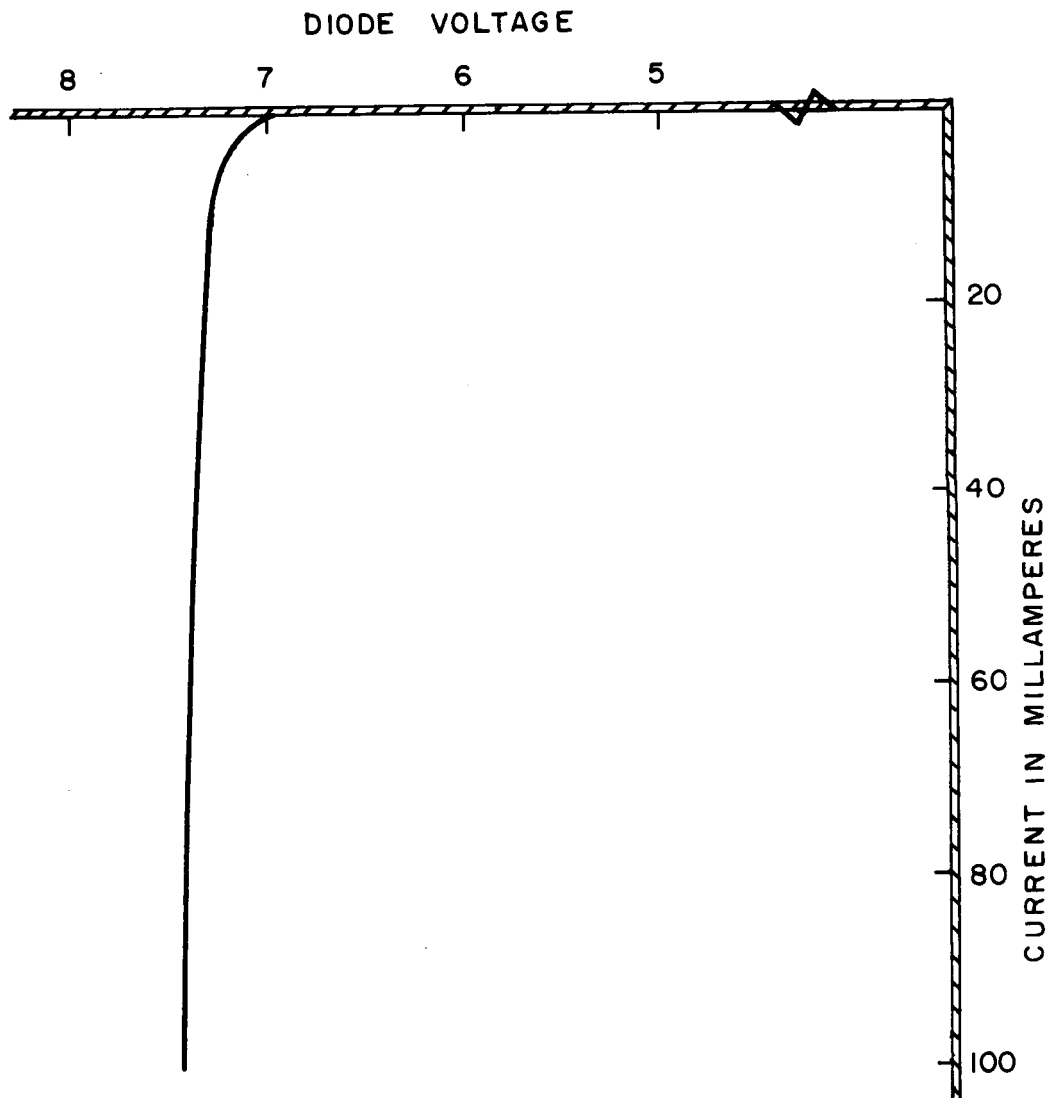
FIG. 73.   CHARACTERISTIC CURVE OF TRANSITRON TYPE
SV-908 ZENER DIODE
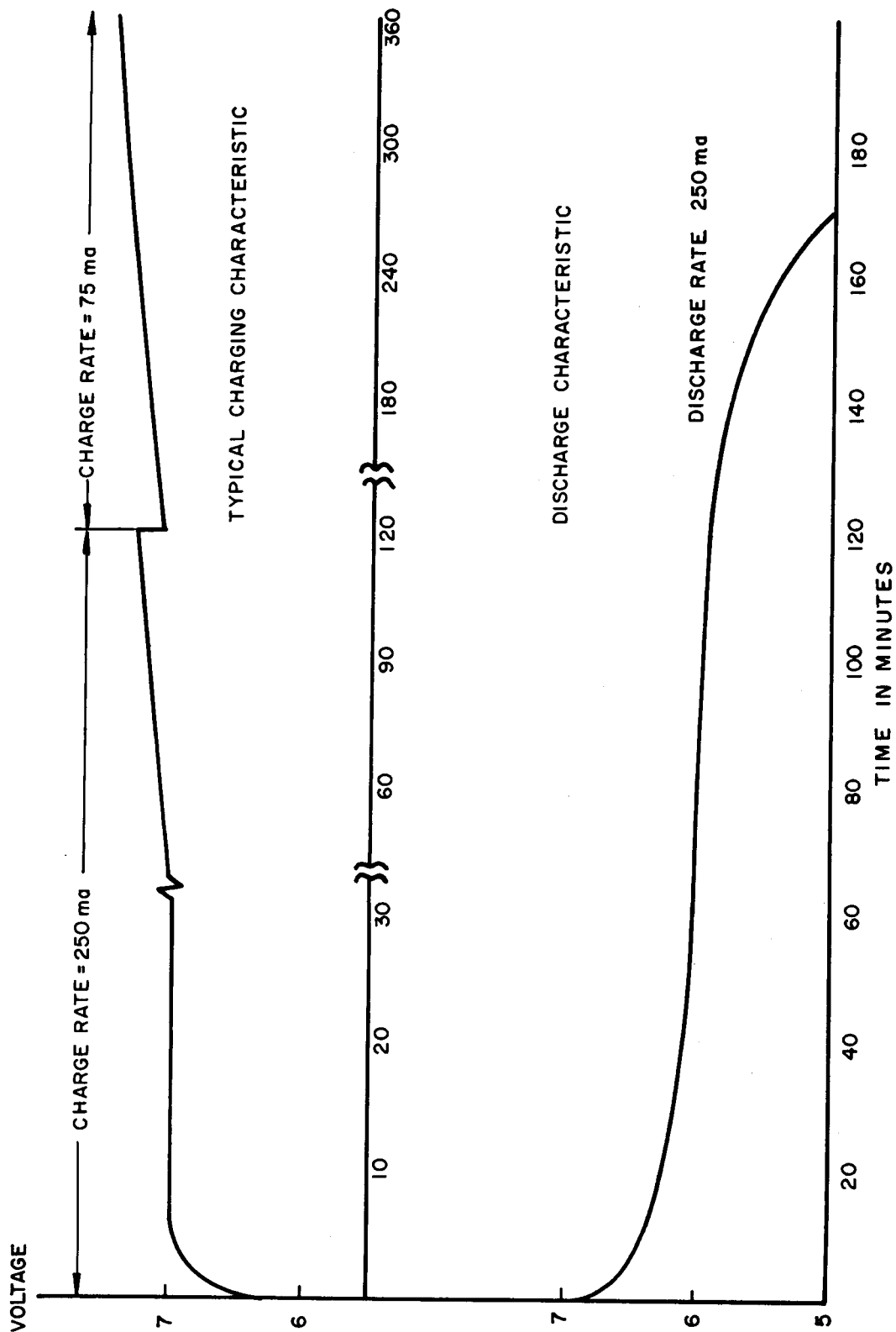
FIG. 74. TYPICAL CHARGE AND DISCHARGE CHARACTERISTICS OF A GULTON 5VO-.500 NICKEL-CADMIUM BATTERY

The batteries were packaged and installed in the battery and distributor assembly and then given two additional charge and discharge cycles to assure that no damage had occurred to the batteries.

A fourteen day temperature-vacuum cycling was given to the payload, with batteries operating a portion of the time at the extremes of the temperature range. After completion of this test, the batteries were given a complete discharge and charge cycle to determine if the batteries had deteriorated during the temperature-vacuum test.

SECTION V. BATTERY AND DISTRIBUTOR ASSEMBLY

The battery and distributor assembly shown in Figure 75 housed the nickel-cadmium batteries, served as the satellite's wiring distributor and provided mounting for the transmitter's one year cut-off timer. In conformance with the other instrumentation decks, this assembly was housed in a fiberglas cylinder with an indented wiring channel and was coated externally with polished aluminum foil for thermal control.

Figure 76 shows the instrument column withdrawn from the solar cell assembly and the outer cylinder. The battery and distributor assembly is the lower-most package in the instrument column.

A partially completed battery and distributor assembly and its components appear in Figures 77 and 78. The fiberglas housing and mounting plates weighed approximately 0.25 pounds, the 3 relays weighed about 0.1 pounds, and the one year timer weighed slightly under 0.5 pounds. As discussed in Battery Selection, Section I,5, Gulton button type cells were selected and purchased as series-connected cells of the desired voltage ratings. This configuration was purchased for ease of handling, processing, and to facilitate packaging. The complete power supply consisted of one 8VO-.180 (10.4 volts), one 5VO-.500 (6.5 volts) and three 4VO-.500 (15.6 volts) batteries. The total weight of the power supply was 1.76 pounds.

The completed battery and distributor assembly as it appears in Figure 79 weighed 3.05 pounds including foam potting and aluminum foil.

SECTION VI. NETWORKS

1. **General**

One of the major problems in satellite S-46 fabrication was that of integrating the various assemblies, sensors, and power supplies into a complete and functional system. This required the cooperation

RELAY SIGMA
93295

TERMINAL LUG

BATTERY
GULTON- 8 VO .180

BATTERY
GULTON 4 VO .500

BATTERY
GULTON- 5 VO .500

RELAY
8967567

FOAM POTTING COMPOUND TO BE
FLUSH WITH THIS SURFACE

.100

2.647
REF

CONNECTOR
CONTINENTAL MM 14- 22 SS

.06

.030

POTTING COMPOUND

G (.261) DRILL TWO HOLES

HOLES ARE FOR ROD CLEARANCE
AND ARE SHOWN FOR REF. ONLY

NOTE:

THESE SURFACES TO BE COVERED
WITH ADHESIVE, WATER RESISTANT,
WATERPROOF BARRIER-MATERIAL
MIL.- A-140 TYPE II, CLASS 2
GRADE B.

CONNECTOR
CONTINENTAL-MM 20- 22 SS

TIMER
BULOVA- 116001

CONNECTOR
CONTINENTAL MM 9- 22 PS

4.750 DIA BC

FIG. 75. BATTERY AND DISTRIBUTOR ASSEMBLY

126

Instrument Column

Solar Cell Assy

Cover

Outer Cylinder

FIG. 76. INSTRUMENT COLUMN WITHDRAWN FROM SOLAR CELL BOX AND OUTER CYLINDER
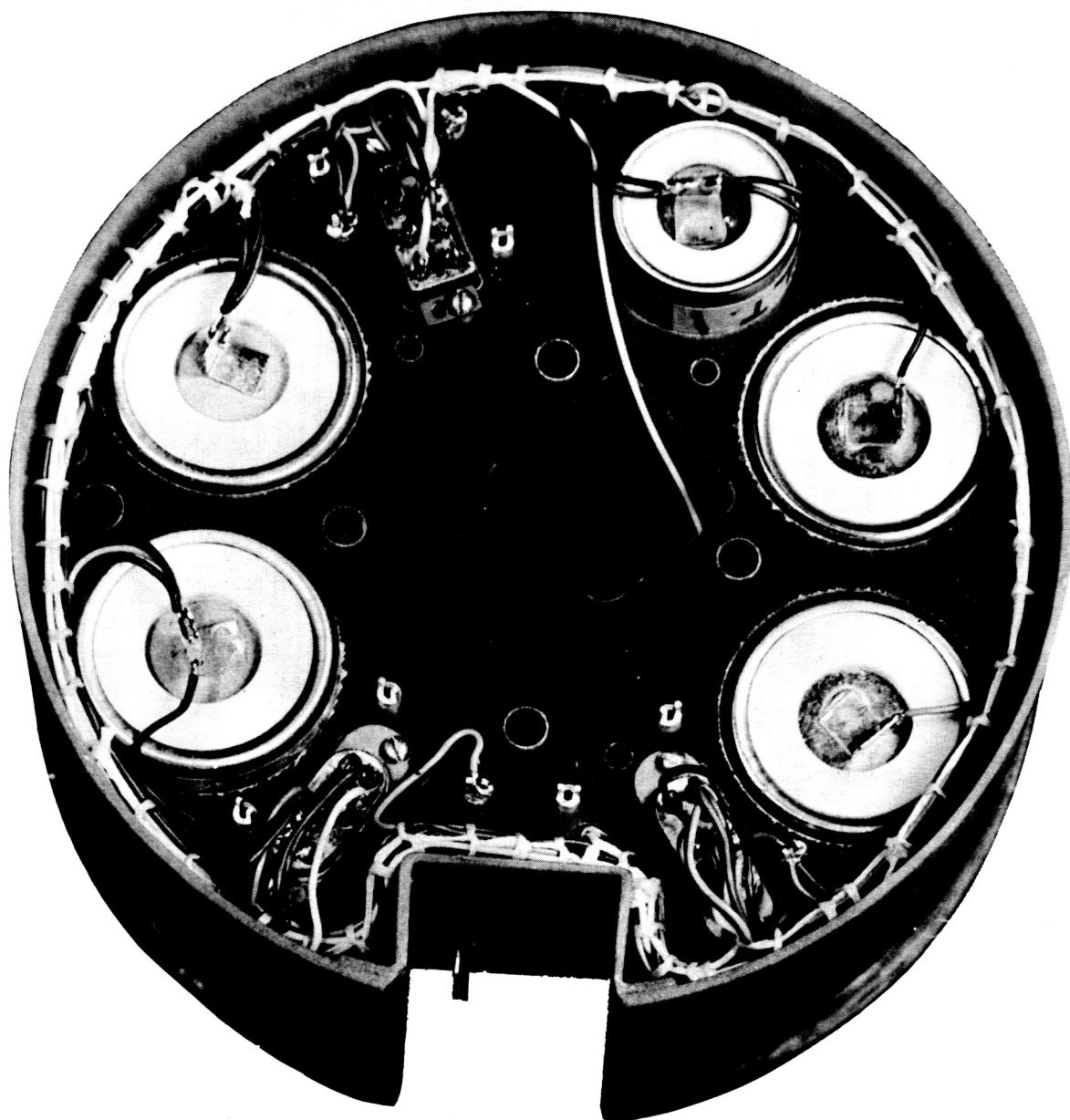
FIG. 77. BATTERY DISTRIBUTOR ASSEMBLY
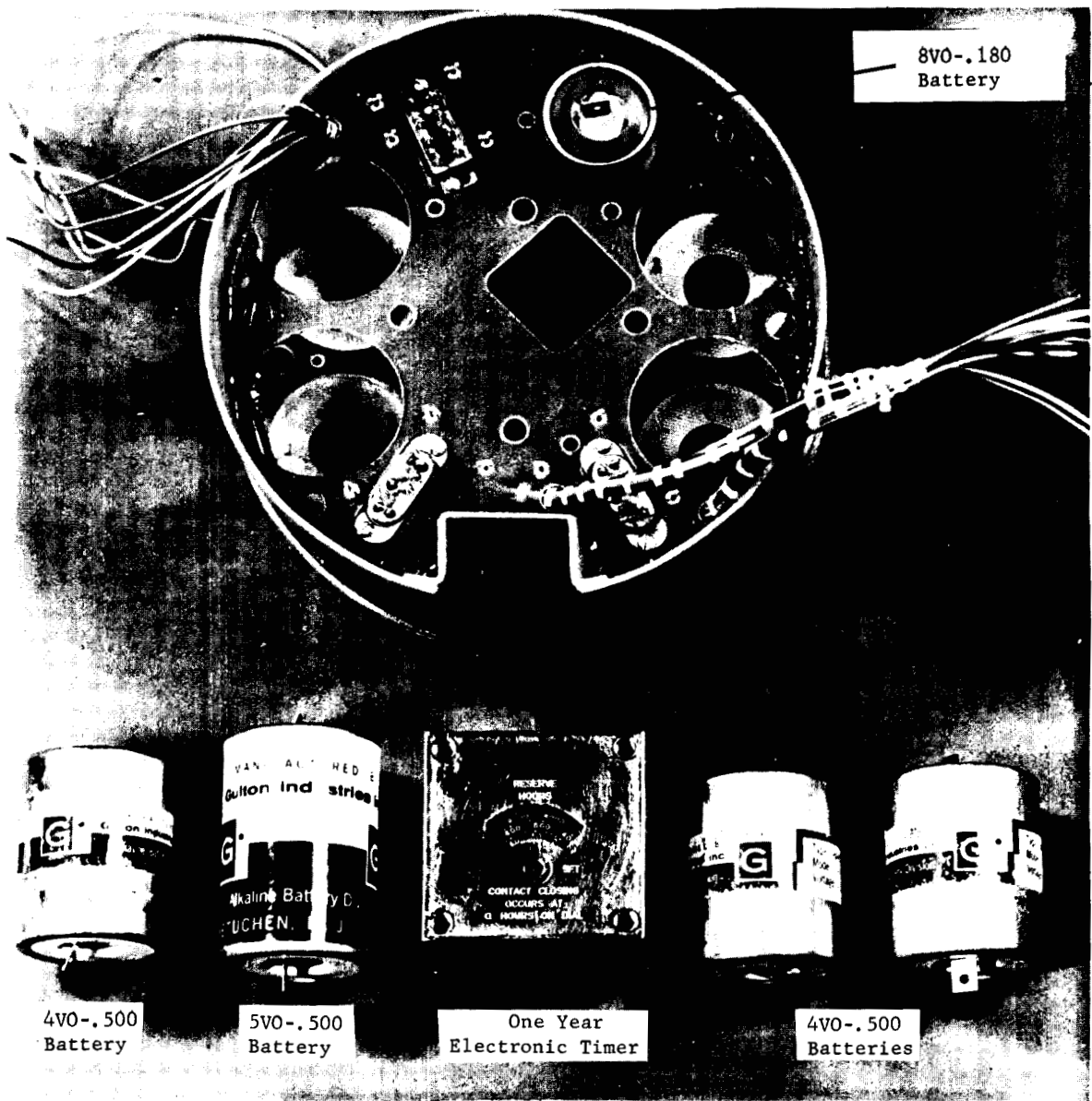
FIG. 78. BATTERY DISTRIBUTOR , BATTERIES, AND TIMER

S-46 Power Supply
and Instrumentation

COSMIC RAY
DETECTOR
PACK

SOLAR CELL
BOX
ASSEMBLY

MULTIPLEXER
ASSEMBLY

DECK "B"
SUB-CARRIER
OSCILLATOR

DECK "A"
SUB-CARRIER
OSCILLATOR

BATTERY
DISTRIBUTOR
ASSEMBLY

INSTRUMENT
HOUSING
ASSEMBLY

COVER
ASSEMBLY
INST. SHELL

RING
AND SPACER
ASSEMBLY

RING, LOWER
PAYLOAD
ADAPTER

RING INST.
SHELL COVER
MOUNTING

SPACER
INSTRUMENT
PACKAGES

TRANSMITTER
ASSEMBLY

RING ASSEMBLY
INSTRUMENT
PACK MOUNTING

ROD ASSEMBLY
INSTRUMENT
PACK

FIG. 79.   POWER SUPPLY AND INSTRUMENTATION ASSEMBLIES FOR S-46 SATELLITE

of the electronic, structural, electrical and thermal designers. For
example, the Tabor sensor for temperature measurements was designed by
the thermal designers in the Research Projects Division, but the struc-
tural designers of the Electro-Mechanical Design Branch designed most of the
hardware and provided for the proper mounting of the sensor. The Electri-
cal Networks Systems Branch provided terminal board space for mounting
calibrated resistors, wired the sensor, and provided cabling and connectors
for completing the sensor circuit to the multiplexer deck. Then, the
electronic designers of the Instrumentation Branch provided a multiplexer
system, the subcarrier oscillator channel and transmitter for relaying the
temperature information to the ground.

2. System Functions

Figure 80 shows a simplified line diagram of the payload power
and control system. The control relays K-1 and K-2 (Filtors, Inc, type
no. P26A1P6A) were used to interrupt the power circuits from the nickel-
cadmium batteries to the satellite's instrumentation during the extended
countdown time thus avoiding excessive discharge. To provide for system
operation and monitoring during countdown, the satellite was equipped
with a system for supplying power and control from the ground. This
system connected into the payload through the two Viking connectors P15
and P16, as illustrated in the lower right portion of Figure 81. The
Electrical Networks Systems Branch coordinated the electrical mating
of the satellite to the JPL cluster, as well as the mating of the cluster
to the booster. The choke assembly 3A1 was required for RF isolation of
the payolad from the fourth stage rocket since the ground control wiring
shunted the antenna gap. The fourth stage casing served as half of the
dipole antenna for the 108 mc transmitter.

Terminal Board 2A7 in Figure 81 served as a collection point for
combining the outputs of the individual solar cell panels and as a
mounting device for the +10.4-volt zener diode voltage regulators. It
was physically located on the internal structure of the solar cell box
assembly as shown by Figure 82.

3. Connectors and Harness

Figure 79 is a display of the various major assemblies which
composed the S-46 satellite. The assembled instrument column and the
payload housing with the solar cell box attached are shown in Figure 82.
It was intended that each instrument deck have its own connector so that
the cable harness could be easily assembled to and removed from the
column. From experience on Explorer VII, it was known that such a fea-
ture is especially desirable during prototype and environmental testing.
However, since the transmitter, sub-carrier oscillators, and multiplexer
were already near fabrication when this was established, connectors
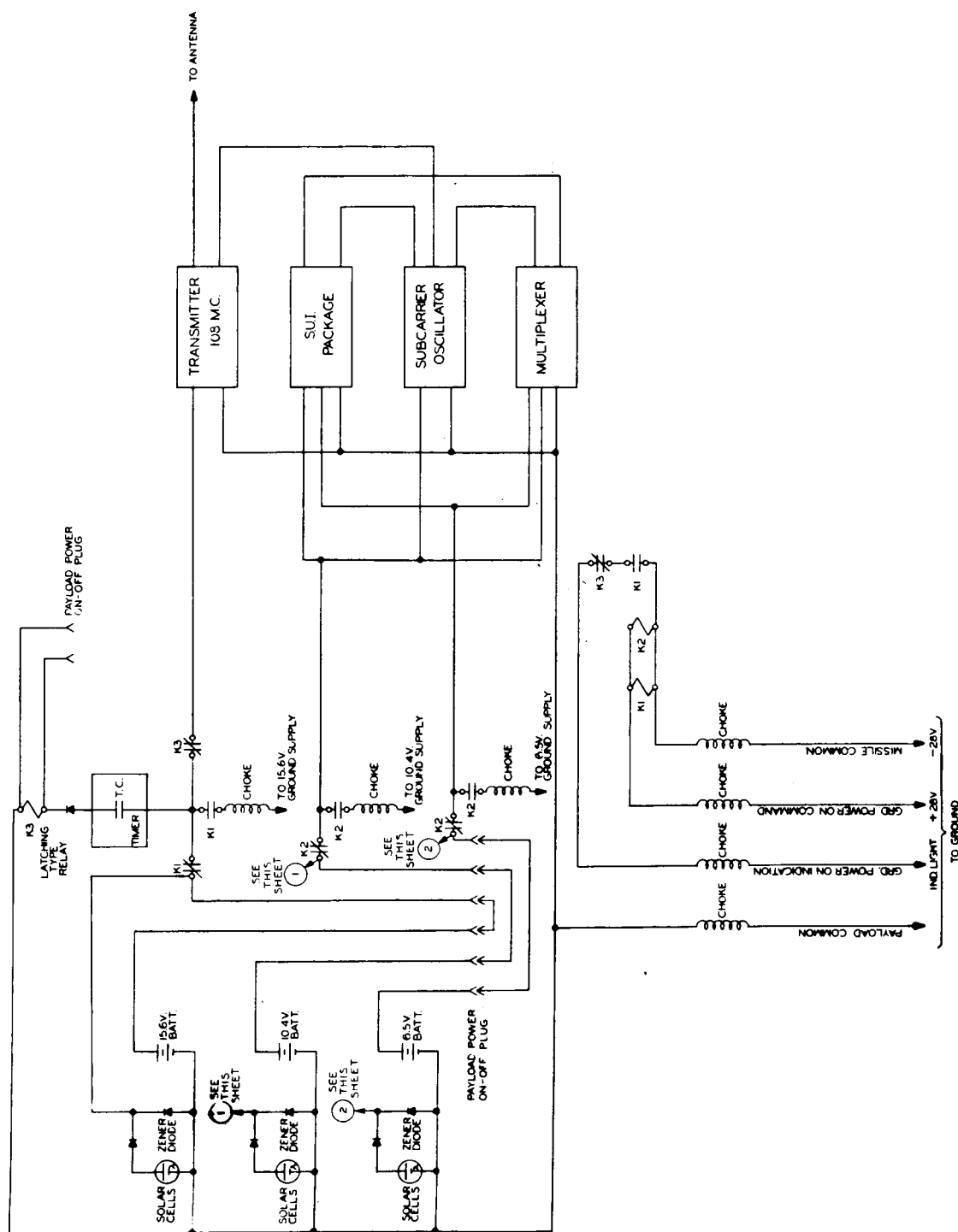
FIG. 80. SINGLE LINE DIAGRAM OF S-46 SATELLITE POWER AND CONTROL CIRCUIT
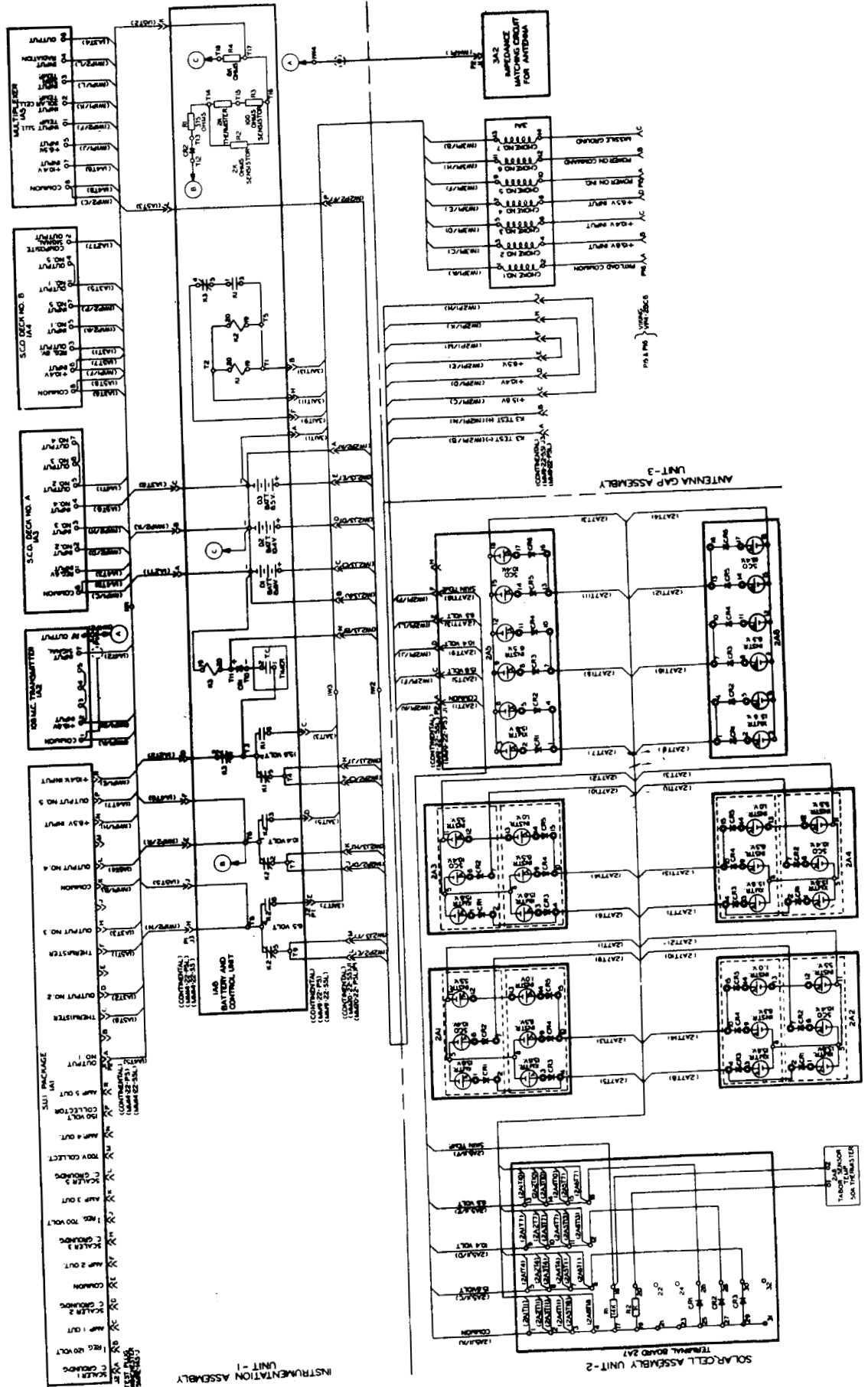
FIGURE 81. WIRING DIAGRAM FOR S-46 SATELLITE
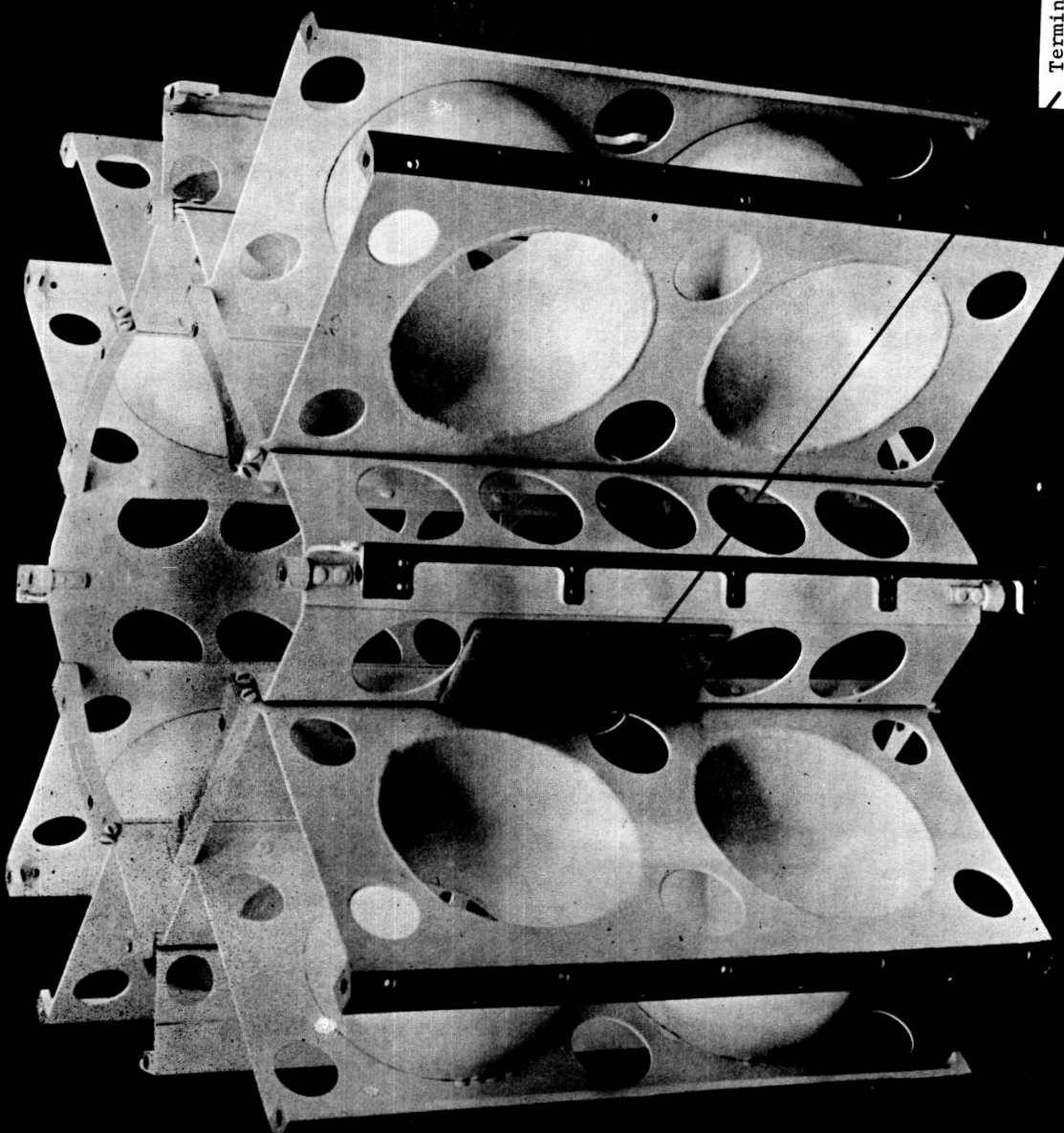
FIG. 82. INTERNAL STRUCTURE OF SOLAR CELL BOX ASSEMBLY

Terminal
Board 2A7

could only be utilized on the SUI (1A1) package, the battery and distrib-
utor assembly (1A6), the solar cell box, etc. The smallest connector
suitable for this.purpose, which had been tested environmentally, was the
Continental micro-miniature series with screw lock. For example, the
connector shown on Figure 77 is connector J-3 in Figure 81 and was a type
MM14-22-SS, 14 pin, no. 22 wire cups, wall-mount, socket connector. For
reliability, the solder cups and wiring were made more rugged with
Armstrong X-81 epoxy resin after soldering and inspection.

4. Test Points

It had been found necessary during the Explorer VII program to
provide ample external test points from the network and instruments to
allow convenient access to circuits which must be monitored during func-
tional and environmental testing. This also eliminates possible damage
caused by repeated disconnections and partial disassembly to obtain meas-
urements. Connectors J-1 on the SUI package and J-3 located on the
antenna gap provided such test points on this satellite. In addition,
the removal of the blind plug P-3 from J-3 allowed the internal battery
circuits to be interrupted to preserve the battery charge during long
standby periods without the need for keeping relays K-1 and K-2 energized.

5. Wiring

In general, the network wiring was 19 strand, AWG no. 24 wire
with an extruded nylon outer jacket. The type used was Surprenant
BUB1936U, Spec. A-10, which was environmentally proven in the Explorer
VII program. Not only had this been excellent wire for environmental
extremes, but it was also light in weight and was easily worked.

SECTION VII. ONE YEAR ELECTRONIC TIMER

To avoid saturating a frequency band with useless radio signals, it
was necessary to include a device to shut off the 108 mc transmitter
after one year of operation, otherwise, the transmitter could possibly
operate as long as the solar cell power system continued to function.

A one year electronic timer was incorporated in the battery and
distributor assembly to provide an accurate and reliable means of inter-
rupting the transmitter after one year of satellite life (Fig. 75). The
timer, Bulova Part No. 664A was the same as the one used in Explorer VII.
It is a precision, electronic watch type mechanism capable of timing long
intervals with an accuracy of better than 0.1%. It was set to operate
after 8760 hours on satellite S-46.

At the end of the preset (one year) period an internal microswitch was to operate which would close the K-3 relay circuit (Fig. 81) to the 15.6-volt supply. Operation of K-3 would interrupt the transmitter power supply and the relay would latch magnetically to permanently withhold transmitter power. K-3 was a Sigma, Inc. type 93295 double pole-double throw, magnetic latching relay with two-ampere contacts. Its coil resistance was 750 ohms and the nominal rating was 12 volts, however, eight volts was sufficient to transfer the contacts.

The latching action of the relay K-3 was necessary to permanently cut off the system since the timer after completing a 10,000 hour cycle, could otherwise restore power to the transmitter.

Chapter 6

THERMAL DESIGN OF S-46

William Snoddy

Space Thermodynamics Branch, Research Projects Division,
National Aeronautics and Space Administration,
Marshall Space Flight Center, Huntsville, Alabama

SECTION I.   INTRODUCTION

The thermal design of satellite S-46 was based on the method of pas-
sive control used in all of the Explorer satellites in the Juno I and II
programs.   This philosophy involves equalizing the satellite skin tempera-
tures as much as possible and thermally insulating the instrument package
from the skin.

In order to evaluate and confirm the effectiveness of the design
scheme, two types of thermal tests, as described in Chapter 7, were
run on one of the prototypes (No. PL-1).   In one test the temperature
of the skin was varied in as near a step-function as possible, while in
the other test the prototype was subjected to heat fluxes similar to
those which would be encountered in space.   The deviations of the meas-
ured data from theoretical values were not considered sufficient to
necessitate any changes in the flight unit design.

SECTION II.   THERMAL DESIGN PHILOSOPHY

The thermal design problems were those involved with maintaining
thermal balance.   Proper thermal balance can be defined as keeping the
temperatures of various parts of the satellite within certain ranges
throughout the instrument lifetime, which was anticipated as one year for
S-46.

Several design philosophies were considered for satellite S-46.   The
passive control method of equalizing the skin temperatures and thermally
insulating the instrument package from the skin was selected.   Equiliza-
tion of the temperatures over the skin would prevent the development of

hot spots, which would lower the efficiency of solar cells in these areas. Skin temperature fluctuates over a wide range as a satellite travels in and out of the earth's shadow. The insulation between the S-46 instrument package and the skin prevented the instrument package temperature from fluctuating as widely as that of the skin, thereby keeping the instrument temperature close to the average value of the skin temperature. The insulation was of even greater importance on this satellite because of the extremely elliptical orbit. The apogee was to be greater than six earth radii, which meant that the satellite would have a period greater than 10 hours. Thus, there was a good chance that sometime during the one-year operating lifetime the orbit would be such that the satellite would spend at least one hour in the earth's shadow during each revolution. Because the average emmissivity of the skin of the satellite must be fairly high to keep the solar cells cool when the satellite is in the sunlight, and the heat capacity was low (the total weight of the S-46 flight unit was only about 22 pounds), the temperature of the skin would drop very fast when the S-46 entered the shadow. Therefore there had to be extremely good insulation between the instruments and the skin to prevent their "freezing out" in the shadow.

Figures 83 and 84 show the external surfaces of the flight unit of S-46. The instrument package shell outside the solar cell box, the package cover, and Geiger tube cover, were sandblasted aluminum. The solar cells were cemented directly to an anodized magnesium box. On the flight payload, each solar cell was covered with a glass slide, introducing an uncertainty into the temperature calculations. Changes in the orbit necessitated replacing the Rokide surface used on the test prototype heat balance strips with a "Tabor" surface, which is very "black" to solar radiation ($\alpha \approx .9$) and has a low infrared emissivity ($\epsilon \approx .3$). The fiberglas antenna gap thermally insulates the payload from the attached fourth stage motor case. The magnesium framework for the solar cell box (Fig. 85) and the part of the instrument package shell inside the solar cell box (Fig. 86) were painted with TiO_2 so the surfaces would have a high emissivity, which would aid in the equalization of skin temperatures. The high emissivity of the anodized surface eliminated the necessity of painting the inside of the solar cell box itself. To save weight, holes were cut in the part of the instrument package shell located under the solar cell box; the holes were then covered with thin aluminum foil except for the top and bottom rows of holes which were left partially uncovered to provide openings for outgassing.

The Dewar flask principle was used to insulate the instrument package from the skin. The inside of the instrument package shell (Fig. 87) and
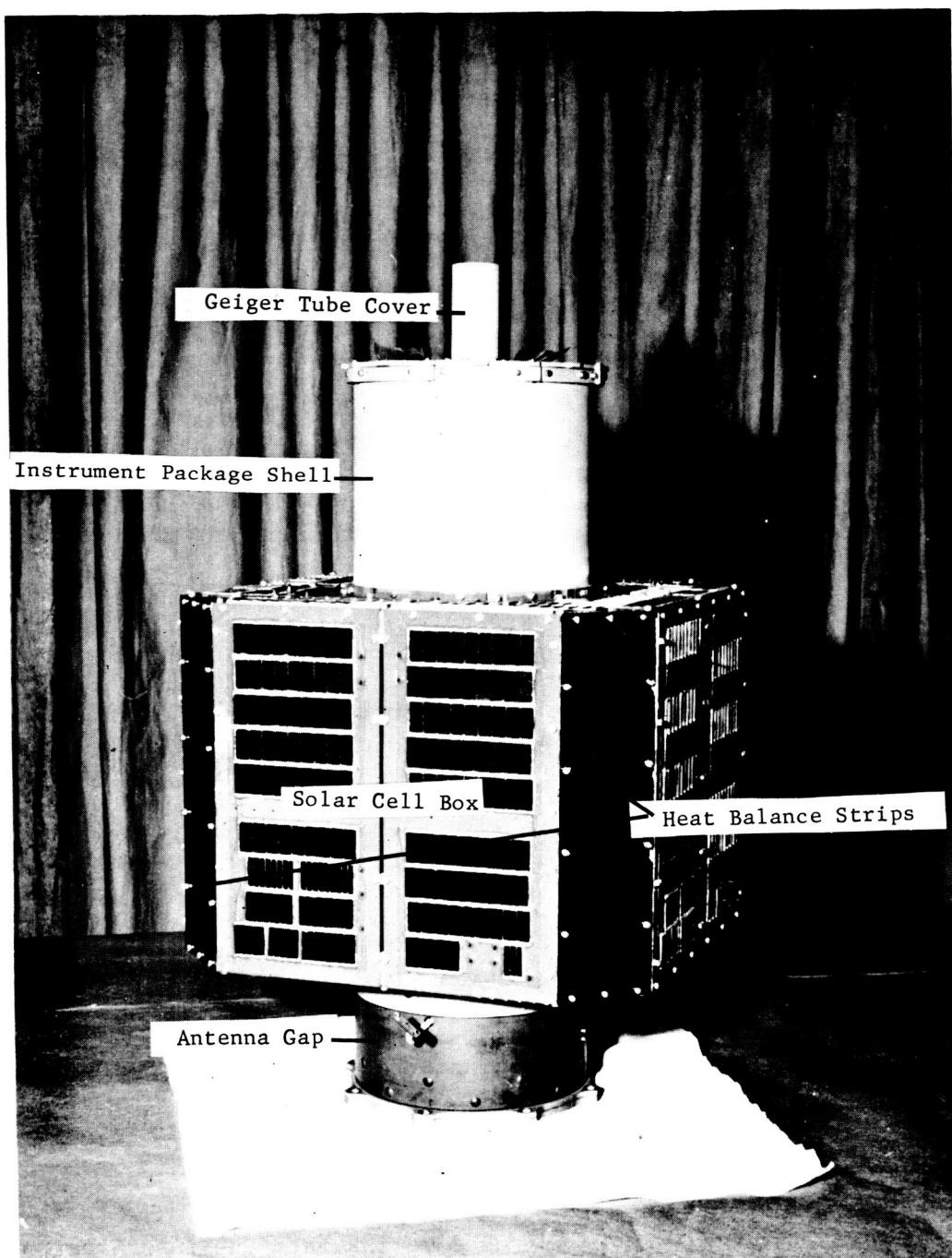
FIG. 83. FLIGHT MODEL OF PAYLOAD S-46
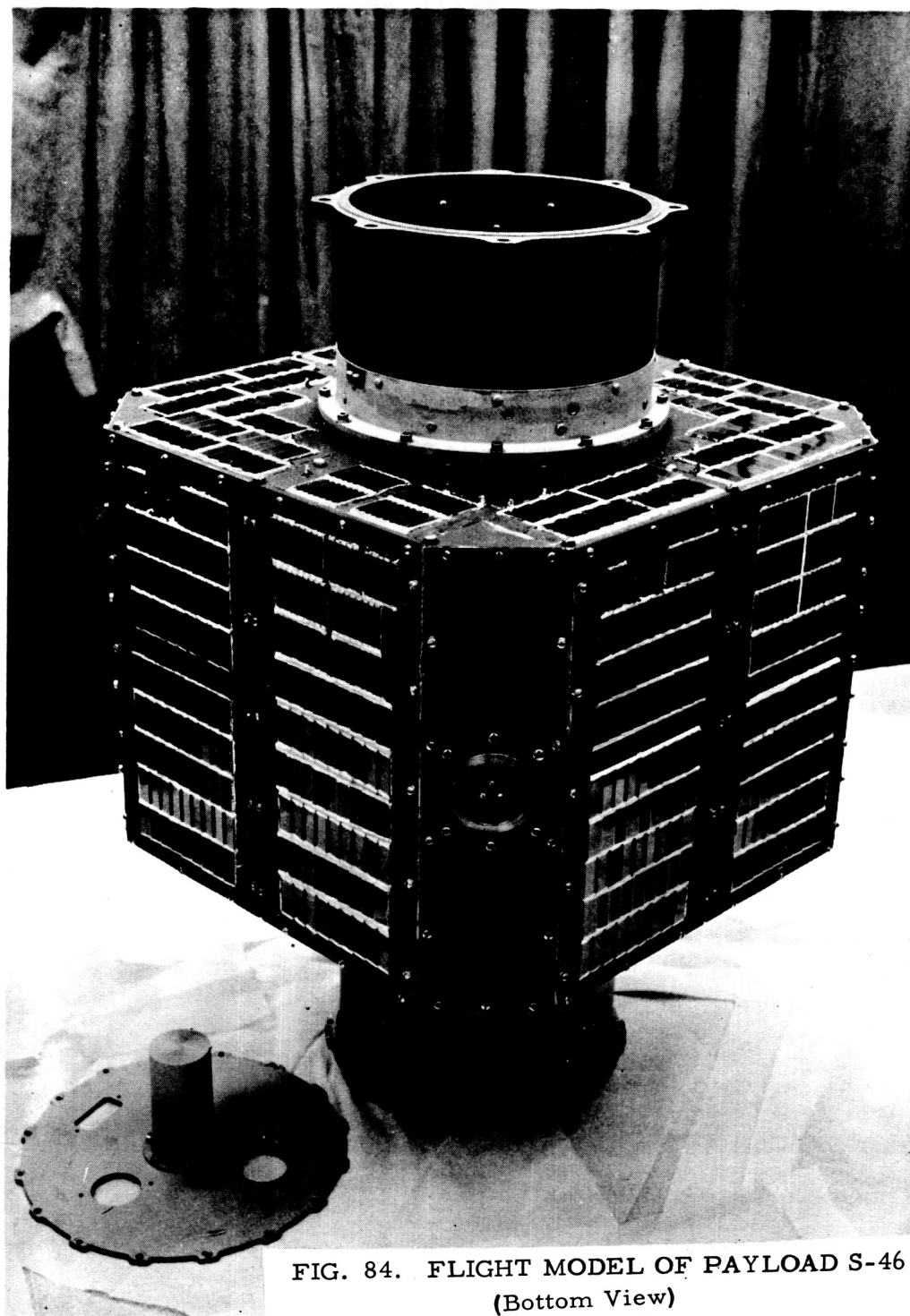
FIG. 84.   FLIGHT MODEL OF PAYLOAD S-46
(Bottom View)
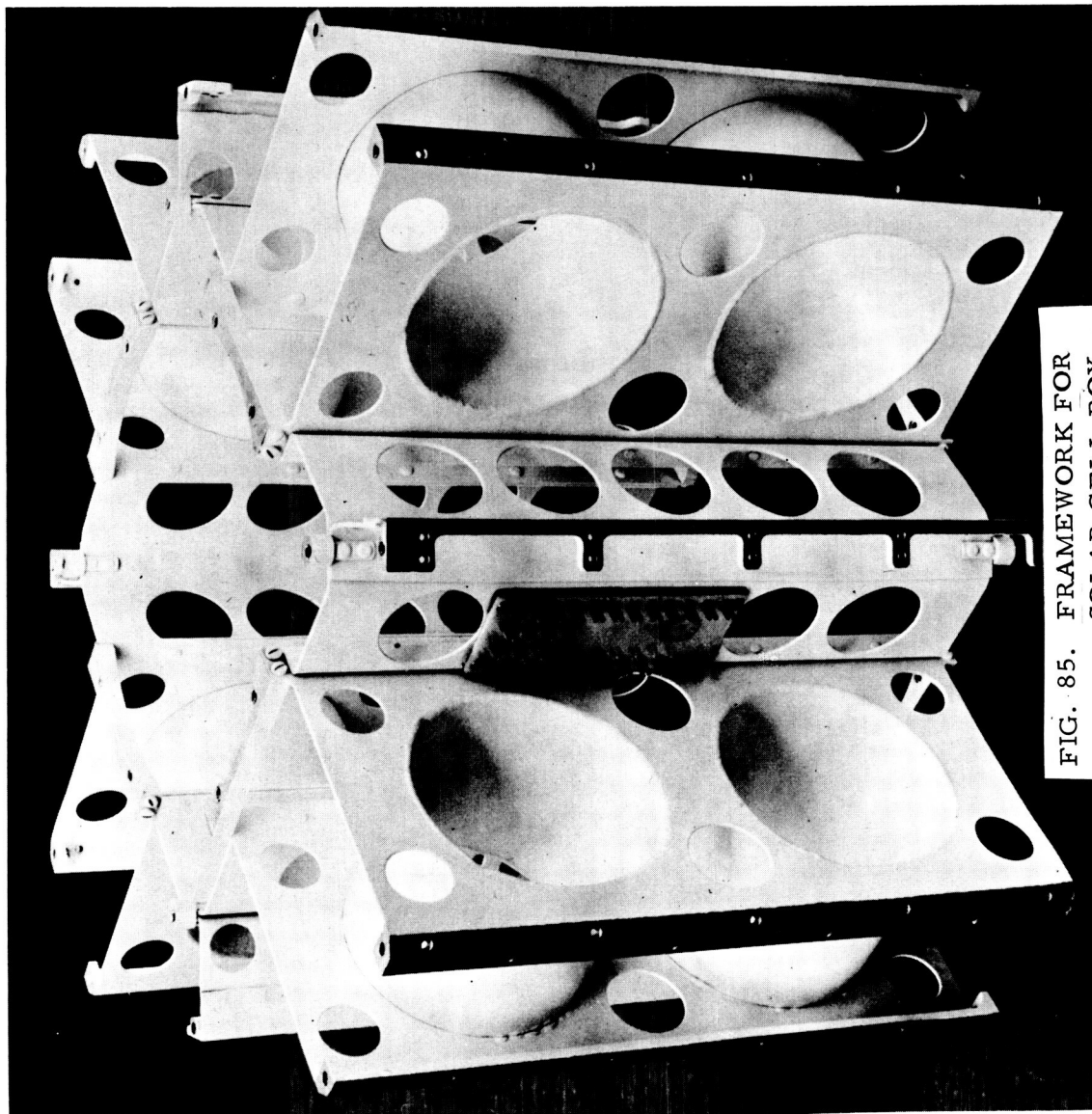
FIG. 85. FRAMEWORK FOR SOLAR CELL BOX

Top, Instrument Package Shell
(sandblasted surface protected by
removeable coating)

The Part of the Shell that is
Inside Solar Cell Box
(Painted with T_1O_2)

Antenna Gap

FIG. 86. INSTRUMENT HOUSING

Inside of Instrument Package Shell
(highly reflective)
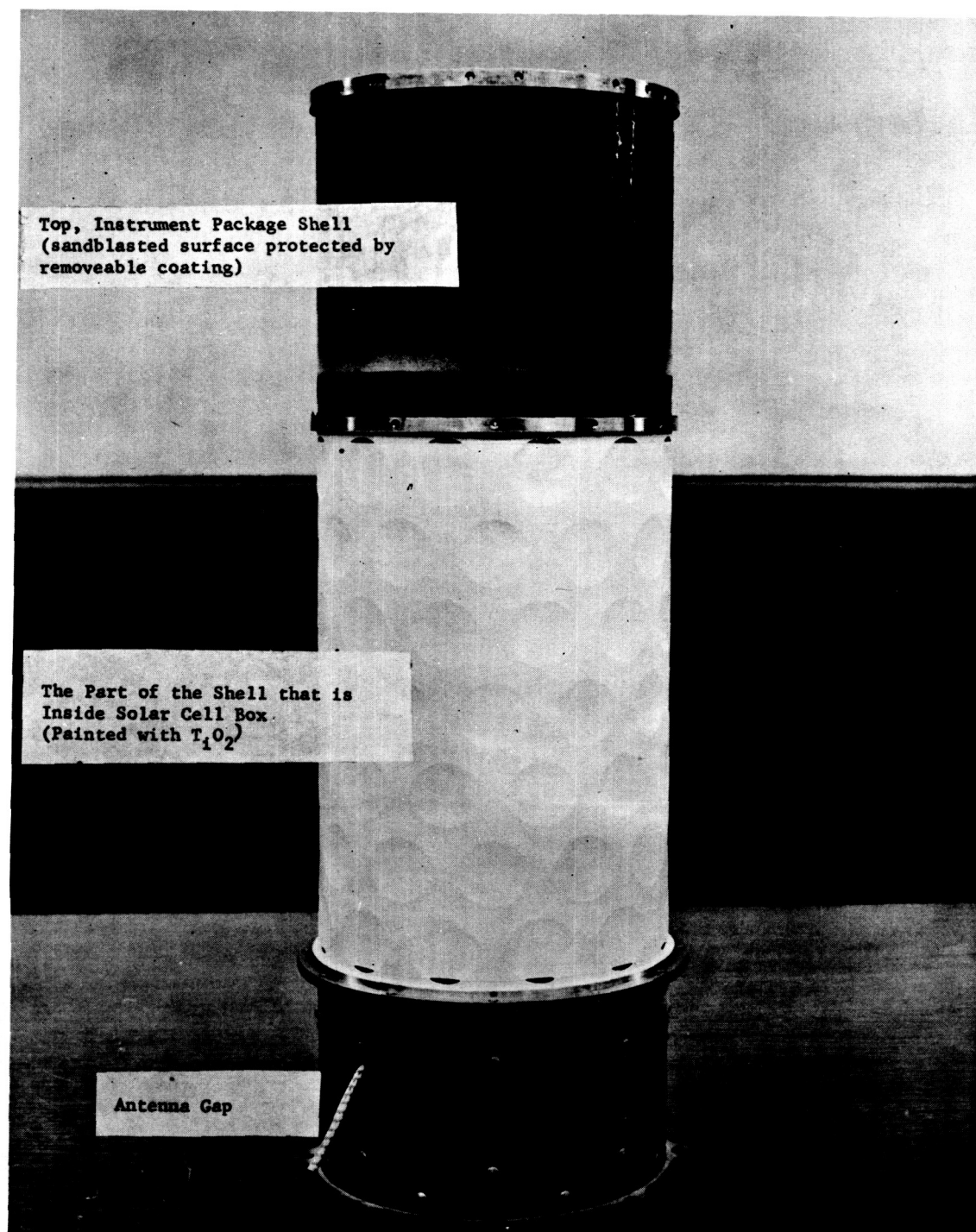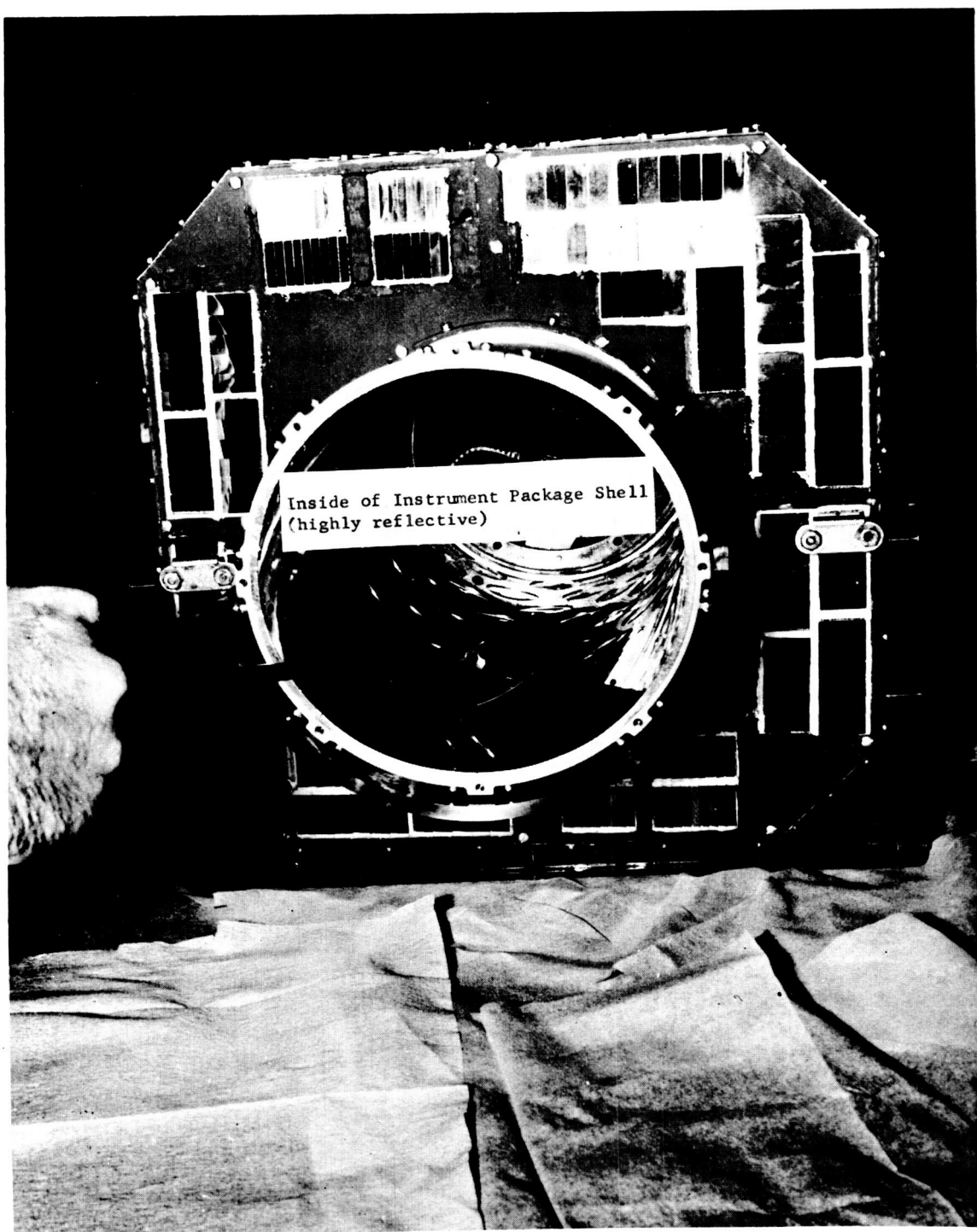
FIG. 87.   INSIDE VIEW OF INSTRUMENT HOUSING

the outside of the instrument package (Fig. 88) are highly polished aluminum to reduce radiation; the support rings between the instrument package and the shell were made of thermally insulated materials (fiber-glas and Kel-F) to reduce conduction; and the vacuum of space along with the outgassing holes assured that convection would be negligible.

SECTION III. RELATION OF THERMAL TEST TO DESIGN PHILOSOPHY

From thermal tests on earlier payloads[1,2,3] it was learned that simulated tests are necessary to determine the conduction and radiation coefficients. Also, many unexpected anomalies were encountered during previous tests which necessitated changes in the payload.

Two types of thermal tests were run on this protoype (Chapter 7, Section IV.4.j.). One consisted of cooling the prototype to a uniform temperature of about -20°C. Then, while in a vacuum of 5 x 10^{-4} mm Hg, or greater, the outside surfaces were raised to a temperature of 80°C as rapidly as possible in an attempt to simulate a step-rise in temperature. The outside temperature was then held to a constant 80°C and the temperatures of various parts of the instrument package were recorded. From these tests it was possible to get over-all thermal transfer coefficients between various parts of the instrument package and the skin.

In the second set of tests the payload was again cooled to a uniform temperature of about -20°C. Then, while under vacuum, heat was applied to those areas the sun would "see" if it were incident at an angle perpendicular to one side of the solar cell box. In space, the net amount of heat entering a surface is equal to the absorbed radiation from the sun, earth, and any other radiating object that the surface can "see", minus the heat that is re-radiated by the surface. A simplified mathematical expression for this is:

$$Q_{net} = A_s \alpha S + A_{se} \alpha B S_g + A_{ie} \epsilon E S_g - A_r \epsilon \sigma T^4$$

1. G. Heller, The Temperature of an Orbiter. ABMA Report No. DV-TN-44, 17 June 1957.

2. W. Snoddy, Heat Transfer Constants of Payloads No. 44 and No. 47. ABMA Report No. DV-TN-59-58, 28 July 1958.

3. B. Jones, Thermal Design Tests of the IGY Satellite (Payload of Missile No. 16). ABMA Report No. DV-TM-23-59, 10 August 1959.
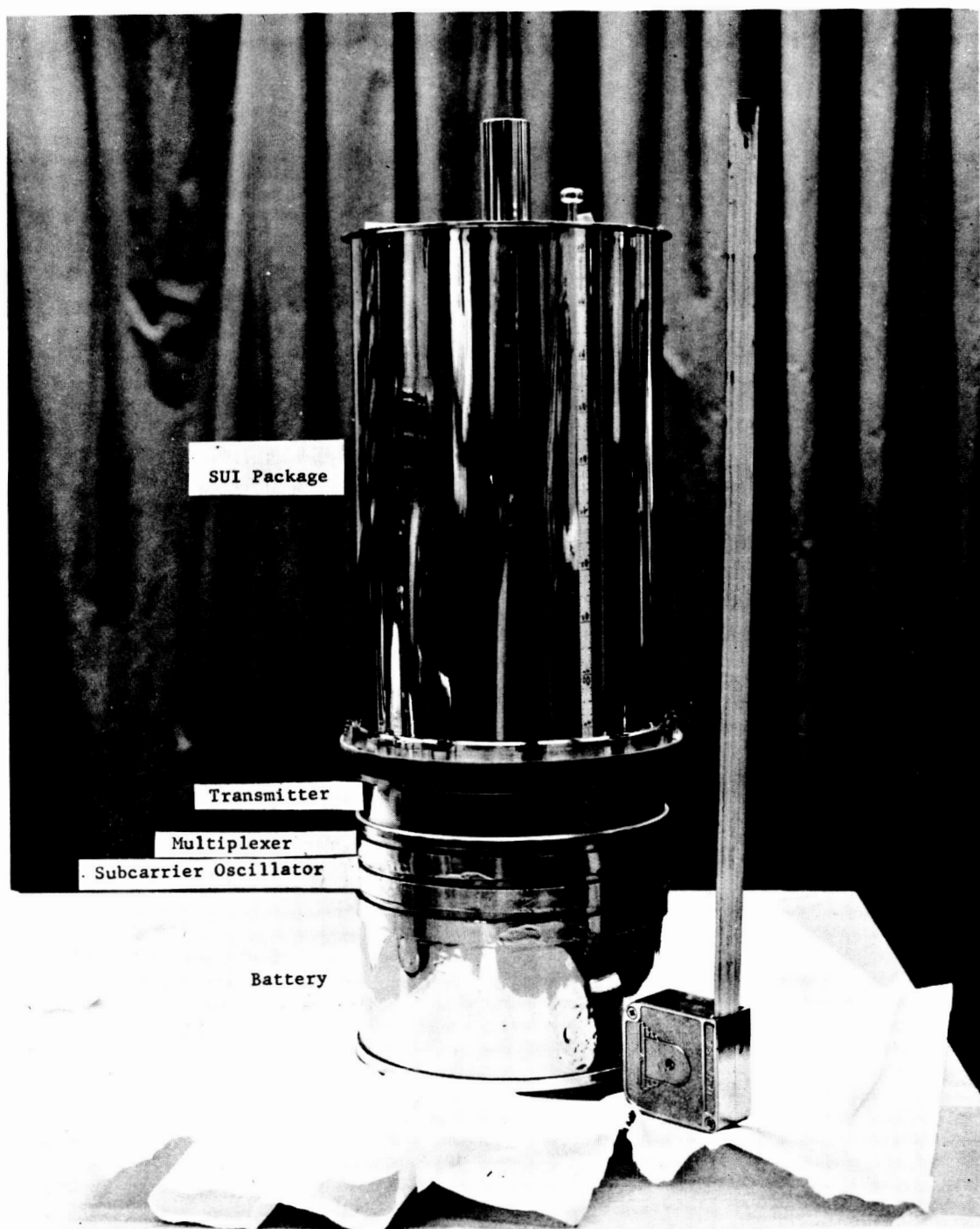
FIG. 88. S-46 INSTRUMENT COLUMN

where:

Q_{net} = net heat flow across the surface

A_s = effective area for solar radiation

α = surface absorptivity for solar radiation

S = solar constant (1200 kcal/hr m^2)

A_{se} = effective area for reflected solar radiation from earth

B = per cent of solar radiation reflected from earth ($\approx$ 40%)

g = altitude factor

A_{ie} = effective area for infrared radiation from earth

ϵ = emissivity of satellite at about room temperature
= absorptivity for earth infrared radiation

E = infrared energy flux from earth as a percentage of solar constant

A_r = radiating area of surface

σ = Stephan-Boltzmann constant

T = temperature of surface

Taking average values of all the factors, except the temperature of the surface, the net heat flow into the surface will be a function of temperature only. Using this equation, the heat inputs to the surfaces were controlled as a function of the temperatures of the surfaces. As the temperatures of the surfaces increased, the heat inputs were decreased to a point where the heat going into the surfaces no longer increased the temperatures of the surfaces, but was conducted and radiated to the unheated parts of the prototype. These unheated surfaces were allowed to radiate as freely as possible. Thus, a steady state condition, very close to the condition in space previously described, was established. Gradients were established between various parts of the satellite; with a knowledge of the heat input, the thermal transfer coefficients could be determined. These coefficients were then put into a computer program to calculate the gradients that exist during various tumbling and spinning motions of the satellite.

The details of these tests are reported in Chapter 7, Section III.

SECTION IV. RESULTS AND CONCLUSIONS

The measured time constant of about five hours for the instrument package gave an over-all thermal transfer coefficient of about

.14 kcal/hr °C, which agreed well with the theoretical value of .18 kcal/hr °C. Thus, if the satellite entered the earth's shadow for one hour, the instrument package temperature would drop about 6°C, depending on other parameters. This amount of insulation was considered sufficient from the standpoint of thermal balance, consequently, no changes were made in the insulation design. From the half-blanket tests, thermal transfer coefficients between various parts of the skin were determined and incorporated into the IBM 704 theoretical orbital temperature program. A qualitative study of the data indicated that the instrument package maintains a uniform temperature even when high gradients exist around the skin and that this uniform value is near the average value of the skin temperature. A comparison between heat input and the steady state temperatures obtained indicated that the tests were a reasonable simulation of space conditions using infrared input instead of radiation in the solar spectrum.

Due to the difficulty involved in removing the instrument package from the prototype because of the thermocouple wires, it was not removed until after completion of the test. At this time a small amount of grease was noted on certain areas of the prototype unit. Analysis showed the grease to be composed of poly-n-butylmethacrylate and an epoxy resin. It had come from the thermocouple wiring. Substitution of another type of thermocouple wire was made for the "soak" test and no more deposits were found.

A better simulation of environmental conditions can be made for future tests by increasing the effective area of the liquid nitrogen coil system, so that the radiating surfaces will have a better sink. Also, the surface emissivity of the coils should be increased to make them more effective in absorbing the infrared radiation from the satellite. With these changes it is felt that a close approximation to actual orbital temperature conditions can be made. Under these conditions not only can various transfer coefficients be determined, but the actual value of the orbital temperatures can be obtained.

The greatest error would be in the assumption of the solar absorptivity and infrared emissivity of the heated surfaces which are used in calculating the blanket control curves (see Fig. 95). Another highly desirable improvement would be to substitute a radiation source which has the intensity and spectral distribution of the sun for the heat blankets. This would eliminate the necessity for assuming the solar absorptivity and infrared emissivity, and even allow the actual surface characteristics to be determined from the test results. With this type of setup, tests could be run on flight units to check out surface characteristics and internal transfer coefficients. In the past, many changes have been made on the design of the flight unit between the thermal tests on the prototype and the completion of the construction of the flight unit. These changes produce uncertainties in the theoretical temperature calculations.

Highly critical surfaces make the use of blankets undesirable in measuring characteristics of the flight units. However, if the radiation setup were used, the check could be made without affecting the flight unit.

Such a radiation setup would be extremely desirable for future satellite thermal tests because of the complex nature of their design. This setup would also be useful in the evaluation of temperature data telemetered from satellites by allowing experimental investigation of anomalies that occur in the satellites, using a prototype or the "backup" flight unit.

Chapter 7

TESTING

SECTION I.   INTRODUCTION

Past experience has indicated the importance of testing in insuring successful performance of an instrumented satellite. Consequently, a comprehensive set of tests was performed on the S-46 payloads to give maximum assurance of a low probability for electrical or mechanical failure during launch and in orbit. In electrical and electronic instrumentation, in general, the probability of failure rises exponentially as the number of components increases. The S-46 SUI radiation package alone contained 255 transistors. Overall reliability will be high only if the probability of failure of individual electrical or electronic components is very low. As for the mechanical structure, making the parts large to provide a good strength safety factor was not a solution for the S-46 because of the requirement for minimum weight. The solution was to utilize an extensive structural testing program in order to obtain a trustworthy estimate of the probability of failure.

Five satellite units were manufactured for the S-46 program. Table 2 sets forth the ABMA payload identification numbers, the related SUI radiation package numbers, and the way each payload was utilized in the program.

In the remainder of this chapter a description is given of the tests performed on the radiation package at SUI, the thermal, electronic, and environmental tests performed on the ABMA portions of the payloads (telemetry, low voltage power supply, structure, etc.), and the tests performed on the completed S-46 prototype and flight units. Complete test procedures and specifications for the tests, both at SUI and at ABMA are included in separate sections.

SECTION II.   TEST PROGRAM AT SUI

The testing program which the State University of Iowa followed in its part of the S-46 program can be divided into four major divisions:

1. Testing of Individual Components

Individual electronic components (and structural elements in some cases) were carefully checked both mechanically and electrically

before insertion into the circuits. At SUI most components were tested, aged, and retested. The aging process was accelerated by placing them in an oven at a temperature of 120°C for a period of approximately 15 days. It was required that the parameters of the components not change excessively during the aging period. An outline of the component test procedures and specifications is contained in Section IV.1 for the SUI instrumentation. The testing program followed at ABMA for the components used in the telemetry and power systems was somewhat similar and is described in Section III.1.

2. Testing of Modules Before Encapsulation

An extensive series of tests was employed at SUI following assembly of the electronics circuits to insure that the electrical design had been sufficiently conservative to allow for changes in component parameters under various operating conditions, to select critical components where necessary to assure reliable operation, and to discover components which were functioning abnormally. Individual module performance was recorded at this time for future reference and for comparison with later readings. Each solder joint was visually inspected under a microscope to detect improperly soldered connections and the modules were mechanically inspected by an ABMA inspector. Following these tests and inspections, the modules were encapsulated.

As in paragraph 1, a parallel testing program on the telemetry modules and power supply was followed at ABMA and is reported in Section III.2. The SUI program is outlined in Section IV.2.

3. Subassembly Testing

Following assembly of the SUI instrumentation package by stacking and wiring the modules, the package was subjected to a series of electrical and mechanical tests and detector calibrations. The primary purpose of the tests was to ascertain that the completed package was a reliable and fully operational unit before it was delivered to ABMA. The calibrations were made to gain as complete an understanding of the detector characteristics as possible. This was the last complete set of tests performed on the SUI instruments by the builders. Although an SUI representative was present at ABMA during the conduct of the payload assembly and environmental testing program there, freedom to work on the SUI instruments was necessarily curtailed at the time they were delivered to ABMA. Access was assured in the event of failure or suspicion of abnormality and for final payload calibration at the launch site.

An outline of the SUI package testing program is contained in Section IV.3. The environmental tests performed at SUI included vibration, temperature, and vacuum, these conditions being by far the most stringent.

Several abnormalities occurred at SUI during this testing program. They were:

     a. PT-1, vibration test in thrust direction at 25 g RMS; channel three counting rate equal to zero after test; failure of G-M counter; counter replaced.

     b. PT-2, vibration test perpendicular to thrust direction and to spectrometer counter axis at 15 g RMS; channel four counting rate equal to zero after test; breakage of G-M counter center wire; counter replaced.

     c. PT-3, vibration test; change in channel one rate; dirt particle in detector A aperture; dislodged.

     d. PT-3, vacuum test; arc-over of 700 volt power supply; incomplete bonding of foam to circuit components; not repaired since unit was to be used for thermal constant measurement; 700 volt system in all other units coated with epoxy resin to obtain more complete seal.

     e. FU-1, vacuum test; arc-over of 700 volt power supply; incomplete bonding of epoxy resin; repaired.

The specifications for these SUI tests were in many cases more severe than the specifications established by ABMA. Although this may have been unnecessary, it is interesting to consider the small number of abnormalities which developed after the SUI packages left the State University of Iowa laboratory. There were no failures of the flight unit packages which required cutting into the foam for repair. The abnormalities are listed in the next paragraph.

4.   Testing of the Complete Payload at ABMA

Final test of the SUI packages took place as a part of the complete payload tests performed at ABMA. These tests, reported in Section III.4, were in accordance with the payload test specifications contained in Section IV.

It is felt that the SUI reliability program achieved its objectives, as evidenced by the small number of failures incurred during the ABMA testing program, and by the fact that the instrumentation operated properly during its launch trajectory. A complete list of all abnormalities which developed in the SUI assembly during the ABMA testing is as follows. (The failures which occurred in the ABMA components of the payloads are reported in Section III.4).

a. PT-2, preliminary testing; intermittent high channel three switching rate; improper quenching of detector C G-M counter; new detector C and D G-M counters installed at SUI.

b. PT-2, temperature-vacuum soak test; change in 700 volt power supply regulator current after six hours at 50°C; failure of transistor in power supply; transistors and bias resistor changed.

c. PT-2, temperature-vacuum soak test; intermittent change by a factor of two in the channel three switching rate after 12 hours at 50°C and 12 hours at 0°C, on way to room temperature; failure of transistor in scalar stage four; transistor changed at SUI after completion of tests.

d. PT-2, temperature-vacuum soak test; slow drift in channel five output voltage after about five days at 50°C; change in characteristics of 2N338 transistor in output amplifier; transistor changed at SUI after completion of tests.

e. PT-2, temperature-vacuum soak test; SUI temperature measurement inoperative; open circuit in thermistor; not changed.

f. FU-1, vibration test; change in channel two rate; dirt particle in detector B aperture; removed.

g. FU-2, vibration test; change in channel one rate; paint chip in detector A aperture; removed.

h. FU-2, temperature-vacuum calibration; inability to ground the channel one integrating circuit capacitor through the TS shorting plug; open circuit between wiring channel and test socket; capacitor grounded by soldered jumper in wiring channel during Cape Canaveral checkout.

SECTION III. TEST PROGRAM AT ABMA

The testing program which the Army Ballistic Missile Agency (transferred to NASA) followed in testing its part of the S-46 satellite and in testing the completed payloads which included the SUI packages, is divided into four major divisions similar to those for the SUI test program in Section II.

152

1. <u>Testing of Individual Components</u>

    a. <u>Transmitter</u>

        (1) <u>Resistors, capacitors, and inductors</u>. Circuits were, in almost all cases, designed to work with the usual ±10% tolerance components. Only on critical items of this type was special testing performed.

        (2) <u>Semiconductor devices</u>. Satellite transmitters represent a state of the art several years ahead of usual commercial transmitter practice in simultaneously obtaining maximum power output, minimum power input, lowest possible weight, smallest size, maximum reliability, and utmost stability. Some of the leading semiconductor devices manufacturers have drawn upon the experience and advanced techniques knowledge of the transmitter design group for evaluation of the manufacturers' new developments. This has been of mutual advantage since these manufacturers provide samples of new products, readily change parameters in their devices to suit the designer's requirements, make first production of their items available, and even make quantities of a new item available in advance of production, all at modest cost to NASA since most of the costs can be charged to the manufacturers' development expense. Items thus supplied by the manufacturers are in a "custom built" category and represent the manufacturers' best efforts. In these cases it is mostly a matter of the transmitter designers' verifying the manufacturers' measured data on the devices. In some instances the quantity supplied permits of selection.

    In the commercially available semiconductor devices, the procurement is usually in quantities which permit of selection of the highest efficiency items.

    b. <u>Telemetry</u>

        (1) <u>Capacitors</u>. Capacitors must have a long term stability. For telemetry applications this was assured by giving the capacitors a modest preaging baking at 100°C for 200 hours after which they were carefully measured, then placed on the shelf and periodically monitored for stability over the six months aging period. Those showing the greatest stability were used in the flight units.

        (2) <u>Semiconductor devices</u>. Transistors and diodes for telemetry applications were put in an oven and baked for 500 hours at 150°C to stabilize the good units and to show up the weak or contaminated units. After baking, the components were checked against the Guidance and Control Division (MSFC) specifications. These specifications are usually about the same as the manufacturer's specifications, but in some cases may be more stringent and in a few cases more lenient. For critical applications, items were specially selected.

(3) <u>Inductors and fine-wire resistors</u>. These items were given a one month vacuum soak test before they were used in the telemetry equipment.

(4) <u>All electronic components</u>. Just prior to assembly all important parameters of all electronic components for the telemetry were completely checked against the governing specifications.

c. <u>Antenna</u>. No test of antenna individual components was considered warranted.

2. <u>Testing of Modules</u>

a. <u>Transmitter</u>. Each satellite, depending on its mission, has a range of temperature in which it must perform. For a normal anticipated operating temperature range for S-46 of 0°C to 50°C, the transmitter modules were tested for satisfactory performance at 10°C above and below this range.

b. <u>Telemetry</u>. A reliability confidence test was made on each telemetry module before encapsulation. Testing at elevated temperature and at depressed temperature was used to provide a "confidence factor" on the basis that reliability over a period of time in the anticipated environment can be related to ability to perform satisfactorily in high and low temperature tests. For the S-46 a three year mean time to failure was desired. The telemetry circuits were analyzed, and by working backward it was concluded that testing the modules at -50°C and +100°C would reasonably simulate three years of actual performance. Tests of the telemetry modules were successfully carried out at these temperatures before the modules were encapsulated.

After encapsulation the telemetry modules were given a mild vibration test and electrically tested again.

3. <u>Subassembly Testing</u>

In general, a subassembly test program analogous to that of the SUI program described in Section II.3 was not carried out at ABMA at a corresponding stage of the testing, but was accomplished during the payload testing program discussed in the rest of this section.

4. <u>Testing of Complete Payloads</u>

a. <u>General</u>. The completely assembled payloads were given a series of mechanical, electrical, and rf tests at ABMA. These tests fall into two main groups, the prototype approval tests performed on PL-1, PL-2, and PL-3, and the flight acceptance tests performed on the flight units PL-4 and PL-5.

The prototype approval test is designed to assure that the newly developed configuration operates as an integral unit exactly as planned and that it possesses sufficient strength to survive the conditions imposed at the time of launch and in orbit. The test levels are set at a sufficiently high level to encompass variations in the encountered environmental conditions and to allow for variations in the strengths of the individual payloads. On the basis of these tests approval or rejection of the design and/or the need for modifications is decided. After being subjected to this series of tests, a unit is usually considered not suitable for flight because of the possibility that the structure may have been weakened by the tests.

The flight acceptance tests are performed on each potential flight unit to assist in determining the operating characteristics of the completed units and to test for mechanical integrity of the completely assembled payloads. On the basis of these tests a unit is either accepted or rejected for flight. In addition, information gained during these tests often assists in the selection of the preferred flight unit from the group of possible flight payloads.

A complete outline of both sets of payload test specifications is contained in Section IV.

b. Payload PL-1 - Prototype Thermal Tests

(1) Test setup. The theoretical thermal design described in Chapter 6 was verified and the transfer coefficients empirically determined by actual test on the PL-1 prototype payload. The test requirements were specified to the Electro-Mechanical Branch of Guidance and Control Laboratory (ABMA) by the Space Thermodynamics Branch of Research Projects Laboratory (ABMA) and were made a part of the test specifications (Section IV.4.j). A detailed procedure was set up by the Electro-Mechanical Branch to apply the same methods of blankets for heating and liquid nitrogen for cooling as was used in the thermal tests of Explorer VII.[1]

The vacuum requirement was met by running the test in a large chamber capable of attaining a pressure of about 3×10^{-7} mm Hg. The chamber and associated equipment are shown in Figure 89.

_____

1. B. Jones, Thermal Design Tests of the IGY Satellite (Payload of Missile No. 16), ABMA Report No. DV-TM-23-59, 10 August 1959.
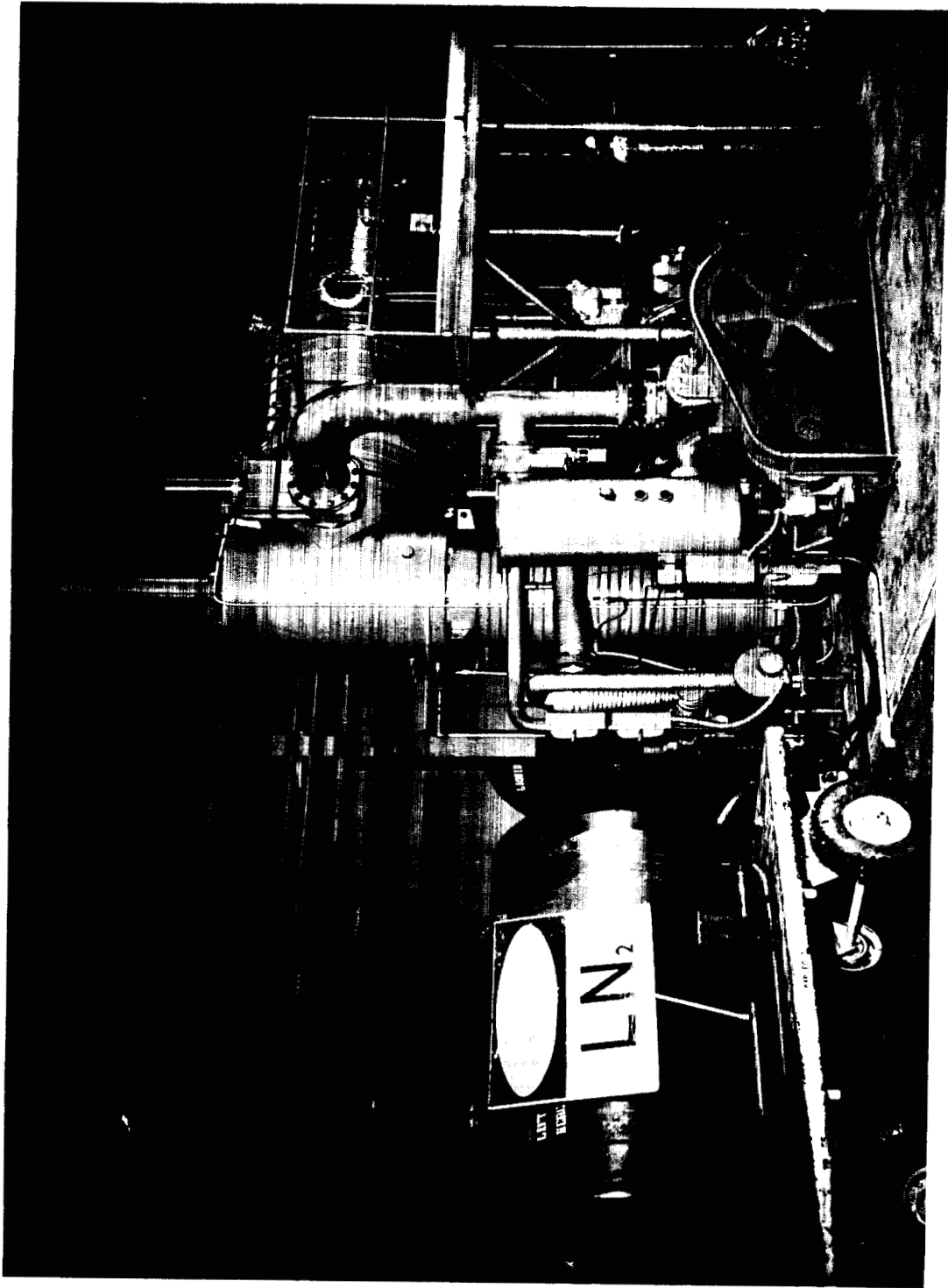
FIG. 89. VACUUM CHAMBER

The payload was cooled to low initial conditions by running liquid nitrogen through a set of coils inside the vacuum chamber, as shown in Figure 90. The chamber was filled with dry nitrogen; the payload was then cooled by convection and radiation. When the temperature equalized, at about -20°C, the dry nitrogen was pumped out and heat applied to the various surfaces of the payload by special heater blankets. During these tests, up to 37 thermocouples recorded the temperature of various parts of the payload, heater blankets, and vacuum chamber. Using a stepping switch, the thermocouple readings were recorded on strip charts in the control room where the controls for the blanket circuits were located.

The temperature measurements were taken at the rate of one reading every half minute for the first five minutes after the blankets were turned on, then every minute for the first hour, every five minutes for the next three hours and every ten minutes for the remainder of the test. On the half-blanket tests, the blanket energy input data points were established at the same rate. Pressure readings were taken at a rate commensurate with noted fluctuations. The locations of the thermocouples are given in Table 6.

(2) *First test series (full-blanket tests)*. In both of the full blanket tests the prototype payload, PL-1, was cooled to a uniform temperature of about -20°C. Then, while in a 5×10^{-4} mm Hg or greater vacuum, heat was applied to all external surfaces of the payload to approximate a step function in temperature, the temperature being raised as rapidly as possible to 80°C. The outside temperature of the payload was then held to a constant 80°C and the temperatures of various parts of the instrument package were recorded. It was thus possible to get overall thermal transfer coefficients between various parts of the instrument package and the skin.

As the term "full-blanket" implies, a full heater blanket was used (Fig. 91). Some of the results from one of these tests are shown in Figure 92. The rapidly rising curves are two typical external temperatures. The three slowly rising curves are typical instrument package temperatures. Figure 93 shows the temperature difference between a typical skin temperature and a typical instrument package temperature. From Figure 93 it can be seen that the time constant (time for temperature difference to decrease by one-half) was five hours.

(3) *Second test series (half-blanket tests)*. In the two tests which were run in this series, the heat was applied in the manner described in (2), simulating heat energy input anticipated in space. In these tests, however, the heater blankets covered only those areas the sun would "see" if it were incident at an angle perpendicular to one side of the solar cell box (Fig. 94). The heat outputs of the blankets were determined by measuring and recording the current and voltage through each of the three blanket circuits. Aluminum foil was
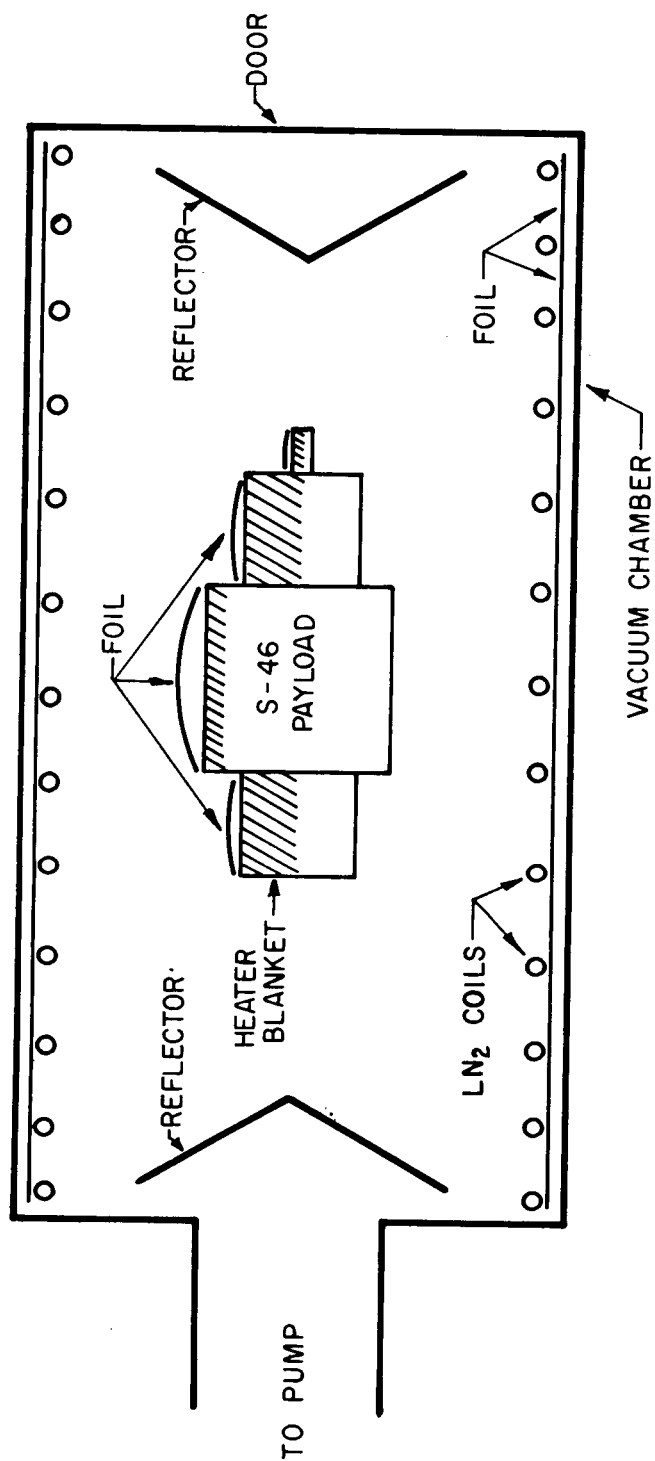
FIG. 90. TEST SETUP FOR HALF-BLANKET TEST

Table 6

LOCATION OF THERMOCOUPLES

Thermo-couple Number	Location around Longitudinal Axis	Location on Payload
1	12:00	Center of each side of solar cell box
2	3:00	
3	6:00	
4	9:00	
5	12:00	Top of solar cell box halfway between aluminum shell
6	6:00	and edge
7	12:00	Bottom of solar cell box halfway between aluminum
8	6:00	shell and edge
9	12:00	Aluminum shell 4 inches from top of shell
10	6:00	
11	12:00	Aluminum shell in center of solar cell box
12	6:00	
13	12:00	Aluminum shell 1/2 inch from bottom of shell
14	6:00	
15	12:00	Base of Geiger tube cover
16	-----	At base of and in center of battery pack
17	-----	Near center of battery pack
18	-----	Near center of transmitter
19	-----	Near center of and at base of SUI package
20	-----	On outside of SUI package directly under #15
21	3:00	On outside of SUI package halfway between #9 & #10
22	3:00	On outside of transmitter halfway between #11 & #12
23	3:00	On outside of battery pack halfway between #11 & #12
24	-----	On shield of foil experiment

Table 6 (Continued):

Thermo-couple Number	Location around Longitudinal Axis	Location on Payload
25	-----	On the experimental foil
26, 27	-----	On each end of vacuum chamber
28, 29	-----	On vacuum chamber directly above and below payload
30	-----	On shield in the "half-blanket tests"
31, 32	-----	Center of heat balance strips, 180° apart
33, 37	-----	On a solar cell of the side of the box which would be heated during the "half-blanket tests'
34, 35	-----	On solar cell of each box end
36	-----	On blanket covering solar cell box
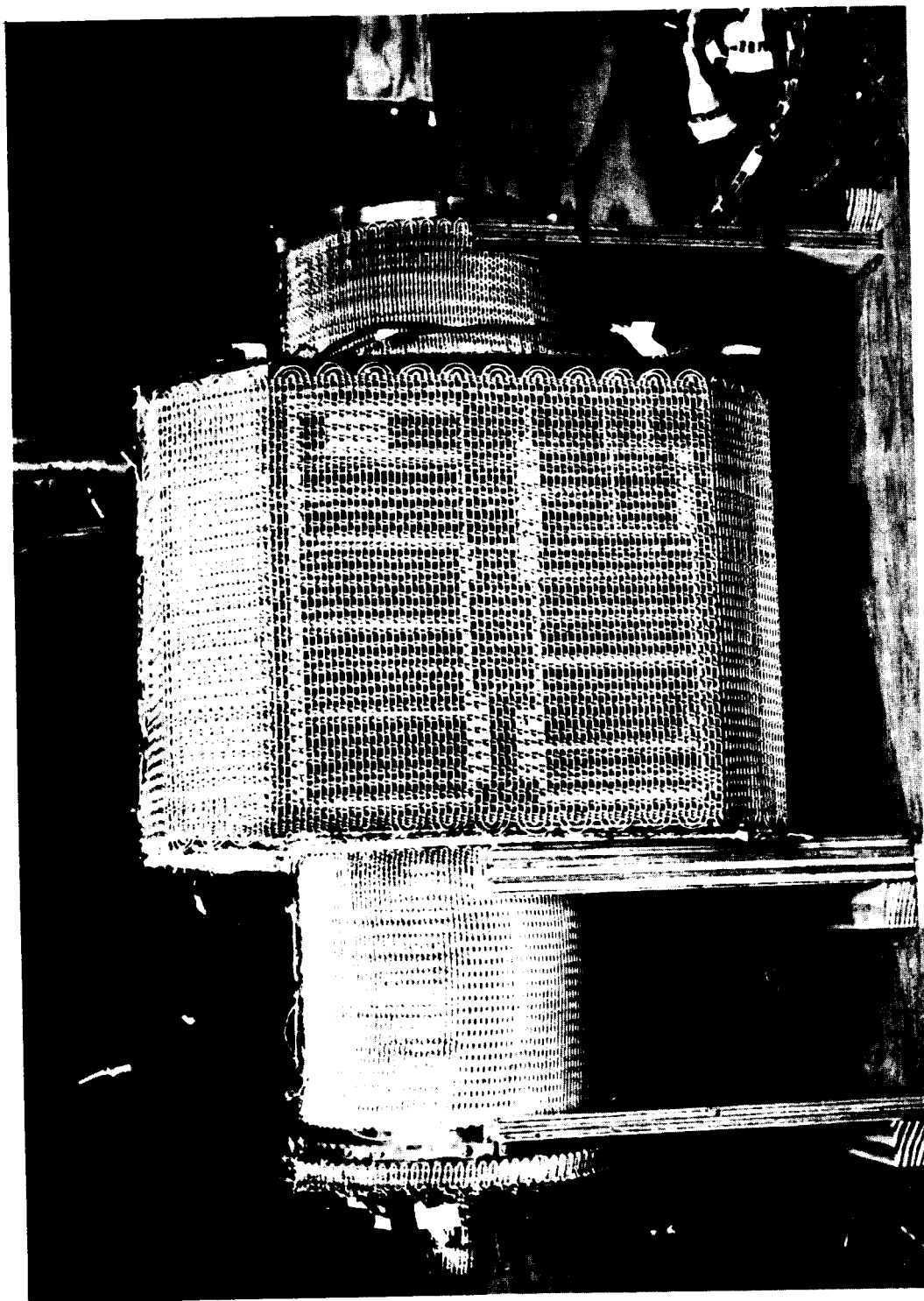
FIG. 91. FULL-BLANKET IN POSITION ON PROTOTYPE
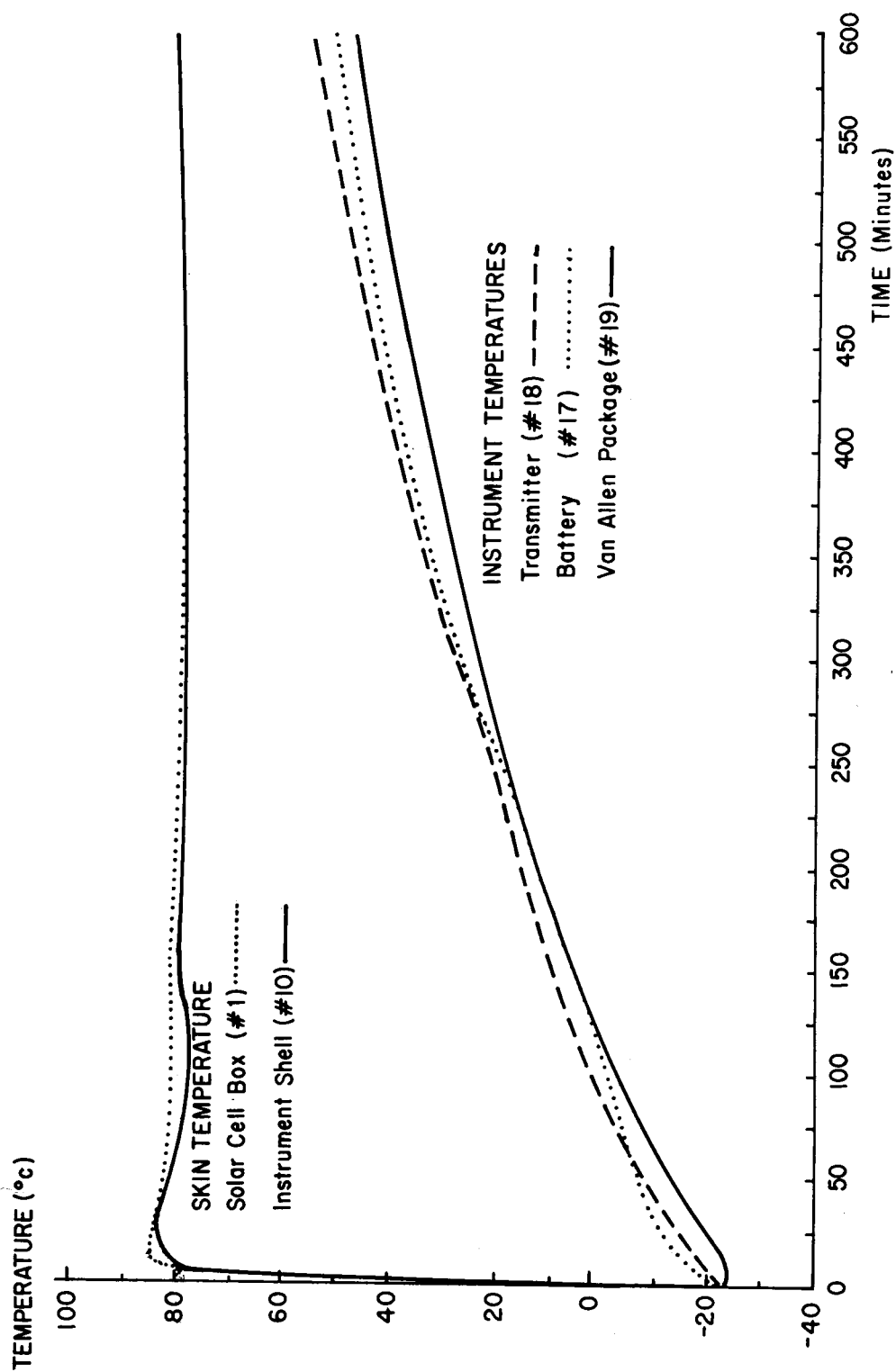
FIG. 92. FULL-BLANKET TEST ON S-46
(Test 132004)

162
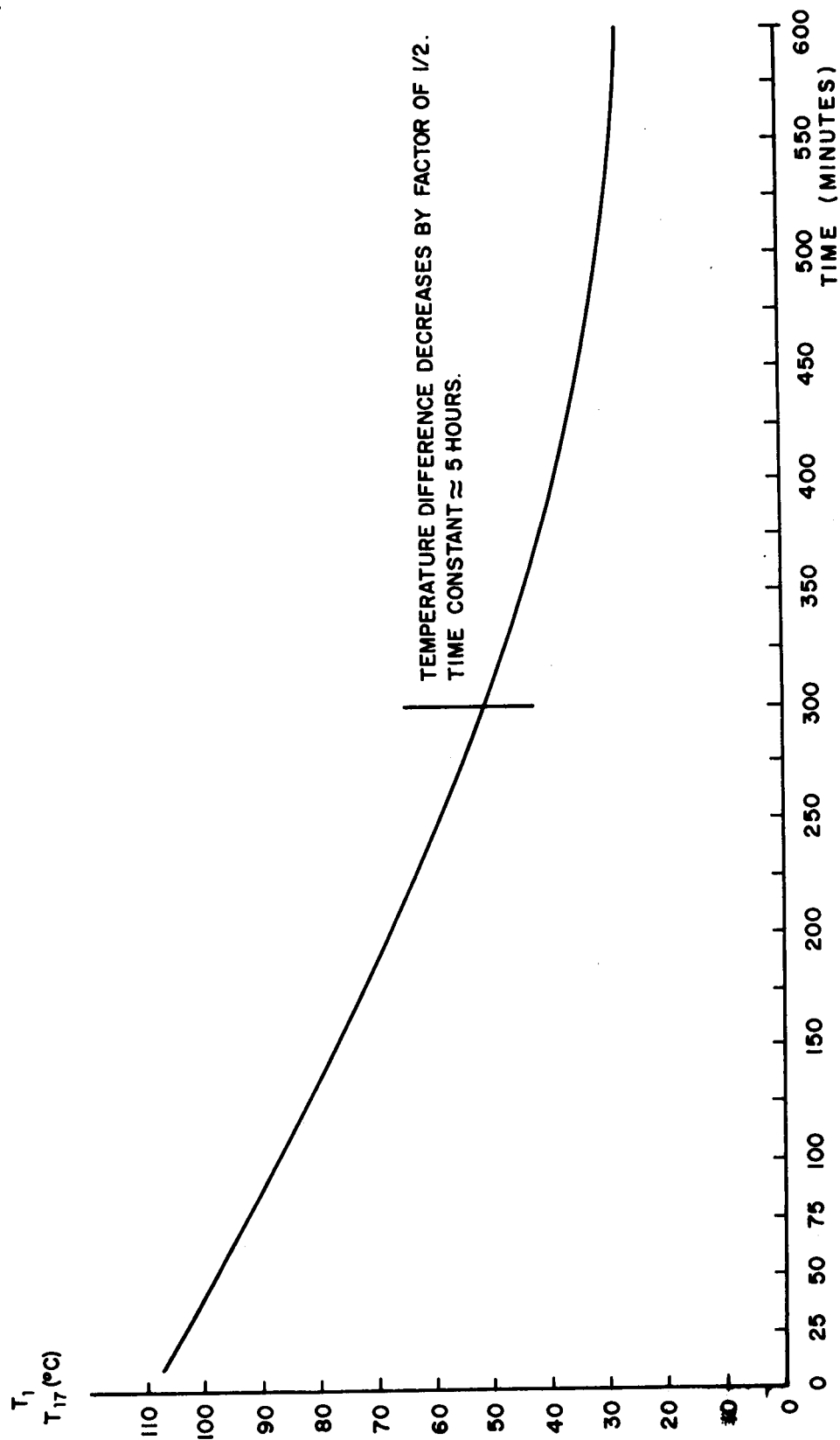
FIG. 93. FULL-BLANKET TEST -- SKIN TEMPERATURE (T_1) AND
BATTERY TEMPERATURE (T_{17}) VS. TIME FOR S-46
(Test #132004)
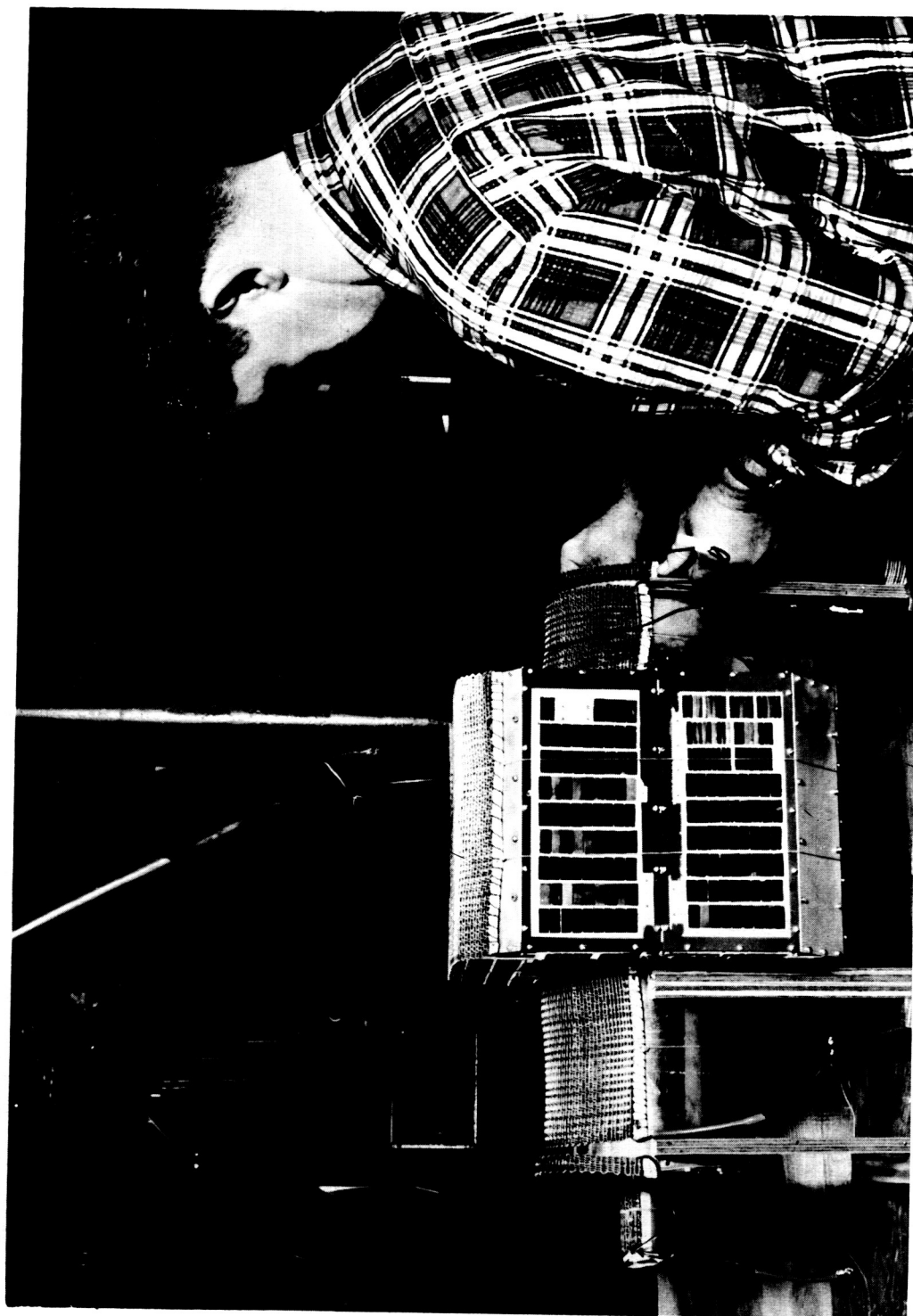
FIG. 94. HALF-BLANKET IN POSITION ON PROTOTYPE

placed behind the blankets (Fig. 90) so that most of their heat output
went into the payload. Those parts of the payload surface which were
not heated were allowed to radiate freely to the cooling coils through
which liquid nitrogen flowed throughout the tests, unlike the full-
blanket tests where it was cut off when heating began. Aluminum foil
between the cooling coils and the walls of the vacuum chamber and the
conical aluminum reflectors placed at each end of the chamber reduced
radiation exchange between the payload and the chamber. A heat input
curve for each of the three blanket circuits was furnished to the test
personnel. The curve for circuit No. 2, shown in Figure 95, is for the
blanket circuit covering the side of the solar cell box. During the
test, the temperature of the surface was monitored continuously and the
energy input from the blanket adjusted by use of this curve. The results
obtained from this circuit in one of the tests are shown in Figure 96.
As the temperature of the heated surface of the solar cell box increased,
the energy from the blanket was decreased, using the control curve in
Figure 95. A point was reached where the energy going into the surface
did not cause a rise in the temperature of the surface; this was the
desired steady state condition. The "theoretical" energy input curve
was plotted using the temperature curve and Figure 95. It is apparent
that the actual input energy was closely controlled.

Figure 97 shows some of the temperatures during a half-blanket
test. The curves show that a steady state temperature difference of
about 55°C existed between the heated side of the solar cell box and
the opposite unheated side. By knowing the blanket energy input, an
effective thermal transfer constant between opposite sides of the solar
cell box was calculated. Other transfer constants were calculated from
other temperature measurements.

It can also be seen from Figure 97 that the aluminum instrument
shell (which "drives" the instrument package temperature) under the
solar cell box, settled at a temperature halfway between the two extremes
on the solar cell box. This shows that even if large temperature
gradients exist around the solar cell box, the instrument package will
still assume an average value. The fact that the temperature of the
heat shield around the blanket remained low throughout the test shows
the effectiveness of the shield and further supports the assumption that
all of the energy output from the blankets went into the payload.

c. Payload PL-2 - Prototype Electronic Tests

(1) Payload checkout. The electronic prototype, PL-2, was
ready for test on October 29, 1959. During this payload checkout
procedure (Section IV.4.a) presence of intermodulation on the 400 cycle
channel was detected. Since this intermodulation was the only deviation
from the specifications (Section IV.4) it was decided to start the tests.
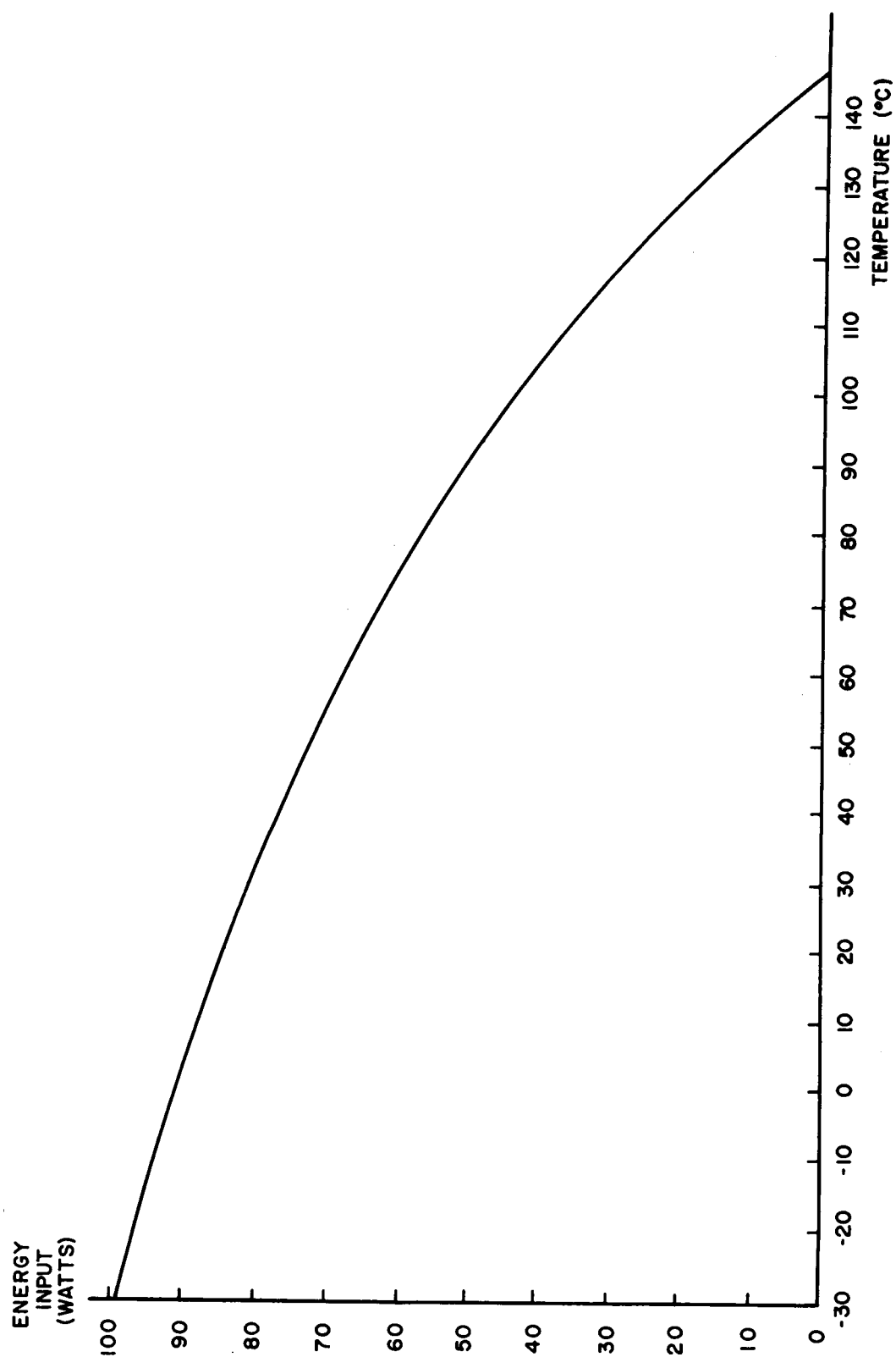
FIG. 95. HALF-BLANKET TEST S-46 -- ENERGY INPUT TO SOLAR CELL
BOX VS. TEMPERATURE. (Used to Control Blanket Power)
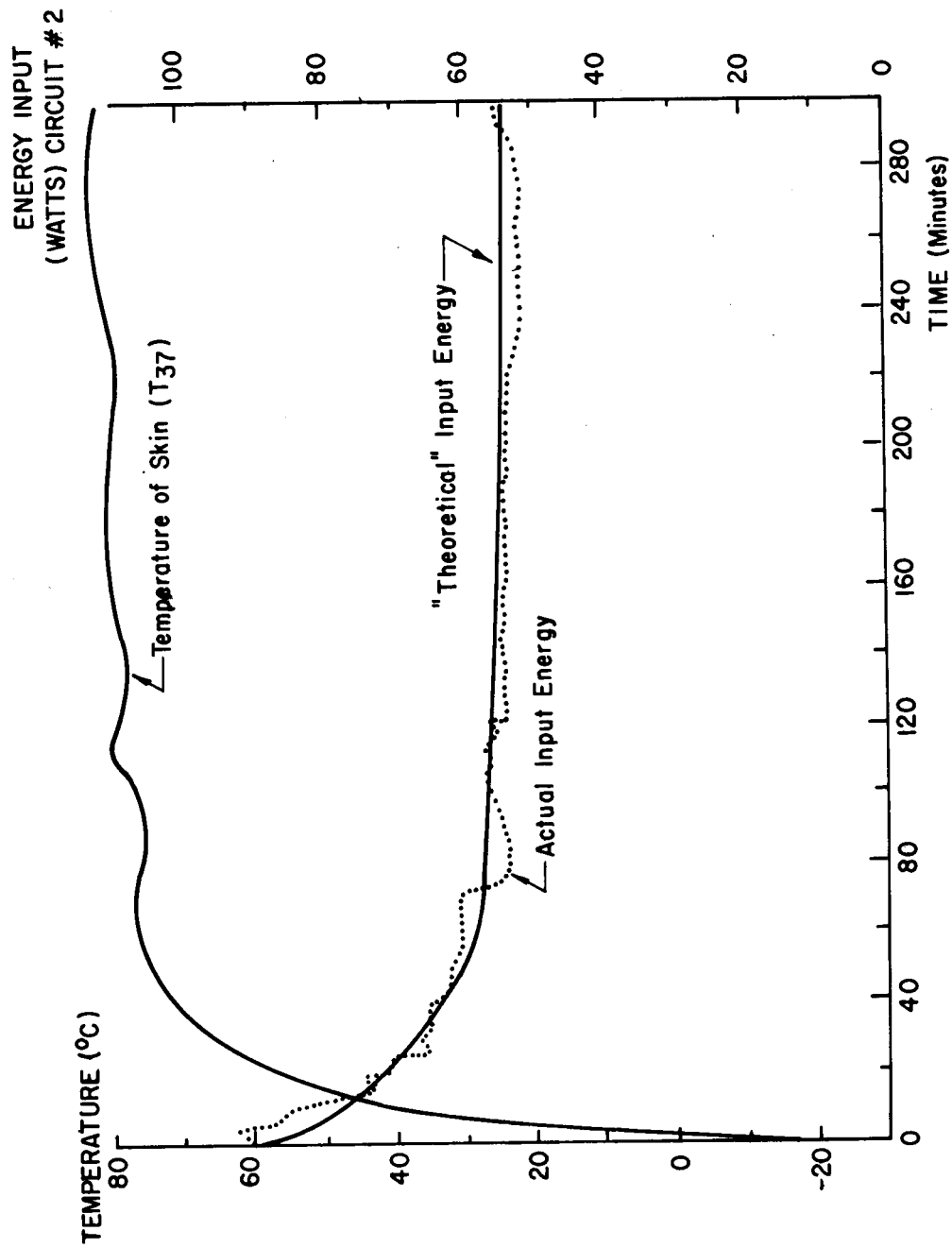
FIG. 96. HALF-BLANKET TEST ON S-46
(Test 132002)
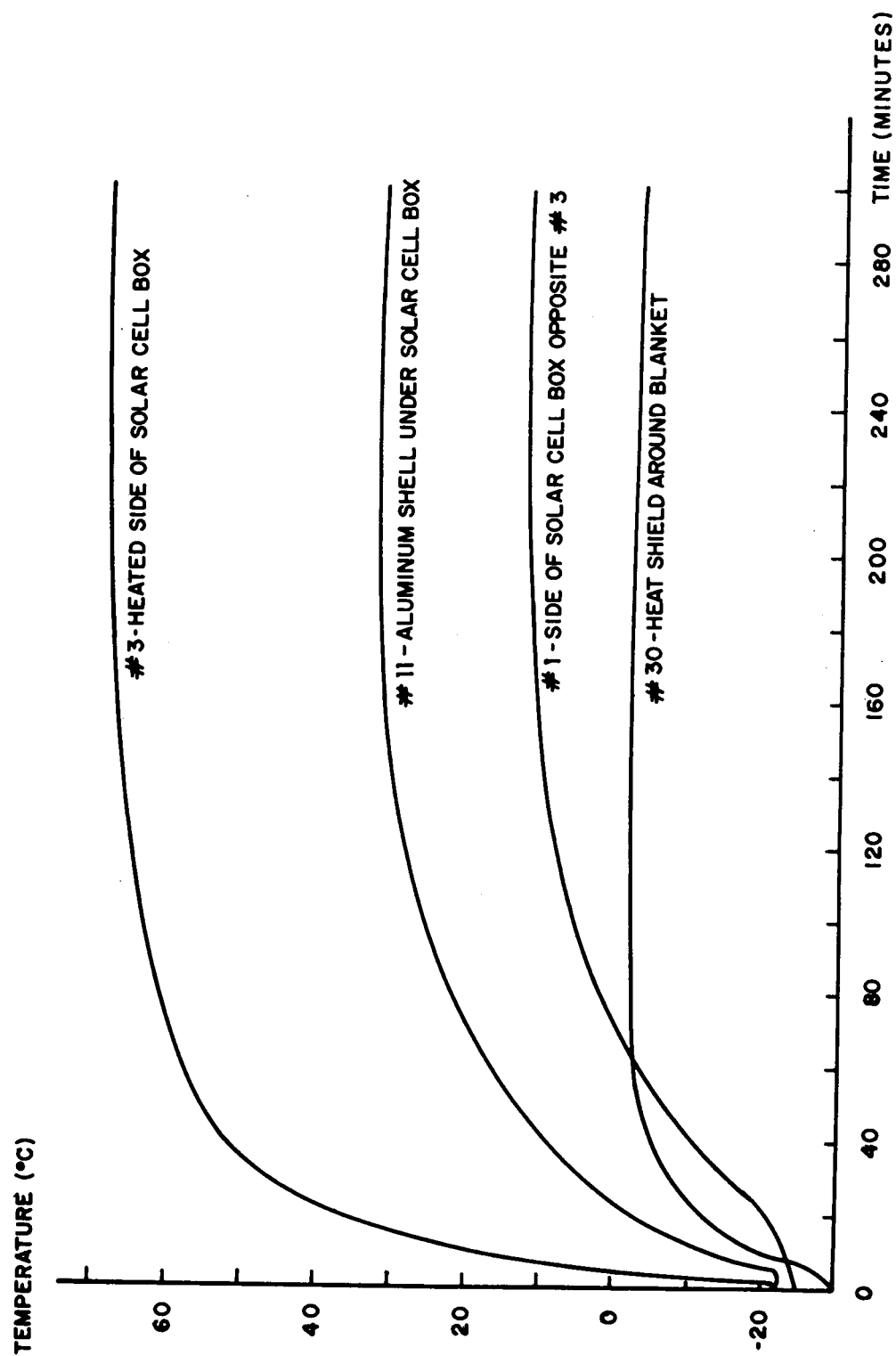
FIG. 97.   HALF-BLANKET TEST ON S-46
(Test 132002)

(2) <u>Dynamic balancing</u>. Since the satellite would be spun during launch, dynamic balancing of the payload about the longitudinal axis was necessary. This was accomplished in PL-2 by properly locating weights on the top and bottom of the solar battery structure. The positions of the weights were chosen so that the perpendicular distance from the center of gravity of the payload to the nominal axis of rotation did not exceed 0.51 mm. The specifications governing this are given in Section IV.4.b.

(3) <u>Vibration test</u>. The payload successfully passed both the thrust direction and perpendicular to thrust direction vibration tests required by the specifications (Section IV.4.e).

(4) <u>Vacuum soak test</u>. On November 9, 1959, this payload was operationally checked out and installed in the vacuum test chamber to undergo the temperature-vacuum soak test required by the test specifications (Section IV.4.h). Various troubles occurred during this test, the first being a loss of vacuum due to improper potting of the plug in the side of the test chamber. A new plug was installed and the test got under way, only to have the 400 cycle subcarrier oscillator stop oscillating. A defective resistor in the subcarrier oscillator was determined to have caused this failure. The necessary repair was made and the test resumed. On November 12 the SUI 1300 cycle channel failed after six hours at 50°C. SUI traced this failure to a change in the 700 volt power supply regulator current due to a transistor failure in the power supply. It was corrected by changing transistors and the base bias resistors on the primary side of the high voltage supply. When further operational electronic checks were made, however, it was found that the 1300 cycle subcarrier was still absent. The cause this time was an open coil in the output filter. The coil was replaced and the vacuum test resumed on November 16. In a few hours the SUI 730 cycle channel became erratic with an intermittent high switching rate caused by improper quenching of the detector C G-M counter in the SUI package. The package was sent to SUI for repair. After installation of new detector C and D G-M counters the package was returned to ABMA on November 30, 1959.

A bench check of the SUI package after its return to ABMA revealed that the SUI temperature measuring network was inoperative. The cause was an open circuit in the thermistor. It was decided to undertake the vacuum test without this network. Because of the discontinuous nature of the vacuum test to that time it was decided to start the 14 day vacuum soak anew. The new test was begun on November 30, 1959. The PL-2 electronic prototype payload successfully passed the test, which was completed on December 14. Figure 98 shows the transmitter frequency and temperature at hourly intervals throughout this test.
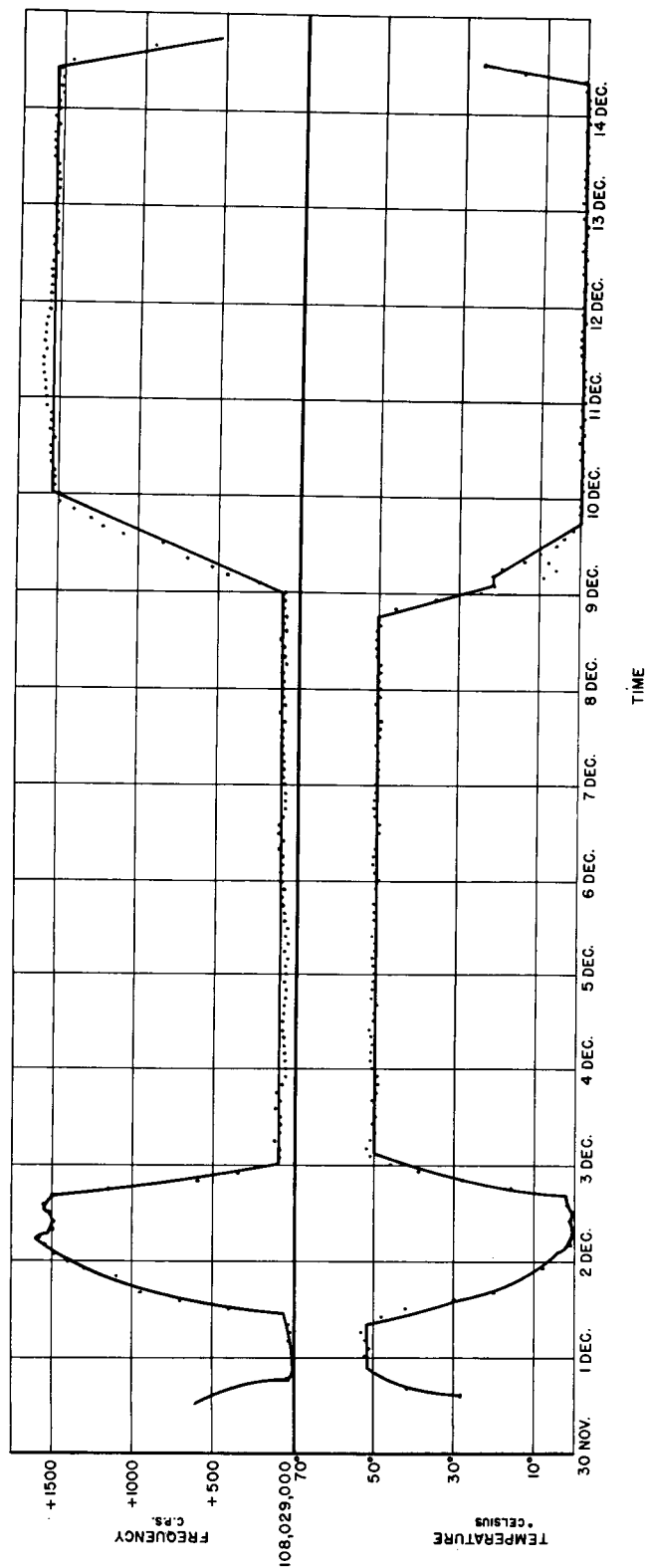
FIG. 98.   VARIATION OF TEMPERATURE AND TRANSMITTER
FREQUENCY DURING VACUUM-SOAK TEST ON PL-2 PROTOTYPE

During the vacuum-soak test some minor irregularities occurred, the exact causes of which were not evident. Some of these difficulties involved sub-components of the SUI package. The package was returned to the State University of Iowa for further investigation. The SUI findings were as follows:

     (a) An intermittent change by a factor of two in the channel three (730 cps) switching rate after 12 hours at 50°C and 12 hours at 0°C, on the way to room temperature, was due to transistor failure in scaler stage four. The transistor was changed at SUI after completion of the test program.

     (b) A slow drift in channel five (1300 cps) output voltage after about five days at 50°C was due to a change in characteristics of the 2N338 transistor in the output amplifier. This transistor was changed at SUI after completion of the test program.

In the components of ABMA responsibility, the 960 cps subcarrier oscillator was intermittent for a short time while at the high temperature but corrected itself and returned to normal operation. This subcarrier oscillator was checked for reoccurrence of the intermittent functioning by temperature cycling but it operated normally. The SUI package from PL-2 was then checked at SUI where it was discovered that the output from some channels varied with temperature on account of the inherent characteristics of the cadmium sulfide detectors. A temperature calibration curve was plotted to give corrections for this variation in counting rate.

The other subcarriers operated properly throughout the test, as did the transmitter, multiplexer, and temperature sensors, and the internal power supply when it was used.

This completed the required tests on the complete electronic prototype payload PL-2.

d. Payload PL-3 -- Prototype Environmental Tests

     (1) Payload checkout. The environmental prototype, PL-3, was given the same checkout as given PL-2, this being required by the test specifications (Section IV.4.a). The intermodulation that was present on the electronic prototype PL-2 (c(1) above) was reduced on the environmental model by adjustments of the subcarrier outputs.

     (2) Dynamic balancing. PL-3 was balanced in the same way as described for PL-2 in paragraph c(2) above.

     (3) Shock test. PL-3 payload was subjected to the required shock test (Section IV.4.d) on November 11, 1959. The payload checkout

procedure, repeated after the test, showed that the payload successfully passed the test.

(4) Vibration test. Following the shock test, PL-3 was given the vibration in the thrust direction test specified in Section IV.4.e. Loss of rf signal occurred during this test. It was caused by a bad connection at the transmitter. The cable was more securely attached and the unit was then vibrated successfully in three planes for short time durations and then was vibrated for two minutes in the thrust and transverse to thrust directions (Section IV.4.e(4)(a)). During vibration in the perpendicular to thrust direction the antenna gap insulator cracked due to too small an antenna collar. After a new and stronger collar was installed the unit was successfully revibrated in two mutually perpendicular directions perpendicular to the thrust axis. Revibration in the thrust direction was done at a later date with the SUI instrument column from PL-1 installed instead of the PL-3 column in order to limit the shake time on the latter column. This vibration test was successful and proved the new antenna gap was satisfactory from the vibration standpoint.

(5) Spin test. Prototype PL-3 was satisfactorily checked out to test specifications, Section IV.4.a both before and after the spin test on November 25, 1959. The testing was performed as specified in Section IV.4.c.

(6) Solar cell continuity during spin test. This test (Section IV.4.g) was conducted on November 30. The solar cells and electronic equipment operated properly both before and after the test. Solar cell networks maintained continuity throughout the test.

(7) Linear acceleration with spin test. On December 5, 1959, the environmental prototype was successfully given the centrifuge and spin test required by the test specifications in Section IV.4.f.

(8) Temperature calibration and vacuum test. The vacuum-calibration test prescribed in Section IV.4.i was started on prototype PL-3 on December 7, 1959 and continued on December 8. An intermittent condition was found to exist on the 400 cycle channel but the transmitted information was readable and the unit was considered to have passed the test satisfactorily. The intermittent condition disappeared when the unit returned to room temperature and atmospheric pressure after the test. An investigation disclosed that the erratic operation of the 400 cycle channel was due to a faulty transistor in the scaler output amplifier.

(9) Bench check of instrument column No. 3. A special bench check was made on the instrument column No. 3 which had been removed from PL-3 as mentioned in the vibration test, paragraph (3) above.

The check was made without radiation source present. The check revealed
that some of the subcarriers were driven out of the passband of the
discriminators by the output from the SUI channels. The corrective
action taken was to add a resistor and capacitor to a multivibrator in
the SUI package. This network always put the multivibrator in the
correct output bias condition.

(10) Rf field test. An rf field check on PL-3 prototype
was started on December 16, 1959 after a correct matching device was
obtained. In this test the payload was operated on internal power,
exactly as it would be in flight, for a check on transmitter loading.
The current measured in this test was in close agreement with the current
previously measured into a standard 50 ohm load. The payload was spun on
the launcher on December 21, 1959 and the rf signals were monitored both
in the test equipment trailer and at the ground station on Madkin Mountain,
Redstone Arsenal, Alabama. The results of the rf field tests were entirely
satisfactory. This concluded the test program on the PL-3 prototype
payload.

e. Flight unit FU-1 (Payload PL-4) -- Acceptance Tests

(1) Payload checkout. Payload checkout (Section IV.4.a)
was accomplished on the flight payload FU-1 (a designation to indicate
the potential flight application of PL-4 as differentiated from the
prototype applications of PL-1, PL-2, and PL-3). Preliminary tests were
made on the subcarrier oscillators and transmitters. Intermodulation,
which had been a problem on prototype PL-2, was negligible after proper
adjustments similar to those found efficacious on PL-3 (paragraph d(1)).
The instrument column for FU-1 was checked out on January 27, 1960. The
SUI package was checked without the presence of a radiation source and
operated the subcarriers within the band limits.

(2) Dynamic balancing. The preliminary dynamic balancing
was performed on February 4, 1960. Forty-five grams of weights were
added to PL-4, the weights being almost exactly opposite the Tabor
sensor (which prompted personnel of Stability and Weight Control Section
in Structures and Mechanics Division to note the feasibility of shifting
this sensor 180° with a net saving in weight might profitably be
investigated). The 0730 and 0900 positions were shimmed .002 inch
previous to the balance operation, for a total indicator runout of .002
inch on the can just above the solar cell box.

Final balancing, as required by specifications of Section IV.4.b,
was done on February 26. Fifty grams total weight was required almost
opposite the Tabor sensor. It was estimated that less than 50% of the
dynamic balance tolerance was used in the final weight locations.
Positioning of the solar battery diodes (located inside the solar battery
framework) and the choke coils (located in the antenna gap (paragraph (8)
below) undoubtedly aided in reducing the balance weights needed. It

was planned to shift the sensor 180°, as previously suggested, after the unit reached Florida.

(3) <u>Vibration test</u>. The flight acceptance tests for vibration (Section IV.4.e) were performed on February 5, 1960. During the test in the thrust direction an erratic count rate on channel No. 3 (SUI) was observed which disappeared when the vibration was stopped. The first vibration perpendicular to thrust direction was accomplished on February 5, also. In this test a change in count rate was observed in channel No. 2 (SUI) both during and after vibration. The SUI package was removed and checked but no electronic flaws could be found. It was thought that the light source, an incandescent lamp suspended over the sensor, might have shifted and caused the count rate change. A diffuse source of light covering a large area was prepared for the next test.

When the vibration test was performed on February 8 in the other perpendicular to thrust direction a decrease in the count rate in channel No. 2 (SUI) occurred again during the vibration. A tiny crumb of Eccofoam was found in the sensor. When this was removed the counting rate returned to normal.

(4) <u>Linear acceleration with spin</u>. Prototype payload PL-3 was used to check out the centrifuge setup prior to testing the FU-1 unit. A shield was fabricated to protect the payload from oil spray from the spin drive. A new reinforcing sleeve was placed over the sleeve previously used in the prototype testing to support the bearing rollers at the forward end of the payload. Two layers of Velumoid were employed to distribute the load over the can and sleeve surfaces. On February 10, 1960, the test was successfully performed on FU-1 in accordance with specifications (Section IV.4.f).

(5) <u>Solar cell continuity during spin</u>. This test, as prescribed in Section IV.4.g, was successfully performed on FU-1 on February 11, 1959.

(6) <u>Moments of inertia, weight, and C.G. location measurements</u>. On February 12 the final mass measurements of payload No. 4 (FU-1) were determined. With reference to Figure 99, the results were as follows:

Weight in pounds	Center of Gravity (inches)	Mass Moment of Inertia in pounds-inch-second squared Axis		
		X-X	Y-Y	Z-Z
22.72	9.64	0.879	1.99	1.98

174

CONVENTIONAL AXES
REFERENCE SYSTEM USED
IN MASS MOMENTS OF
INERTIA DETERMINATIONS

GUIDANCE & CONTROL AXES
REFERENCE SYSTEM

FLIGHT DIRECTION

9.64
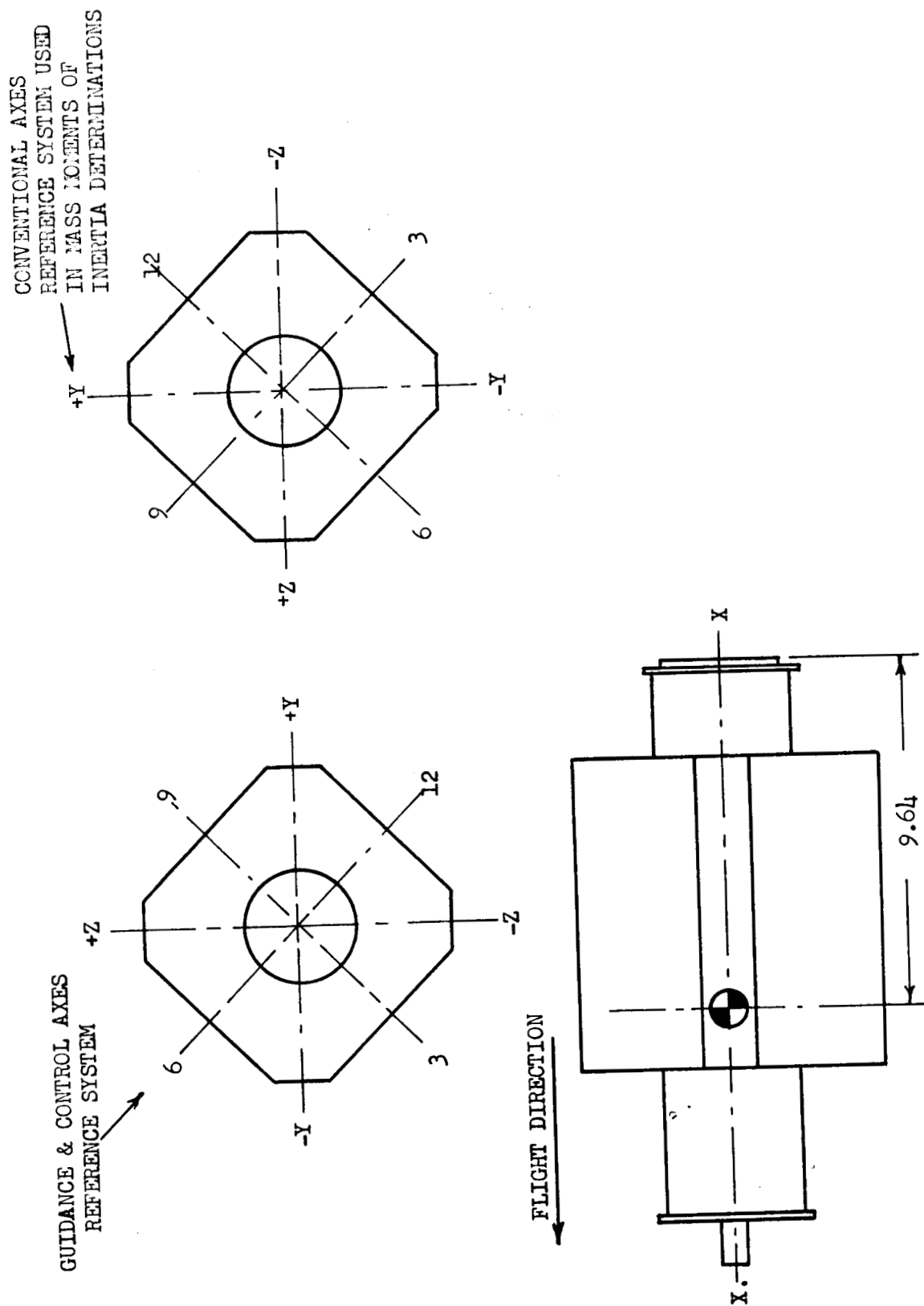
FIG. 99.   MASS MEASUREMENTS DIAGRAM -- FLIGHT UNIT NUMBER 1

The accuracy of this data is: Weight, ±0.03 lb; C of G, ±0.03 inch; roll mass moment of inertia (X-X), ±0.01 lb in sec^2; pitch and yaw mass moment of inertia, ±0.25 lb in sec^2. The mass moment of inertia data are referenced to the center of gravity of the payload (which was 9.64 inches above the extreme lower surface of the adapter ring) and to standard gravity of 32.174 ft/sec^2. The mass moment of inertia measurements about the Y-Y and Z-Z axes were taken by swinging the payload in a bifilar pendulum as shown in Figure 100. The moment of inertia about the X-X (roll) axis was determined by swinging the payload in the torsion pendulum setup shown in Figure 101.

The longitudinal center of gravity of FU-1 was determined by two methods, (a) the two point suspension method using a shadowgraph scale supporting a knife edge for one support and suspended from a 0.035 inch diameter music wire at the other support, and (b) by a beam balancing arrangement shown in Figure 102.

(7) Temperature calibration and vacuum test. The temperature vacuum calibration test required by Section IV.4.i was begun on FU-1 at the 0°C step on February 15, 1960. On February 16 the ambient (25°C) step of the test was completed but after 15 minutes in the 50°C step the power level of the transmitter dropped sharply when the payload was switched from internal to external power. The test was halted and the transmitter removed. Tuning slugs in the transmitter were found to be loose. The transmitter was retuned and the slug locks were replaced. The transmitter was then tested by itself and the failure did not recur so the transmitter was reinstalled in the payload. The temperature vacuum calibration test was resumed and again the transmitter failed at 50°C. This time the failure at 50°C was reproduced in the laboratory on an individual transmitter check. A slight mistuning of the driver stage corrected the malfunction. The transmitter was again installed in the payload unit. The temperature vacuum calibration test was then successfully carried on through 0°, 25°, and 50°C at 100 microns vacuum during February 18 and 19.

(8) Rf field tests. On February 19, 1960, the antenna match on FU-1 was checked and found to be satisfactory. However, during the pole test of the FU-1 the next day a discrepancy was shown to exist between the transmitter and the antenna although the transmitter had been loaded exactly as it would be in flight. The transmitter current was 70 ma when feeding into the payload antenna but when the transmitter output was fed into a 50 ohm wattmeter the current was only 60 ma. The high current was due to unsatisfactory antenna impedance which was caused by the seven wires which connected in the third stage, crossed the antenna gap and connected in the fourth stage. These seven conductors had to pass through the antenna gap to provide external power to the payload while it was mounted on the rocket vehicle during countdown, to
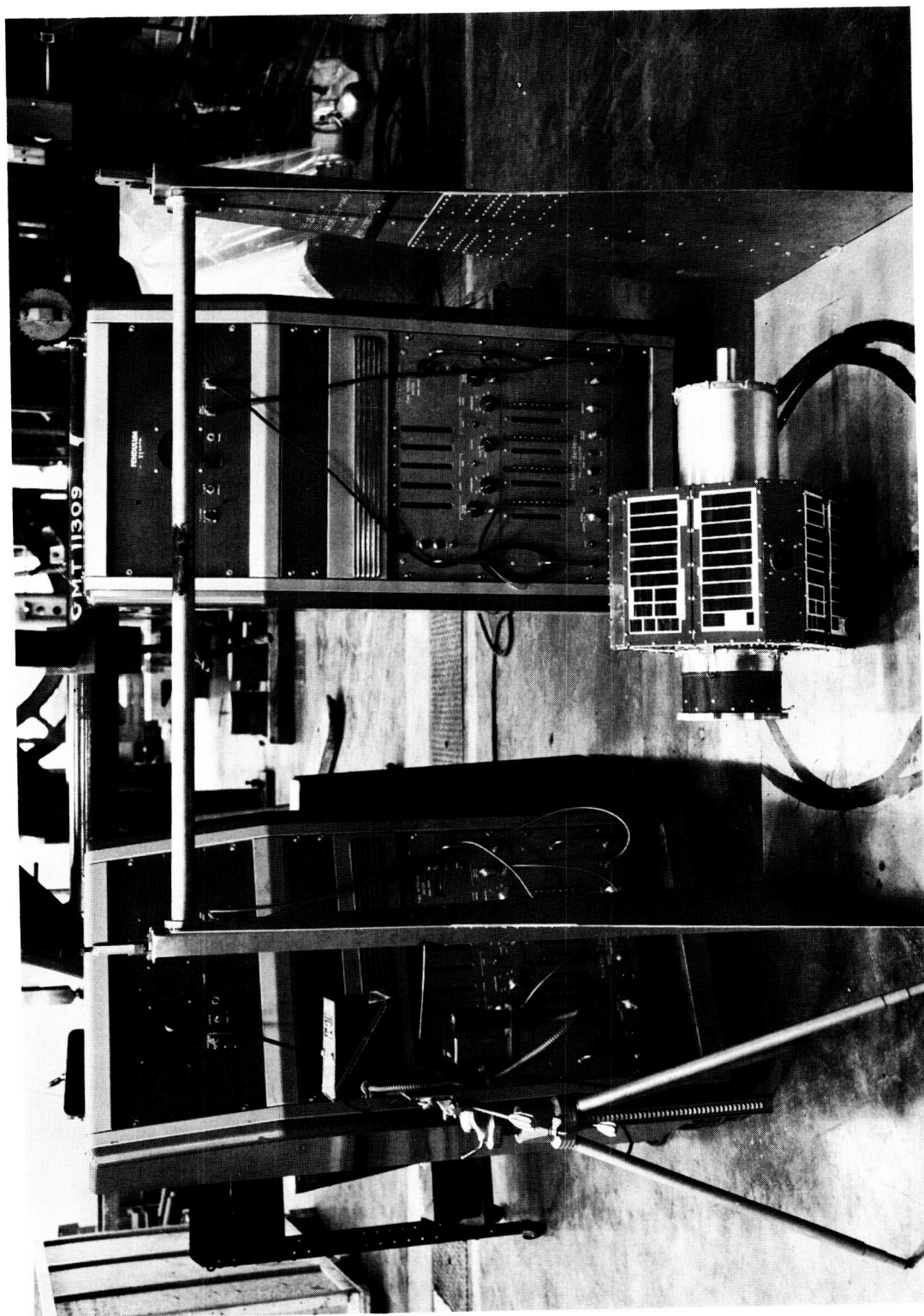
FIG. 100. SETUP FOR TRANSVERSE AXES MOMENT OF INERTIA DETERMINATIONS. The electronic timer and counter are shown in the background. The photo-electric pickup is at the left.
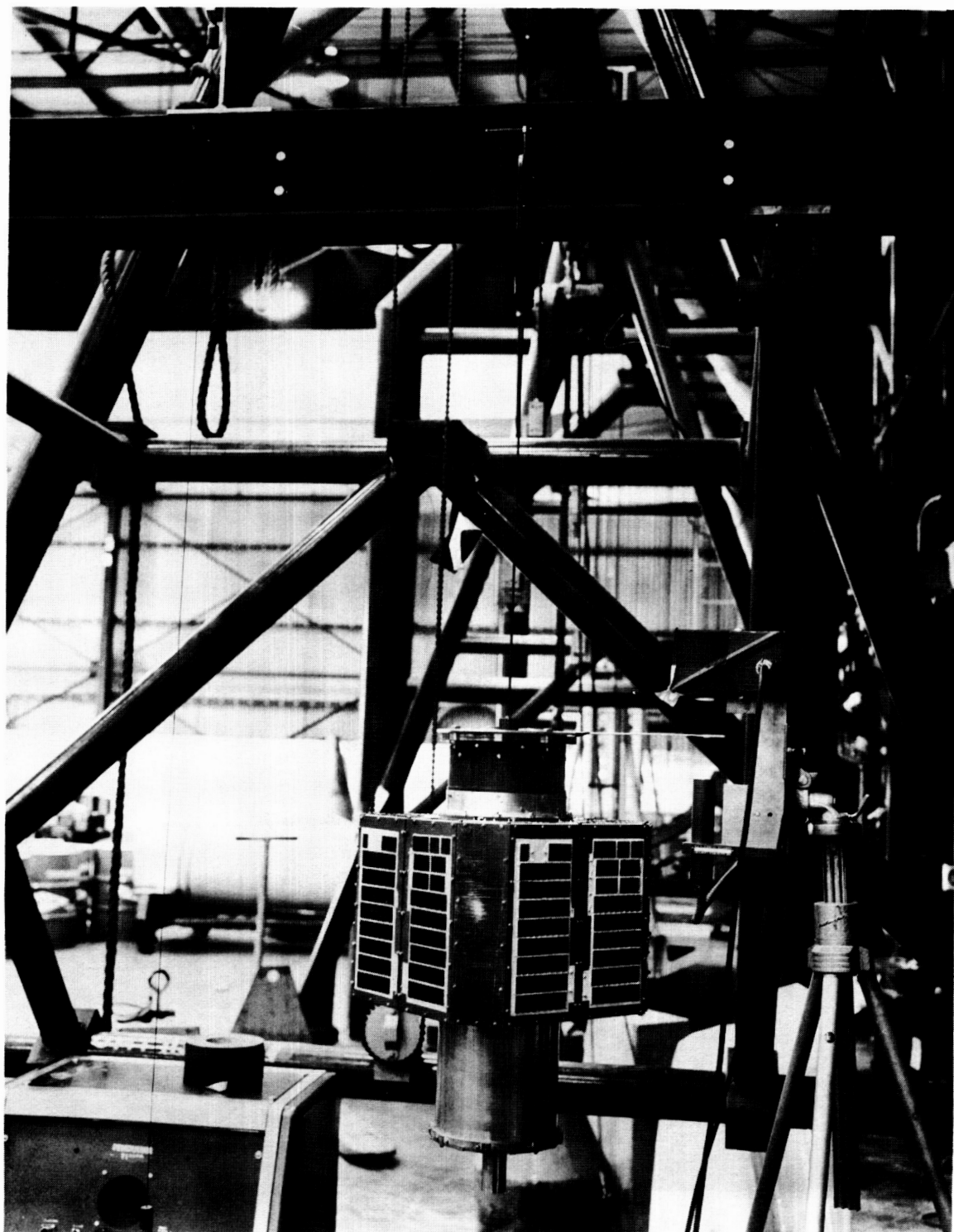
FIG. 101. SETUP FOR ROLL AXIS MOMENT OF INERTIA DETERMINATION
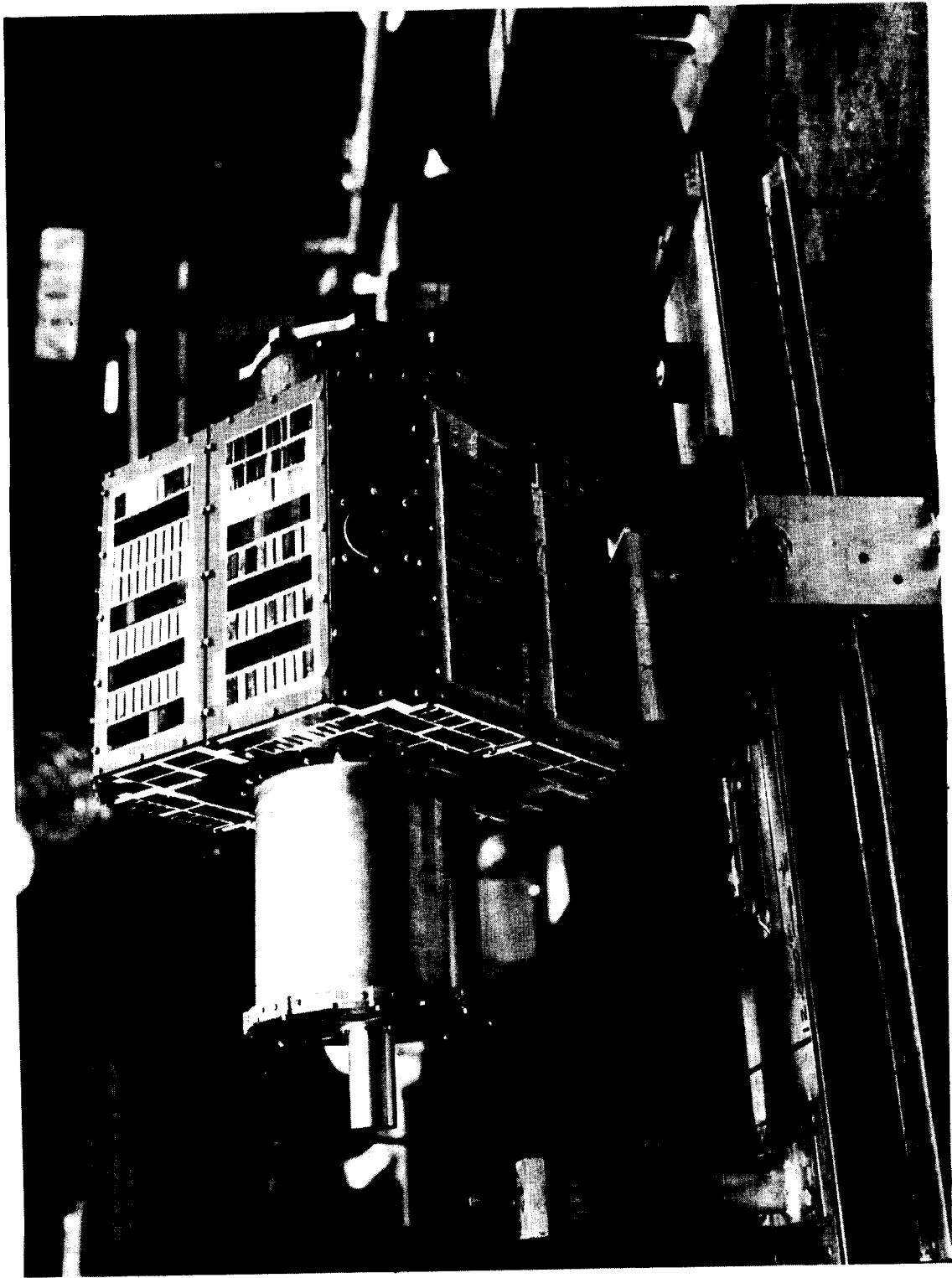
FIG. 102. SETUP FOR CENTER OF GRAVITY DETERMINATION

switch the internal power on and off, and to monitor the switching operation. All this was necessary because the payload would be mounted on the Juno II about eight hours prior to launch time, the solar cells would be covered by the payload shroud, and it was desired to launch the payload with its chemical batteries fully charged. The effect of the control wires on the antenna impedance was corrected by winding the complete cable in a series of small toroidal inductors which were mounted in the antenna insulator as indicated in Figures 30 and 103 so they did not short the antenna input. This arrangement replaced the original choke coil assembly with a net weight increase of only about 15 grams, including ruggedizing. The positioning of these chokes in the antenna gap was chosen to assist in dynamically balancing the payload for spin about its longitudinal axis, as mentioned in (2) above.

During the rf test the signals were monitored both in the checkout trailer and at the Madkin Mountain, Redstone Arsenal, tracking station. The data recorded were entirely satisfactory. There was no evidence of the counting rates in the SUI package being affected by any induced radio frequency currents.

The payload was spun at 450 rpm on internal power and the records obtained were satisfactory. External power was supplied to check the rf chokes. No pickup problems appeared. The shroud was mounted on the vehicle and another record was obtained at the tracking station and in the trailer. The signal level at the tracking station was approximately -120 dbm during spin. The signal was reduced to -145 dbm before becoming indistinguishable.

On March 3, 1960, the FU-1 was shipped to Cape Canaveral, Florida.

(9) Final testing at Cape Canaveral. Flight unit FU-1 was turned over to the Instrumentation Development Branch at Patrick Air Force Base, Cape Canaveral, and was given a complete rf checkout on March 4, 1960. On March 7 the payload was connected to the dummy fourth stage and an rf field test was run. The signal strength was monitored in both the checkout trailer and the microlock station. Performance was satisfactory. The signal strength recorded at the microlock station was -90 dbm.

On March 8 the SUI package was removed from the instrument column for calibration. Calibration required two days, after which the package was returned to the instrument column for further tests.

On March 12 the FU-1 payload was operated for a short time to verify the correct operation of the monitoring equipment in Blockhouse 56. The blockhouse equipment was to be used for rf monitoring during the spin interference test and on launch day. On March 14, before installation of the payload on the Juno II vehicle, another short check was performed,

LEAD 1

LEAD 2

LEAD 3

LEAD 4

LEAD 5

LEAD 6

LEAD 7
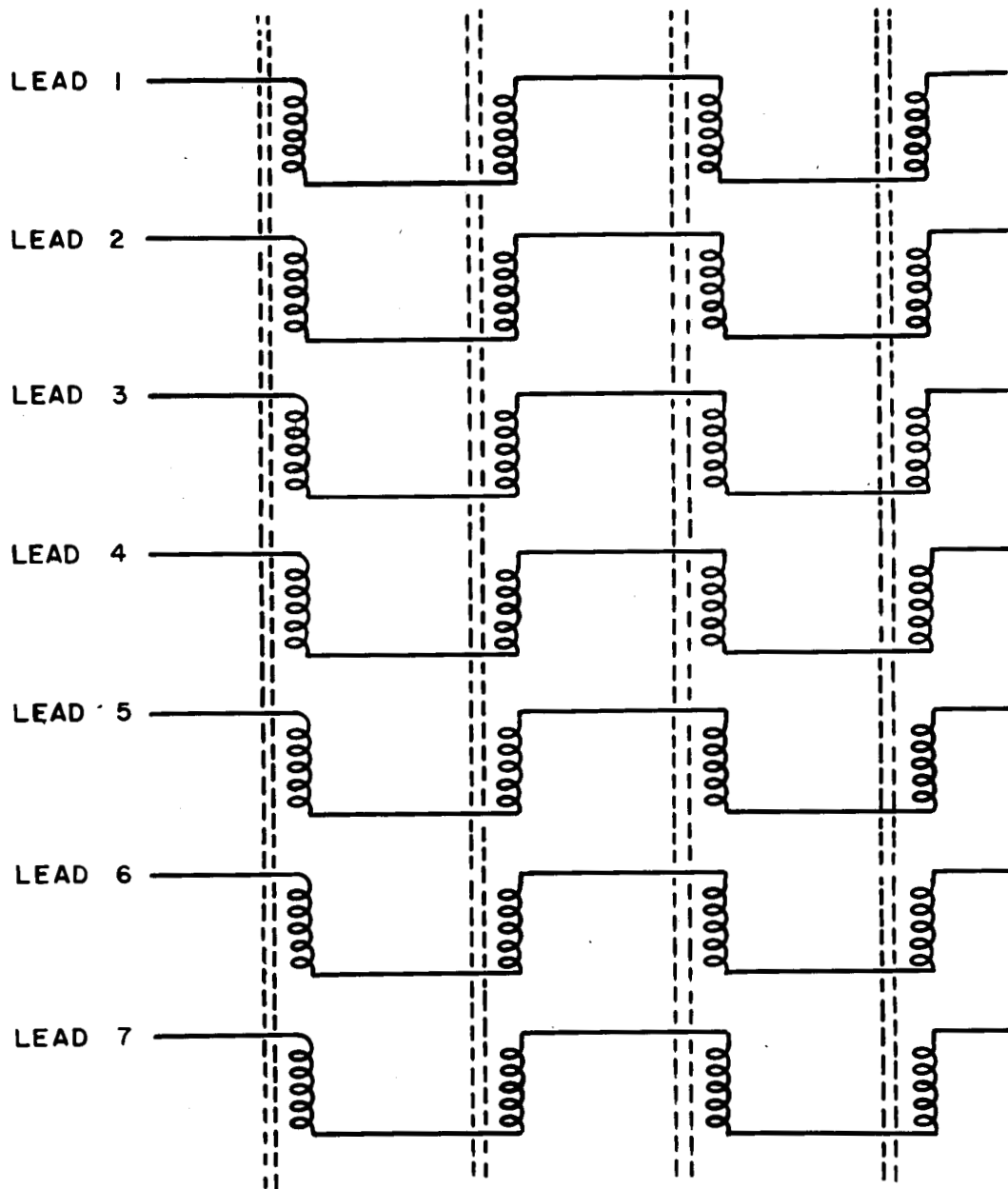
NOTES:
1. ALL COILS 5 TURNS
2. ALL FERRITE CORES GENERAL CERAMICS CORP. TYPE Q-2

FIG. 103. EXTERNAL LEAD ISOLATING FILTERS

using the equipment in Blockhouse 56. Equipment and payload operated correctly.

The FU-1 was next installed on the Juno II but a wiring error applied incorrect voltage to the payload. The wiring was corrected and the payload was rechecked for any detrimental effects, but none were found. The payload was then reinstalled and an rf check was made without the shroud. On March 15, 1960, an rf check was made before and during the spin interference test. Blockhouse 56 and the microlock station monitored both of these tests. The test results were satisfactory.

  f. <u>Flight unit FU-2 (Payload PL-5) -- Acceptance Tests</u>

   (1) <u>Payload checkout.</u> Instrument column checkout (Section IV.4.a) was successfully accomplished on February 9, 1960.

   (2) <u>Dynamic balancing.</u> Initial balancing was done in accordance with the balancing specifications in Section IV.4.b. This required 20 grams on the upper edge of the box at 0600 and 15 grams on the lower edge at 1045. An exact balance was not attempted at that time. The weights added reduced the unbalance to about 50% of the specified tolerance.

After the FU-2 was subjected to many of the acceptance tests, as indicated by the dates of the tests given in the following paragraphs, the final balancing was performed on March 2. A final balance weight of 30 grams on the upper edge of the box at 0600, and of 40 grams on the lower edge, 141° away in a clockwise direction from the upper weight gave a dynamic balance to within about seven inch-grams (1/4 inch-ounce). The setup for balancing is shown in Figure 104.

   (3) <u>Vibration test.</u> Vibration testing in three planes, as specified in Section IV.4.e, was successfully performed on February 16. Figure 105 shows the setup for a vibration test. In thrust direction a SUI light sensor in channel No. 2 was temporarily blocked by foreign matter with resulting reduced counting rates. An unidentified particle, possibly Eccofoam, was the cause. Channels 3, 4, and 5 showed momentary erratic counting rates during vibration but then returned to normal. The test was considered satisfactory.

Vibration in one direction perpendicular to thrust showed a fast count on channel No. 3 which returned to normal after vibration. This was considered acceptable.

Vibration in the other perpendicular to thrust direction caused a change in the channel No. 1 count rate. In this instance the trouble was caused by what appeared to be a flake of dark blue enamel which had been applied over a zinc chromate primer.
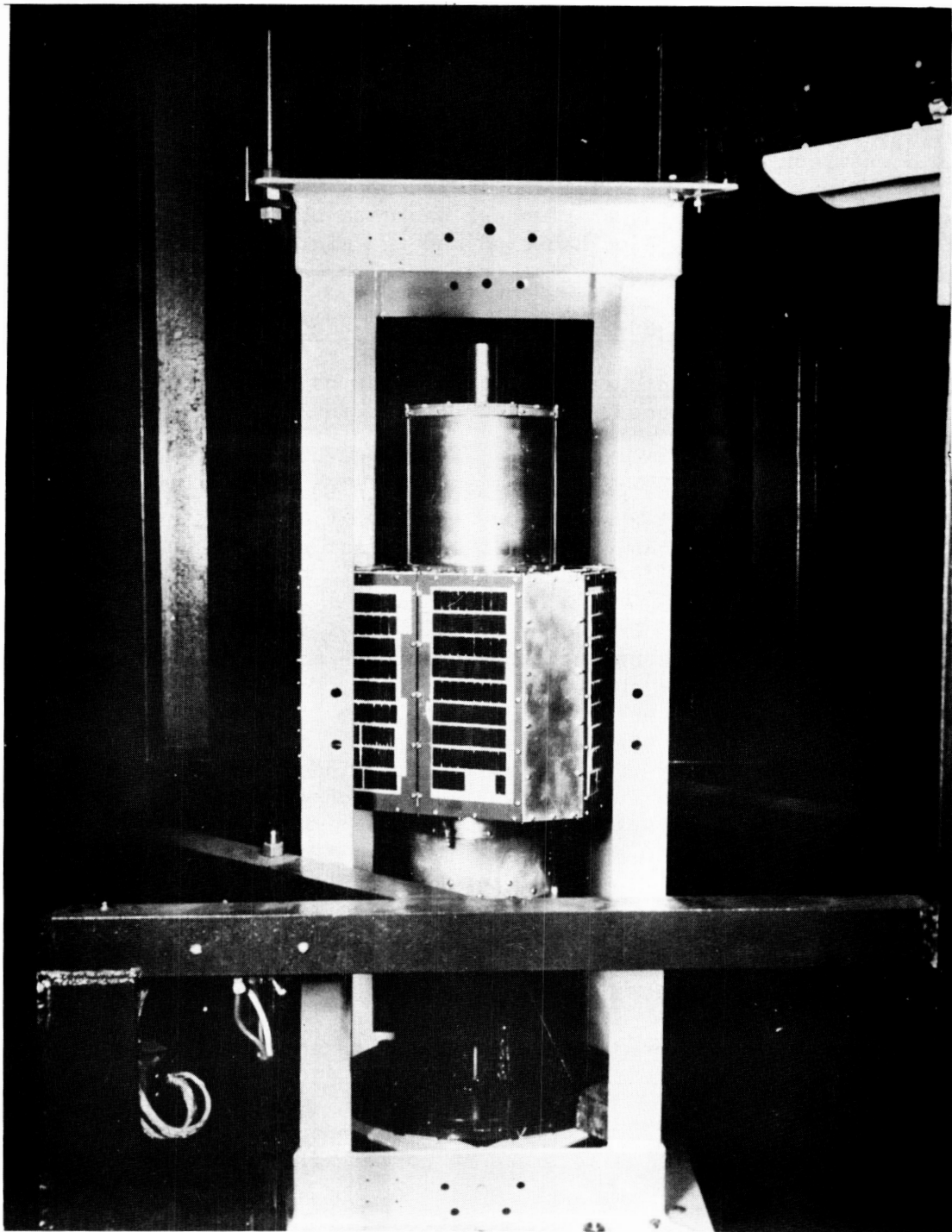
FIG. 104. PAYLOAD SET UP FOR DYNAMIC BALANCING
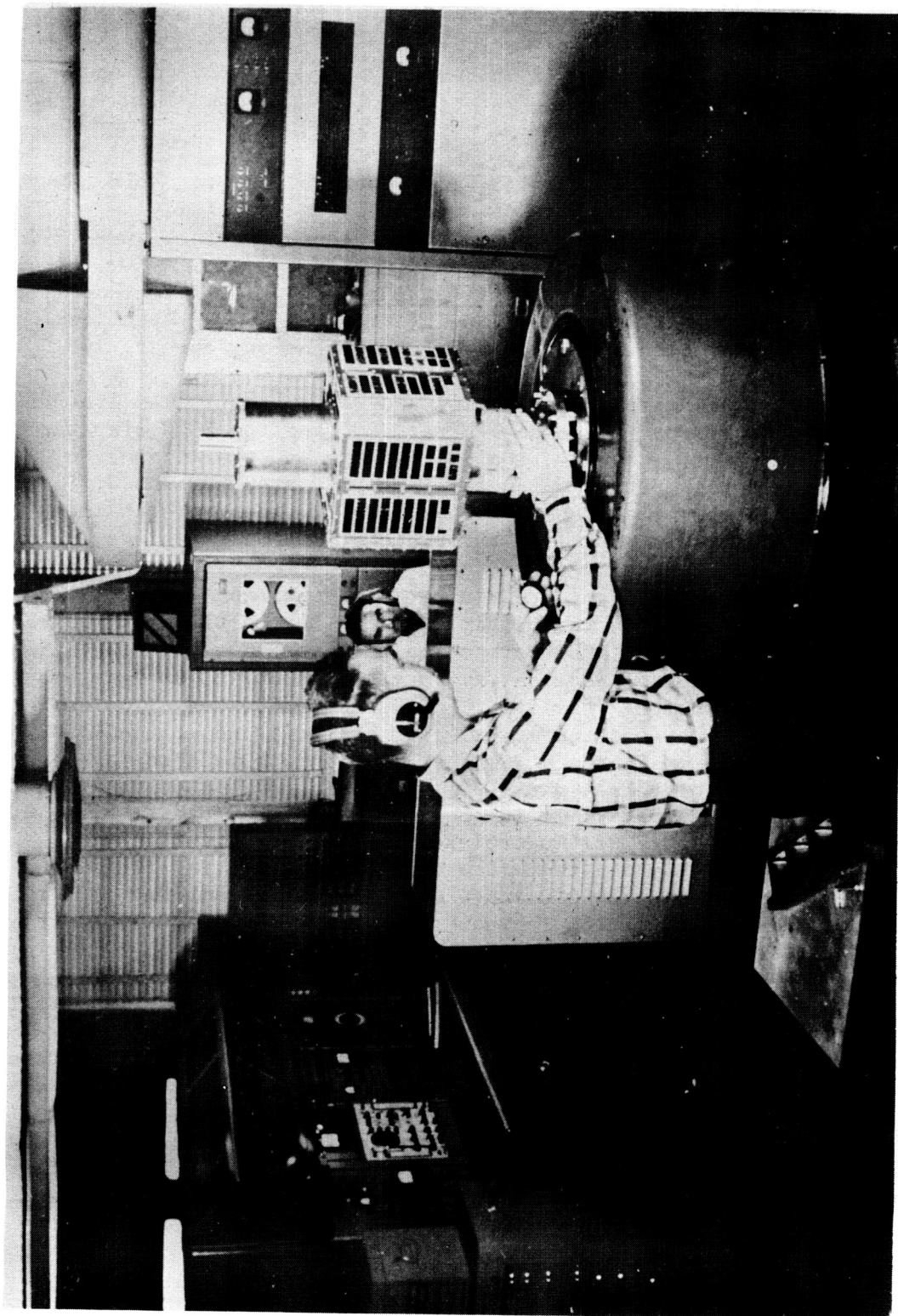
FIG. 105. A PAYLOAD VIBRATION TEST

(4) <u>Linear acceleration with spin</u>. The centrifuge with spin test, included as part of the flight acceptance tests (Section IV.4.f), was successfully performed on FU-2 on February 17. The payload and spinning gear, all mounted on the centrifuge platform, are shown in Figure 106.

(5) <u>Spin test</u>. The flight acceptance test for spin (Section IV.4.c) at 600 rpm for three minutes was successfully accomplished on February 19, 1960, using the setup shown in Figure 107.

(6) <u>Solar cell continuity during spin</u>. The flight acceptance test for solar cell continuity during spin, required by the specifications (Section IV.4.g), was also successfully accomplished on February 19.

(7) <u>Temperature calibration and vacuum test</u>. Temperature vacuum calibration of FU-2 began on February 23, and the 50°C step was successfully completed. However, the SUI package and the channel No. 2 of the multiplexer both performed unsatisfactorily at 0°C. The difficulty in the SUI package was established as inability to ground the channel No. 1 integrating circuit capacitor through the TS shorting plug, due to an open circuit between the wiring channel and the test socket. The capacitor was grounded by a soldered jumper in the wiring channel. Three transistors were replaced in the multiplexer and the multiplexer was then vibrated 16 seconds in the thrust direction in accordance with the flight acceptance specification of Section IV.4.e after which it was reassembled into FU-2 payload. The FU-2 payload then passed the 50°C step of the temperature calibration, but the multiplexer again failed at the 0°C step. At this point, on February 26, the decision was made to take the multiplexer from prototype payload PL-2, modify it to function as required in a flight model, and install it in the FU-2 flight payload in place of the malfunctioning PL-5 (FU-2) multiplexer. After the exchange of multiplexers the FU-2 payload temperature-vacuum calibration test was successfully accomplished at 50°C and 0°C. The test at ambient temperature was successfully carried out on February 27. Figure 108 shows preparations for one of these tests.

(8) <u>Rf field tests</u>. As a preliminary to the rf field tests, the transmitter current of FU-2 was checked with an empty fourth stage attached. The same current conditions were found as had been encountered in FU-1 as reported in e(8) above. The same antenna impedance difficulty due to the seven control wires was also found to exist. The same solution of small toroidal inductors was applied to FU-2 and corrected the trouble.

The rf field tests were carried out on March 3, 1960, in the same manner as for the FU-1 payload (e(8) above). Results were satisfactory.
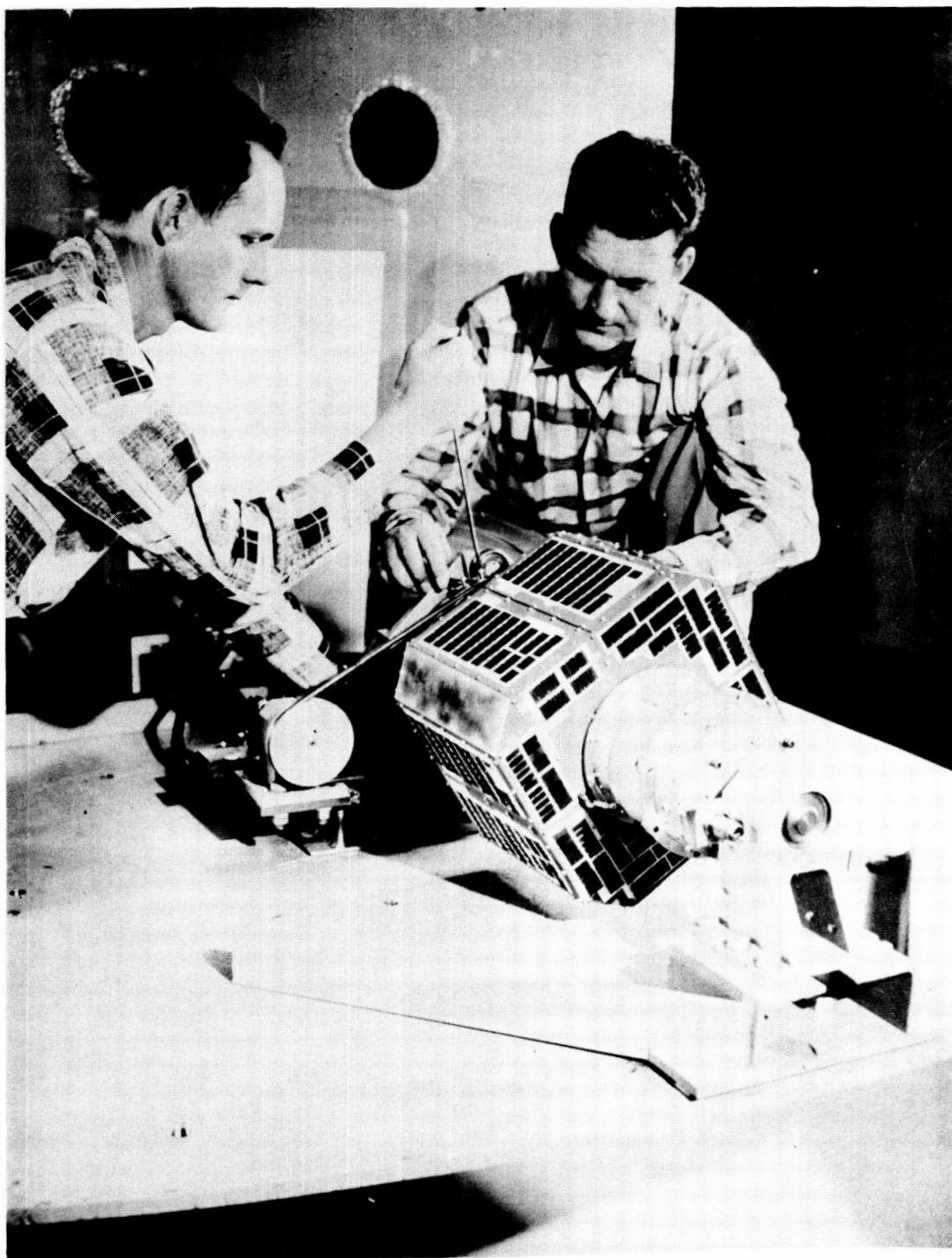
FIG. 106. PAYLOAD BEING SET UP FOR LINEAR
ACCELERATION WITH SPIN TEST
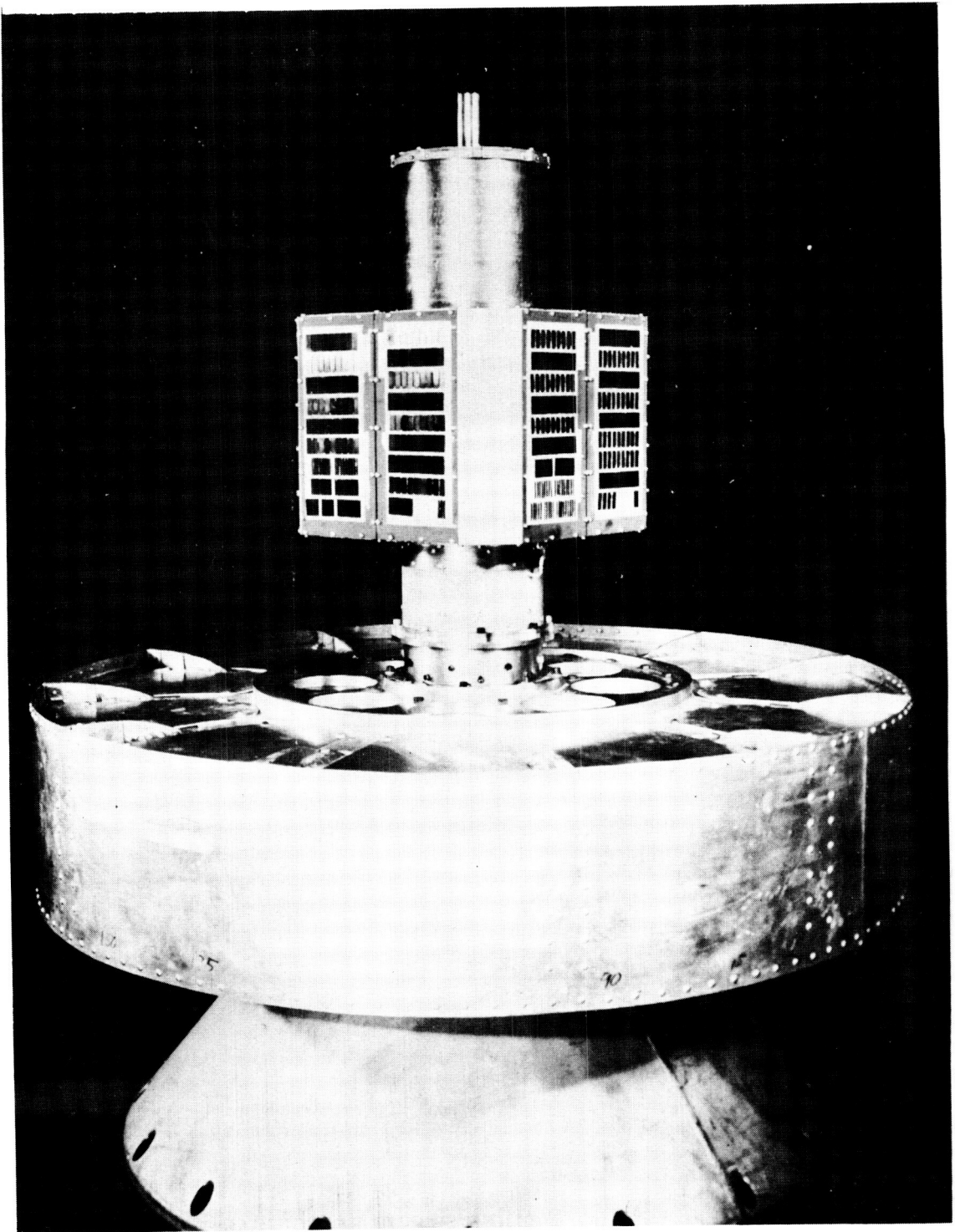
FIG. 107. PAYLOAD SET UP FOR SPIN TEST
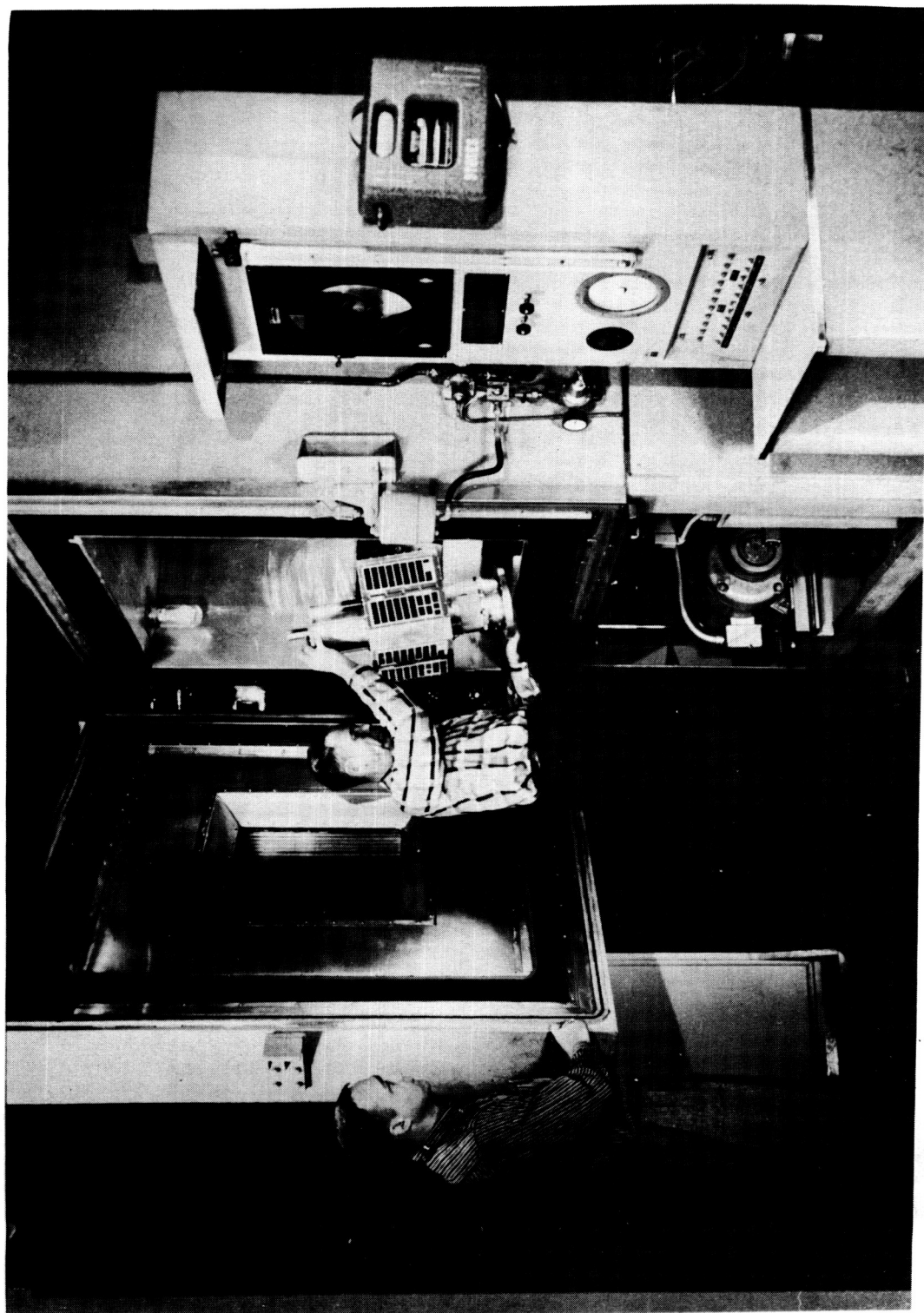
FIG. 108. PREPARATION FOR TEMPERATURE-VACUUM CALIBRATION TEST

(9) Moments of inertia, weight, and C.G. location
measurements. On March 4, 1960 the final mass measurements of payload
No. 5 (FU-2) were determined. With reference to Figure 109, the results
were as follows:

Weight in pounds	Center of Gravity (inches)	Mass Moment of Inertia in pounds-inch-second squared Axis		
		X-X	a-a	b-b
22.58	10.32	0.86	1.96	1.94

Accuracy of this data is: weight, ±0.03 lb; C of G, ±0.03 inch; roll
mass moment of inertia (X-X), ±0.10 lb in sec^2; pitch and yaw mass moment
of inertia, ±0.10 lb in sec^2. The mass moments of inertia are referenced
to the center of gravity of the payload (10.32 inches, measured forward
from the mating flange of the payload) and to standard gravity of 32.174
ft/sec^2. Figures 100 and 101 show the bifilar pendulum and torsion
pendulum setups used in making the moment of inertia measurements.

The longitudinal center of gravity of FU-2 was determined by the two
point suspension method using a shadowgraph scale supporting a knife edge
and suspended from a 0.035 inch diameter music wire at the other support.

(10) Final testing at Cape Canaveral. Flight unit FU-2 was
turned over to the Instrumentation Development Branch at Patrick Air
Force Base on March 4, 1960. The FU-2 payload was connected to a dummy
fourth stage on March 7 and a rf field test made. It was found that the
transmitter current was 45 milliamperes when connected to the antenna and
was 60 ma when connected to a 50 ohm standard load.

g. Final tests before launch. The transmitter current response
of FU-2 (paragraph f(10)) clinched the decision that the FU-2 transmitter
would be second choice for the unit to be launched.

On March 10, 1960, the SUI package of FU-2 was removed from the
instrument column for calibration, which took two days. The preference
of the State University of Iowa personnel was to fly the SUI package of
FU-2 while the preference of ABMA personnel was to fly the instrument
column of FU-1. This was resolved by replacing the SUI package of FU-1
with the package from FU-2. The new instrument column was then checked
and found ready for flight.

Final flight preparations were made on March 22. Both payloads, the
FU-1 flight unit (with the SUI package originally in FU-2) and the FU-2
spare flight unit (with the SUI package originally in FU-1), were each
mounted on a dummy fourth stage and their operation checked by microlock
station and monitor in Blockhouse 56. The tests on both were satisfactory.

AXES REFERENCE
SYSTEM USED IN
MASS MOMENTS
OF INERTIA
DETERMINATIONS

GUIDANCE & CONTROL AXES
REFERENCE SYSTEM

FLIGHT DIRECTION

10.32
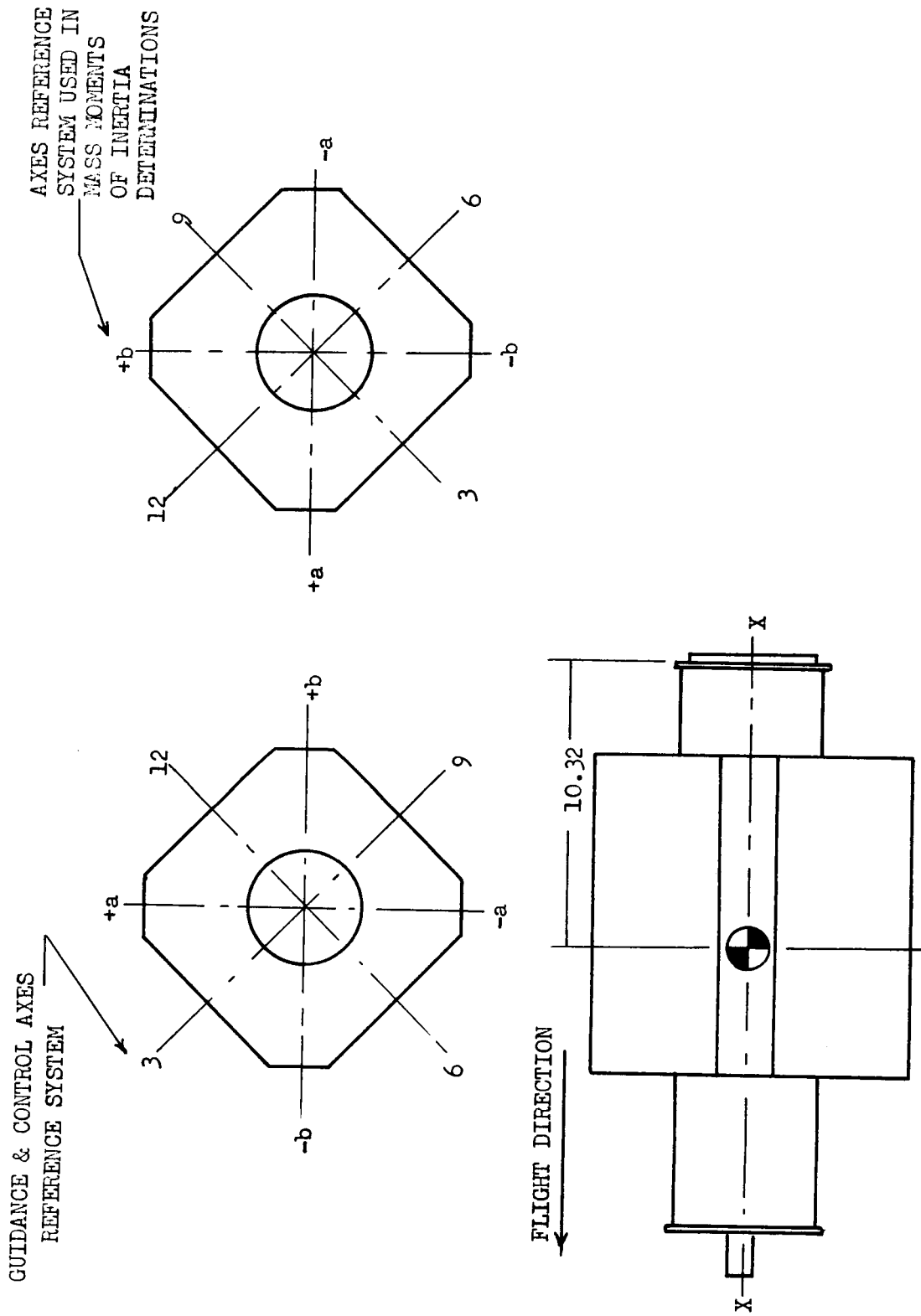
FIG. 109. MASS MEASUREMENTS DIAGRAM -- FLIGHT UNIT NUMBER 2

During a last visual inspection, paint chips were found in one of the cadmium sulfide detectors of the flight unit SUI package. The unit had to be dismantled, cleaned, and repainted. Bench check after reassembly was satisfactory.

After mounting the FU-1 flight unit on the rocket cluster, several rf checks were made. Channel No. 4 (Tabor Sensor) of the multiplexer increased in value after the shroud was mounted. Check with dry ice on the sensor showed that the thermistor was still responding so it was decided to fly the unit without further checks on the channel after it was assured that malfunction of this channel would not affect the remaining channels. The FU-1 payload functioned properly at liftoff and the transmitter signal was monitored from Blockhouse 56 until T + 50 seconds. The performance details are given in Chapter 2.

SECTION IV. TEST PROCEDURES AND SPECIFICATIONS

1. Testing of Individual Components at SUI Before Assembly

Individual components were mechanically and electrically inspected upon receipt from the manufacturers. They were then aged at a temperature of 120°C for approximately two weeks and retested. Parameter change patterns were determined, and components whose changes differed appreciably from the normal patterns were discarded.

Several critical components, such as G-M counters, were tested much more extensively following aging, in order to determine their operating characteristics and to facilitate selection of the best units.

The following is a listing of the tests and the criteria for rejection of abnormal components:

a. Transistors

(1) Check beta before and after aging.

(a) Beta to be within manufacturer's tolerance before and after aging.

(b) Change in beta to be less than ±5 percent

(2) Check switching time, before and after aging, in a grounded emitter amplifier circuit with $V_{cc} = 6.5$ volts, $R_L = 47$ K ohms, and a 47 K ohm resistor between base and the low impedance output of a square wave generator adjusted to switch between zero and ±3 volts.

(a) Rise time (to within e^{-1} of final value) to be less than five microseconds before and after aging.

(b) Change in rise time to be less than ±10 percent.

b. Diodes, 1N625

(1) Back resistance as measured with a Simpson model 260 meter to be greater than 20 M ohms before and after aging.

(2) Forward resistance as measured with a Simpson model 260 meter to be 1 K ohms ±30 percent before and after aging. Change in forward resistance to be less than +5 percent.

c. Diodes, 608C. Same as 1N625 except back resistance to be greater than 5 M ohms and forward resistance to be between 20 and 35 ohms.

d. Diodes, zener, 650C0 and 652C3. Zener voltage to be within manufacturer's tolerance before and after aging.

e. Diodes, zener, 1N1327

(1) Zener voltage to be within manufacturer's tolerance before and after aging.

(2) Flight unit diodes selected on the basis of zener voltage dependence on diode current and temperature.

f. Diodes, high voltage, HR10318

(1) Forward resistance as measured with a Simpson model 269 meter to be between 18 and 24 ohms before and after aging.

(2) Back resistance as measured with a Simpson model 269 meter (10^5 scale) to be greater than 200 M ohms before and after aging.

(3) Read reverse current with the diode, a 135 volt battery and a Keithley electrometer in series, with the diode at 75°C.

(a) Reverse current to be below 0.2 μA before and after aging.

(b) Change in reverse current to be less than 0.1 μA.

192

g. Resistors, Allen Bradley type TR

(1) Resistor value to be within manufacturer's tolerance before and after aging.

(2) Change in resistance to be less than minus five percent, plus zero.

h. Resistors, Dale Products type DC (used in series with 700 volt regulator)

(1) Resistor value to be within manufacturer's tolerance before and after aging.

(2) Change in resistance to be less than minus zero, plus one percent.

i. Capacitors, RMC (for high voltage power supplies). Read leakage current with the capacitor, a 700 volt battery, a 10 M ohm resistor, and a Keithley electrometer in series before and after aging. Leakage current to be less than 10^{-9} amp before and after aging.

j. Capacitors, Glenco ceramic. Check before and after aging for abnormally high leakage current at 67-1/2 volts.

k. Capacitors, Sprague type 150D tantalum. Check before and after aging for abnormally high leakage current at rated voltage.

l. Transformers, Rayco type 0-3767A. Check in test circuit before and after aging.

(1) Overall circuit power efficiency to be 42 ± 3 percent.

(2) Change in efficiency to be less than ± 1 percent.

(3) Transformers having the highest efficiencies to be set aside as flight components.

m. Transformers, Rayco type 0-3753. Check in test circuit before and after aging.

(1) Overall circuit power efficiency to be 51 ± 3 percent.

(2) Change in efficiency to be less than ± 1 percent.

(3) Transformers having the highest efficiencies to be set aside as flight components.

n. <u>Voltage regulator tubes, Victoreen, 700 volt</u>. NOTE: Aging temperature for regulator tubes 100°C.

(1) Check regulator voltage as a function of regulator current at room temperature before aging in test circuit (with tube paralleled by a series connected 0.01 μfd capacitor and 100 K ohm resistor). Voltage and regulation to be within manufacturer's tolerance.

(2) Stabilize regulator tube operation after aging by running at about 20 μA for 12 hours at room temperature.

(3) After aging check regulator voltage as a function of regulator current in test circuit at 75, 50, 25, 0, -25, and -50°C.

(a) Room temperature characteristics to be essentially the same as those before aging.

(b) Tubes having the best regulation characteristics to be set aside as flight components.

o. <u>Neon lamps</u>. Selected on the basis of firing voltage stability as a function of temperature and leakage resistance.

p. <u>Cadmium sulfide detectors</u>. Selected on the basis of dark current, response time, physical size, physical structure, electron sensitivity, and X-ray sensitivity.

q. <u>G-M counters</u>. Selected on the basis of threshold voltage, constancy of threshold voltage, shape of the counting rate versus voltage and temperature curves, and effectiveness of quenching (absence of double pulses and continuous discharge).

2. <u>Inspection and Testing of SUI Modules Before Stacking</u>

Following assembly of the components on the deck cards, the modules were subjected to a series of inspections and tests to make sure that they would operate according to specifications.

a. <u>Preliminary inspection of scaler decks</u>

(1) Check alignment of interdeck spacers and terminal boards.

(2) Inspect each solder joint under a binocular microscope (10X).

(3) Visually check wire clearances and security of parts.

b. <u>Preliminary inspection of detector assembly</u>

(1) Inspect each solder joint under a microscope.

(2) Visually check wire clearances and security of parts.

c. <u>Preliminary electrical check of scaler decks</u> (room temperature)

(1) Connect decks to test panel. Apply power (6.50 and 10.40 volts) to deck F and check the regulator voltage (5.0 ± 0.2 volts) and the input currents. Deck F must remain on during all other tests.

(2) Turn on the other scaler decks in turn and check the input currents.

(3) With the test panel time constant switch on "fast" (capacitors ungrounded) feed a test signal to one deck at a time and check the scaling factors. Input pulse requirements are width = 5 μsec, amplitude = 3.1 volts, polarity = negative, rise time < 0.1 μsec, source impedance = 50 ohms.

(4) Check scaler operation, one deck at a time, as a function of input pulse rate. Decks E and G should count to at least 30,000 sec^{-1} and decks C, D and F to at least 10,000 sec^{-1}.

(5) Adjust the 820 K ohm and 1.2 M ohm nominal value resistors in the logic summing circuits so that the maximum and minimum output voltages are 5.0 ± 0.2 and 1.0 ± 0.1.

(6) Ground the logic circuit RC capacitors and check that the time constants are 5 ± 1 sec.

(7) Repeat steps 2c(1) through 2c(4) with the supply voltages equal to 5.50 and 9.40, and 7.50 and 11.40 volts.

d. <u>Preliminary electrical check on detector assembly</u> (room temperature)

(1) Connect assembly to test panel with AB and TS cables (with all scaler decks also connected). Apply power and check currents.

(2) Adjust the two power supply bias resistors separately. The 160 volt supply should draw 6.0 ± 0.1 ma at V_{cc2} = 6.50 volts (R ≈ 47 K ohms), producing 125 ± 7 μA regulator diode current. The 700 volt supply should draw 11.0 ± 0.2 ma at V_{cc2} = 6.50 volts (R ≈ 22 K ohms), producing 45 ± 5 μA regulator tube current. These resistors should be deposited carbon.

(3) With the appropriate detectors connected to the inputs, check the pulse shaping amplifier output pulse heights (3.2 ± 0.1 volt), rise times (less than one microsecond), widths at half amplitude (22 ± 2 μsec for detectors A and B, 9 ± 3 μsec for detectors C and D, and 13 ± 3 μsec for detector E), and widths at full height (about 2 μsec less than at half height).

(4) Check that the current (regulated 5.0 volts) to the pulse shaping amplifiers is less than 15 μA total (no sources near detectors).

(5) Repeat steps 2d(1), (3), and (4) with the supply voltages equal to 5.50 and 9.40, and to 7.50 and 11.40 volts.

e. Temperature cycle test of scaler decks

(1) Locate modules in temperature chamber and connect to the test panel. Provide a pulse source to all five scalers and monitor the outputs continuously.

(2) Temperature cycle between 100° and -50°C. Check operation after stabilization following each temperature change.

(3) Continue the test for at least one complete cycle after repairing the last difficulty, but in any event for at least three full cycles.

f. Temperature cycle test of detector assembly

(1) Locate assembly in temperature chamber and connect through AB and TS cables to test panel. Connect all scaler modules to test panel. Provide appropriate radioactive and light sources to stimulate the detectors.

(2) Temperature cycle between 75° and -50°C. Do not exceed 75°C. Check operation after stabilization following each temperature change.

(3) Same as 2e(3) above.

g. Temperature-voltage test of scaler decks

(1) Connect the modules as in 2e above. Use the following test conditions:

(a) Temperature = 25, 100, 50, 0, and -50°C (in that order).

(b) V_{cc1} = 9.40, 10,40, and 11.40 when V_{cc2} = 5.50, 6.50, and 7.50 volts, respectively.

(2) Check and record:

(a) Minimum supply voltage V_{cc2} (min) for proper operation (voltage at which scaling factor changes) with V_{cc1} = 9.40, pulse rate = 1000 sec^{-1} for decks C, D, and F, pulse rate = 10,000 sec^{-1} for decks E and G.

(b) Same as (a) except determine the supply voltage at which the output amplifier state 8 output voltage begins to decrease appreciably.

(c) Power supply current to each module from each supply.

(d) Maximum counting rate for each scaler.

(e) Output amplifier minimum and maximum voltages.

(f) Voltage from the nominal 5.0 volt regulator.

(3) Upon completion of test elevate package temperature before opening chamber to prevent condensation of moisture on instruments.

h. Temperature-voltage test of detector assembly

(1) Connect the modules as in 2f(1) above. Use the same test conditions as in 2g(1) above. Locate sources at appropriate fixed distances for the duration of the complete test.

(2) Check and record:

(a) Power supply current from the nominal 6.5 volt supply.

(b) 700 volt supply regulator tube current.

(c) 160 volt supply regulator diode current.

(d) 700 volt supply voltage. Measure with electrostatic voltmeter, with V_{cc2} adjusted for regulator currents of 5, 10, 30, 50 and 70 μA.

(e) 160 volt supply voltage. Measure with Simpson type 269 (100,000 ohms per volt) meter on 400 volt scale, with V_{cc2} adjusted

for regulator diode currents of 20, 40, 60, 80, 100, 120, and 140 μA. Disconnect voltmeter for all other tests.

(f) Pulse shaping amplifier pulse amplitudes, rise times, widths at half amplitude, and widths at full amplitude.

(g) Counting rates of the five detectors with the sources located in their standard positions.

i. Test of modules after encapsulation

(1) Inspect for voids and trim.

(2) Connect to test panel. Check currents, regulated voltage, scaling factors and logic circuit operation, maximum scaling rates, output voltages, pulse shaping amplifier output waveforms, and high voltage power supply regulator currents at room temperature.

(3) Mark modules with deck identification and serial number.

3. Testing of the Completely Assembled Instrumentation Package at SUI

a. Inspection following final assembly and channel wiring

(1) Before applying power, check all wiring with a terminal-to-terminal continuity check.

(2) Connect to the test panel with the PP and TS cables.

(3) Apply power and measure currents.

(4) Check high voltage power supply regulator currents.

(5) Check power supply collector waveforms.

(6) Check pulse shaping amplifier output waveforms.

(7) With sources in their standard positions, read counting rates and compare with earlier readings.

(8) Check scaling factors and operation of the logic circuits and output amplifiers.

(9) Ground the integrating capacitors in the logic circuits and check the time constants.

b. <u>Vibration test</u>

(1) Mount package on the table in the proper position. Vibrate along the thrust axis, transverse to the thrust axis and along the spectrometer axis, and transverse to the thrust and spectrometer axes. Connect to test panel through PP and TS cables. Connect output signal to data recording system.

(2) Locate sources to give appropriate counting rates.

(3) Before each run equalize the shake system with the instrument assembly in place. Do not exceed one g vibration level during equalization.

(4) Before and after each test check and compare with previous readings:

(a) Supply currents.

(b) Regulator currents.

(c) Pulse shaping amplifier output waveforms.

(d) Scaling factors and logic circuit operation.

(5) Before, during, and after each test record the outputs of all five channels simultaneously and continuously to check for faulty operation. Record the counting rates.

(6) Vibrate according to the following schedule. All tests are random noise, uniform spectral density over range of 20-1500 cycles per second.

(a) Direction of thrust

Prototype units - 25 g's RMS for two minutes.

Flight units - 20 g's RMS for 30 seconds.

(b) Both transverse axes

Prototype units - 15 g's RMS for two minutes.

Flight units - 12 g's RMS for 30 seconds.

c. <u>Vacuum test</u>

(1) Install instrumentation package in vacuum chamber. Connect to test panel through PP and TS cables. Record both high voltage power supply currents continuously throughout duration of test on a moving chart recorder.

(2) Reduce pressure to less than 100 microns Hg (preferably to less than 10 microns Hg) and monitor for at least one hour. Power supply arc-over is indicated by downward deflections of the current readings.

(3) Remove power from package and allow it to remain overnight at a pressure of less than 100 microns.

(4) Apply power, run for at least one hour, checking continuously for arc-over.

(5) Increase pressure to atmospheric and check continuously for arc-over for at least one hour.

d. <u>Temperature test and calibration</u>

(1) Locate instrumentation package in temperature chamber and connect to test panel through PP and TS cables. Connect output signal to data recording system.

(2) Locate sources in standard positions.

(3) Use the following test conditions:

(a) Temperature = 25, 75, 50, 0, -50°C (in that order).

(b) V_{cc1} = 9.40, 10.40, and 11.40 when V_{cc2} = 5.50, 6.50, and 7.50 volts, respectively.

(4) Allow package to stabilize at each new temperature as determined by monitoring the rate of change of the SUI thermistor resistance. At least three hours is required for stabilization after a 50°C change.

(5) Check and record:

(a) Power supply current to the package from each supply.

(b) Both high voltage power supply currents.

(c) Pulse shaping amplifier output pulse amplitude and width at half height.

(d) Counting rates of all five detectors.

(e) Steady-state resistance of the SUI thermistor.

(6) Upon completion of the test, elevate package temperature before opening chamber to prevent condensation of moisture on instruments.

e. Temperature soak

(1) Connect package as in 3d(1) and (2) above. Place silica gel in chamber during the low temperature soak.

(2) Allow the package to remain for twelve hours at 65° and -25°C.

(3) Using the test conditions outlined in 3d(3)(b) above, check and record the data outlined in 3d(5) above before each temperature change and two hours after each temperature change.

(4) Upon completion of the test elevate the package temperature before opening chamber to prevent condensation of moisture on instruments.

4. Testing of the Completely Assembled Payload at ABMA

A complete set of electrical, mechanical, and rf tests was made following final assembly of the payloads at ABMA.

a. Payload checkout procedure. Before and after each phase of the testing program, perform an operational check to determine whether a malfunction results from the test. During the environmental tests make those operational checks which are possible in view of the limited access to the payload during the test, and which are necessary to determine the occurrence of a malfunction.

(1) Connecting the payload

(a) Connect the external power supply to the payload.

(b) Connect the SUI package TS cable to the SUI test panel. NOTE: Whenever power is applied to the SUI package either the test panel must be connected to the TS socket or a shorting plug must be in place.

(c)   Connect the transmitter output cable to an rf wattmeter through a two db attenuator. NOTE: The transmitter must always be terminated in a proper load whenever input power is supplied.

(d)   Provide standard radioactive and light sources for the detectors. NOTE: The source strength and position must be the same for all tests in order that changes in detector sensitivity and scaling factors can be easily discovered.

(2)   Activation of the payload

(a)   Allow all test equipment to warm up.

(b)   Apply the 15.6, 10.4, and 6.5 volt power, either from the external or internal supply as necessary.

(c)   Read and record the supply voltages and currents.

(d)   Read and record the SUI high voltage power supply regulator currents.

(3)   Transmitter measurements

(a)   Read and record the power output. This should be 300 ± 30 mw.

(b)   Connect the transmitter output to the AM and PM detectors. NOTE: Always turn the 15.6 volt power off when disconnecting the transmitter load. Read and record the relative amplitudes of the outputs of the AM and PM detectors.

(c)   Connect the transmitter output to the frequency counter. Read and record the transmitter center frequency. This should be 108.0300 ± 0.0015 mc/sec.

(4)   Subcarrier oscillator measurements

(a)   Connect the transmitter output to the modified Clarke receiver, and the receiver output to the subcarrier discriminators, Sanborn recorder, and, if necessary, to the tape recorders. Calibrate the equipment.

(b)   Obtain a Sanborn record of the telemetered data.

(c)   Observe from the calibrated Sanborn record that the subcarrier oscillators are operating properly.

(5) Electronic commutator check. Obtain at least one full cycle of the commutator (multiplexer) and ascertain that all channels are operating properly.

(6) SUI package measurements

(a) Read and record the counting rates of all five detectors from the Sanborn record.

(b) Read and record the pulse shaping amplifier output pulse heights and widths from the SUI test panel. NOTE: It is necessary to perform this test only every few days during the testing program.

(c) Ground the integrating capacitors at the SUI test panel and check the time constants as observed on the Sanborn record.

(7) Deactivation of payload

(a) Turn the power supplies off.

(b) Remove the external cables and radioactive and light sources.

b. Dynamic balancing

(1) Applicability: PL-2, 3, 4 and 5.

(2) Operational checks: None required.

(3) Specifications:

(a) Spin rate during balancing not to exceed 600 rpm.

(b) Final balance to be such that the perpendicular distance from the center of gravity to the nominal axis of rotation does not exceed 0.51 mm.

c. Spin

(1) Applicability:

(a) Prototype approval test to PL-3.

(b) Flight acceptance test to PL-4 and PL-5.

(2) Operational checks:

(a) Before and after test. See 4a above.

(b) During test. Monitor demodulated signals on Sanborn recorder.

(3) Specifications:

(a) Prototype approval test

$\underline{1}$ Spin rate: 750 rpm.

$\underline{2}$ Duration: 20 minutes.

(b) Flight acceptance test

$\underline{1}$ Spin rate: 600 rpm.

$\underline{2}$ Duration: 3 minutes

d. Shock

(1) Applicability: PL-3

(2) Operational checks: See 4a above.

(3) Specifications:

(a) Number of shocks: 45.

(b) Linear acceleration: 25 g's near shock.

(c) Impulse rise time: about 90 msec.

e. Vibration

(1) Applicability:

(a) Prototype approval test to PL-3.

(b) Flight acceptance test to PL-2, 4, and 5.

(2) Operational checks:

(a) Before and after each phase. See 4a above. In addition solar batteries to be carefully checked.

    (b) During tests. Monitor demodulated signals on Sanborn recorder.

    (3) Method of application: Tests to be performed along three axes; the thrust axis and two mutually perpendicular transverse axes.

    (a) Thrust axis. Payload to be mounted vertically on the horizontal vibration table.

    (b) Transverse to thrust axis. Payload to be mounted to table with L-shaped fixture. Table vibrating surface to be vertical. Payload to be vertical. Payload and fixture weight to be supported by two elastic supports fastened to ceiling.

    (4) Specifications: All tests to be random noise, uniform spectral density in frequency range 20 to 1500 cycles per second.

    (a) Prototype approval test

Direction	RMS g Level	Duration (sec)
Thrust	25	0.2
	15	7.8
	25	0.2
	15	7.8
	25	0.2
	15	7.8
	25	0.2
	15	7.8
	20	120.0
Transverse to Thrust	20	0.2
	12	7.8
	15	120.0

(b)   Flight acceptance test

Direction	RMS g Level	Duration (sec)
Thrust	20	0.2
	12	7.8
	20	0.2
	12	7.8
Transverse to Thrust	12.5	0.2
	7.5	7.8

f.   **Linear acceleration and spin combined**

(1)   Applicability:

(a)   Prototype approval test to PL-3.

(b)   Flight approval test to PL-4 and PL-5.

(2)   Operational checks:

(a)   Before and after test. See a above.

(b)   During test. Monitor demodulated signals on Sanborn recorder.

(3)   Method of application: Payload to be mounted with nose toward centrifuge axis. Base of payload to be 2.285 meters from centrifuge center.

(4)   Specifications:

(a)   Prototype approval test. Radial acceleration of 99 g's corresponds to centrifuge speed of 148 rpm.

Accumulative time (min)	Payload spin rate (rpm)	Radial Acceleration (g)
0-15	735	0
15-17	735	0-99
17-18	735	99
18-20	735	99-0
20-25	735	0

(b) Flight acceptance test. Radial acceleration of 35 g's corresponds to centrifuge speed of 88 rpm.

Accumulative time (min)	Payload spin rate (rpm)	Radial Acceleration (g)
0-5	437	0
5-7	437	0-35
7-8	437	35-0
8-10	437	0

g. Solar cell continuity during spin

(1) Applicability:

(a) Prototype approval test to PL-3.

(b) Flight acceptance test to PL-4 and PL-5.

(2) Operational checks:

During test check continuity of all solar cells.

(3) Specifications:

(a) Prototype approval test. Spin rate to be 750 rpm for as long as necessary to conduct continuity check.

(b) Flight acceptance test. Spin rate to be 500 rpm for as long as necessary to conduct continuity check.

h. Temperature-vacuum soak

(1) Applicability: PL-2

(2) Operational checks: Satellite instrumentation to be operated continuously throughout test, and demodulated signal to be recorded and checked on Sanborn recorder continuously throughout test. External power to be used except as specified below.

(3) Specifications:

(a) Vacuum of 5 x 10^{-4} mm Hg or better to be maintained throughout test.

(b) Total duration of test to be 14 days.

(c) No part of the payload is to be permitted to fall below -20°C or to rise above 75°C during the test.

(d) Temperatures to be maintained within ± 5°C of specifications and to be read with an accuracy of ± 1°C.

(e) Test to begin with the establishment of vacuum at room temperature.

(f) Heat and stabilize payload temperature at 50°C. Stabilization will require about six hours. Maintain at 50°C for 12 hours after stabilization.

(g) Cool and stabilize payload temperature at 0°C and maintain at that temperature for 12 hours after stabilization.

(h) Heat and stabilize payload temperature at 25°C. Calibrate payload temperature measurements and read counting rates.

(i) Heat and stabilize payload temperature at 50°C. Maintain at that temperature for half of the remainder of the 14 day period. Calibrate payload temperature measurements and read counting rates near beginning and end of this period. Operate instrumentation on internal power for the last 40 minutes.

(j) Cool and stabilize payload temperature at 0°C. Maintain at that temperature for all but six hours of the remainder of the 14 day period. Calibrate payload temperature measurements and read counting rates near beginning and end of this period. Operate instrumentation on internal power for the last 40 minutes.

(k) Heat payload to room temperature and terminate test.

(1) Chemical batteries to be subjected to a discharge-charge cycle at ambient pressure following termination of test.

i. Temperature calibration and vacuum test

(1) Applicability:

(a) See paragraph h above for calibration and vacuum test of PL-2.

(b) This paragraph applies to PL-3, PL-4, and PL-5.

(2) Specifications:

(a) Vacuum of 0.1 mm Hg or better to be maintained throughout test.

(b) SUI high voltage power supply regulator currents to be monitored and recorded continuously throughout test.

(c) No part of the payload is to be permitted to fall below -20°C or to rise above 75°C during the calibration and test.

(d) Calibrations to be made at 0°, 25°, and 50°C. Payload temperature is to be completely stabilized before making readings.

(e) Calibration is to include calibration of the payload temperature measurements and reading of the detector counting rates.

(f) The occurrence of any rapid downward deflections of the high voltage power supply regulator currents is to be interpreted as failure of the payload to pass the vacuum test and will require resealing of the high voltage power supply.

j. Determination of thermal characteristics

(1) Applicability: PL-1.

(2) Instrumentation is not to be operated during the test. Operational checks are not required.

(3) Thermistors are to be located in the payload in such a manner that the temperatures of all sections of the payload can be measured.

(4) Vacuum of 5 x 10^{-4} mm Hg or better to be maintained throughout tests.

(5) Test 1 (perform twice) to determine thermal time constant. Stabilize temperature at -20°C. Heat all external surfaces rapidly to 70°C and hold constant until internal payload temperature is nearly stabilized. Step-change in temperature to be accomplished in such a manner that the external surfaces rise from -20°C to 60°C in less than three minutes.

(6) Test 2 (perform twice) to determine thermal characteristics when illuminated by the sun from a direction normal to one side of satellite. Stabilize temperature at -20°C. Heat external surfaces on one side of payload. Heat input to be known and variable over range zero to at least one watt per square inch. Heat input to be varied as determined from consideration of detailed thermal design. Unheated surfaces to exchange radiant energy with either highly reflective surfaces or surfaces at the temperature of liquid nitrogen. Test to end when payload temperatures stabilize.

Chapter 8

THE DEVELOPMENT OF A
CORPUSCULAR RADIATION EXPERIMENT
FOR AN EARTH SATELLITE*

George H. Ludwig
Research Fellow of the U.S. Steel Foundation

SECTION I.   INTRODUCTION

During a large part of the past decade the State University of Iowa
(SUI) cosmic ray group has been engaged in a program of study of the cor-
puscular radiation in the vicinity of the earth and in extra-terrestrial
space.   The most important single finding of this program has been the
discovery in 1958 of belts of radiation consisting of reservoirs of
charged particles trapped by the earth's magnetic field.   The study of
these trapped particles and the associated phenomena by the use of earth
satellite and space probe borne instrumentation has occupied an increas-
ingly large fraction of the laboratory's effort.

This chapter describes the preparation of the SUI experiments for
satellite S-46.   It is hoped, in spite of the fact that this payload
failed to orbit following the launch attempt on March 23, 1960, that the
complete description of this project will serve as a valuable reference
for those engaged in similar projects.

SECTION II.   HISTORY OF THE RADIATION EXPERIMENTS

The work of the SUI laboratory began in 1952 with the use of balloon
and rockoon borne experiments to investigate the lower energy end of the

---

primary cosmic-ray spectrum.[1] An unexpected result was observed in 1953 in the vicinity of the northern auroral zone when the counting rates of G-M counters were observed to rise to very high rates at altitudes above about 40 km.[2] During the following five years the effect was observed repeatedly, and was interpreted as being due to the bremsstrahlung from low energy (< 100 kev) electrons incident on the high atmosphere and on the material of the rocket instrumentation. It was believed that this was a direct detection of the particles which produced the visible aurorae.[3,4,5,6]

In 1956, after it was realized that this country had advanced technologically to the point where satellites could be launched, instruments for the investigation of the primary cosmic rays were designed to take advantage of their ability to gather data for long periods of time over large fractions of the earth's surface. The first instruments used in the SUI program were contained in satellite 1958 Alpha (Explorer I),[7] launched on February 1, 1958 (universal time). The first data from this satellite, obtained from receiving stations located in the United States, and therefore transmitted while the satellite was near perigee height, indicated that the instrumentation was operating as planned. The G-M counter rate was plotted as a function of height in the vicinity of California, and this curve, when extrapolated down to altitudes previously investigated by rockets, agreed with the earlier data. During the second week in March the first tapes from stations in South America were reduced. These data were obtained while the satellite was at a greater height and near the equator, and showed an immediately unexplainable apparent counting rate of zero. This phenomenon was still being investigated at the time satellite 1958 Gamma (Explorer III)[8] was successfully launched on March

1. J. A. Van Allen, The Cosmic Ray Intensity Above the Atmosphere Near the Geomagnetic Pole, Il Nuovo cimento 10, 630,1953.

2. L. H. Meredith, M. B. Gottlieb, and J. A. Van Allen, Direct Detection of Soft Radiation Above 50 Kilometers in the Auroral Zone, Phys. Rev. 97, 201, 1955.

3. F. B. McDonald, R. A. Ellis, and M. B. Gottlieb, Rocket Observations on Soft Radiation at Northern Latitudes, Phys. Rev. 99, 609, 1955. (abstr)

4. J. A. Van Allen, Direct Detection of Auroral Radiation with Rocket Equipment, Proc. Natl. Acad. Sci. U.S., 43, 57, 1957.

5. C. E. McIlwain, Direct Measurement of Radiation Associated with Visible Aurorae, IGY Rocket Report Series No. 1, Natl. Acad. Sci., 164, July 1958.

6. C. E. McIlwain, Direct Measurement of Particles Producing Visible Aurorae, J. Geophys. Research, in press, 1960.

7. G. H. Ludwig, Cosmic Ray Instrumentation in the First U.S. Earth Satellite, Rev. Sci. Instr. 30, 223, 1959.

8. G. H. Ludwig, The Instrumentation in Earth Satellite 1958 Gamma, M.S. Thesis, State University of Iowa research report 59-3, February 1959.

26, 1958. The first recording of the internal storage mechanism in the satellite was received at SUI on April 3, 1958, and almost immediately the conclusion was reached that the zero apparent rate was due to counter saturation and that the earth was therefore surrounded by a region of intense radiation. The later recordings from this satellite yielded the first crude survey of the spatial extent of this region of radiation.[1]

These two early satellites had originally been instrumented to investigate the cosmic ray and cosmic ray albedo corpuscular radiation, and the high intensity trapped radiation had been quite unexpected. As soon as the general characteristics of the belt became known from the Explorer I and III data, it was decided to instrument another payload with detectors having a much greater dynamic range and able to provide some information about the radiation belt particle type and energy spectrum. As a result satellite 1958 Epsilon (Explorer IV) was launched on July 26, 1958.[2] This satellite provided:

1. A more complete survey of the spatial distribution of the radiation at heights up to 2220 km, and to a latitude of ±51° geographic (The earlier U.S. satellites had inclinations of 33°.)

2. A measure of the radiation intensity by detectors having several different characteristics and under various amounts of absorber

3. Some information on particle identification

4. Several points on the particle energy spectrum curve for a wide range of positions

5. A rough indication of the angular distribution of the trapped particles

6. Important information about the trapping mechanism obtained as a result of project Argus[3]

The USSR satellite 1957 Beta (Sputnik II), launched November 3, 1957, had carried a G-M counter for the study of cosmic rays, but because its orbit was so low over the USSR, and because their ground receiver network was confined almost entirely to the USSR, only a very small counting rate increase at the latitude corresponding to the lower extreme of the outer

1. J. A. Van Allen, G. H. Ludwig, E. C. Ray, and C. E. McIlwain, Observations of High Intensity Radiation by Satellites 1958 Alpha and Gamma, IGY Bulletin, Trans. Am. Geophys. Union 39, 767, 1958. Also Jet Propulsion 28, 588, 1958.

2. J. A. Van Allen, C. E. McIlwain, and G. H. Ludwig, Radiation Observations with Satellite 1958 Epsilon, J. of Geophys. Research 64, 271, 1959.

3. J. A. Van Allen, C. E. McIlwain, and G. H. Ludwig, Satellite Observations of Electrons Artificially Injected into the Geomagnetic Field, J. Geophys. Research 64, 877, 1959.

belt was detected, and the proper significance was not attached to it.[1,2] Upon learning of the Explorer I and III results, they included equipment on satellite 1958 Delta (Sputnik III, launched on May 15, 1958) to study the high intensity radiation. The results obtained from this experiment confirmed, in general, our earlier findings and those obtained from Explorer IV.[3]

The experiments described above were carried in satellites having apogee heights of less than 2500 km. As a result, the configuration of the higher altitude regions of the belt structure was not known. The existence of two separate belts had not been unambiguously indicated by the low altitude data, although its possibility was realized, as indicated in private communications by C. E. McIlwain in October 1958.

The importance of extending the spatial survey to greater radial distances was evident. As a result, radiation detectors were prepared for the Pioneer series of space probes. The data received from Pioneer I, which was launched on October 11, 1958, and which traveled to a radial distance of about 110,000 km, indicated that the high intensity radiation was confined to the region near the earth and did not extend into extra-terrestrial space. It did not, however, show the existence of the two distinct belts due to gaps in telemetry coverage and failure of the probe equipment.[4] Pioneer III, launched on December 6, 1958, to a comparable radial distance, made two cuts through the trapping region and revealed the existence of the two great belts.[5] The USSR solar orbiting vehicle

1. S. N. Vernov, N. I. Grigorov, Yu. I. Logachev, and A. Ye. Chudakov, Artificial Satellite Measurements of Cosmic Radiation, Doklady Akad. Nauk S.S.S.R. 125, 1231, 1958.

2. Soviet Artificial Earth Satellites - Some of the Results of Scientific Researches on the First Two Artificial Earth Satellites, Report of IGY Committee of USSR, May 1958.

3. Annals of the International Geophysical Year, Vol. X, contains the following papers: V. I. Krassovsky, Y. M. Kushnir, G. A. Bordovsky, G. F. Zakharov, and E. M. Svetlitsky, A Discovery of Corpuscular Fluxes by Means of the Third Sputnik ; S. N. Vernov, A. Ye. Chudakov, E. V. Gorchakov, Yu. I. Logachev and P. V. Vakulov, A Study of Cosmic-Ray Soft Component by the Third Soviet Earth Satellite ; A. Ye. Chukakov, A Photon Study on the Third Sputnik.

4. P. J. Coleman, Jr., C. P. Sonett, and A. Rosen, Ionizing Radiation at Altitudes of 3500 to 36,000 km., Pioneer I, Bull. Am. Phys. Soc., Series II 4, 223, 1959.

5. J. A. Van Allen and L. A. Frank, Radiation Around the Earth to a Radial Distance of 107,400 Kilometers, Nature 183, 430, February 1959.

Mechta launched January 2, 1959 confirmed the findings of Pioneer III.[1] They were further confirmed following the launching of Pioneer IV on March 3, 1959 into a solar orbit. More importantly, the Pioneer IV data, by comparison with the earlier data, showed that the position, intensity, and composition of the outer belt were variable and apparently related to solar activity, thus indicating the high probability of the solar origin of the particles responsible for the outer belt.[2]

Plans were begun as early as March 1958 for a satellite having a high orbital inclination (51°) and long lifetime to serve as a temporal monitor for the corpuscular radiations above the atmosphere. With the discovery of the high intensity belts it was realized that such an experiment would be extremely valuable as an aid to the study of the injection and storage mechanisms for the trapped particles. This program was temporarily delayed by the Explorer IV program and other projects, but became a reality on October 13, 1959, when satellite 1959 Iota (Explorer VII) was launched into orbit.[3] That experiment, described in Volume I, has yielded a wealth of information about variations in the intensity, structure, and nature of the outer belt and their correlations with solar storms and flares, magnetic field variations, aurorae, and radio noise. The relative stability of the inner belt has been shown, and the instruments have shown the arrival of solar protons at high latitudes on several occasions.[4] Comparison of results with those of the contemporary experiments in satellite 1959 Delta (Explorer VI) and space probe Pioneer V are particularly interesting.[5,6,7,8]

1. S. N. Vernov, A. Ye. Chudakov, P. V. Vakulov, and Yu. I. Logachev, Study of Terrestrial Corpuscular Radiation and Cosmic Rays During Flight of the Cosmic Rocket, Doklady Akad. Nauk S.S.S.R. 125, 304, April 1959. (Translation available from U.S.Dept. of Commerce, Information on Soviet Bloc International Geophysical Cooperation - 1959, PB131632-64 of May 1, 1959, also Soviet Phys. JETP 4, 338, 1959.)

2. J. A. Van Allen and L. A. Frank, Radiation Measurements to 648,300 km with Pioneer IV, Nature 184, 219, 1959.

3. G. H. Ludwig and W. A. Whelpley, Corpuscular Radiation Experiment of Satellite 1959 Iota (Explorer VII), J. Geophys. Research 65, 1119, 1960.

4. B. J. O'Brien and G. H. Ludwig, Development of Multiple Radiation Zones on 18 October 1959, J. Geophys. Research, in press, 1960.

5. R. L. Arnoldy, R. A. Hoffman, and J. R. Winckler, Observations of the Van Allen Radiation Regions during August and September 1959, Part 1, J. Geophys. Research 65, 1361, 1960.

6. J. A. Van Allen and W. C. Lin, Outer Radiation Belt and Solar Proton Observations with Explorer VII during March-April 1960, J. Geophys. Research 65, 2998, 1960.

7. R. L. Arnoldy, R. A. Hoffman, and J. R. Winckler, Solar Cosmic Rays and Soft Radiation Observed at 5,000,000 km from Earth, J. Geophys. Research 65, 3004, 1960.

8. C. Y. Fan, P. Meyer, and J. A. Simpson, Preliminary Results from the Space Probe Pioneer V, J. Geophys. Research 65, 1862, 1960. (ltr.)

From this point the investigation was to be carried forward by satellite S-46 as explained in Chapter I. The design and development of the SUI instrumentation for S-46 is the subject of the rest of this chapter.

SECTION III. PAYLOAD INSTRUMENTATION

1. General

This section contains a detailed description of those elements of the flight unit assembly which were furnished by the State University of Iowa. The physical location in the payload of the modules containing the various circuits can be seen in the drawings of Figures 110 and 111, and their functions can be seen in the block diagram of Figure 112. The block diagram also indicates the division of responsibility between SUI and ABMA for the development and production of the various circuits. The circuits of ABMA responsibility are described in Chapter 4. ABMA was also responsible for the thermal design, the power system, and most of the payload structure which are described in Chapters 6, 5, and 3 respectively.

Five S-46 payloads were fabricated in this program, as set forth in Table 1. There were a number of differences between the payloads, especially between the prototype units and the flight units. Representative of this were the different counter types used in different payloads. The prototype payloads and flight unit number one used Anton type 302 counters, which are similar to the ones used in Explorers IV, VI, and VII and Pioneers III, IV, and V. In flight unit two a change was made to a smaller Anton type 213 counter for two reasons. First, because of the smaller size the counter would be able to measure a larger particle intensity (the outer belt intensity measured by the type 302 counter in Pioneer IV was high enough to cause partial counter saturation); and second, because the supply of fully calibrated type 302 counters was low at the time of payload assembly, and the best available counters had somewhat undesirable characteristics. The differences in the prototype and flight units insofar as SUI equipment is concerned are summarized in Table 7.

2. Radiation Detectors (Fig. 112)

a. Detector B. Detector B is one of five detectors used in the experiment. It is a low energy particle detector developed at SUI by Freeman, Pizzella, and Thissell following earlier work of C. E. McIlwain.

The basic detector element is a doped single semiconducting crystal of of cadmium sulfide (CdS) of a type which is in general use as a photoelectric detector. The CdS resistance is a known function of the rate of energy loss for charged particles in the crystals. No material is located between the active volume of the crystal and the outside of the satellite.

Table 7

TABULATION OF PAYLOAD DIFFERENCES

	Item	Figure Reference	Remarks
1.	Glass solar cell cover plates	71, 76	Not present on prototype units. Prototype testing was accomplished on test panel and flight units.
2.	Commutated solar cell voltage measurement.	19	This was a solar cell temperature measurement on PT units.
3.	CdS Detectors Detectors A,B	114, 117	Detectors in SUI PT-3 fixed in place rather than plug in. Lead absorber in aperture system not used in PT units. Thinner magnetic shielding used in PT units. Clairex Cl-2P CdS crystals used in PT-2 and PT-3 units.
4.	Electron spectrometer. Detectors C,D	119	Different magnet pole shape used in PT units. Different aperture system used in PT units. Lead baffle and shield in line with detector opening was not used in PT units.
5.	G-M counter. Detector E	115	Type 302 G-M counter used in PT units and FU-1, type 213 counter used in FU-2. Container for 302 counter had 0.020 inch aluminum wall, that for 213 counter had 0.093 inch aluminum wall. Flight cover for 302 counter had 0.125 inch aluminum wall, that for 213 counter had 0.032 aluminum wall.
6.	Thermistor network.	120	14 K ohm shunt resistor in FU units was 30 K ohm in PT units.

Table 7 (cont)

Item	Figure Reference	Remarks
7. 160 volt power supply	120	(2) 6.2 M ohm resistors at output of supply in flight units were 10 M ohm in PT units. 1N1327 zener diode in regulator circuit of flight units was a Victoreen type RCA-125 trigger tube in the PT units.
8. 700 volt power supply	120	Transformer was Rayco type 0-5263 in PT units. 390 K ohm secondary circuit current limiting resistor was 100 K in PT units. 4.7 M ohm regulator resistor was 2.7 M ohm in PT units. (4) 5.6 M ohm resistors at output of supply in flight units were not used in PT units.
9. Step limiting MV no. 1	136, 137, 138	Input circuit contained unnecessary components in PT units. Initializing RC network was not used in PT units.
10. Step limiting MV no. 2	136, 137, 138	Initializing RC network was not used in PT units.
11. Antenna matching network	30	Shunt 0.47 h choke not used in PT units. 1 M ohm resistor in parallel with capacitor in PT units.

G. M. COUNTER

DETECTOR ASSEMBLY

SOLAR CELL STRUCTURE

SCALING AND LOGIC CIRCUITS

TRANSMITTER COMMUTATOR

SUB-CARRIER OSCILLATORS

BATTERY PACK

ANTENNA GAP

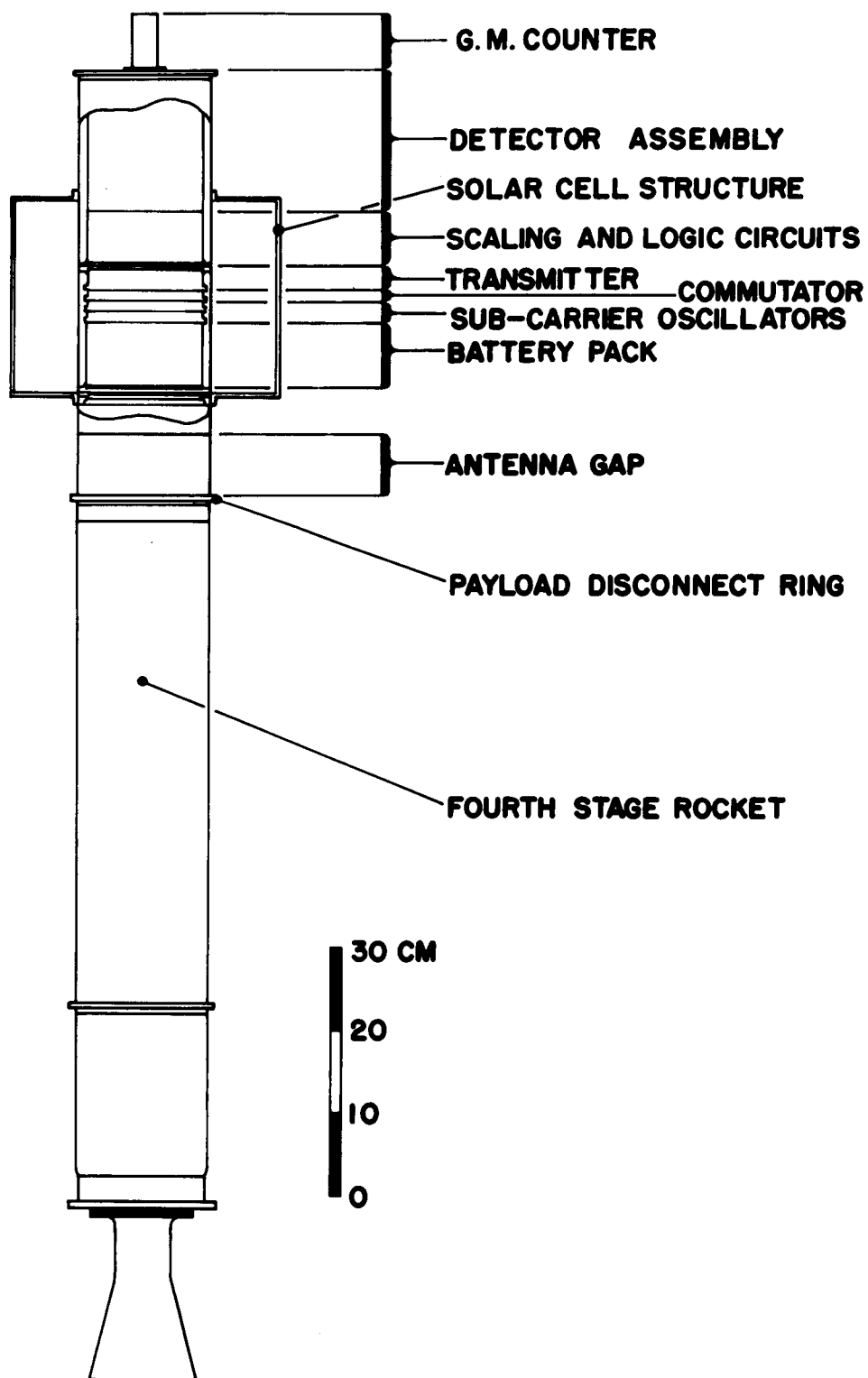PAYLOAD DISCONNECT RING

FOURTH STAGE ROCKET

30 CM

20

10

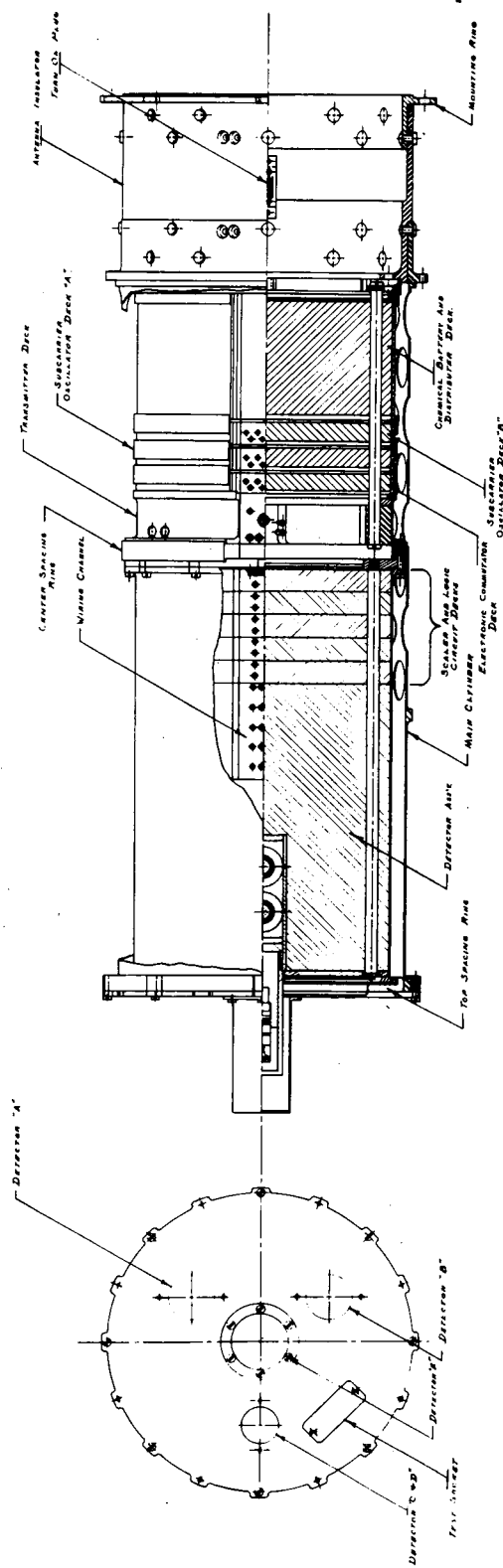0

FIG. 110. OUTLINE DRAWING OF SATELLITE S-46

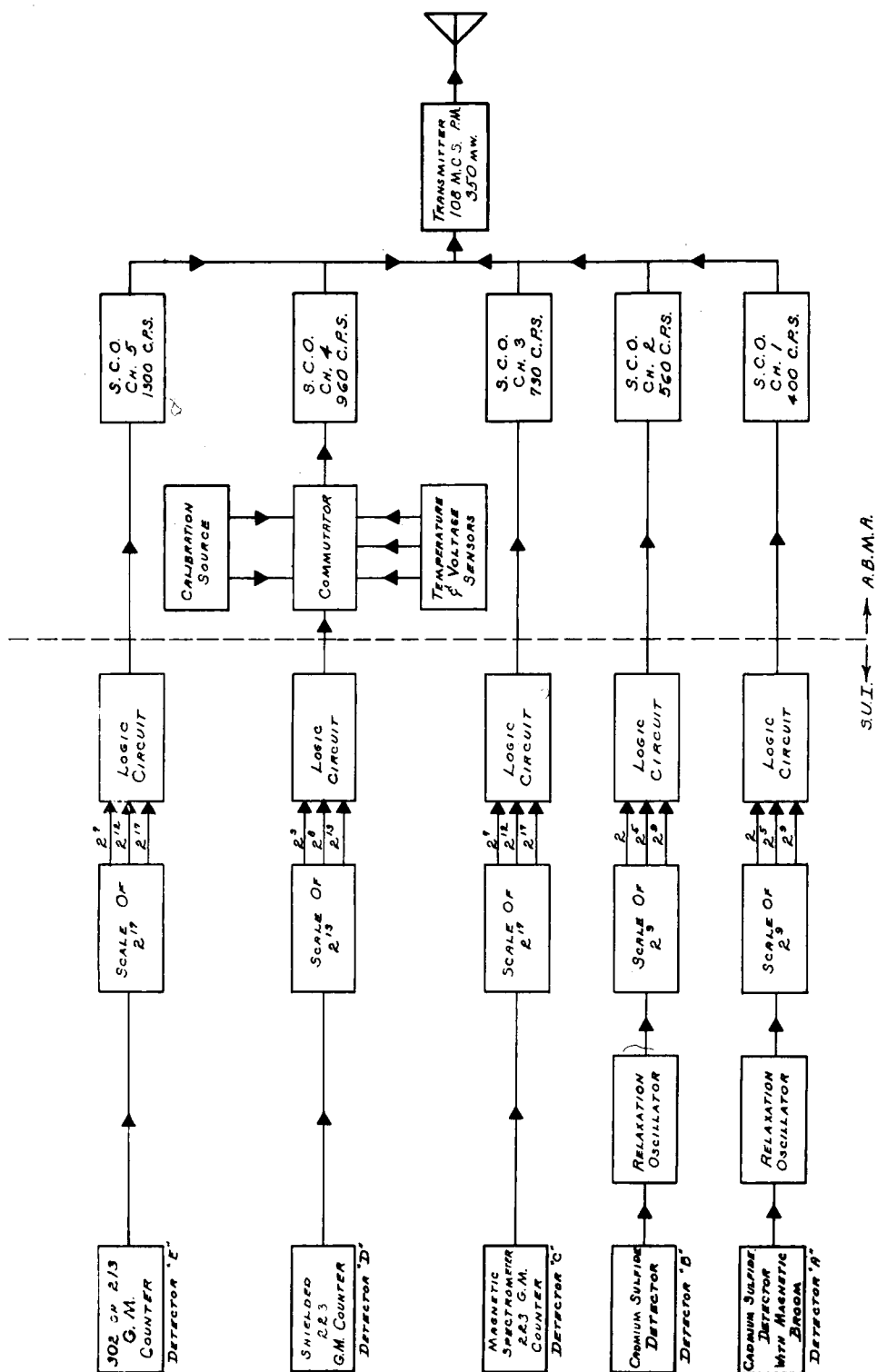FIG. 111.   ASSEMBLY DRAWING OF THE S-46 PAYLOAD COLUMN

FIG. 112. BLOCK DIAGRAM OF THE S-46 INSTRUMENTATION

The absorption of charged particles in the body of the crystal by inelastic collision results in the creation of electron-hole pairs. Until these carriers are lost by recombination, the conductivity of the crystal is increased. The recombination time of the electrons is relatively long; therefore they act as the majority carriers. The minimum particle energy which can be detected is the sum of the energy required to create an electron-hole pair and the work function of the surface (a total of about 2.5 ev).[1] Mr. Pizzella has indicated, in a private communication, that the number of electron-hole pairs created per unit energy lost in the crystal per unit time rises from zero for incident electrons with energies of a few electron volts to a nearly constant value for particle energies above about 50 ev. Above this energy the conduction current through the crystal from a constant potential supply is nearly proportional to the time rate of loss of particle energy by absorption within the crystal.

The conductivity is also related to T, the absolute temperature. For low incident fluxes, where the conductivity is primarily the intrinsic conductivity of the bulk material, the conductivity is proportional to $T^{-3/2}$ in the neighborhood of room temperature. For high incident fluxes the amount of the decrease in conductivity with increasing temperature is somewhat less. The temperature coefficient varies from crystal to crystal, but is typically of the order of -0.3 per cent per degree centigrade.

When a change in energy flux occurs, the adjustment of the conductivity to its new value occurs quite slowly, the speed of response depending on the final value of the conductivity. This is illustrated in Figure 113 in which the pulse rate of the relaxation oscillator (proportional to current) is plotted as a function of time, as the intensity of a light source illuminating the crystal is changed in discontinuous steps.

The Clairex type C1-2 CdS crystals used in the S-46 payloads have a typical area of 3 mm^2 and thickness of 0.5 mm. This thickness corresponds to the range of approximately 700 kev electrons or 13 mev protens.

The detector conductivity is also increased by incident light due to the creation of electron-hole pairs by the photoelectric effect. For this reason a series of light baffles is provided to eliminate its light sensitivity except over a solid angle of about 10^{-3} steradian (see the assembly drawing, Fig. 114). These baffles and a lead aperture act also as the geometry determining collimator for all particles not sufficiently energetic to penetrate the material of the assembly. In addition, the detector is mounted in a lead and stainless steel cylindrical absorber to further reduce the contribution from the X-rays (bremsstrahlung) produced in the payload structure and from energetic particles arriving from outside the angle of collimator acceptance.

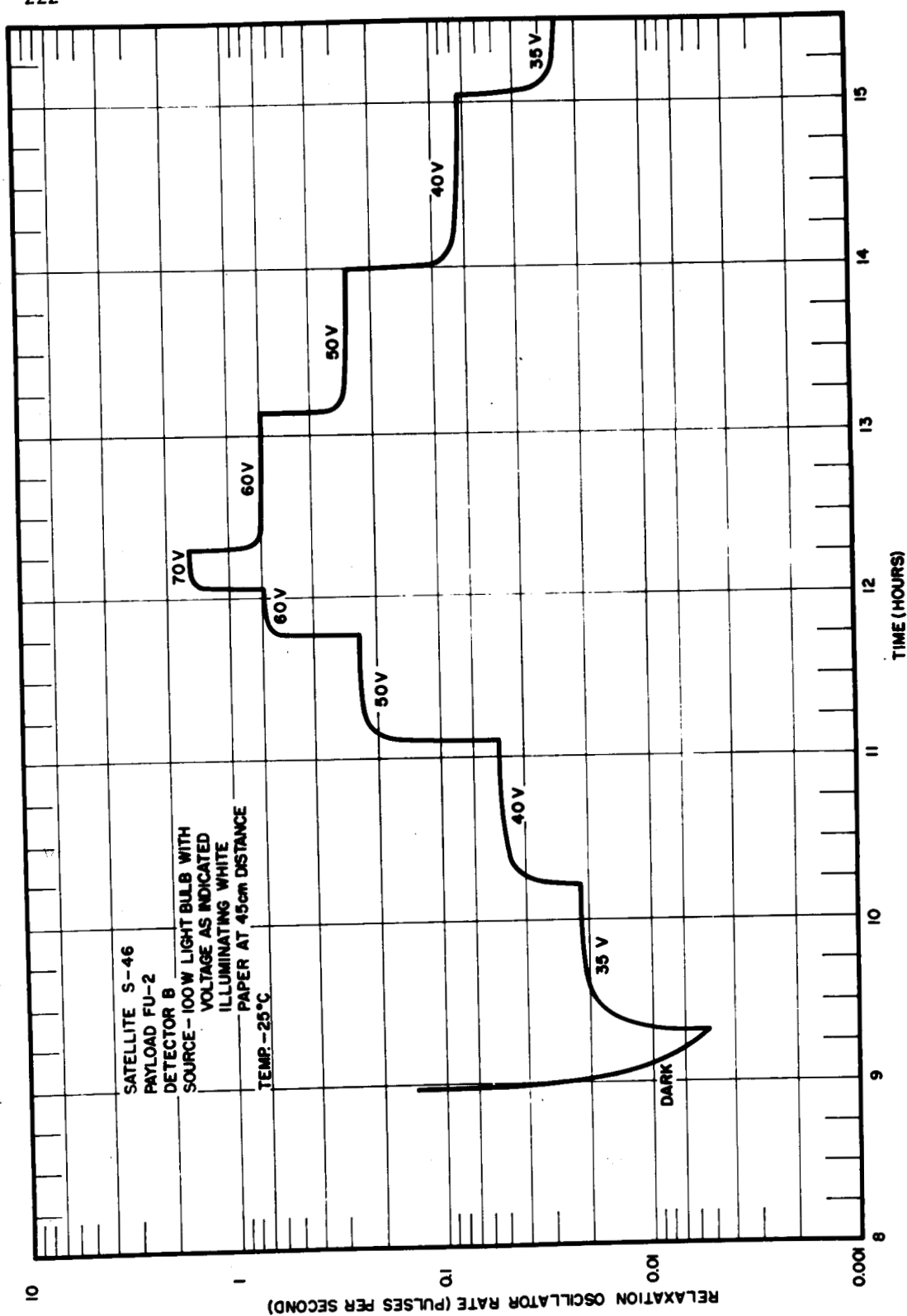1. Li Chin-Tsien, Physics Abstracts 63, No. 745, p. 605 (Abstr.).

FIG. 113. CADMIUM SULFIDE DETECTOR RELAXATION CHARACTERISTICS FOR
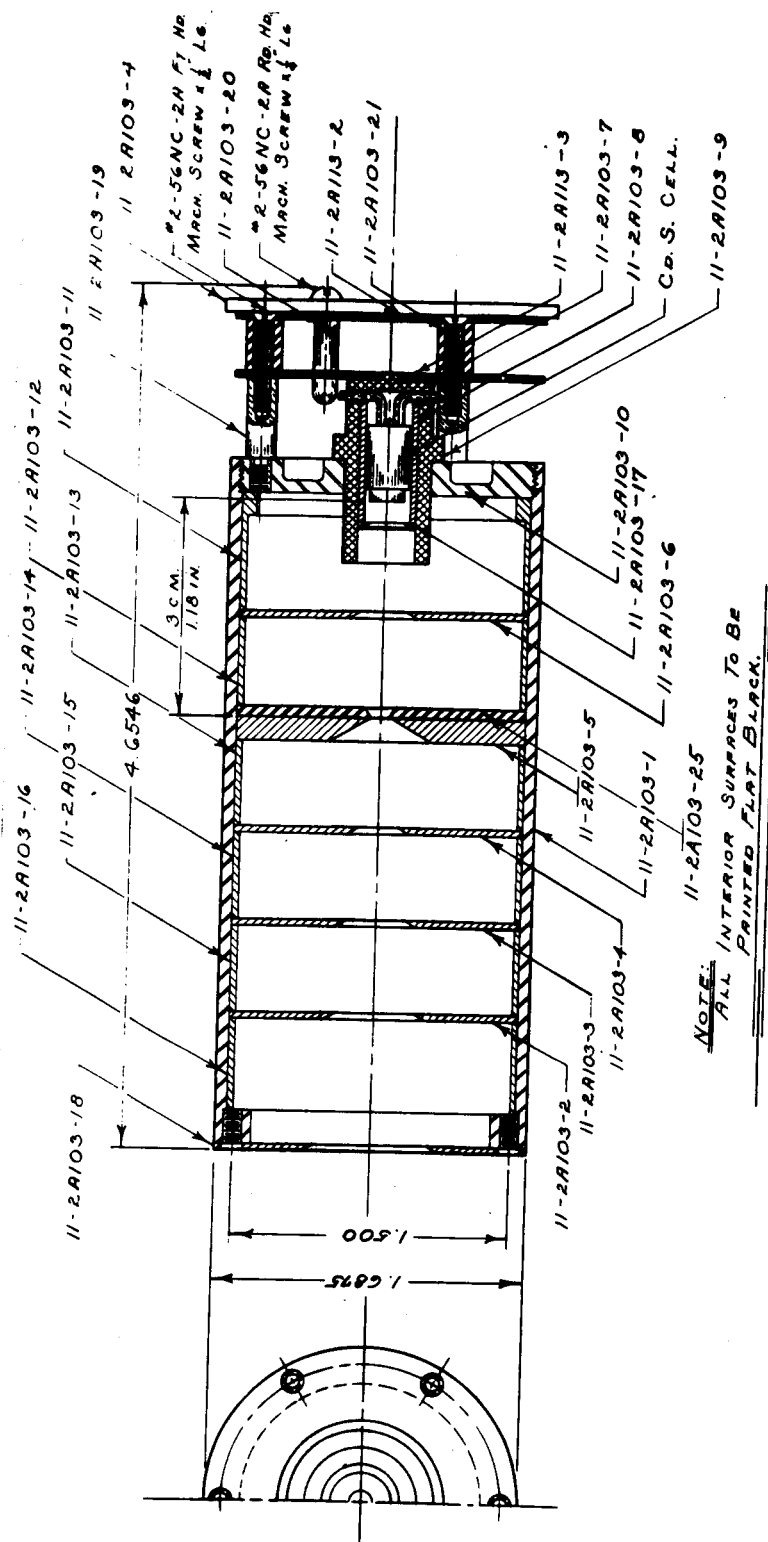DISCONTINUOUS CHANGES IN LIGHT ILLUMINATION

FIG. 114. ASSEMBLY DRAWING OF CADMIUM SULFIDE DETECTOR B
From Dept of Physics, State Univ. of Iowa Drawing B11-2A001

To reduce the effects of external magnetic fields on the arrival of low energy electrons at the detector, it is surrounded by a sheet of 0.51 mm thick Perfection Mica Co. type NETIC S-3 high permeability magnetic shielding material.

The conductivity of the crystal is measured, in practice, by measuring the current through the crystal from a regulated 160 volt power supply (Fig. 115). This current charges a capacitor in a relaxation oscillator until the ionizing potential of a neon lamp (NE-76 or NE-81) is reached, at which time the capacitor is discharged through the lamp. The discharge pulse obtained across a resistor in the discharge path is shaped and used to drive a scalar (Para. 4). The pulse rate from the relaxation oscillator is proportional to crystal current over a large range of current. Figure 116 shows the relationship between the crystal current and pulse period for the FU-2 circuit at room temperature. The variation in pulse rate with changes in temperature for an input current in the range from 10^{-5} to 10^{-9} ampere can be made less than 2.5 per cent over a temperature range from -25°C to +75°C by proper selection of the neon lamp.

b. Detector A. This detector is identical to detector B except for the addition of a permanent magnet with a field strength of about 500 gauss in the aperture system to sweep aside low energy electrons (Fig. 117). With this field strength electrons having energies less than 500 ±100 kev are deflected from the crystal. Thus, the simultaneous measurements of detectors A and B yield independently the flux of all particles with $E > \approx 50$ ev, and the flux of all of these particles except for electrons with $E < \approx 500$ kev.

c. Detector C. Detectors C and D are contained in the spectrometer assembly, designed at SUI by C. D. Laughlin. Figures 118 and 119 are, respectively, a photograph and an assembly drawing of the unit.

The spectrometer proper (detector C) consists of a stainless steel aperture system having a known geometric configuration to admit the particles, a magnet to deflect them through a 90° angle, another aperture to further define the geometry, and a thin window G-M counter to detect the particles. The magnet field strength (1050 ± 25 gauss) is adjusted to deflect electrons in the desired energy range through the proper angle so that they will enter the G-M counter. The spectrometer unit in FU-2 had an electron energy "window" from about 47 kev to 56 kev measured at the half height of the response curve.

The counter is heavily shielded by lead and stainless steel absorbers to reduce the contribution from particles traversing the payload structure and from X-rays produced by inelastic collisions of electrons in the payload structure. The load thickness is 0.442 cm (5.0 gm/cm^2) corresponding
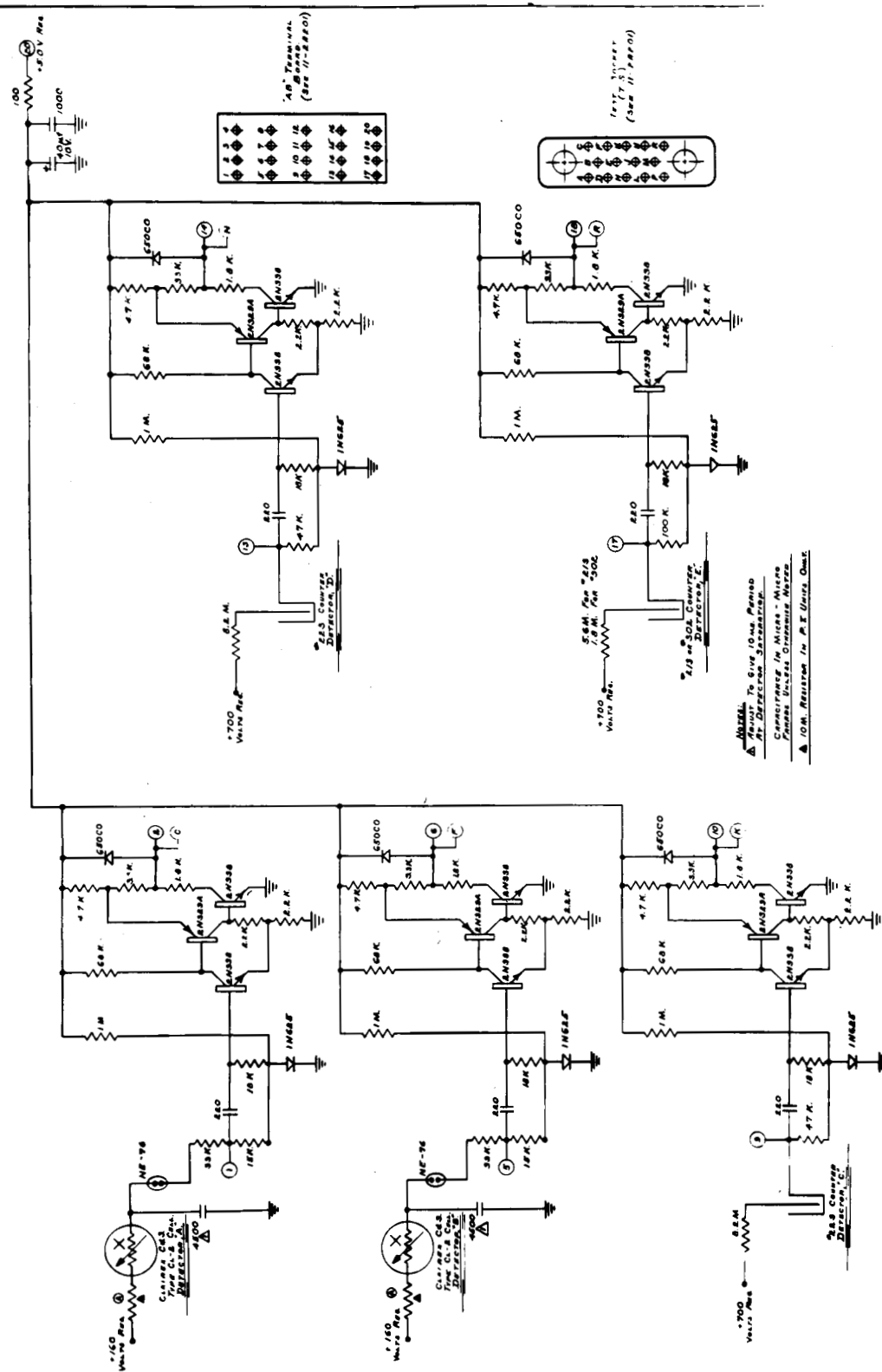
FIG. 115. SCHEMATIC DIAGRAM OF THE DETECTOR CIRCUITS AND PULSE SHAPING AMPLIFIERS, DECK B

226

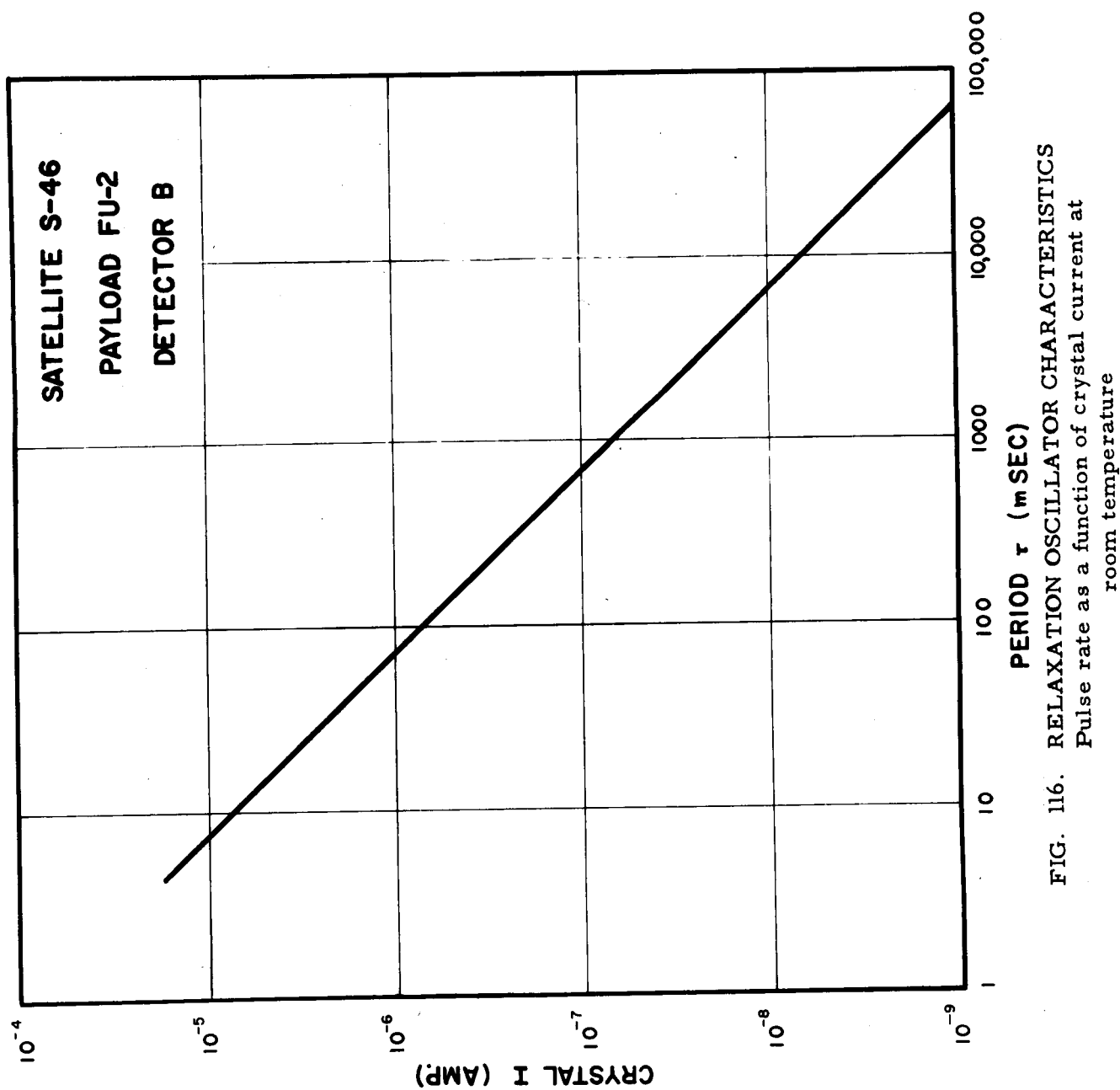FIG. 116.   RELAXATION OSCILLATOR CHARACTERISTICS
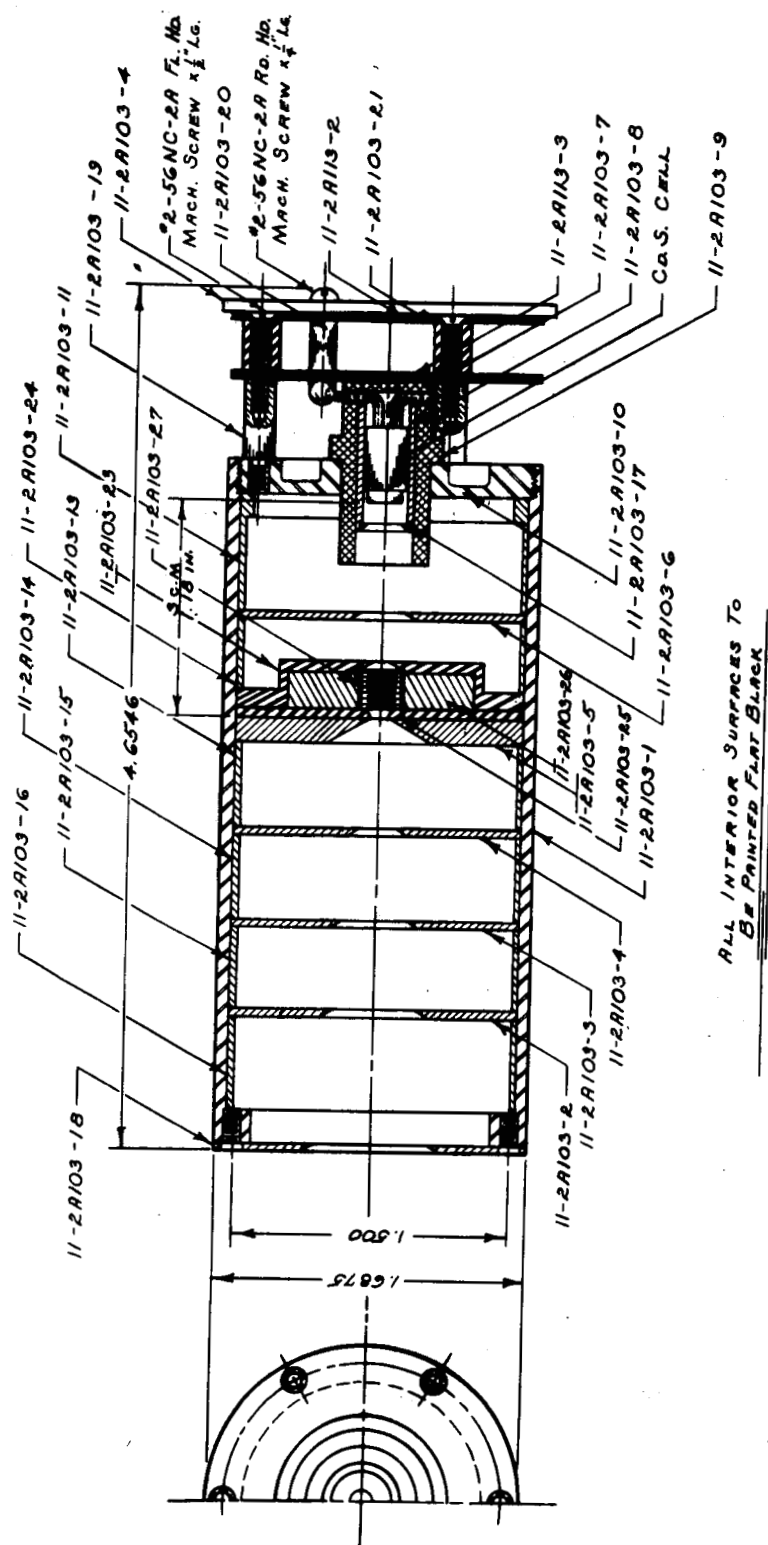Pulse rate as a function of crystal current at
room temperature

FIG. 117. ASSEMBLY DRAWING OF CADMIUM SULFIDE DETECTOR A
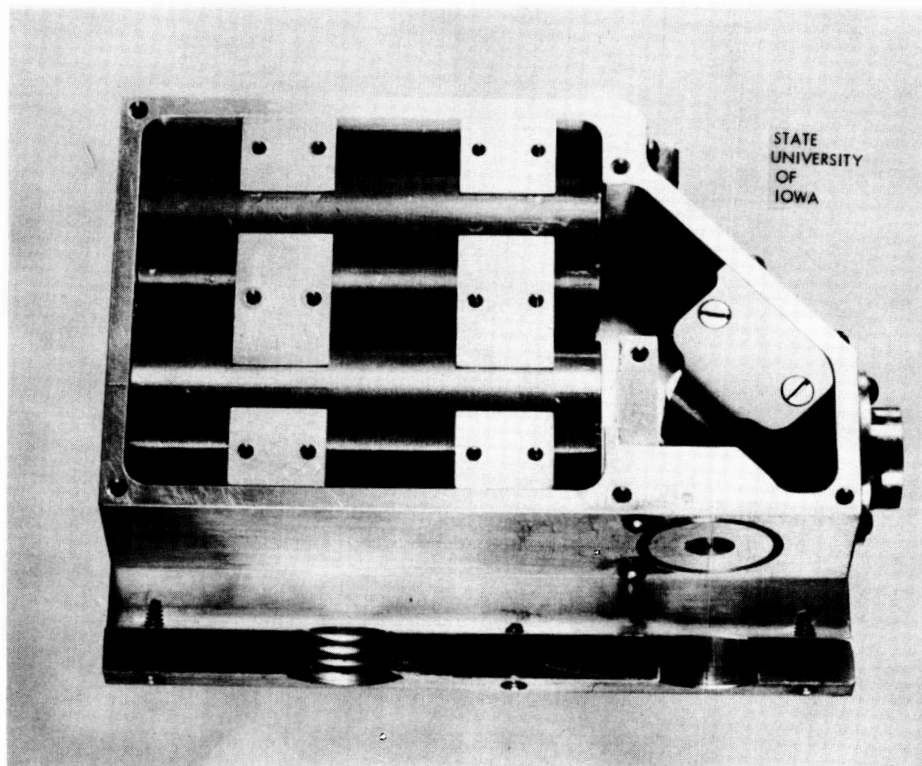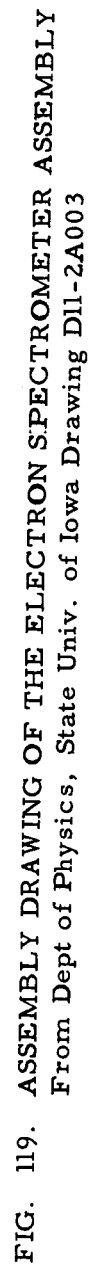From Dept of Physics, State Univ. of Iowa Drawing B11-2A002

FIG. 118. ELECTRON SPECTROMETER ASSEMBLY

FIG. 119. ASSEMBLY DRAWING OF THE ELECTRON SPECTROMETER ASSEMBLY
From Dept of Physics, State Univ. of Iowa Drawing D11-2A003

to the ranges of approximately 10 mev electrons and 50 mev protons. The stainless steel absorber thickness is 0.40 gm/cm^2.

The G-M counter used as the spectrometer detector is an Anton type 223 halogen quenched counter having a mica window with a thickness of 1.2 ± 0.2 mg/cm^2 (27 kev energy loss for electrons). The designation of this counter has recently been changed from 223 to 213 without ceramic button, by its manufacturer. The practice adopted in this report is to refer to the counters used in detectors C and D as 223 counters and the counter with the ceramic button over the mica used as detector E in FU-1 as a 213 counter. The effective omnidirectional factor (ϵG_o) of both types is typically

$$\epsilon G_o = 0.12 \text{ cm}^2$$

The effective geometric factor (ϵg_c) of the complete spectrometer assembly for electrons incident within a cone of angles about the initial aperture system axis, assuming an idealized rectangular counting rate versus electron energy curve with upper and lower edges at the half height energies of the actual curve, is

$$\epsilon g_c = 1.7 \times 10^{-5} \text{ cm}^2 \text{ steradians}$$

for the unit in FU-2. Hence, the unidirectional intensity (j_c) of electrons in this range of energy is:

$$j_c = \frac{R_c}{\epsilon g_c} = (5.9 \times 10^4) R_c \text{ cm}^{-2} \text{ sec}^{-1} \text{ ster}^{-1}$$

where R_c is the true counting rate of the G-M counter, if the counting rate contributions from all other sources are zero.

d. <u>Detector D.</u> This detector is identical to the cylindrical counter and absorber assembly in the electron spectrometer in every respect except that no window is provided in the lead and stainless steel absorbers, so that all low energy charged particles and almost all locally produced bremsstrahlung are excluded from the counter. This counter was included to permit a correction of the electron spectrometer rates for the counting rate contribution from particles not entering through its opening, and to give additional information about the particle absorption spectrum.

e. <u>Detector E.</u> Detector E protrudes from the top of the payload, and employs a G-M counter surrounded by a relatively thin absorber. Both Anton types 302 and 213 halogen quenched G-M counters were used as indicated in Table 7. Typical values of their most important characteristics are listed in Table 8.

Table 8

DETECTOR E CHARACTERISTICS
(Typical Values)

Item	213 Counter	302 Counter
Effective omnidirectional geometric factor, ϵG_o	0.12 cm^2	0.59 cm^2
Omnidirectional intensity of energetic charged particles, J_o	8.7 R$_{213}$	1.7 R$_{302}$
Counter wall thickness (stainless steel)	0.4 gm/cm^2	0.40 gm/cm^2
Thickness of mounting thimble plus flight cover (aluminum)	0.86 gm/cm^2	0.99 gm/cm^2

3. <u>High Voltage Power Supplies</u>

Two high voltages were required in the S-46 SUI instrumentation, 700 volts for the G-M counters and 160 volts for the CdS detectors. They were provided by independent transistor saturating core converters, voltage multipliers, and voltage regulators. The schematic diagrams of these supplies are contained in Figure 120; the bottom view of a completed power supply assembly is shown in Figure 121.

The basic high voltage power supply circuit was originally developed by the Power Sources Division of the Signal Corps Engineering Laboratories for Explorer I.[1] The S-46 supplies were modifications of this design.

a. <u>700 Volt Supply.</u> The 700 volt supply utilizes two transistors in a conventional transformer feedback oscillator circuit in which core saturation is employed to stabilize the operating conditions and to obtain high power supply efficiency.

The type 0-3767A transformer was designed and wound by the Rayco Electronic Manufacturing Company of North Hollywood, California. It employs an Arnold Engineering Company Supermalloy type 4168-S1 tape wound core, and is wound with 532 turns (center tapped) for the primary winding, 80 turns (center tapped) for the feedback winding, and 13,500 turns for the secondary winding. The secondary winding is both bank wound and split wound to minimize distributed capacitance.

1. G. H. Ludwig, <u>Cosmic Ray Instrumentation in the First U.S. Earth Satellite</u>, Rev. Sci. Instru. <u>30</u>,223,1959.
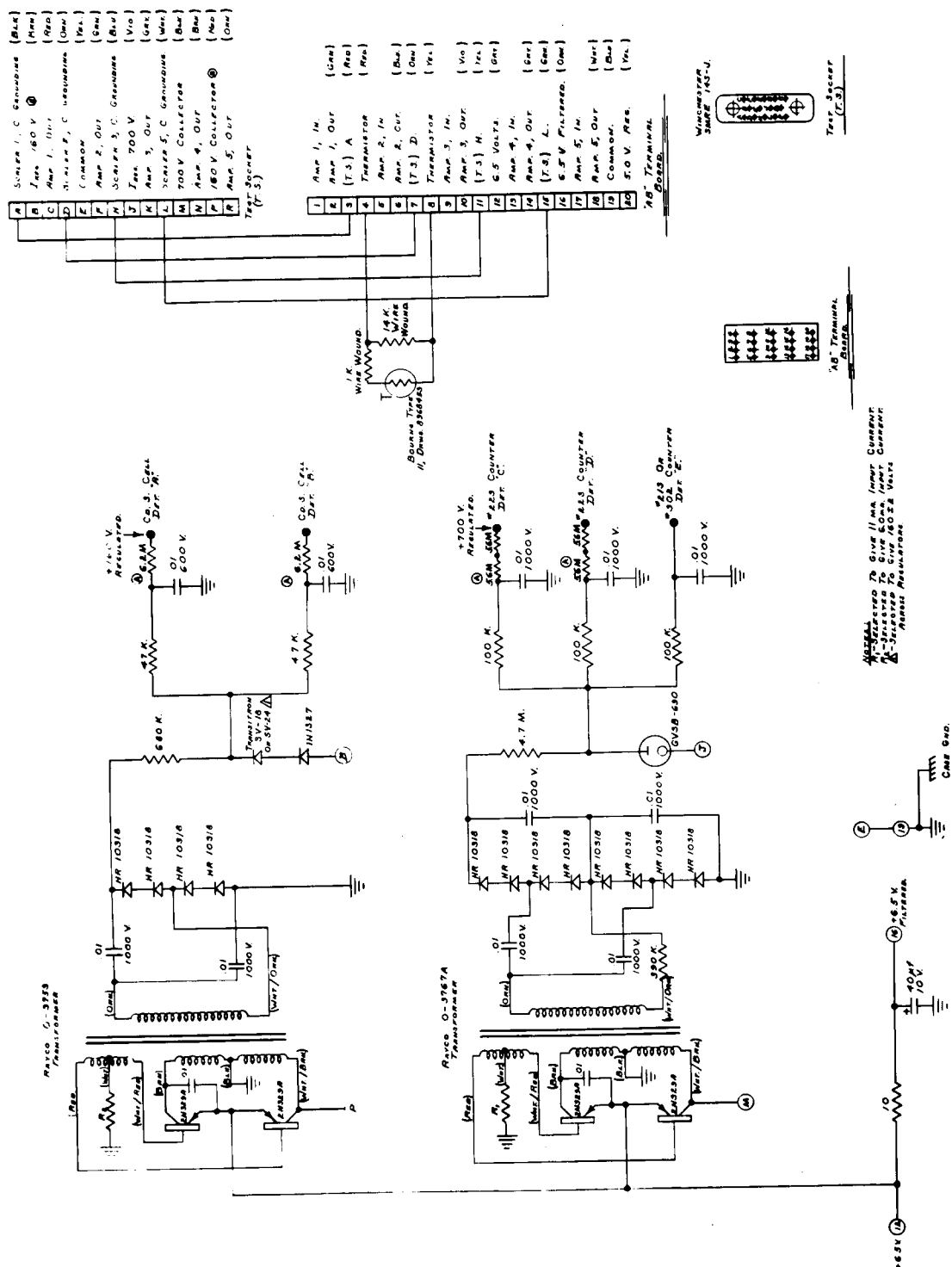
232

FIG. 120. SCHEMATIC DIAGRAM OF THE 160 AND 700 VOLT POWER SUPPLIES, DECK A
From Dept of Physics, State Univ. of Iowa Drawing D11-2A201
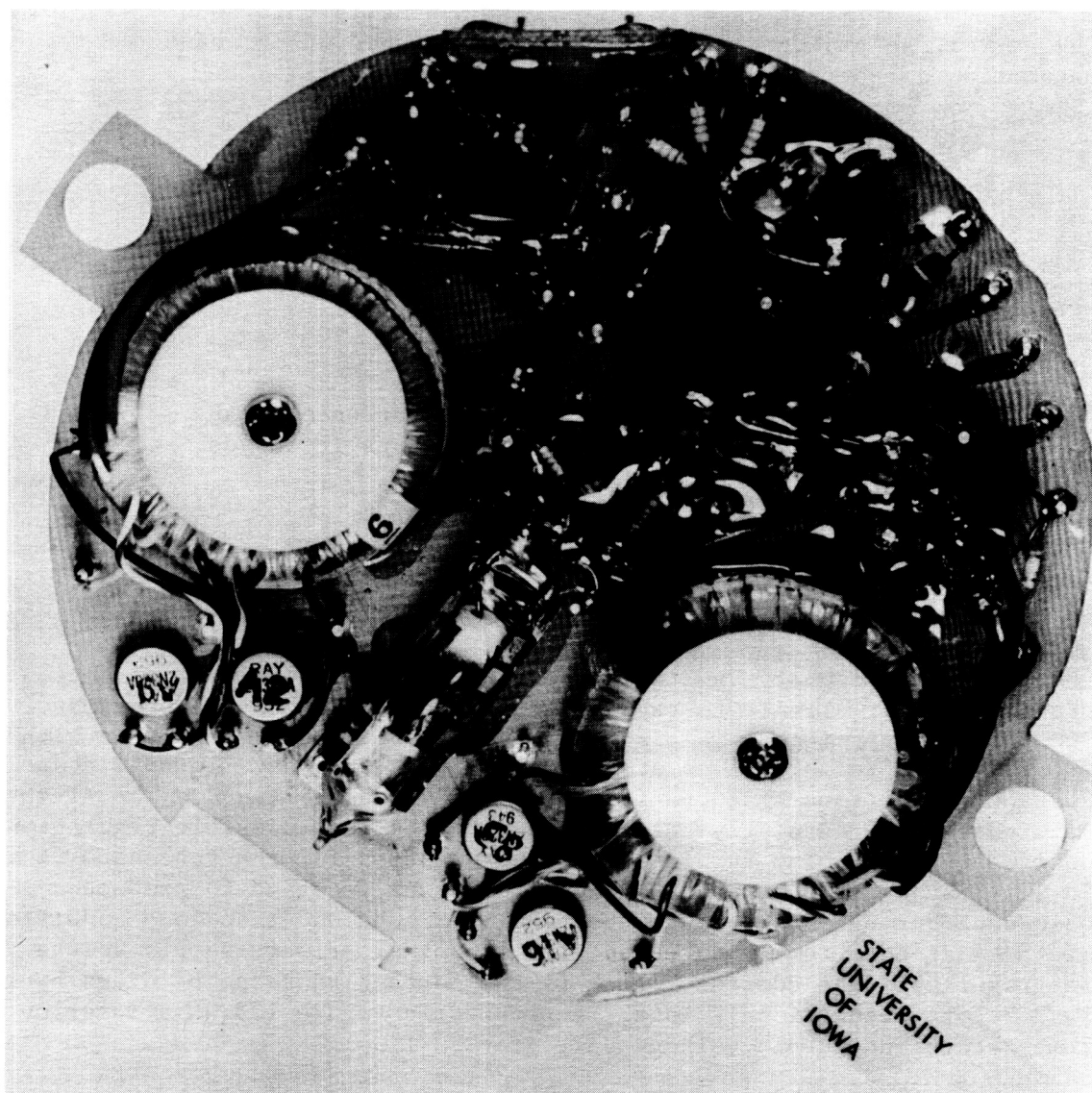
FIG. 121. BOTTOM VIEW OF H. V. POWER SUPPLY FOR SUI INSTRUMENTATION

The frequency of oscillation is about 900 cycles per second for an input voltage of 6.50 volts, and the peak-to-peak amplitude of the collector square waveform is 12.0 volts. This is transformed to an approximate peak-to-peak square wave amplitude of 475 volts at the secondary. A voltage quadrupler is used to multiply and rectify this square waveform. The dc voltage produced at the output of the quadrupler, based on the assumption of perfect diodes and capacitors, is:[1,2]

$$V_{mult} = nE - \frac{i \left(\frac{2n^3}{3} + \frac{n^2}{2} + \frac{n}{6}\right)}{fC}$$

where n is the number of doubler stages,

E is the peak-to-peak input voltage,
i is the output current in amperes,
f is the operating frequency in cycles per second, and
C is the value of the multiplier capacitors in farads.

In the S-46 case n = 2, E = 475, f = 900, and C = 10^{-8}, so

$$V_{mult} = 950 - 0.78 \, i$$

where i is now in microamperes. Thus, for i = 45 μA, V_{mult} = 915.

A corona discharge voltage regulator tube is used in a conventional shunt regulator circuit to regulate the output voltage at approximately 700 volts. Capacitance is placed across the regulator (in series with the 100 K ohm resistors) to stabilize the regulation at low regulator currents. The tube employed is a Victoreen type GV 3B-690. The flight unit tubes were carefully selected to give the best possible regulation characteristics. The regulation characteristics for the tube used in FU-1 are shown in Figure 122. The circuit was designed to produce a quiescent current I_{ss} through the regulator tube under no-load conditions of 45 μA at room temperature and with a nominal primary supply voltage. The regulator tube current, which is the current that can be drawn by the load before regulation is lost, is plotted in Figure 123 as a function of temperature and supply voltage V_{cc2} (for FU-1).

1. W. R. Arnold, A 500-Kilovolt Linear Accelerator Using Selenium Rectifiers, Rev. Sci. Instr. 21, 796, 1950.

2. Von A. Bouwers and A. Kuntke, Ein Generator fur drei Millionen Volt Gleichspannung, Z. technische Physik 8, 27, 1937.
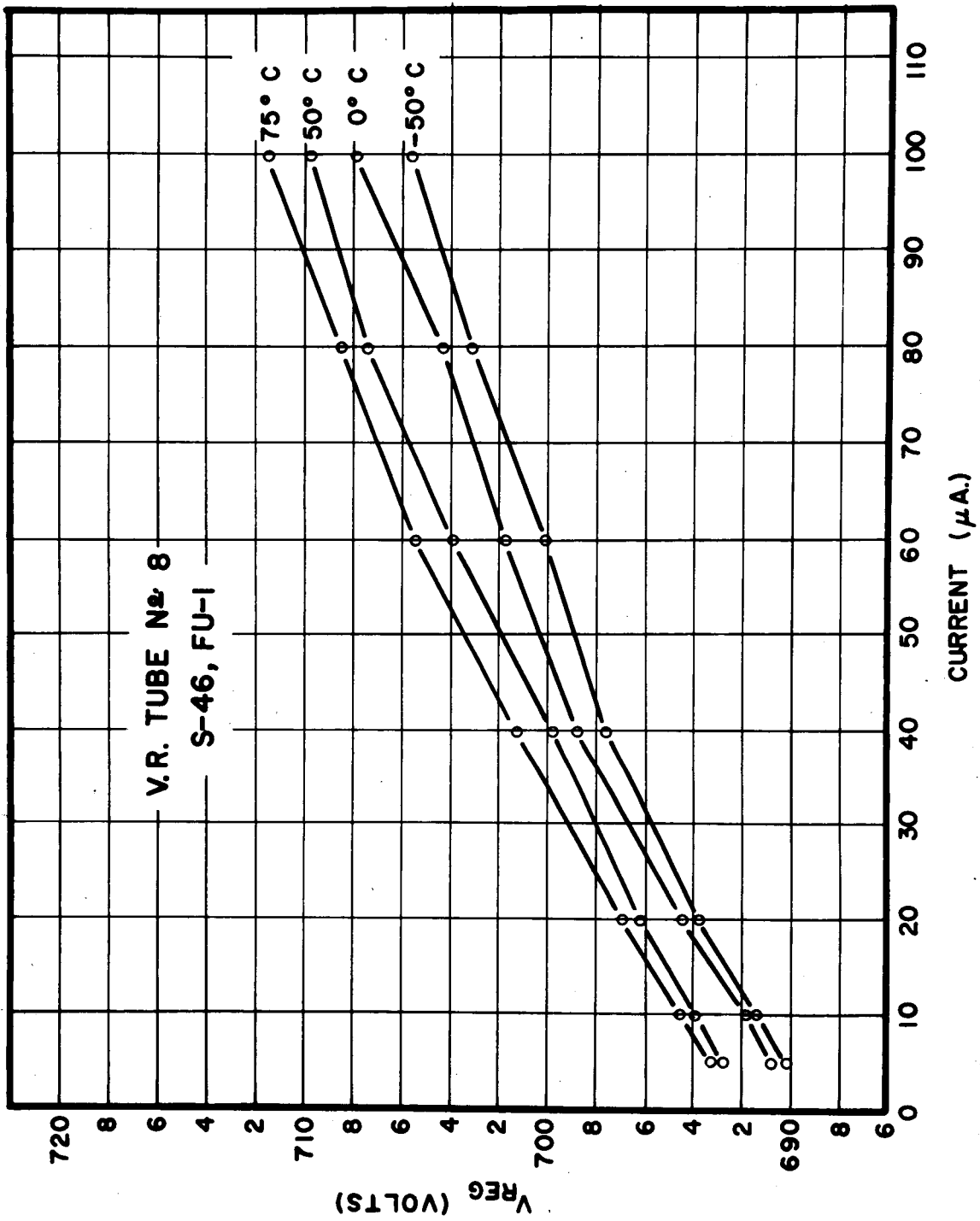
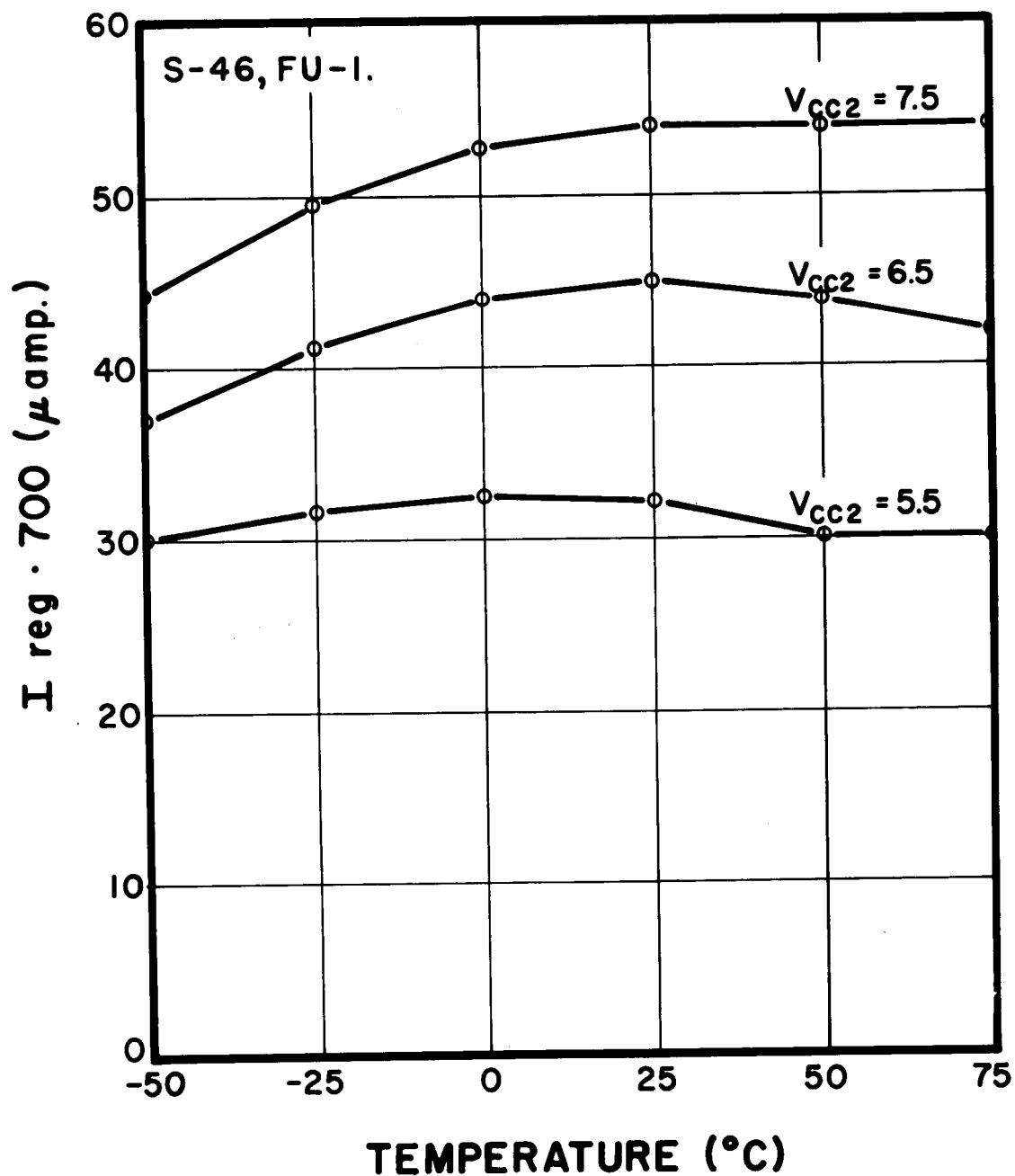FIG. 122. TYPE GV3B-690 VOLTAGE REGULATOR TUBE CHARACTERISTICS

FIG. 123. VARIATION OF REGULATOR TUBE CURRENT WITH CHANGES
IN TEMPERATURE AND INPUT VOLTAGE FOR THE 700 VOLT
POWER SUPPLY UNDER NO LOAD CONDITIONS

The G-M counter series resistors were chosen so that the total current drawn by the counters under the saturated condition would not exceed the regulator current. The current requirements for the saturated counters when operating from a 700 volt supply are approximately 6.7 μA for a 223 counter with 19.4 megohms series resistance, 29 μA for a 213 counter with 5.6 megohms series resistance, and 18.5 μA for a 302 counter with a 1.8 megohm series resistance. The design was finalized on the basis of the requirements of two type 223 and one type 302 counters as used in FU-1, which require a total of 31.9 μA if all three counters are saturated at the same time. This is available under all operating conditions for $V_{cc2} \geq 5.62$ volts. This is acceptable because the supply voltage is not expected to fall below 5.85 volts in practice. When the decision was made to substitute a type 213 counter in FU-2, it was done with the knowledge that the supply could not have delivered the 42.4 μA required if all counters were saturated simultaneously, if the supply voltage became less than 6.5 volts. This was not considered a serious limitation, however, because the probability of simultaneously saturating all three counters, with their assorted absorber thicknesses and different geometric factors, at the same time is very small. Furthermore, the overloading of the supply does not cause the supply to cease operating. It simply reduces the voltage below the regulated value, and a new operating point is established. The fact that the counter calibrations are no longer valid is obvious from the data by the fact that the channel C, D, and E rates are all very high.

b. <u>160 Volt Supply</u>. The 160 volt supply is, in general, similar to the 700 volt supply. The transformer is a Rayco type 0-3753 transformer with 532 (center tapped) primary turns, 80 (center tapped) feedback turns, and 5500 secondary turns wound on the same core type as that in the 700 volt supply. Since the output voltage is relatively low, a voltage doubler circuit is used rather than the quadrupler. And since 160 volts is below the range for which satisfactory corona discharge regulators are available, zener diodes are used for voltage regulation. The zener diode regulation characteristics are shown in Figure 124 for the regulator in FU-1. The large variation in the regulated voltage with changes in temperature is not considered serious because high accuracy is not required for the CdS detectors in this experiment, and that the temperature of the detector assembly, within which the power supplies are located, is measured by one of the thermistors.

The diode current, which is the available load current, is plotted in Figure 125 as a function of temperature and primary supply voltage for flight unit number one. The graph indicates that a minimum of 64 μA is available under all possible operating conditions. Thus, regulation is maintained even if the terminals on the load side of the series resistors are grounded, in which case the current would be 52 μA. Actually, the maximum current drawn from this supply when both detectors are saturated by a strong light source is only 32 μA due to the manner of operating of the relaxation oscillator circuit.
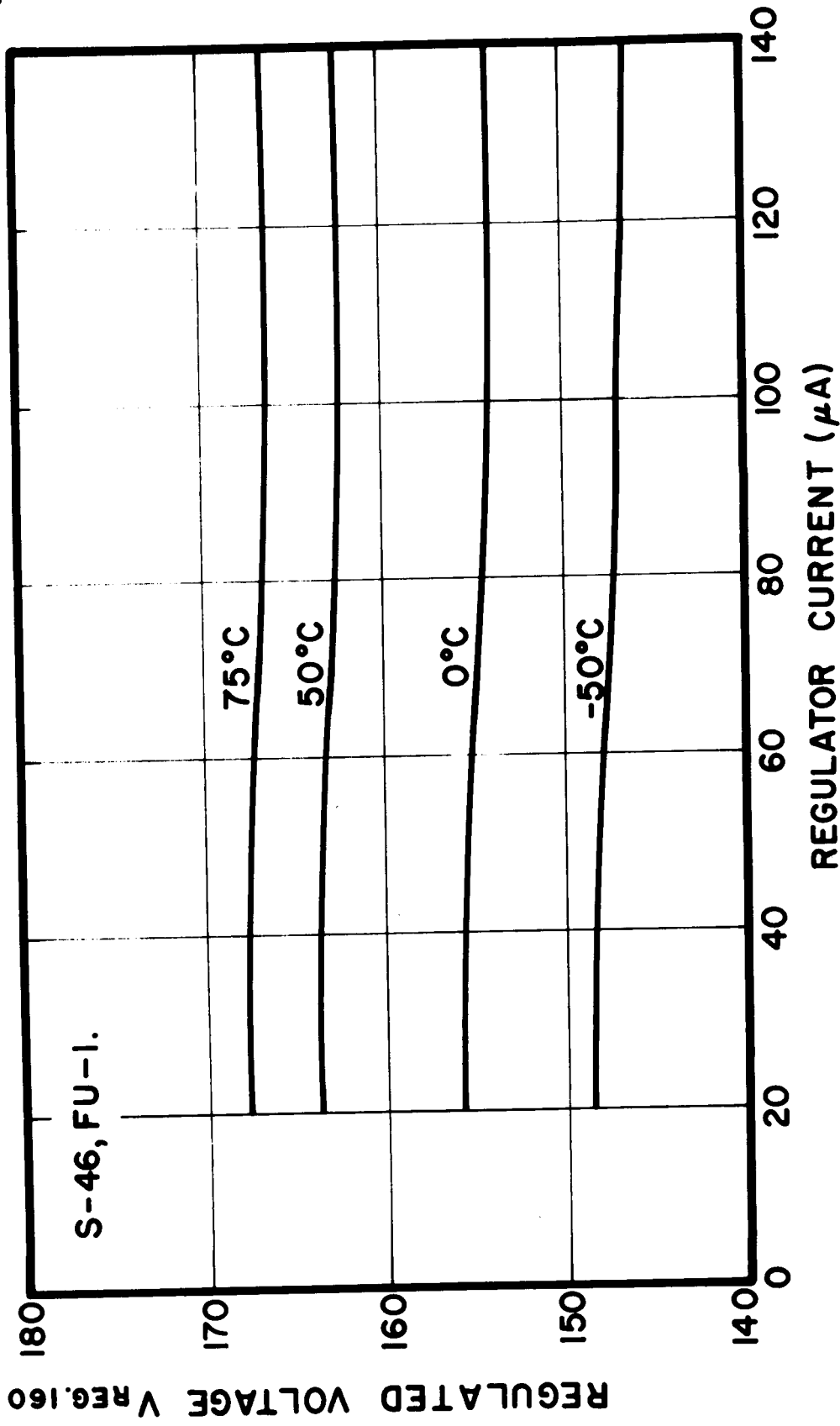
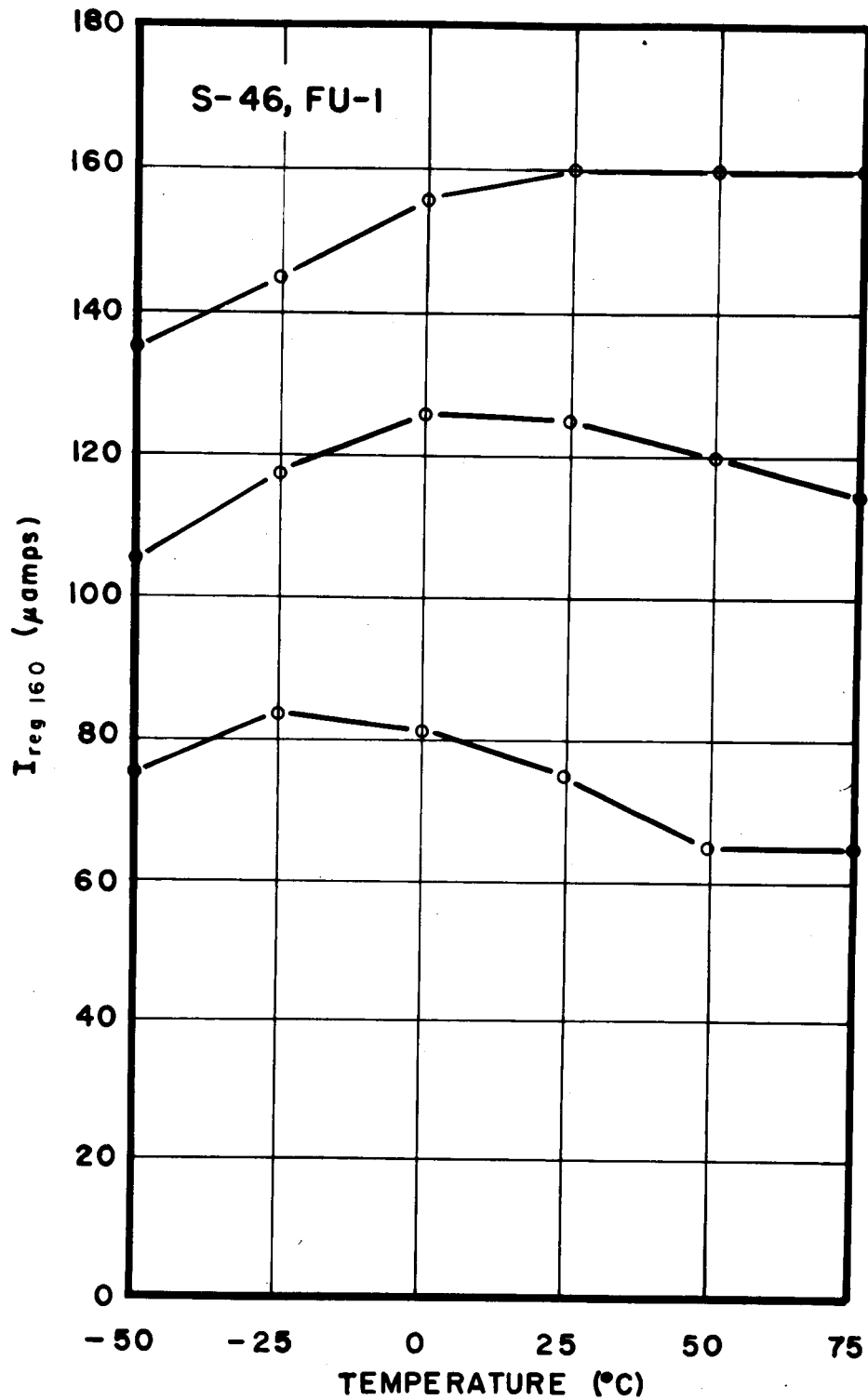FIG. 124. TYPE 1N1327 ZENER DIODE VOLTAGE REGULATION CHARACTERISTICS

FIG. 125. VARIATION OF ZENER DIODE CURRENT WITH CHANGES
IN TEMPERATURE AND INPUT VOLTAGE FOR THE 160
VOLT POWER SUPPLY UNDER NO LOAD CONDITIONS.

4. Pulse Shaping Circuits

The function of the pulse shaping circuit is to furnish a stabilized optimum shaped pulse to the scaler circuits. Its use is particularly necessary with the G-M counters to minimize the effects of changes in temperature and supply voltage on the counting rates when these rates are very high. They are also used with the CdS detectors to prevent the load from influencing the operation of the relaxation oscillators.

Figure 126 shows the envelope of the G-M counter pulses following an initial pulse. Whenever a pulse occurs at time t_0 and another occurs at time t_1, as in Figure 126, then the amplitude of the second pulse is as indicated by the envelope. The pulses drive a scaling circuit where the threshold voltage of the combined shaping circuit and scaler is V_t. When the particle flux is sufficiently great so that there is a high probability that some pulses will be separated by less than the dead time $t_1 - t_0$, then the counting rate varies with changes in the dead time, the threshold voltage, and the G-M counter pulse amplitude. The pulse shaping circuit used in satellite S-46 establishes a set of operating conditions such that variations in the values of these parameters combine to reduce the overall variation in maximum counting rate to a low value.

The pulse shaping circuit uses a two stage bootstrap amplifier. In order to simplify the discussion of its operation, the basic single stage amplifier, as shown in Figure 127a, is described first. A Z-parameter equivalent circuit of the amplifier is shown in Figure 127b. It has been simplified by omitting the components which introduce the effects of the open circuit reverse transfer impedances Z_{12} and Z'_{12}, since they are small for the transistors used. The calculations are further simplified by ignoring I_3 in all calculations, since for the transistors and resistors used $I_4/I_3 > 10$ over the complete range of operating conditions. With these assumptions,

$$V_1 = \frac{R_2}{R_1 + R_2} V_{out}.$$

The quantity V_{be} is the input transistor base-emitter junction dc voltage, and Z_{11} is the transistor open circuit input impedance. Since Z_{11} is less than 2000 ohms, V_{be} is of the order of 0.5 volt for these transistors, and I_1 is less than 10 microamperes under all operating conditions, the voltage drop across Z_{11} is negligible compared with V_{be}. Thus the dc input-output relationship is

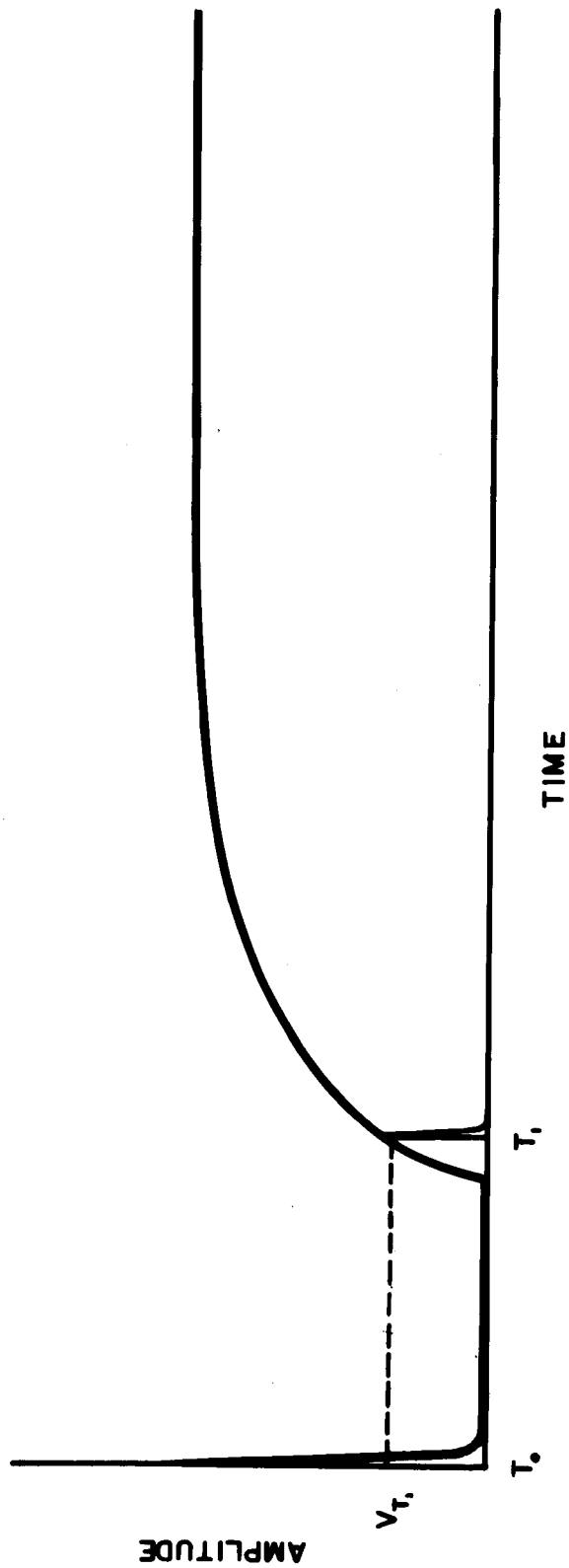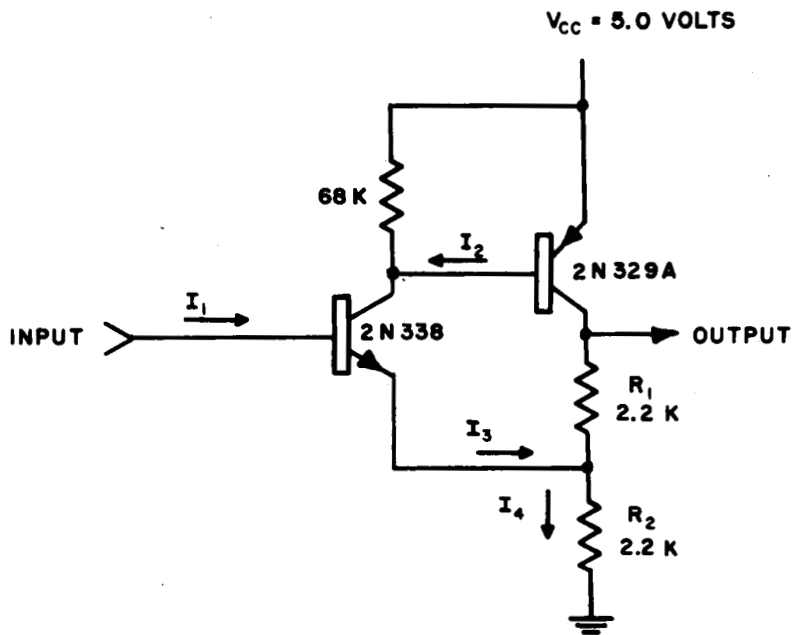$$V_{out} = \frac{R_1 + R_2}{R_2} (V_{in} - V_{be})$$

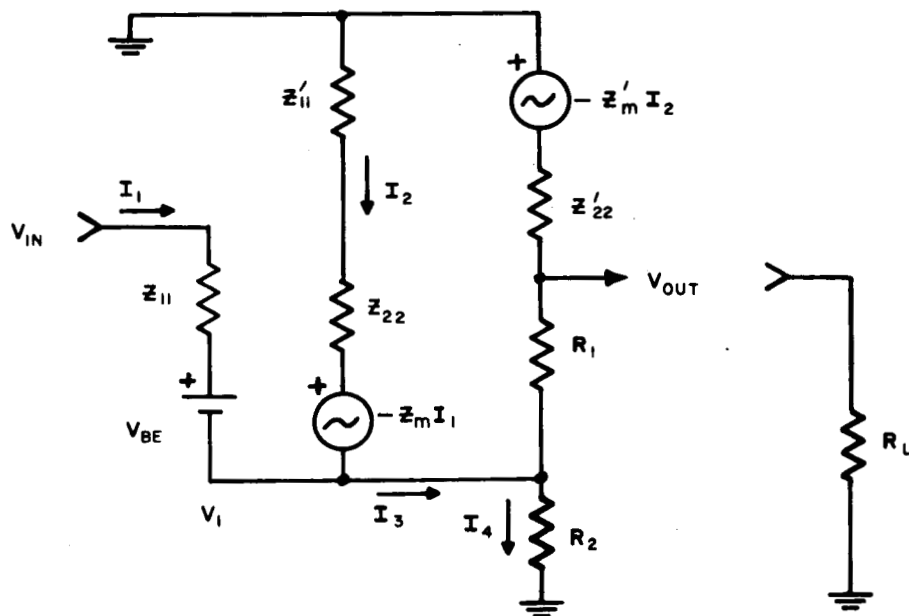FIG. 126.   G-M COUNTER PULSE ENVELOPE

(a) BASIC CIRCUIT

(b) SIMPLIFIED EQUIVALENT
CIRCUIT

FIG. 127.   BASIC BOOTSTRAP AMPLIFIER CIRCUIT

and the dynamic gain is

$$V_{out} = \frac{R_1 + R_2}{R_2} \, V_{in} \, .$$

Both the dc and ac voltage gains, in this approximation, are independent of all circuit parameters except the ratio $(R_1 + R_2)/R_2$. The dc relationship is, however, dependent on temperature, since V_{be} is temperature dependent. A family of dc output voltage versus input voltage curves is given in Figure 128, where temperature is the parameter. The linearity of response over a large fraction of the supply voltage and the constancy of the dynamic gain (the slopes of the curves) can be seen. The x-axis intercepts of the lower extensions of the straight line sections are the values of V_{be} at the temperatures plotted.

Figure 129 shows the independence of the output voltage for fixed input voltages as the supply voltage V_{cc} is varied. The slopes of the linear portions of the curves are less than 0.002.

The dc input impedance of the circuit, $Z_{in} = V_{in}/I_1$, which is a function of V_{in} and temperature, is shown in Figure 130. The effect of output loading on the circuit can be seen in Figure 131, where the output voltage is plotted as a function of the output load resistance R_L, and V_{in} is the parameter. Adding the load causes less than a one per cent change in V_{out} (with V_{in} constant) if $R_L \geqslant 6000$ ohms, and less than a ten per cent change if $R_L \geqslant 1000$ ohms. The output impedance Z_{out}, found from the data used for this plot, is approximately 100 ohms. Thus the impedance ratio Z_{in}/Z_{out} for the circuit is of the order of 10,000. The current ratio I_{out}/I_{in} is about 1300 when the device is terminated in its output impedance of 100 ohms and with $V_{in} = 2.00$, $V_{cc} = 5.00$, and temperature is 25°C.

This basic circuit has been used in a number of previous experiments as a linear pulse amplifier where its high frequency response was useful,[1] as an emitter follower (with $R_1 = 0$),[1] and as a dc voltage amplifier and impedance transformer (Para 6).

The pulse shaping amplifiers employed in the S-46 payloads are shown in schematic form in Figure 115, and Figure 132 is a photograph of the top of the instrumentation deck containing these five circuits. The pulse shaping circuits for the five channels are identical except for the input circuit resistor values, which are selected to produce the proper input pulse amplitudes.

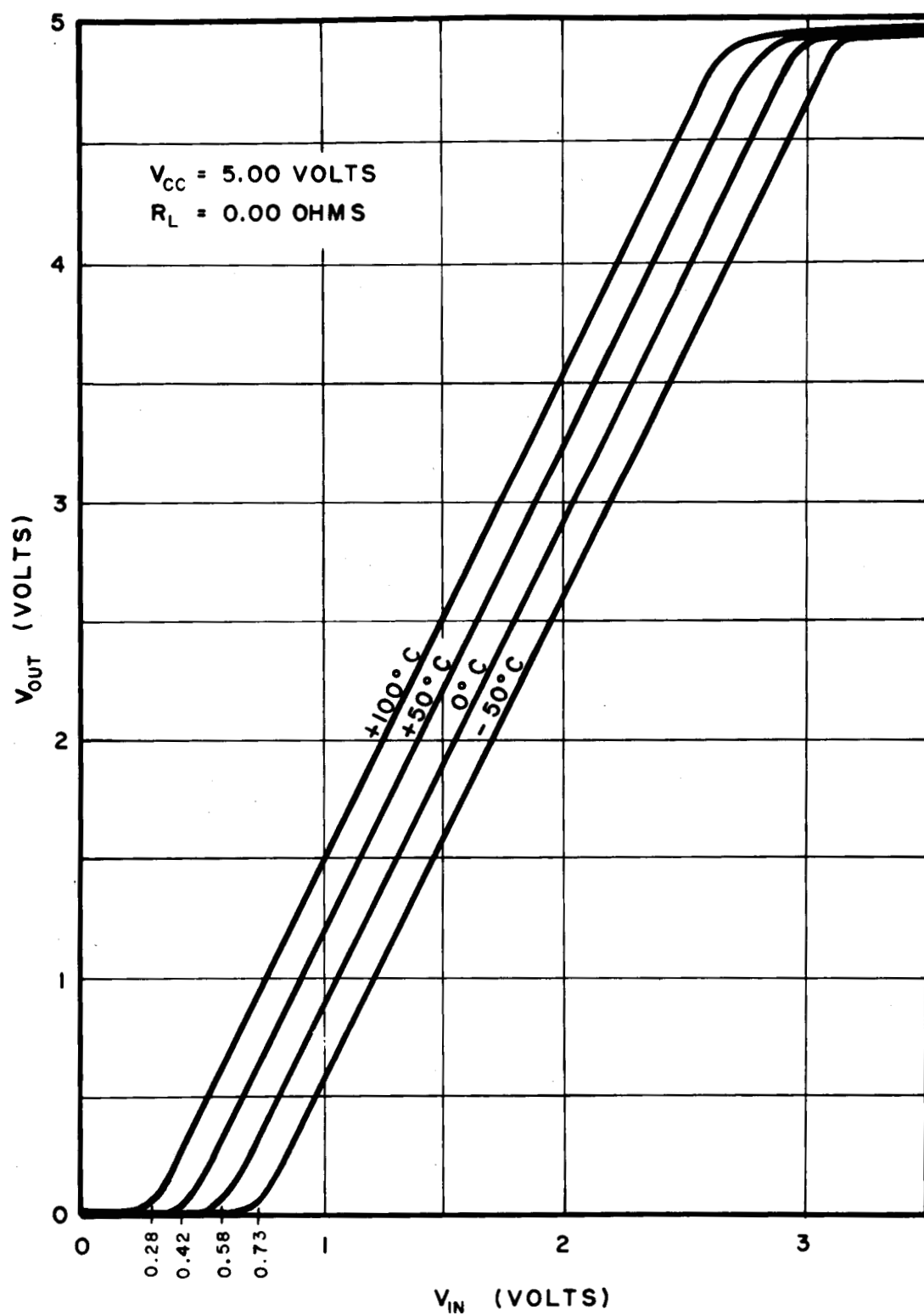1. C. E. McIlwain, <u>Scintillation Counters in Rockets and Satellites</u>, SUI Research Report 60-4, February 1960.

FIG. 128.   BOOTSTRAP AMPLIFIER VOLTAGE GAIN
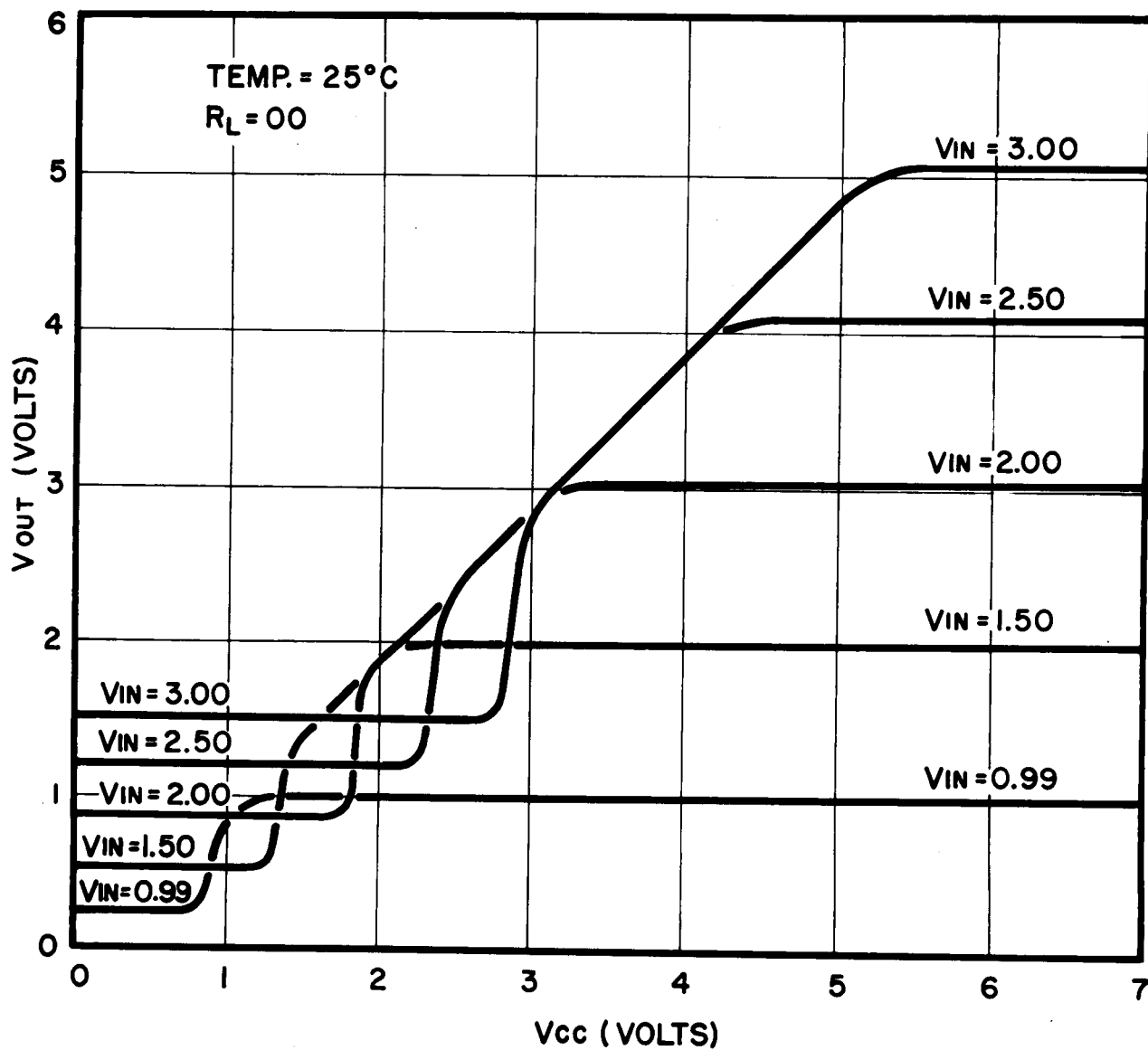
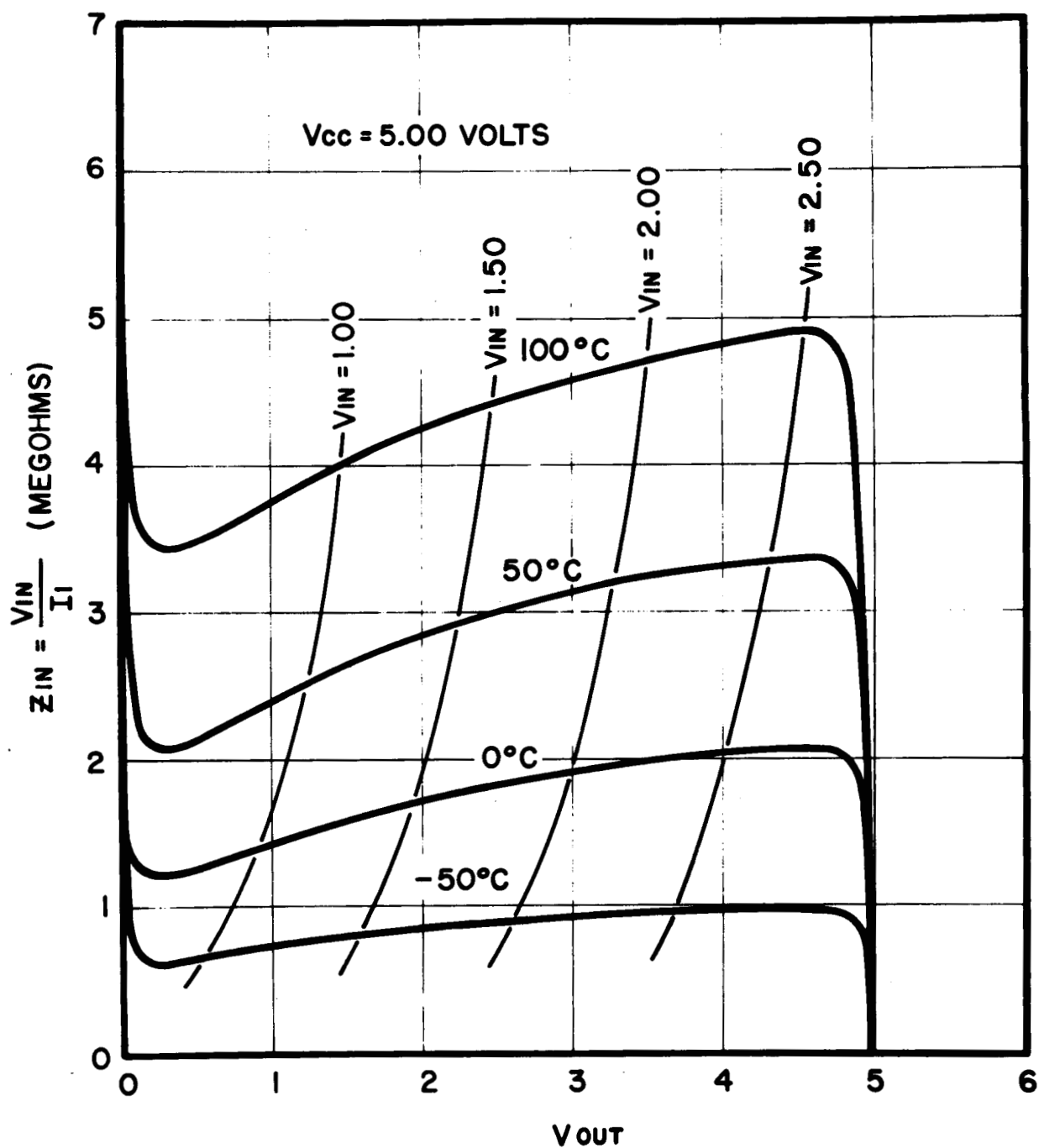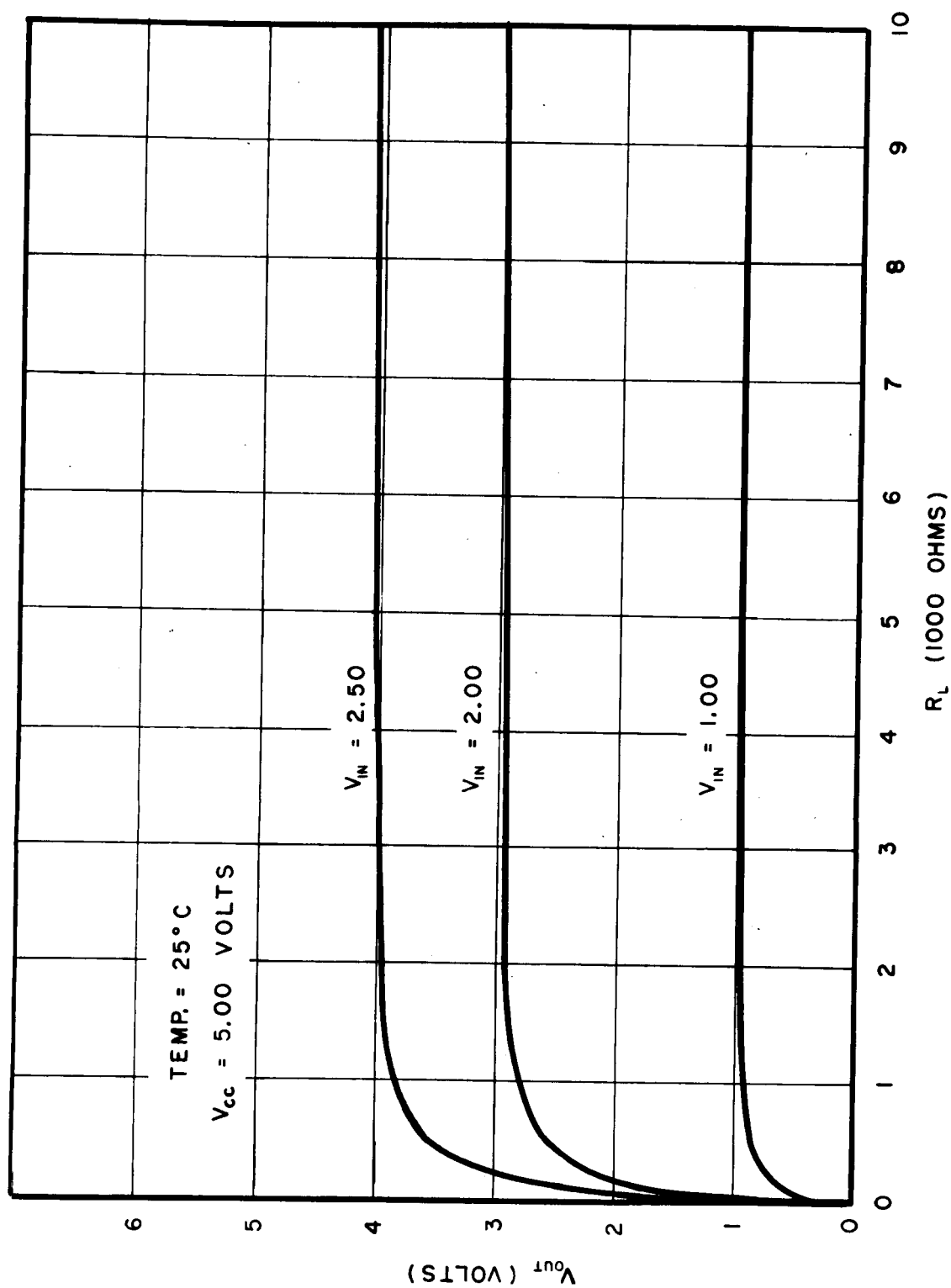FIG. 129. BOOTSTRAP AMPLIFIER PERFORMANCE WITH CHANGE IN V_{cc}

FIG. 130. BOOTSTRAP AMPLIFIER INPUT IMPEDANCE

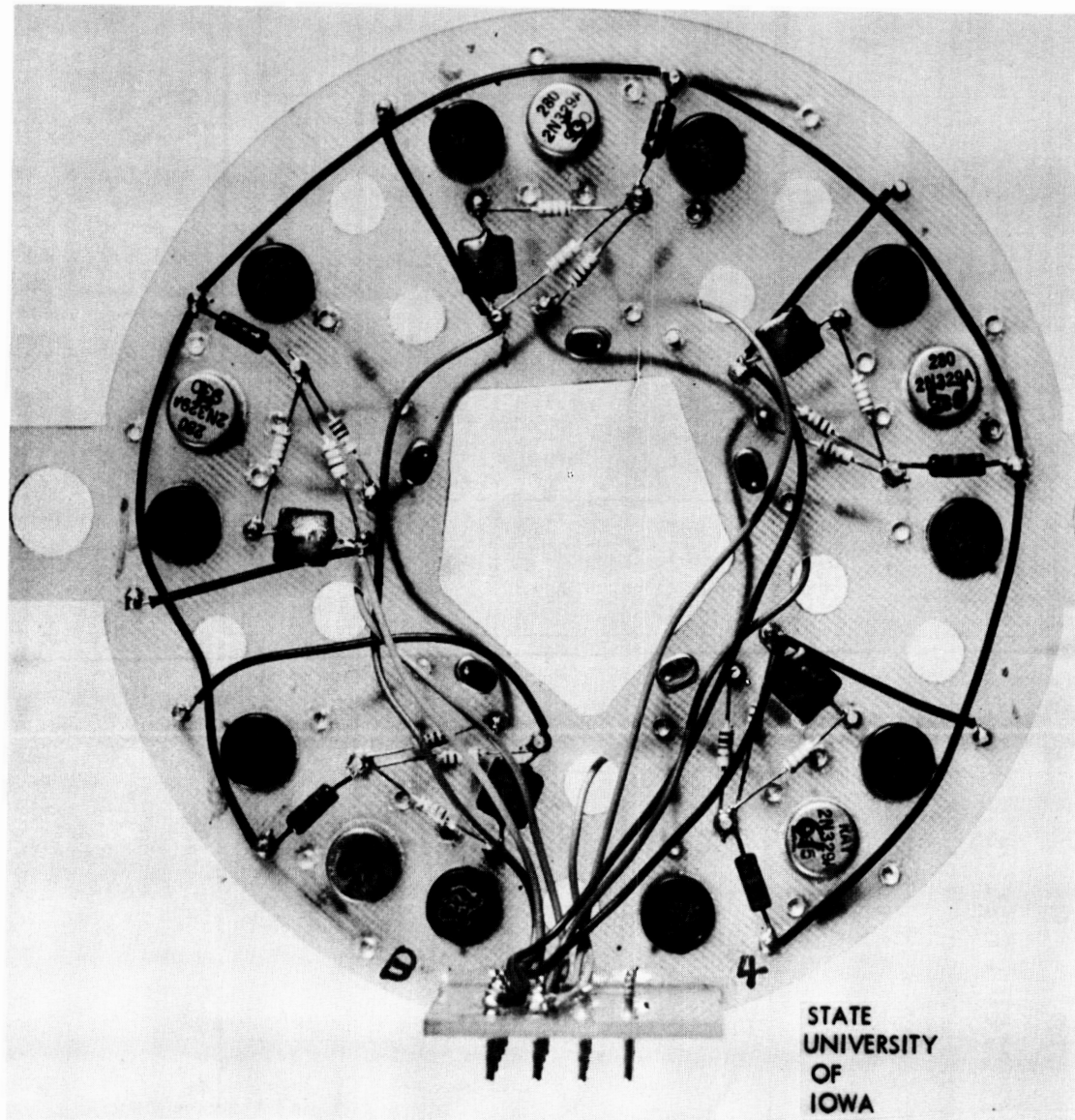FIG. 131. BOOTSTRAP AMPLIFIER PERFORMANCE WITH CHANGE IN R_L

FIG. 132.   TOP VIEW OF THE PULSE SHAPING AMPLIFIER DECK

Two stages of amplification are used in each circuit to provide an overall gain of 3.4. The output transistor of the first stage is used as the input transistor of the second stage, so that only three transistors are required for the two stages instead of four. The circuit is used as a nonlinear amplifier. A zener diode voltage limiter is used at the output to clip the negative pulses at the 3.3 volt level, producing an optimum pulse amplitude for driving the scaler. The threshold effect due to V_{be} is used to establish an input pulse amplitude threshold. The overall effect of the circuit is to produce no output for input pulses just below the threshold, and to provide output pulses having full amplitude for input pulses slightly above threshold. This is illustrated in the graph of Figure 133, in which the output pulse height is plotted as a function of input pulse height.

It was determined experimentally that a diode placed in the input circuit as shown in the schematic diagram effectively reduces the high counting rate temperature dependence of the complete configuration. Its primary effect is to partially balance the temperature dependence of V_{be} by generating an equal voltage with a similar junction placed in a position where their variations subtract. The effectiveness of the overall temperature compensation can be seen in Figure 134, in which the counting rate of detector E with a radioactive source positioned to produce a maximum scaler switching rate is plotted as a function of temperature.

5. Binary Scalers

The binary scalers used in the S-46 payloads are an outgrowth of the circuits designed for Explorers I and III.[1] The major modifications implemented changes proposed by R. J. Parent and V. E. Suomi, of the University of Wisconsin, that the supply voltage be changed from 2.68 volts to 6.50 volts and that appropriate changes be made in the component values. The advantages are a decrease in the power requirements and the ability to drive one stage directly from the output of a preceding stage without the need of interstage coupling amplifiers.

The basic scaling circuit is the bi-stable multivibrator shown in Figure 135. Departures from conventional techniques are the omission of the usual base to negative potential biasing resistors and the use of unusually large collector resistor values to reduce operating power. The dc biasing conditions are as follows:

Assume that T_1 is conducting and that T_2 is cut off. The T_2 collector current is essentially I_{co}, which for the silicon transistors used is negligible (less than one microampere). Then

$$V_{c_2} = V_{cc} - \frac{R_2(V_{cc} - V_{b_1})}{R_2 + R_4} = 3.4 \text{ volts}$$

1. G. H. Ludwig, _Cosmic Ray Instrumentation in the First U.S. Earth Satellite_, Rev. Sci. Instr. __30__, 223, 1959.
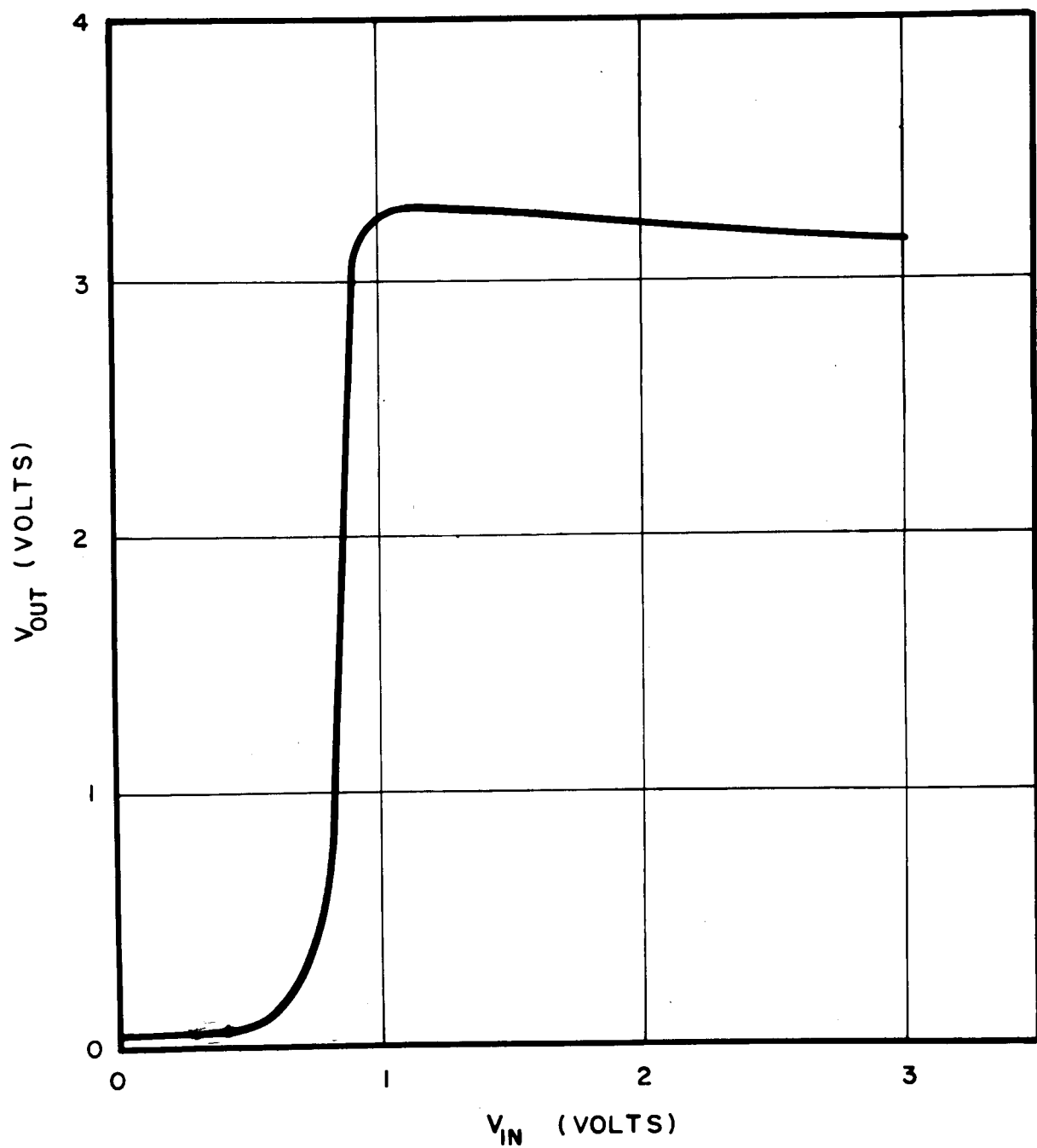
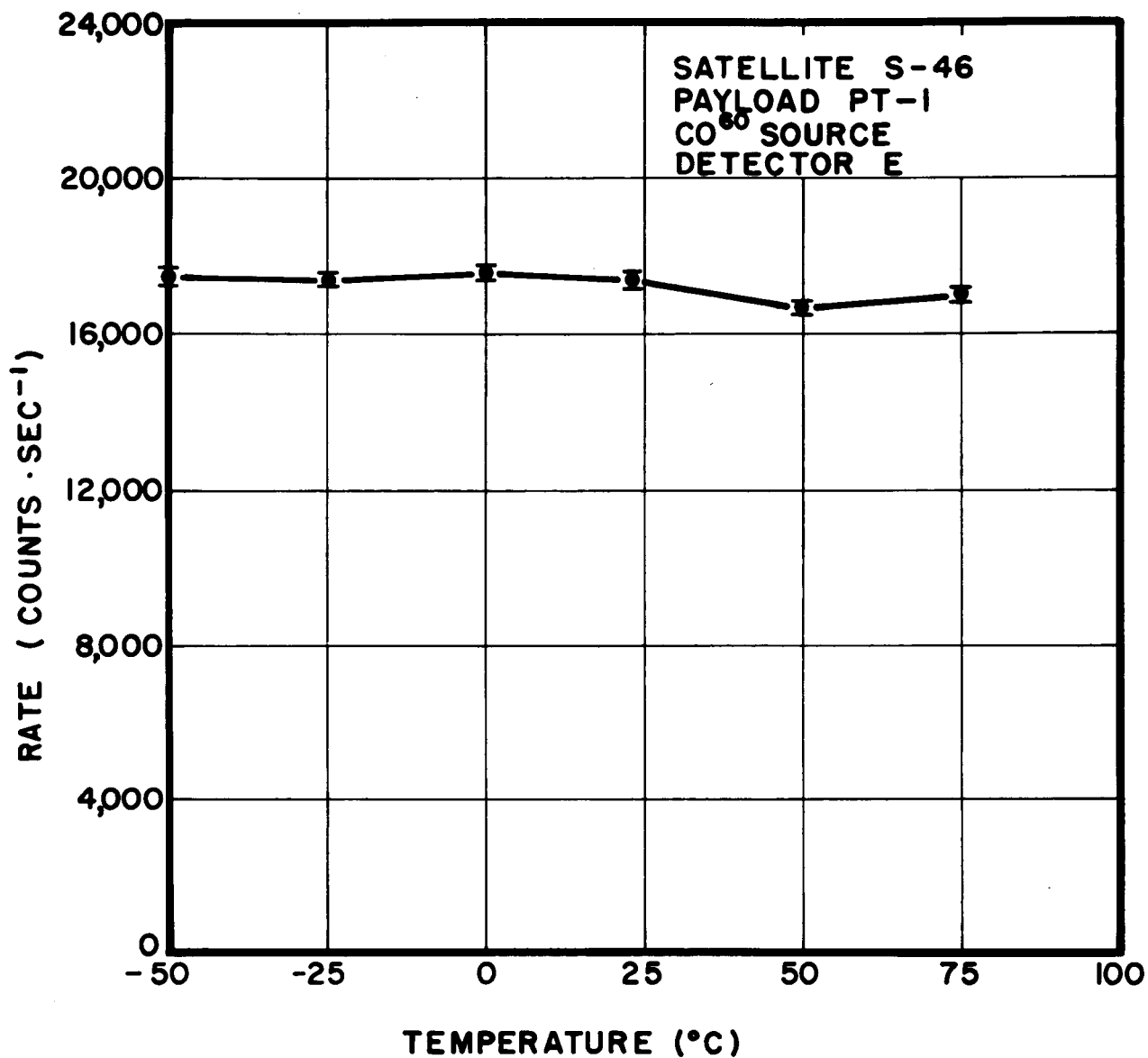FIG. 133. PULSE SHAPING CIRCUIT CHARACTERISTICS

FIG. 134.   DEPENDENCE OF MAXIMUM COUNTING RATE ON TEMPERATURE
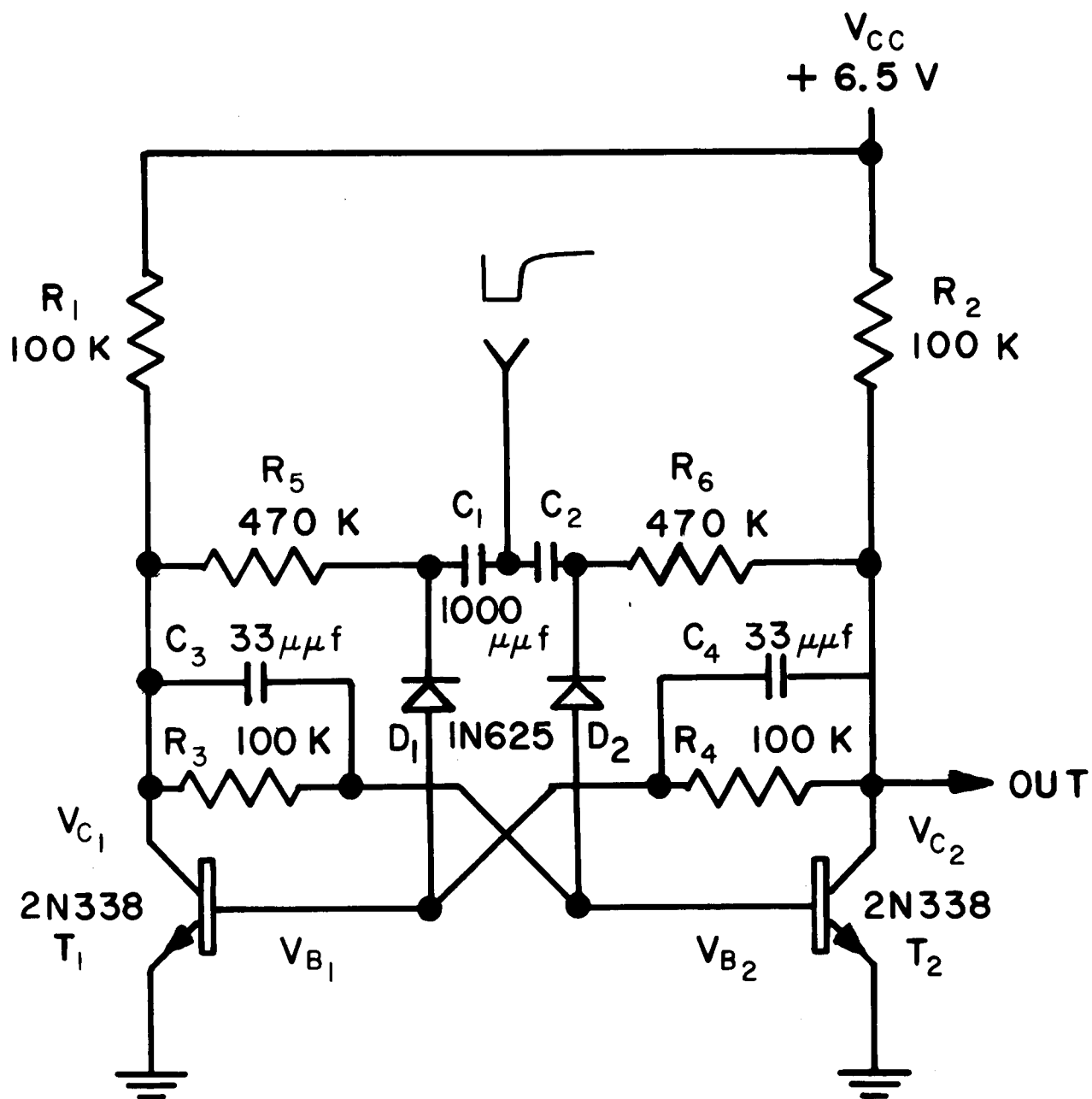
252

FIG. 135. BASIC BINARY SCALER CIRCUIT

for the resistance values indicated and for V_{cc} = 6.5 volts, since V_{b_1} = 0.3 volt when T_1 is conducting. The base current of the conducting transistor is

$$I_{b_1} = \frac{V_{cc} - V_{b_1}}{R_2 + R_4} = 30\mu A$$

which would be great enough to provide I_{c_1} = 1.5 ma (with β_{min} = 50) if this current could be supplied by V_{cc} through R_1. However, the current is limited by R_1 to $I_{c_1} = \frac{V_{cc}}{R_1}$ = 65μA. The result is that V_{c_1} is firmly clamped to ground (V_{c_1} = 0.03 volt).

With V_{c_1} = 0.03 volt the cutoff transistor base voltage (V_{b_2}) is well below the silicon transistor base-emitter junction potential (I_c is only a few microamperes when V_b = 0.2 volt). As a result, T_2 is adequately cut off, and I_{c_2} is negligible as was initially assumed.

Thus it is seen that all biasing conditions for stable operation are met, and that the base to negative potential resistors are not required as a result of the low I_{co} and high base-emitter potential of the silicon transistors, and the low current operating conditions of the circuits. The design is sufficiently conservative so that operation over very wide ranges of temperature and supply voltage is possible.

To trigger a change of state, a negative pulse is applied to the base of the conducting transistor by the pulse steering network consisting of C_1, C_2, R_5, R_6, D_1, and D_2. The two resistors R_5 and R_6 bias the diodes to accomplish the steering action. If T_1 is conducting, diode D_2 is reverse biased by a potential of 3.4 volts, while D_1 has essentially zero bias. A negative pulse applied to the input is conducted by D_1 to the base of T_1 and to the collector of T_2 through the speed-up capacitor C_4, but is not conducted by the reverse biased D_2. Thus the circuit begins a transition to the opposite state, and the regenerative action of the circuit completes the transition. The values of the speed-up capacitors C_3 and C_4 are not critical, the primary requirement being that the time constant of the capacitors and their discharging resistors R_2 and R_4 or R_1 and R_3 be of the order of a few microseconds. A value of 33$\mu\mu$fd is used, giving RC = 1.6 μ sec.

The values of the steering network components were chosen empirically to produce the best operation over a wide range of operating conditions from the waveform obtained from the collector of an identical circuit. The time constant of the input circuit consisting of C_1 and R_5 is 470 microseconds. This establishes a maximum frequency of operation of about 16,000 counts per second ($f_{max} \approx \frac{8}{RC}$). The time constant can be reduced

considerably before serious deterioration of performance results. The values shown in the schematic are used whenever high speed of operation is not necessary. In the cases where faster counting is necessary, a modification of the basic circuit is used in which the operating currents are increased by reducing the values of R_1, R_2, R_3, and R_4, and the input time constants are reduced in value. The first stages of the scaler of Figure 137 are examples of circuits which count at maximum rates of about 39,000 counts per second (RC = 44 microseconds; $f_{max} \approx \frac{2}{RC}$). Even higher speeds of operation are possible, although this requires a somewhat more careful selection of transistors, diodes, and resistor values.

The input pulse amplitude must be considerably greater than the silicon diode junction voltage of the unbiased steering diode (about 1.6 volt). However, if it is made greater than the 3.4 volts by which the other diode is reverse biased, then the performance is deteriorated. The most immediate effect is that the maximum speed of operation decreases. A pulse amplitude of about 3.3 volts is used at all the scaler inputs. The zener diode in the pulse shaping amplifier regulates the first scaler stage input pulse amplitude at this value, and for succeeding stages this amplitude is provided directly by differentiation of the scaler collector waveform.

The output impedance of the scaler circuit is 50 K ohms (with R_1 = R_2 = 100 K ohms).

The values of the scaler components are not critical. Resistor value tolerances are ± 10 per cent, and the transistor forward current gain (β) can be any value greater than about 50. The transistors having the higher values of β are used in the stages which must operate at the higher rates, and an attempt is made to use pairs of transistors in each stage with approximately equal values of β. The capacitor values are also noncritical, although, of course, the scaler has a deadtime versus temperature characteristic which is partially determined by the capacitors C_1 and C_2.

In the S-46 payload, 65 scaler stages are used. The scaler module schematic diagrams of Figures 136,137, and 138 show the manner in which they are connected. Figure 139 is a photograph of the top of the detector E seventeen stage scaler (scale of 131,072) and the logic circuit and output amplifier associated with it.

Several of the performance characteristics of the scaler stages are indicated in Figures 140, 141, and 142. The data used to plot the curves are average values obtained from a number of individual circuits, as indicated in the figures. The signal source for all tests was a pulse generator furnishing a negative 3.1 volt rectangular pulse having a width of 5μsec, a rise time of less than 0.1μsec, and a source impedance of 50 ohms. In all cases the output of the stage under test was loaded by an identical scaler stage input impedance.
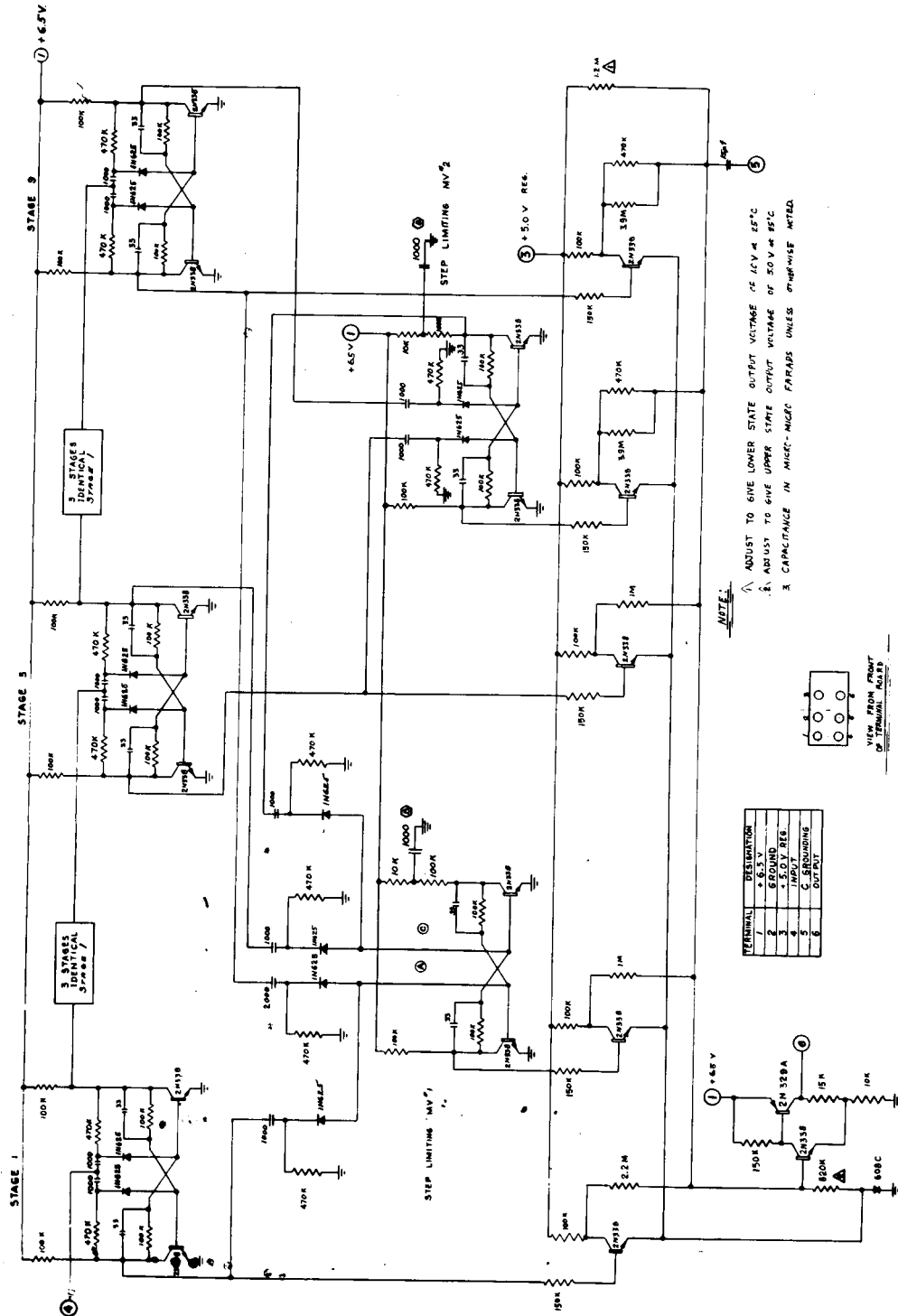
FIG. 136. SCHEMATIC DIAGRAM OF THE CHANNEL A AND B SCALERS, LOGIC CIRCUITS
AND OUTPUT AMPLIFIERS, DECKS C AND D   From the Dept of Physics,
State Univ. of Iowa Drawing D11-2C201

FIG. 137. SCHEMATIC DIAGRAM OF THE CHANNEL C AND E SCALERS, LOGIC CIRCUITS, AND OUTPUT AMPLIFIERS, DECKS E AND G   From Dept of Physics, State Univ. of Iowa Drawing D11-2E201
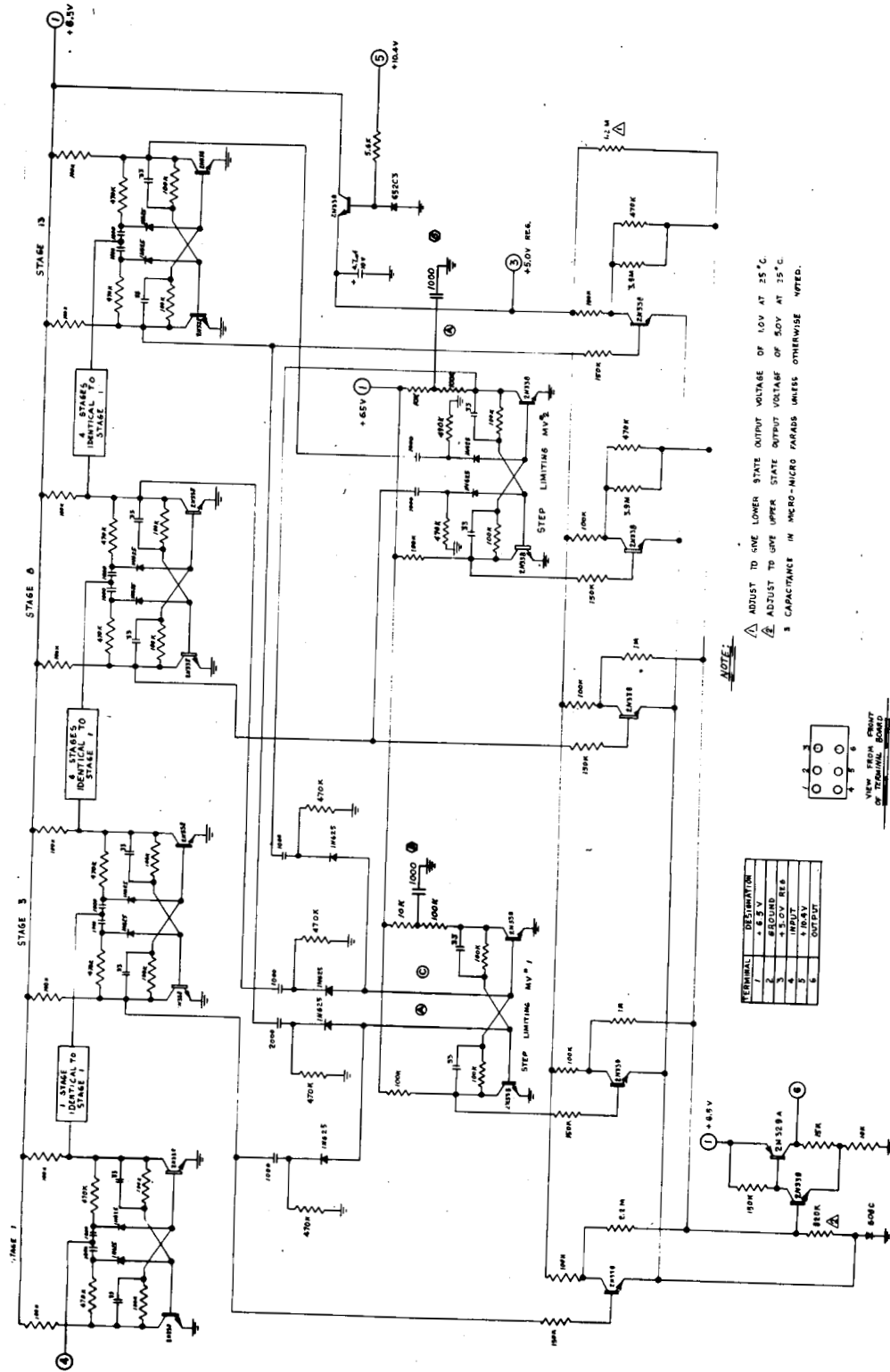
FIG. 138. SCHEMATIC DIAGRAM OF THE CHANNEL D SCALER, LOGIC CIRCUIT, AND OUTPUT AMPLIFIER, AND 5.0 VOLT REGULATOR, DECK F Dept of Physics, State University of Iowa Drawing D11-2F201
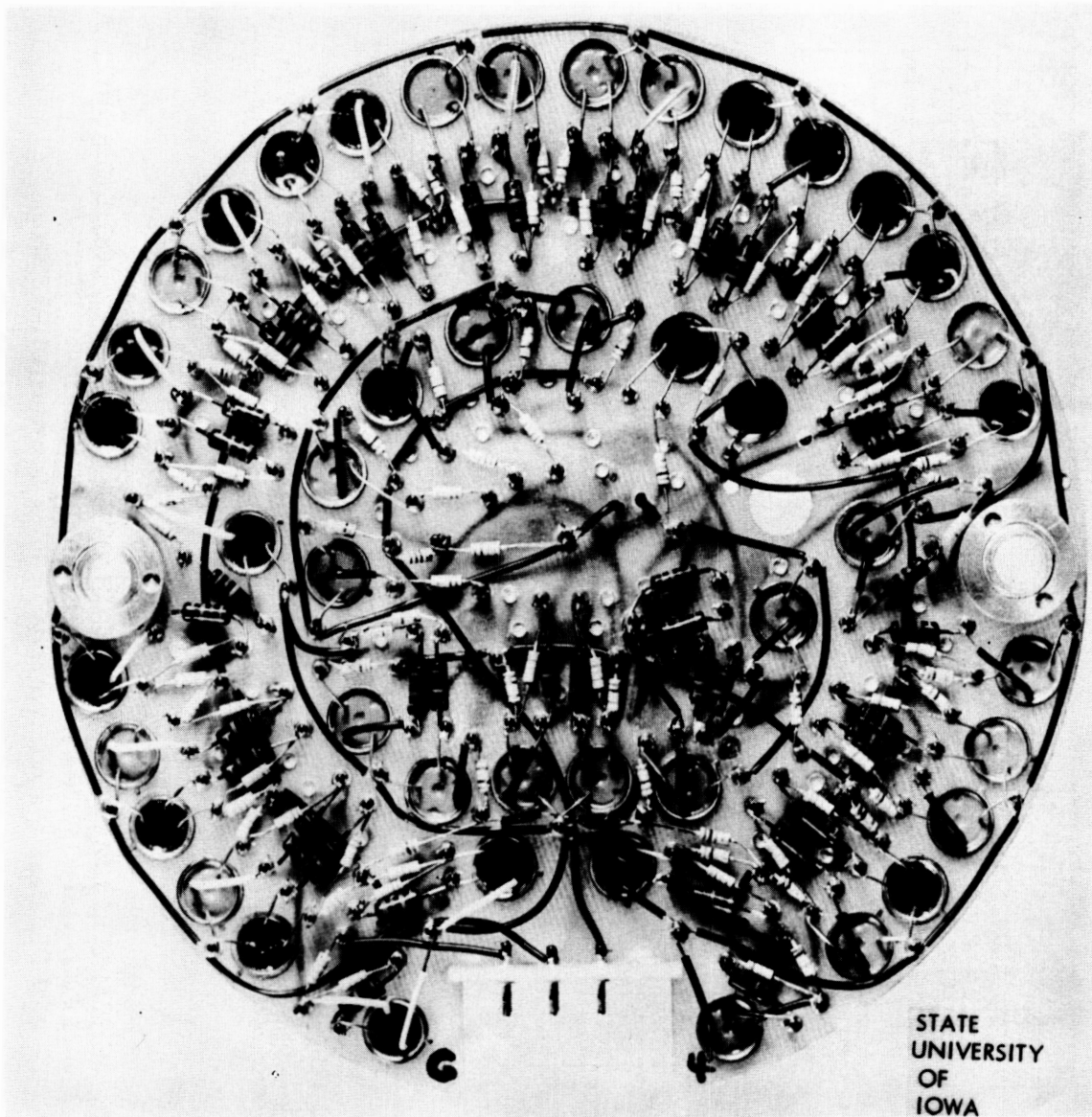
FIG. 139. TOP VIEW OF DECK G CONTAINING THE SEVENTEEN STAGE SCALER, LOGIC CIRCUIT, AND OUTPUT AMPLIFIER FOR DETECTOR E

LOW SPEED SCALER ($R_1 = 100 K ohms$)
COUNTING RATE = 1,000 SEC^{-1}
AVERAGE FOR 12 INPUT STAGES
IN PT-1, PT-2, FU-1, & FU-2.

FIG. 140.   MINIMUM SUPPLY VOLTAGE V_{cc} FOR SCALER OPERATION

LOW SPEED SCALER ($R_1 = 100K \, \Omega$)
COUNTING RATE = 1000 SECOND^{-1}
AVERAGE FOR 148 STAGES
IN PT-1, PT-2, FU-1, FU-2

+100° C

- 50° C

SCALER POWER PER STAGE (MW.)

SUPPLY VOLTAGE V_{CC} (VOLTS)

FIG. 141. SCALER POWER REQUIREMENTS

FIG. 142.   SCALER MAXIMUM COUNTING RATE

The scaler stages operate over a wide range of supply voltage V_{CC}. Figure 140 indicates the minimum value $(V_{CC}$ min) as a function of temperature for the low speed scaler, with the scaler operating at a rate of 1000 sec^{-1}. The analogous curve for the high speed scaler is similar in character but about 0.3 volts higher. The maximum value (V_{CC} max) is in every case greater than 8.0 volts, the highest value attempted.

The operating power per low speed scaler stage is nominally about 0.75 milliwatt with V_{CC} ≈ 6.5 volt. A plot of the operating power as a function of supply voltage is shown in Figure 141 for temperatures of -50°C and +100°C.
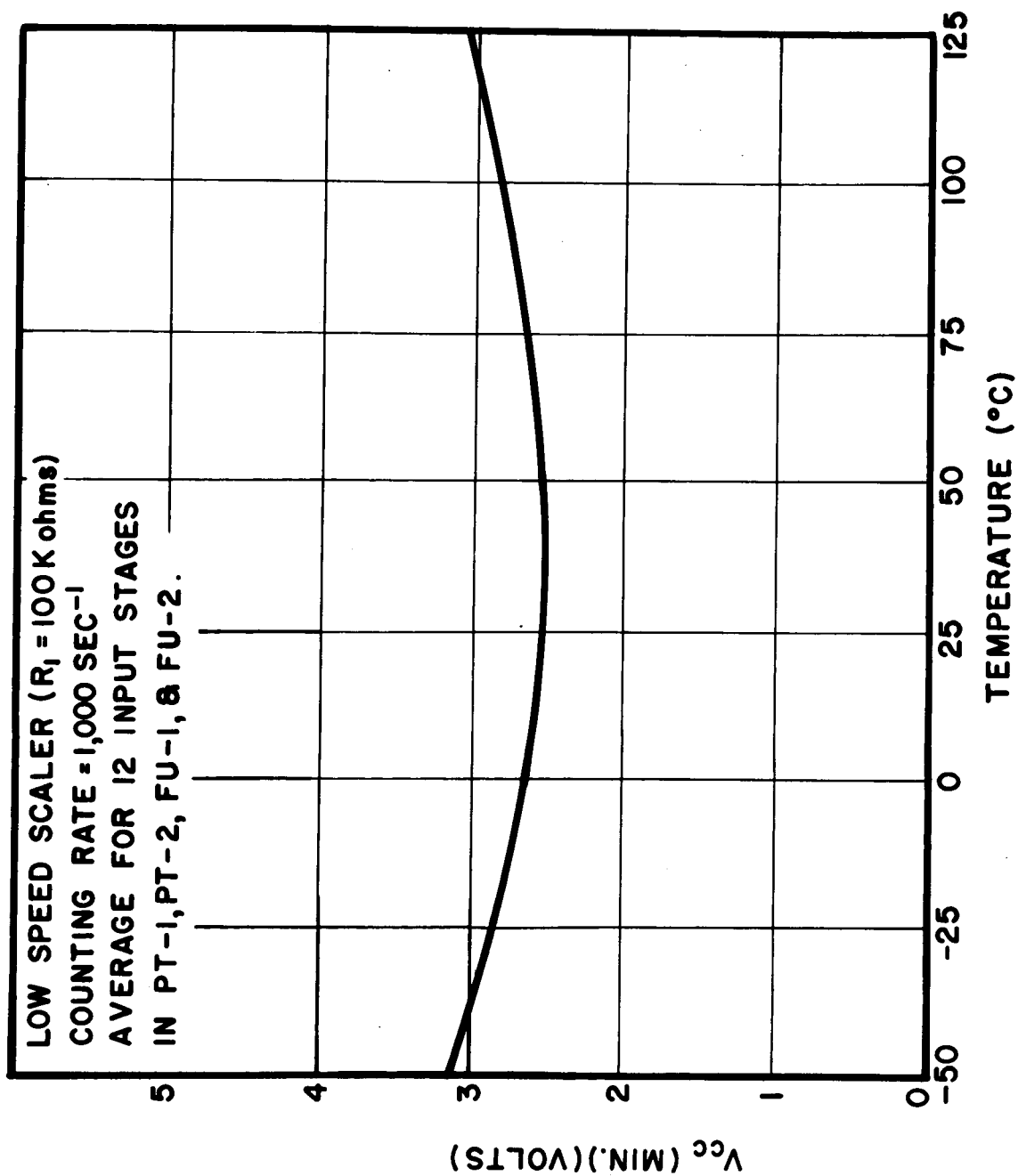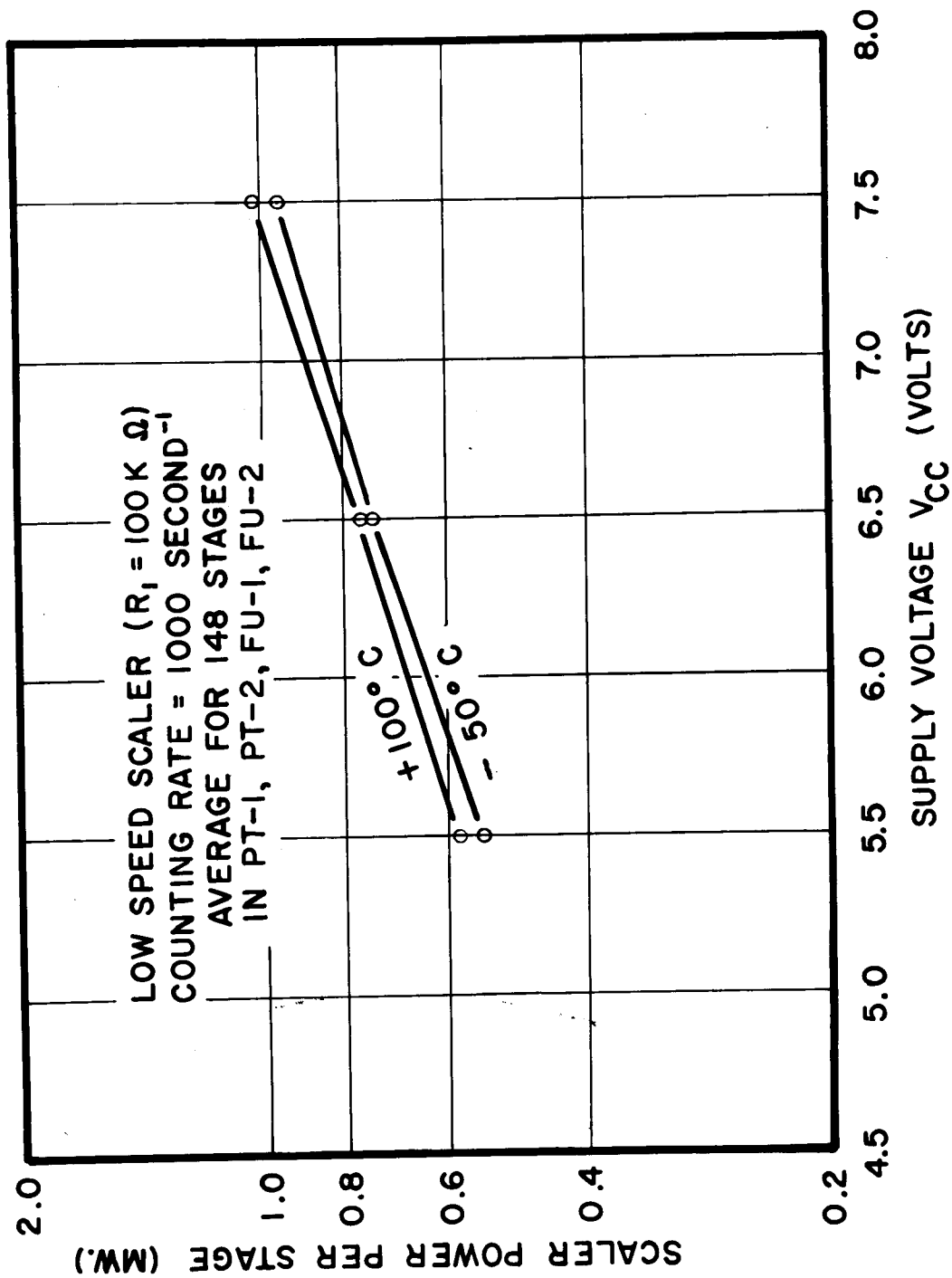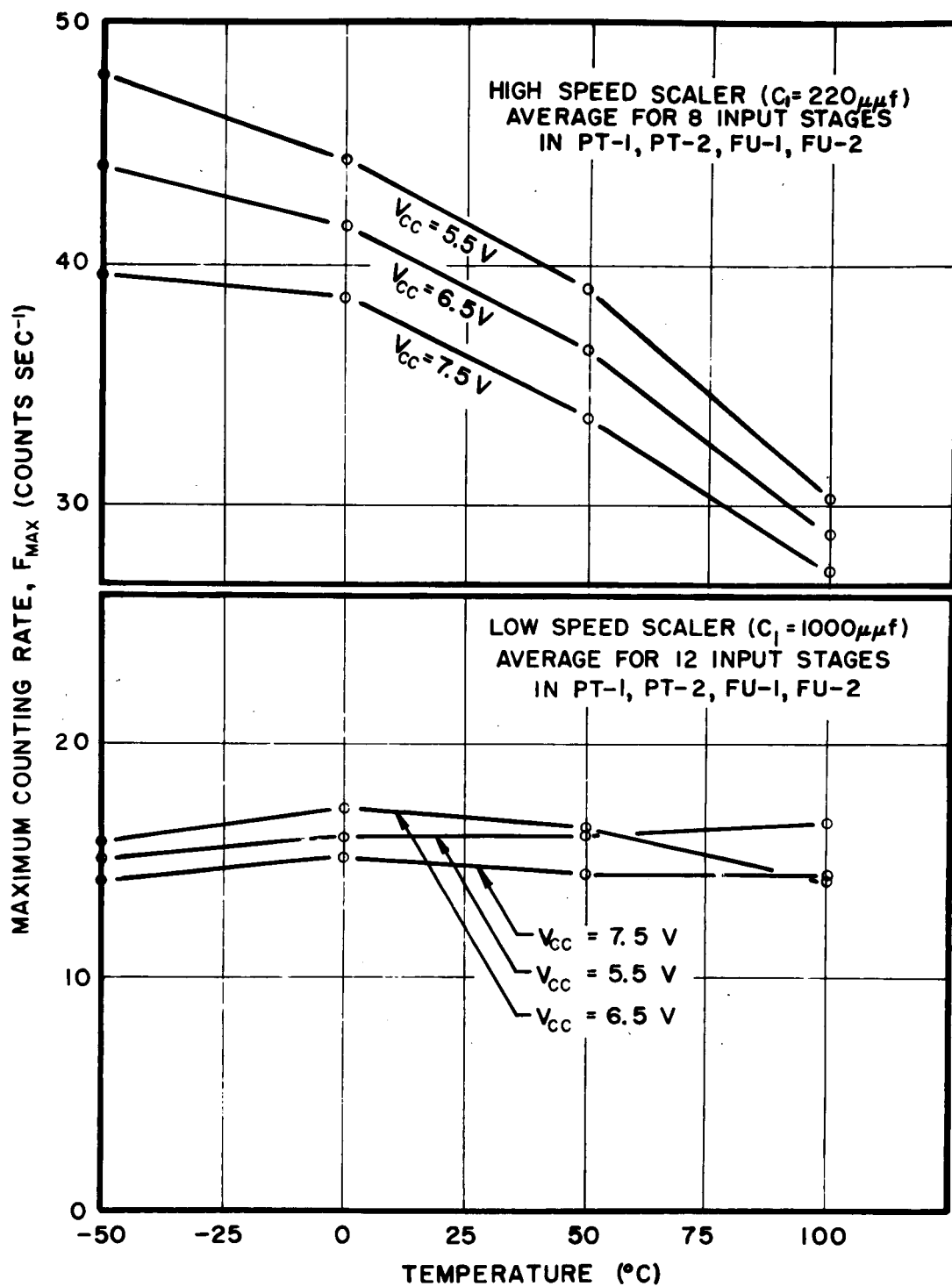
Figure 142 shows the dependence of the maximum counting rate (of the scaler alone) on temperature and supply voltage V_{CC} for both the high and low speed scalers. The difference in temperature characteristics between the two circuits is due primarily to the difference in the input capacitor (C_1 and C_2) temperature coefficients. The high speed scaler uses Glenco Corp. type TC-220-9 (Code Q) 220 μμfd capacitors having a negative temperature coefficient of about 0.2 per cent per degree centigrade, while the low speed scaler uses Glenco Corp. type SSM-001-23 (Code M) 1000 μμfd capacitors having a positive temperature coefficient of somewhat less than 0.14 per cent per degree centigrade. Thus the difference in capacitor coefficients is a little less than 0.34 per cent per degree centigrade. The difference in the slopes of the maximum counting rate curves for the two scalers is of the order of 0.28 per cent per degree centigrade. It is reasonable to assume, then, that the counting rate temperature coefficient for the scaler circuit, if zero temperature coefficient input capacitors were used, would be about -0.14 per cent per degree centigrade. This is due primarily to changes in transistor characteristics with changes in temperature. The variation can be reduced to a low value by the proper selection of input capacitor characteristics. In this particular scaler application the variation in scaler dead time does not affect the maximum G-M counter counting rate because the scaler dead time is significantly less than the counter dead time under all operating conditions (Fig. 134).

6. Logic Circuits and Output Amplifiers

Since a large dynamic range in counting rates is expected for any experiment traversing the high intensity radiation belts, it was considered necessary to telemeter three different scaling factors for each detector. Outputs are obtained from three stages of each scaler. The various scaling factors used in the S-46 instruments are as indicated in the block diagram of Figure 112. These outputs are combined in logic circuits in such a way that all three scaling factors can be identified unambiguously in the single output waveform.

This method of telemetering three scaling factors on a single channel was first proposed in April, 1958. The Jet Propulsion Laboratory designed the first version of the system and used it successfully in the Pioneer III and IV space probes.[1] The present system is an improved design of the JPL system in which the remaining large shifts in SCO frequency are eliminated, less operating power is required, and the operation is more stable.

The operation of the logic circuit can be seen with the aid of the block diagram of Figure 143, the schematic diagrams of Figures 136, 137, and 138, and the waveforms of Figure 144. Inputs from the three scaler stages A, B, and C (which correspond, for example, to stages 1, 5, and 9 respectively of the channel A scaler) operate transistor switches 1, 3, and 5 directly. The collectors of these switches are either at ground potential (0.02 volt) or at 5.0 volts minus the voltage drop across the 100 K ohm collector resistors, depending on whether the switchs are off or on. These voltages produce an eight level waveform in the summing circuit as shown in Figure 144 by waveform (f).

It was found necessary to keep the telemetry bandwidth as low as possible to reduce the transmitter power requirements (Chapter 1, Section II, 7). This was accomplished by choosing the scaling factors large enough so that the highest anticipated counting rates were scaled to rates of less than one cycle per 5 seconds, and by limiting the rate of change of the logic circuit output voltages (and therefore subcarrier oscillator frequencies). This was accomplished by including elements in the logic circuit to prevent all output voltage shifts of greater than one unit, and by passing the output waveform through an RC integrating circuit having a time constant of about five seconds.

The "OR" circuits, step reducing multivibrators, and switches 2 and 4 were added to reduce the large voltage shifts. The step reducing multivibrators produce waveforms which, when used to generate waveforms (b) and (d) of Figure 144 at the outputs of switches 2 and 4, produce the logically perfect waveform (g).

The operation of step reducing multivibrator number two is as follows: Its normal position is with C_2 (collector number two) at ground potential. A negative pulse (the waveforms shown occur at the outputs of the switches where the multivibrator waveforms have been reversed) at B_2 (base number two) coincident with the triggering of scaler stage C at time t_1 switches the multivibrator. The subsequent input to B_1 from scaler stage B at time t_2 resets it, and no further action occurs until another pulse appears at B_2 (at time t_4). The operation of step reducing multivibrator number one is similar, except that an extra pulse is inserted at the time (t_2) that step reducing multivibrator number two resets (through input B of "OR" circuit 2), and a pulse is blanked at the time (t_3) that scaler stage C resets (through input B of "OR" circuit 1). Input B to "OR" circuit 1

1. C. S. Josias, Radiation Instrumentation Electronics for the Pioneer III and IV Space Probes, Proc. IRE 48, 735, 1960.
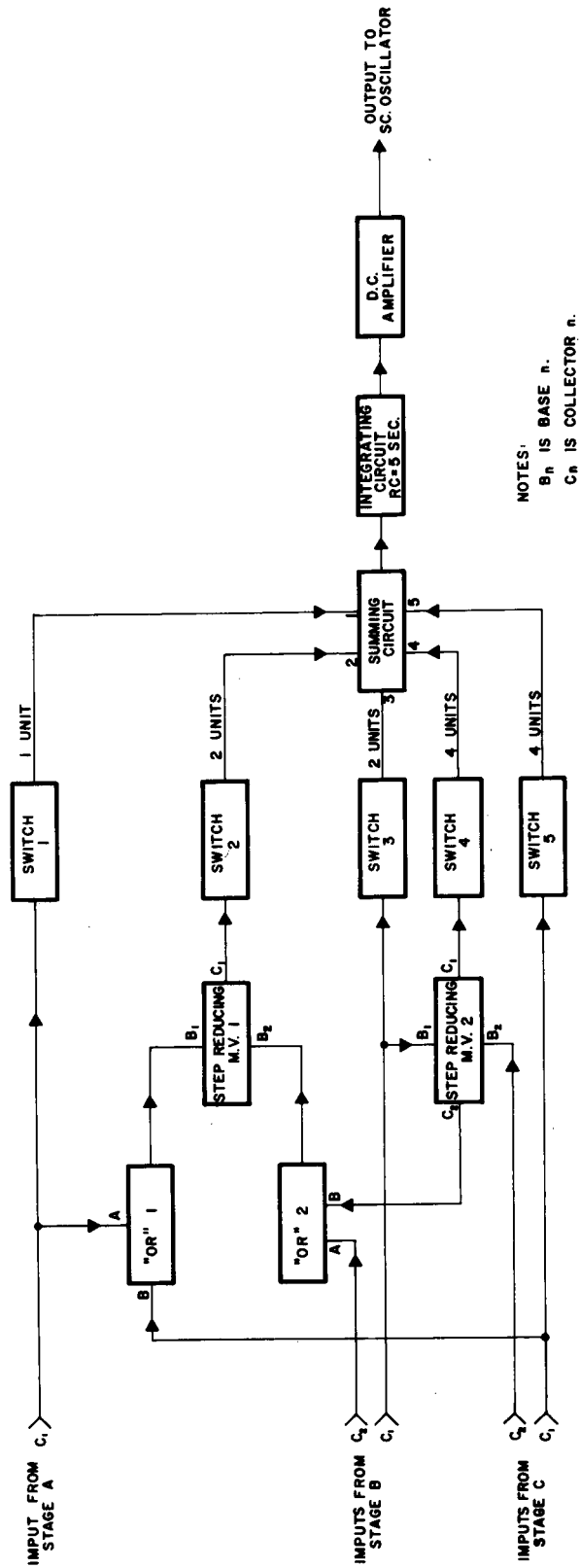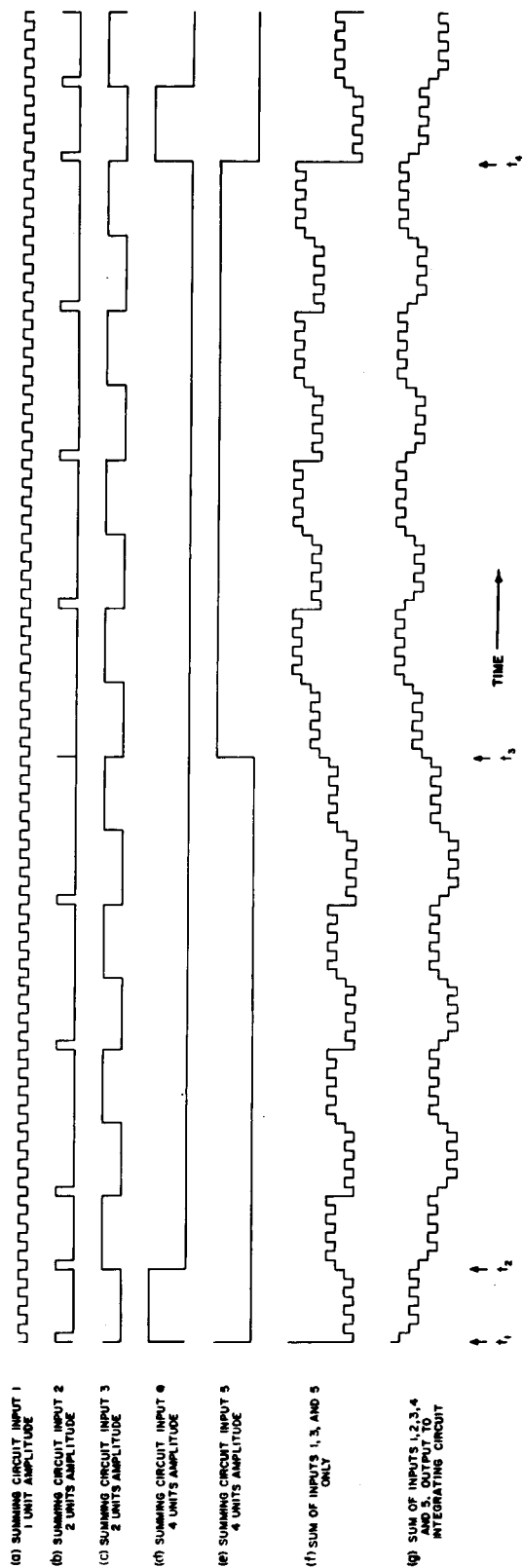
FIG. 143. BLOCK DIAGRAM OF LOGIC AND OUTPUT AMPLIFIER CIRCUITS

FIG. 144. LOGIC CIRCUIT WAVEFORMS

occurs about 40 microseconds later than input A to "OR" circuit 2 due to switching delays in the scaler stages between stages B and C. Therefore the multivibrator is triggered as usual, but is immediately reset. The integrating circuit removes all traces of the 40 microsecond wide pulse which results.

The step reducing multivibrators are identical to the low speed scaler stages except for several minor modifications. They are used as bistable multivibrators with separate inputs. Therefore the diodes are zero biased rather than collector biased. Additional diode networks are added to step reducing multivibrator number one to form the two "OR" circuits. And an RC network is added to one of the collector circuits in each multivibrator. The capacitors hold those collectors at ground potential momentarily when power is applied to cause them to be initially in the "down" state. If this were not done, there would be a probability that more than three of the summing circuit inputs of some channel might be in the "on" state, which would cause that subcarrier oscillator frequency to be out-of-band. This could not be allowed because, during launch, the internal payload power was finally applied only 5.5 minutes prior to rocket liftoff. With the low counting rates observed near the earth's surface, these SCO's would probably have remained out-of-band throughout the launch trajectory, and no launch data would have been obtained from those channels.

The transistor switches are grounded-emitter amplifiers. The common emitter lead connection is maintained at approximately 0.6 volt by the diode at the input to the dc amplifier. When the multivibrator collector driving a switch is in the "off" state (near ground potential), the switch is reverse biased and essentially zero base current results. The transistor is thus cut off and the collector potential is that established by the current through the summing circuit resistors. When the multivibrator collector is in the "on" state, however, base current in the transistor switch results. Its value is about 13 microamperes (the multivibrator collector voltage with this load is 2.58 volts), resulting in full conduction. Thus the collector is within 0.03 volt of the emitter voltage.

The summing circuit consists of 2.2, 1 and 0.42 megohm input resistors (and a 1.2 megohm resistor used to establish one operating point) and a 0.82 megohm shunt resistor. The exact value of the 0.82 megohm nominal value shunt resistor is selected to produce a dc voltage of 1.0 ± 0.1 at the amplifier output with all transistor switches conducting and at room temperature. The 1.2 megohm nominal value resistor is selected to produce 5.0 ± 0.2 volts at the same point with switches 1, 3, and 5 cut off and switches 2 and 4 conducting. These voltages establish the SCO frequencies when the amplifier output waveform is in its lowest and highest states, that is, states one and eight.

The transistor switches and summing circuits are operated from a 5.0 volt supply which is regulated to reduce the output voltage changes with variations in supply voltage. The regulator is shown in the schematic diagram of Figure 138. It is a conventional series transistor regulator for which a reference voltage is established by a type 652C3 5.8 volt zener diode. The regulation characteristics of this regulator are shown in Figure 145, in which the output voltage is plotted as a function of temperature and supply voltages. This circuit maintains the voltage within ±4 per cent of 5.0 volts, which is adequate in this application.

Integration of the output amplifier waveform is provided by the 15 microfarad capacitor and the resistors in the summing circuit. One terminal of this capacitor, shown unconnected in the schematic diagrams, is grounded through the test socket (TS) on top of the payload except during laboratory testing, when the long time constant would result in an unnecessarily long wait to accumulate test data. The capacitor value was chosen to produce a time constant of 5 ± 1 second.

The dc output amplifier is a simple, linearly operated bootstrap amplifier having somewhat higher voltage divider resistor values than the input circuits (which are biased off in the steady-state condition) to keep the power requirements low. The resulting higher output impedance is acceptable in view of the high subcarrier oscillator input impedance. The amplifier dynamic gain is 2.5.

A diode is included in the input circuit of this amplifier to partially compensate the amplifier temperature characteristic. As was indicated in Paragraph 4, the shifts in output voltage with changes in temperature are due primarily to the temperature dependence of the first transistor base-emitter junction voltage. This is balanced by inserting a silicon diode junction having similar characteristics in the input circuit so that the two variations subtract.

Figure 146 shows the variation in the output of this amplifier with changes in temperature and supply voltage with the complete system consisting of the scaler, logic circuit, output amplifier, and voltage regulator operating together. It can be seen that the temperature compensation is not complete. The primary requirement was, however, that the input voltage to the subcarrier oscillators remain between 0.70 and 6.0 volts over the temperature range -20 to +75 degrees centigrade. This condition was adequately met, and more complete compensation was not attempted in order to keep the circuits as simple as possible.
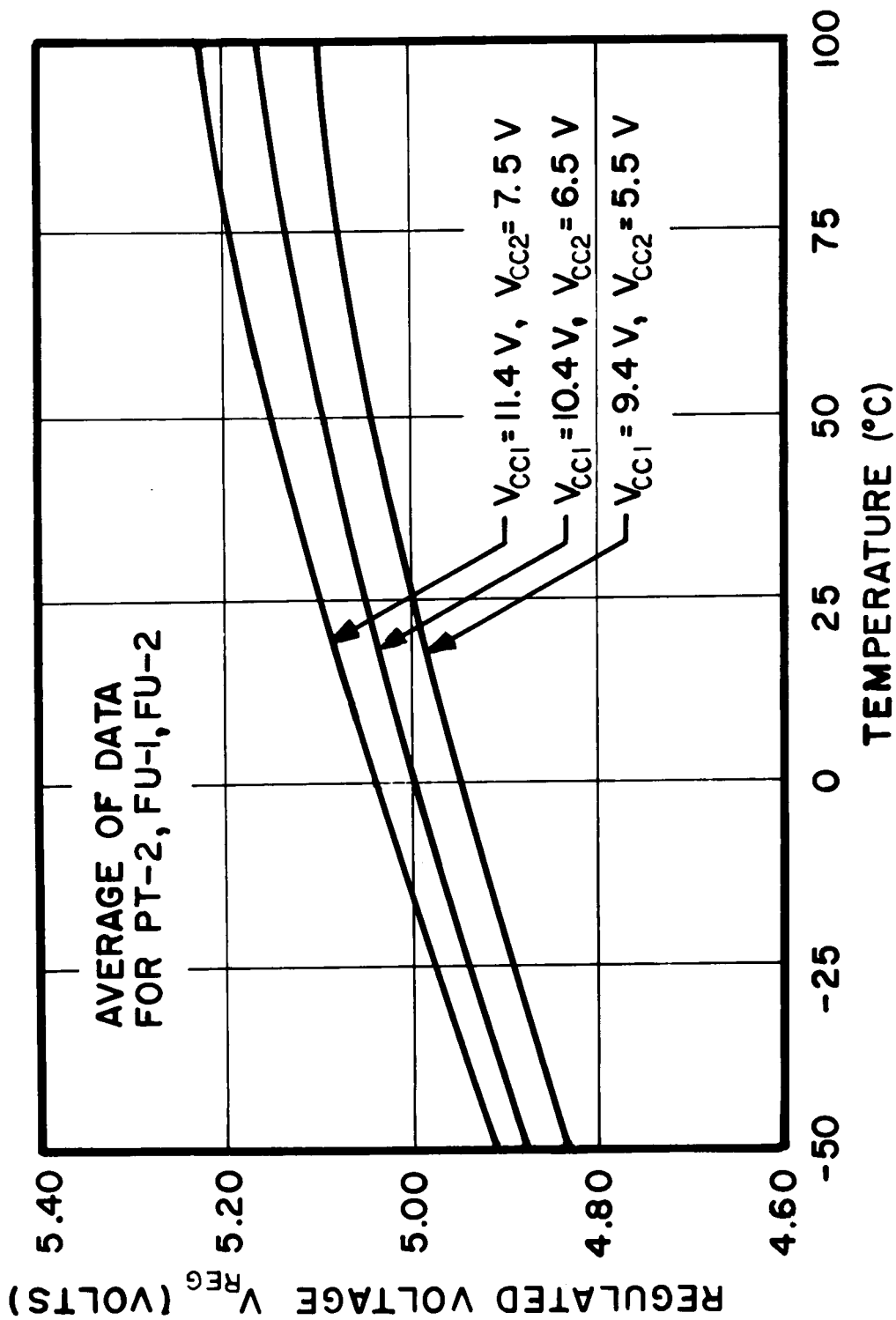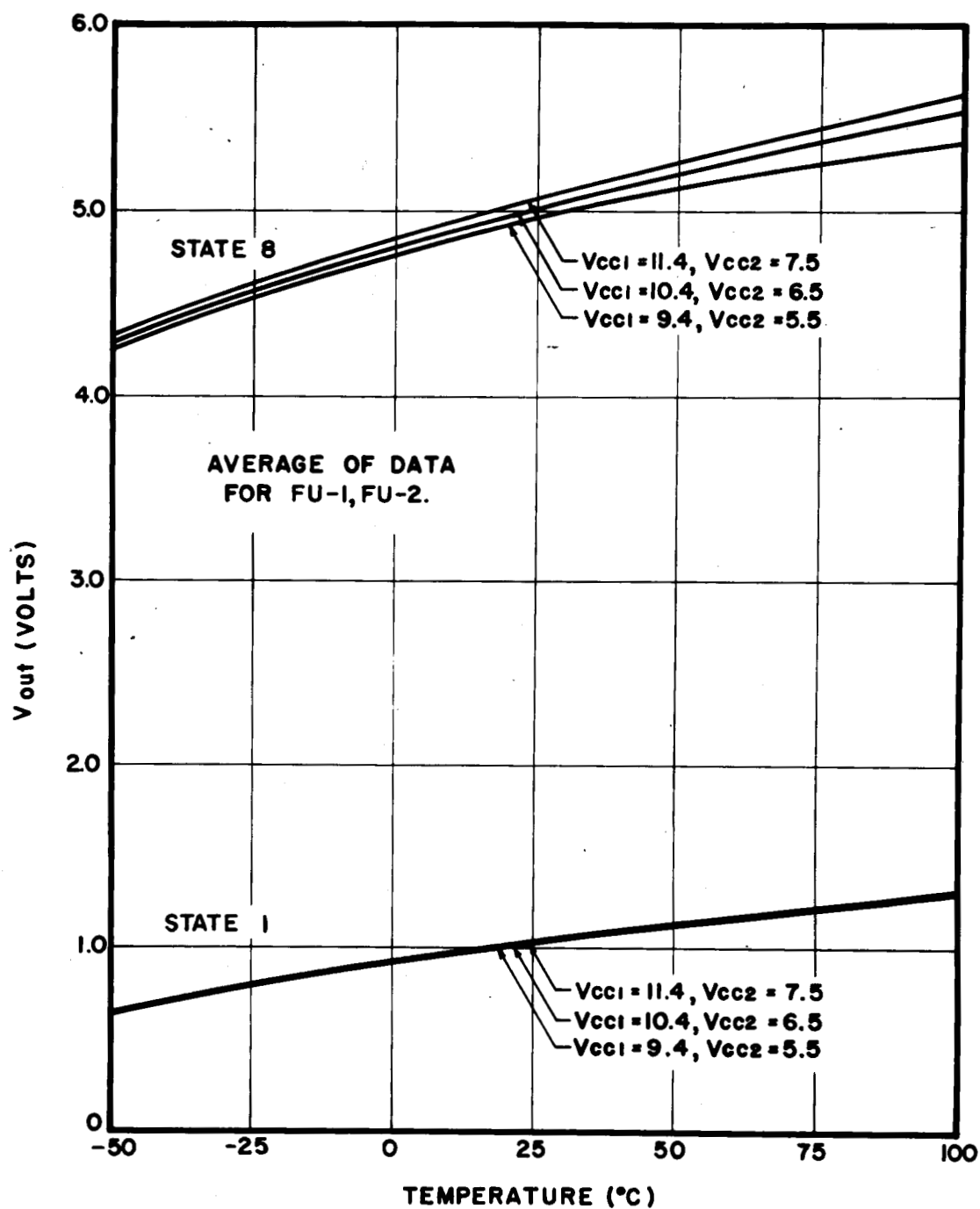
FIG. 145. VOLTAGE REGULATOR CHARACTERISTICS

FIG. 146. OUTPUT VOLTAGE FOR STAGES ONE AND EIGHT

SECTION IV.   FABRICATION OF THE SUI APPARATUS

The method of assembly of the SUI instrumentation package can be seen
in Figures 111, 147, 148, and 149.   The electronics components are mounted
on fiberglass boards. The completed electronics decks are encapsulated in
Eccofoam FP Isocyanate foam mixed in the ratio of one cubic centimeter of
12-6 catalyst to ten grams of prepolymer.   The detectors are mounted on the
top plate of the detector assembly, and are encapsulated in foam in common
with the high voltage power supply and pulse shaping amplifier decks.   All
high voltage points are coated before encapsulation with epoxy resin to
provide a seal to prevent arc-over when the completed unit is placed in
vacuum.   Figure 150 is a photograph of the complete FU-1 detector assem-
bly before encapsulation.

After the modules are encapsulated they are arranged on the stacking
rods.   Thin (0.3 mm) insulating discs are placed between modules to elimi-
nate the possibility of shorts between modules.   Figure 148 is a photograph
of a prototype package (PT-2) which was stacked before encapsulation to
show the internal structure of the assembly and to illustrate the rather
high component density.   Following stacking of the completed modules they
are interconnected by a channel wiring harness.   The wiring diagram is
shown in Figure 151. Figure 149 is a photograph of the completed package.
The completed SUI instrumentation stack is placed in the thin wall (0.56mm)
cylindrical aluminum case shown in Figure 149.   Screwing this case to the
base plate places the module stack in compression to minimize mechanical
oscillation during vibration.

Due to the severe limitation on total weight of the S-46 flight unit
all parts, including those of the SUI package, were made as light as
possible.   The weight of the various parts and groups of the S-46 is given
in Table 3.   A detailed outline of the subassembly weights for the SUI
package only, in FU-2 is given in Table 9.

Extensive testing was performed on the SUI package at the various
stages of manufacture.   Individual components were tested, modules were
tested before encapsulation, subassemblies were tested, and finally the
complete payload was tested.   These tests have been included with ABMA
testing in the overall description of the tests in Chapter 7.

Table 9

BREAKDOWN OF S-46 SUI INSTRUMENT PACKAGE WEIGHT (FU-2)

Assembly	Mass (gm)	Subtotal (kg)
SUI Instrument Package		2.895
Detector Assy, Consisting of:	1702.0	

Power Supply Deck A (153.2 gm)
        Amplifier Deck B (53.0 gm)
        CdS Detector A (229.0 gm)
        CdS Detector B (200.1 gm)
        Spectrometer Assy (589.0 gm)
        213 Counter Assy, Detector E (43.1 gm)
        Hardware and Structure (138.2 gm)
        Encapsulant, Coatings (296.4 gm)		

Scaler Deck C (49.5 gm foam)	139.8	
Scaler Deck D (49.5 gm foam)	139.1	
Scaler Deck E (38.5 gm foam)	169.9	
Scaler Deck F (44.0 gm foam)	157.8	
Scaler Deck G (38.5 gm foam)	169.9	
Case (235), Base Plate (128), and Hardware (53.2)	416.2	

272

FIG. 147. ASSEMBLY DRAWING OF THE SUI INSTRUMENT PACKAGE
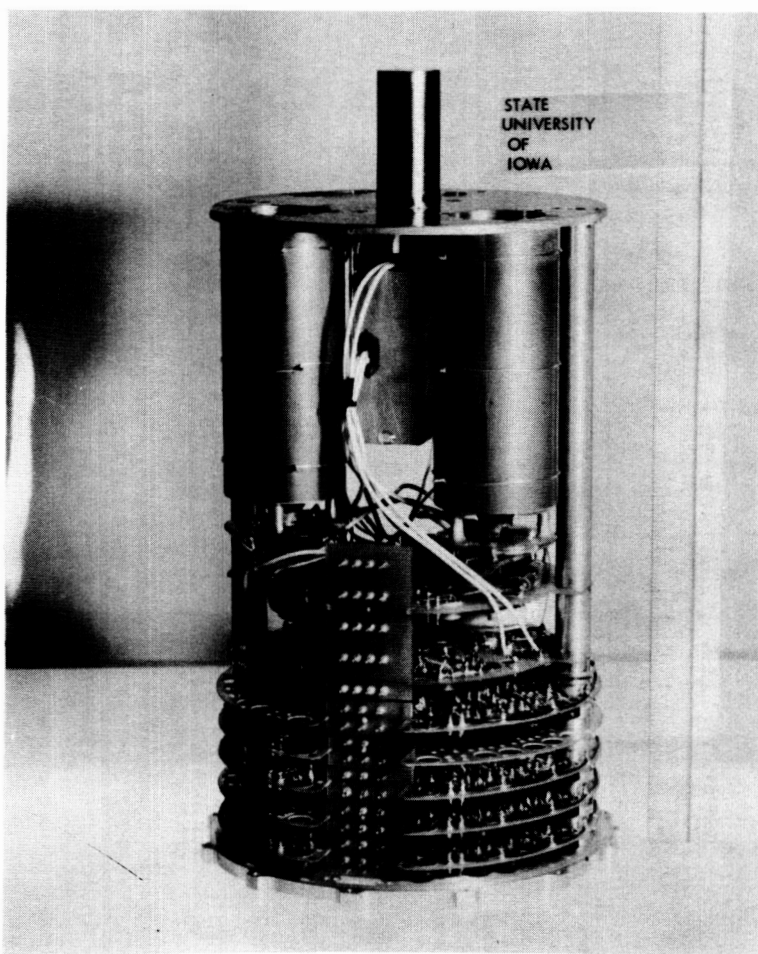Dept of Physics, State Univ. of Iowa Drawing D11-0002

FIG. 148.   THE SUI INSTRUMENT PACKAGE BEFORE ENCAPSULATION
OF INDIVIDUAL MODULES (PT-2 for PL-2)
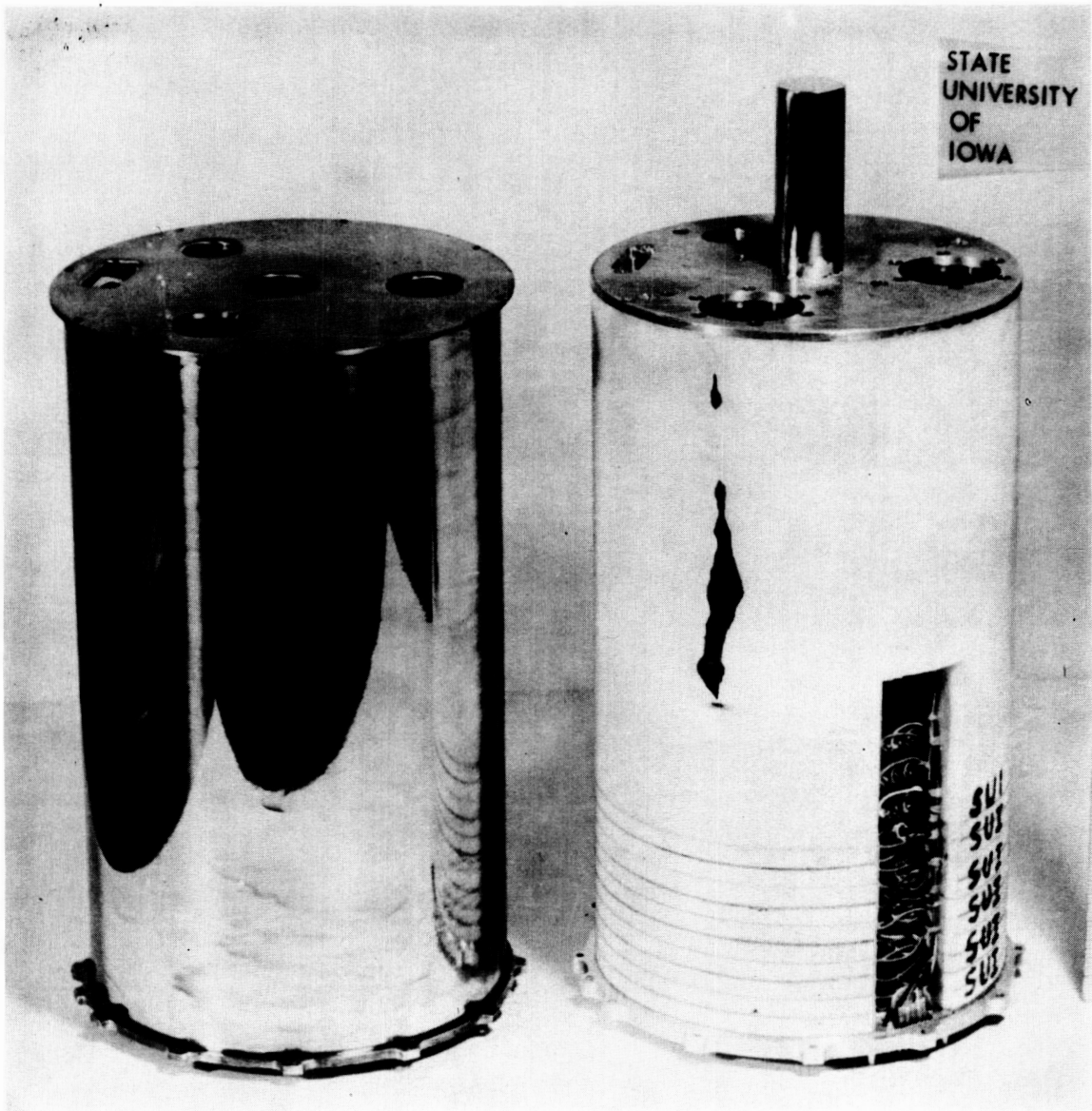
FIG. 149. COMPLETE SUI PACKAGE WITH CASE REMOVED (FU-1)
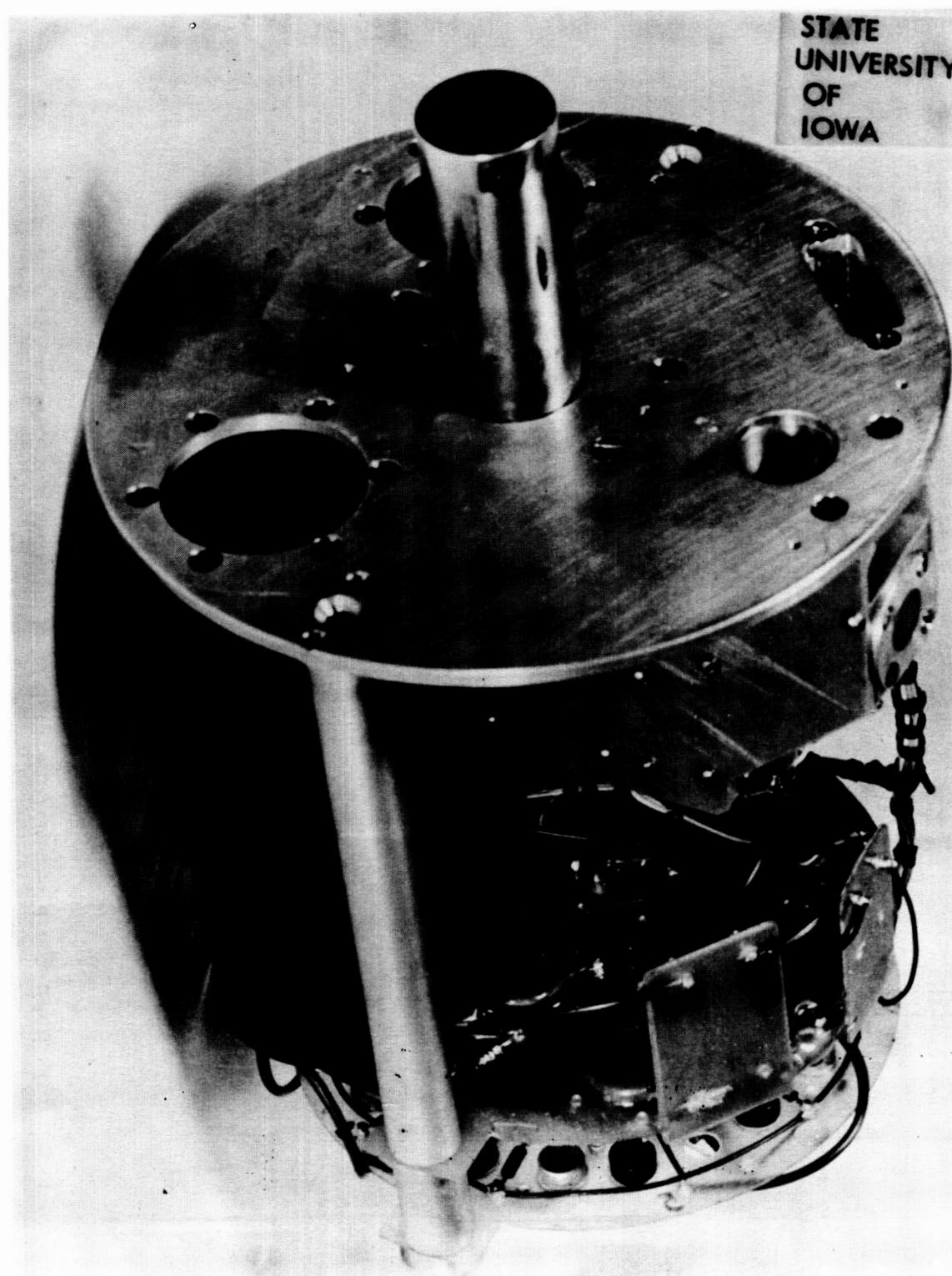
STATE
UNIVERSITY
OF
IOWA

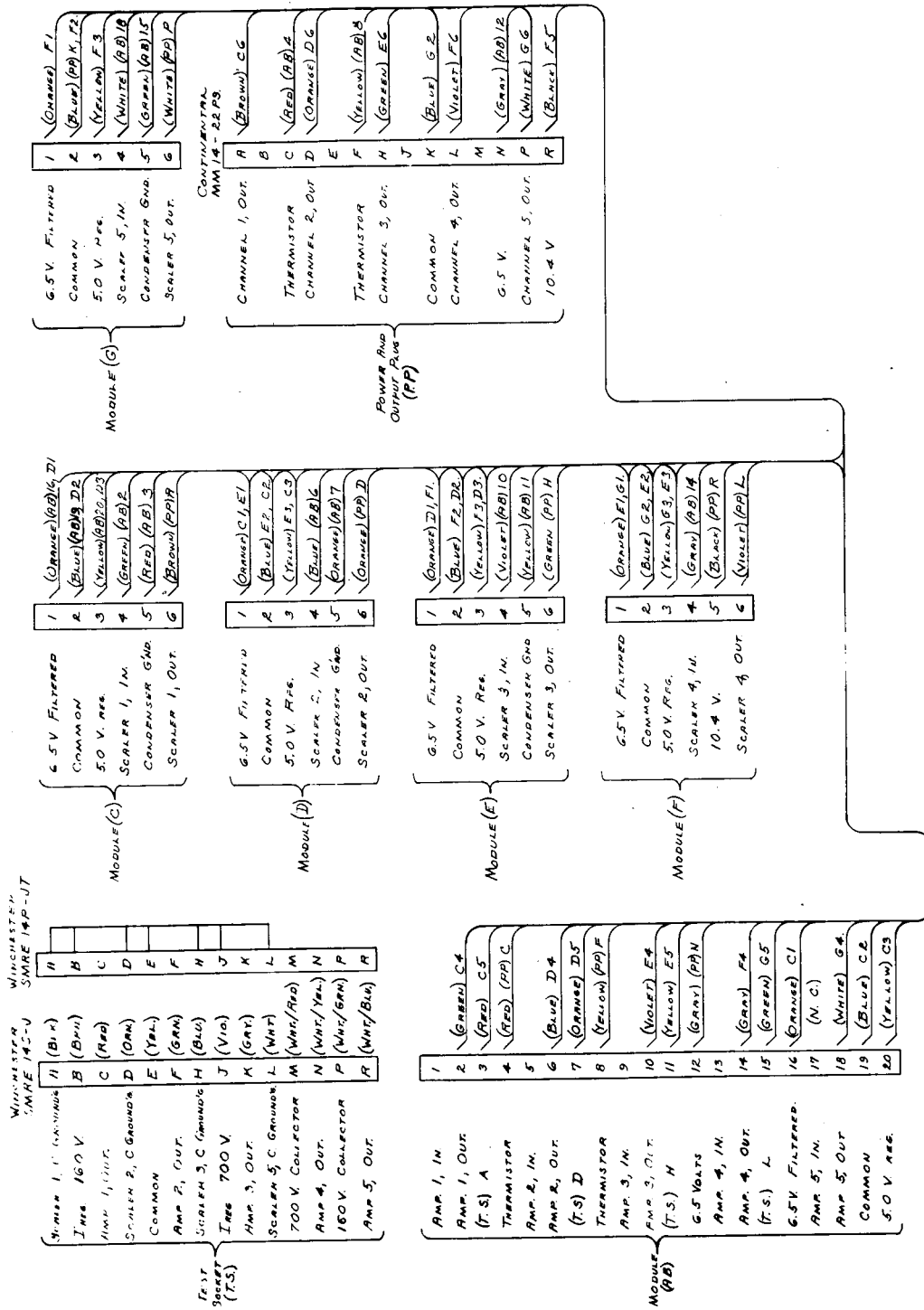FIG. 150. DETECTOR ASSEMBLY BEFORE ENCAPULATION (FU-1)

FIG. 151.   WIRING DIAGRAM OF THE SUI INSTRUMENTATION
Dept of Physics, State Univ. of Iowa Drawing C11-2301

SECTION V.   PAYLOAD CALIBRATIONS

The detectors and electronic circuits in the SUI flight instrumentation packages were fully calibrated before delivery to ABMA for environmental testing. The critical individual components were calibrated before assembly of the modules, and the packages were calibrated as complete, fully operating systems. Table 10 identifies the components selected for the various payloads. The detector A, B, C, and D calibrations were made by their respective designers and the descriptions of the procedures are not available for this report. The detector E G-M counter calibrations were made by Messrs. J. A. Van Allen and L. A. Frank and are outlined as follows:

1.   G-M Counter Plateau Measurement

The counting rate for a fixed Co^{60} source distance as a function of the applied voltage was measured for several temperatures. The results are shown in Figures 152 and 153 for the counters used in FU-1 and FU-2 respectively. These curves can be used in conjunction with those of Figures 122 and 123 to determine the counting rate dependence on temperature. To obtain these measurements the counters were operated in electronic circuits identical to those used in the satellite instruments.

2.   Apparent vs. True Counting Rate

When operated in high radiation fluxes, the observed or apparent counting rate in a G-M counter is no longer proportional to the incident flux. Figure 154 shows the relationships, for the FU-1 and FU-2 counters, between the apparent counting rates and the true counting rates, which are defined as the rates which would be obtained from counters identical to the ones in use in every respect, except that they have zero dead times. The curves were obtained by placing the payloads at various distances from an X-ray source and using the inverse square relationship between X-ray intensity and distance to compute the relative intensities. By making a series of runs with different source intensities it was possible to plot the entire curves shown.

It is interesting to note that, in obtaining the data for the 213 counter in FU-2 such high X-ray intensities were employed in an effort to extend the curve of Figure 154 as high as possible that some radiation damage to the high voltage power supply diodes resulted. It was manifested by a reduction in regulator tube current, signifying an increase in diode reverse leakage current. The power supply made a rapid (overnight) partial recovery and returned to completely normal operation after about two weeks.

Table 10

IDENTIFICATION OF CRITICAL COMPONENTS

| Description	PT-1	PT-2	PT-3	FU-1	FU-2
Detector A CdS Crystal	CL-2/94	CL-2P/63	CL-2P/65	CL-2/131	CL-2/132
Detector A Neon Lamp	NE-76/42	NE-76/41	NE-76/35	NE-76/56	NE-81/43
Detector B CdS Crystal	CL-2/88	CL-2P/66	CL-2P/71	CL-2/102	CL-2/130
Detector B Neon Lamp	NE-76/39	NE-76/37	NE-76/36	NE-81/5	NE-81/1
Spectrometer Assembly	3	2	1	4	6
Detector C G-M Counter	223/18490	223/18092	223/4491	223/17743	223/18094
Detector D G-M Counter	223/18015	223/18163	223/4635	223/18540	223/15415
Detector E Assembly	-	-	-	8	10
Detector E G-M Counter	302/055	302/V316	302/N845	302/X538	213/21013
700 Volt Regulator Tube	GV3B-690S/62	GV3B-690/20	GV3B-690/24	GV3B-690/11-8	VXR-700S/11-6
160 Volt Regulator Diode	RCA-125/14	RCA-125/12	SV-18 and SV-24	1N1327/-	1N1327/6
SUI Thermistor	11/004	11/009	11/001	11/006	11/012
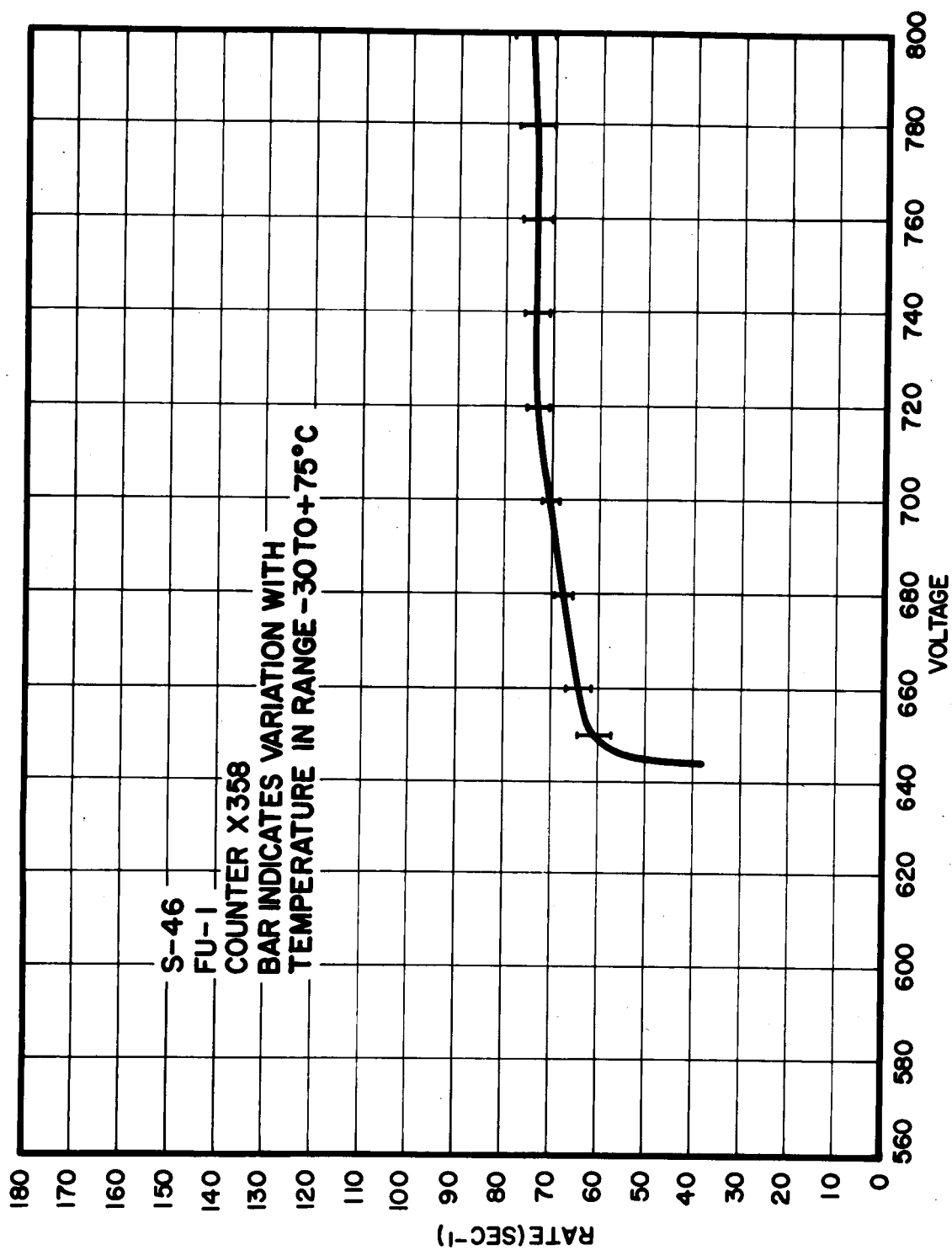
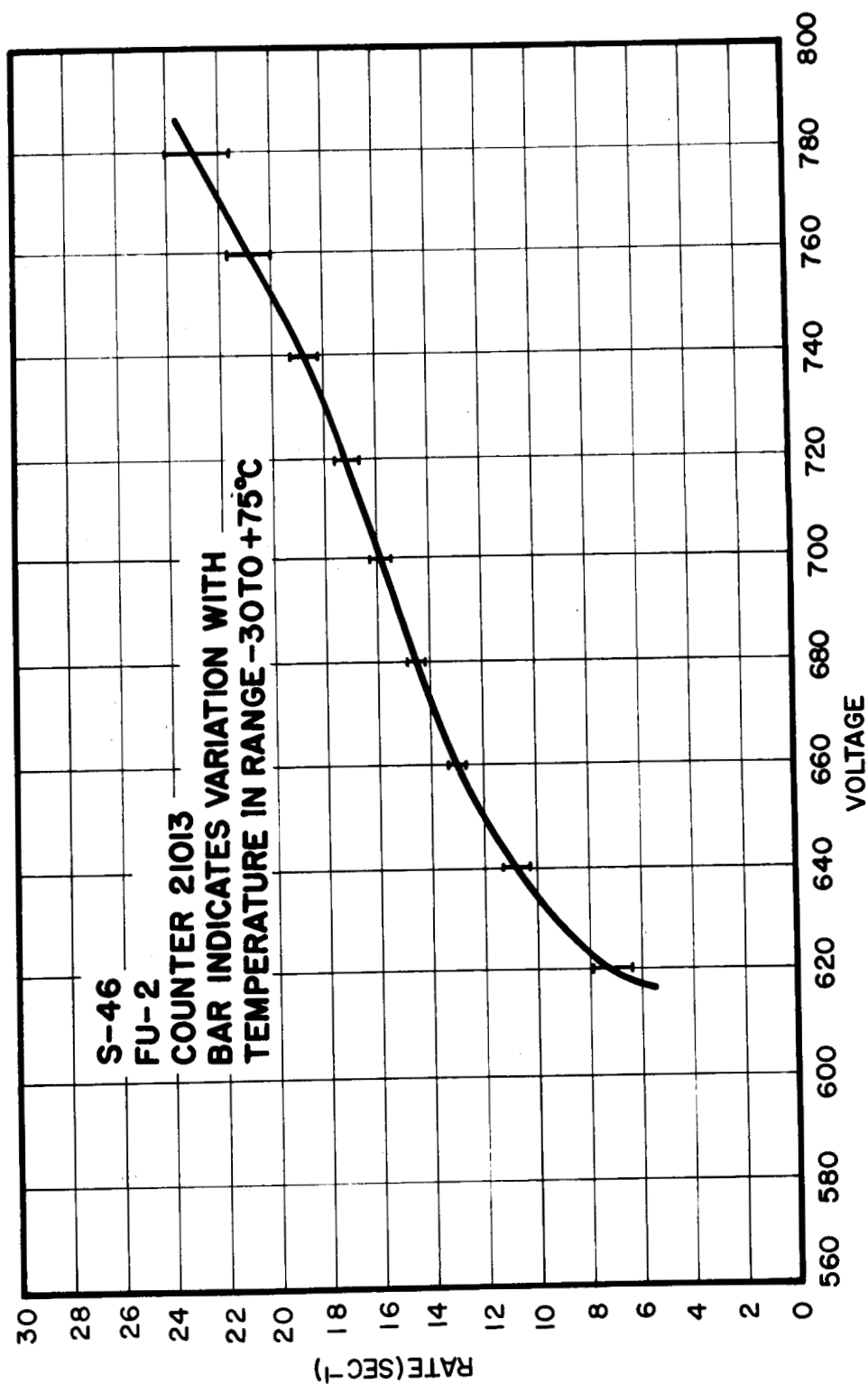FIG. 152. TYPE 302 G-M COUNTER PLATEAU
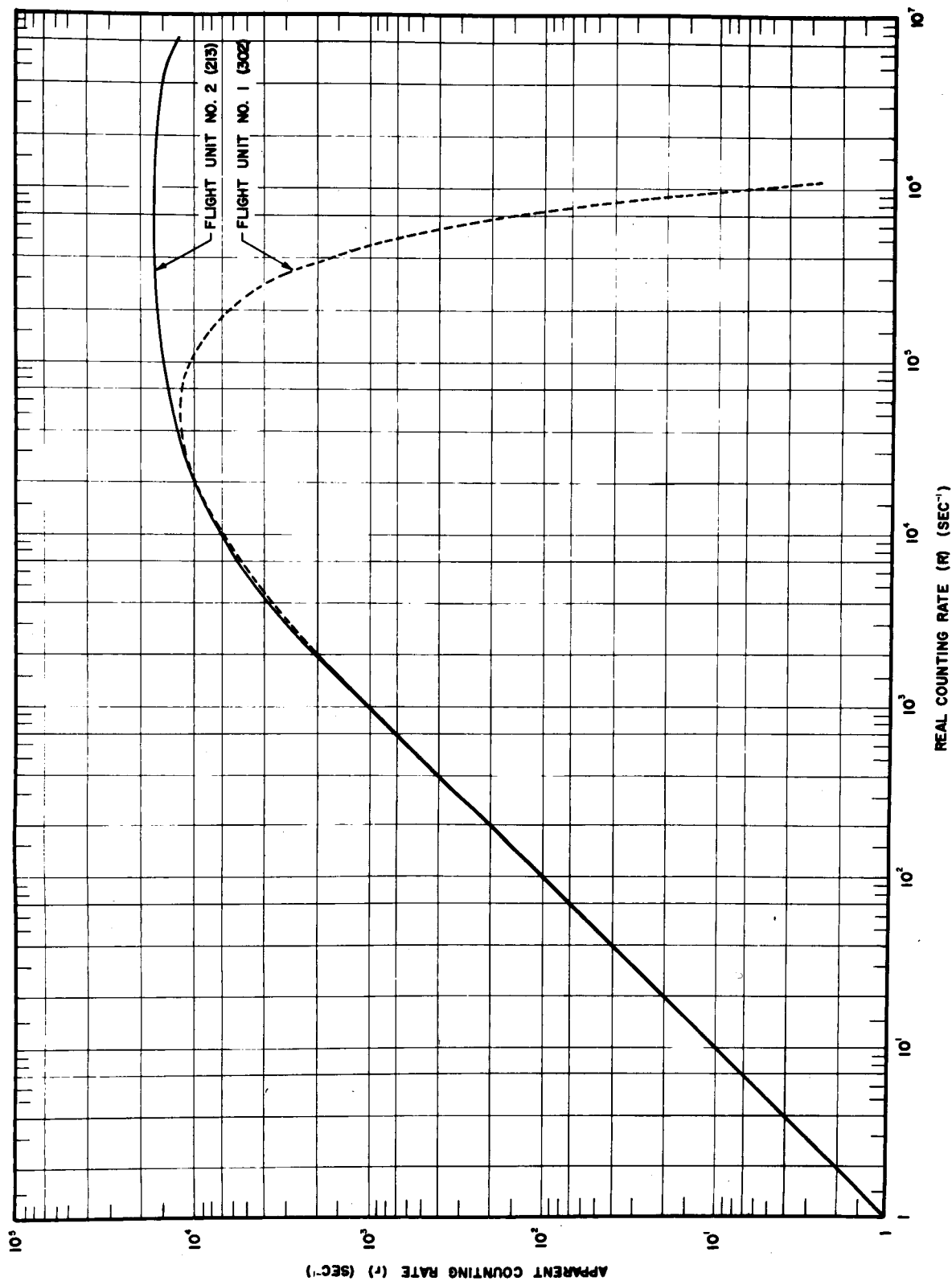
FIG. 153. TYPE 213 G-M COUNTER PLATEAU

FIG. 154. G-M COUNTER APPARENT VERSUS TRUE COUNTING RATE

3. **Determination of Absolute Geometric Factor**

The geometric factor of each flight G-M counter was determined relative to a similar reference counter by a standard source - standard distance (SSSD) Co^{60} gamma measurement. The geometric factor of the reference counter was, in turn, determined relative to a large counter in a cosmic ray telescope. The physical geometry of the large counter was determined by measurements of its effective length and diameter and by determination of its cosmic ray counting efficiency. This indirect approach was necessary because the flight counters were so small that their dimensions and efficiencies could not be directly measured with the necessary accuracy.

Standard source - standard distance measurements were also made periodically during the construction and testing of the payloads to ascertain that no changes occurred in the G-M counter operation.

4. **Determination of Angular Dependence of the Absolute Geometric Factors**

The detailed geometry of the very small counters used for the study of the high intensity radiation is not well defined because the shape of the effective volume is not simple. Therefore the angular dependence of the absolute geometric factor was determined experimentally by orienting the counters at different angles to a Co^{60} source (at a fixed distance).

5. **Determination of Absolute Electron Sensitivity**

When the payload is located in regions in which there are energetic electrons, the electrons are detected primarily by a low efficiency secondary process in which they strike the shell of the satellite, bremsstrahlung is produced in the material of the shell, and these X-rays are detected by the G-M counters. The similar production of bremsstrahlung at the target of an X-ray tube provides a means for establishing the relationship between the incident electron flux and the payload counting rates. A complete set of laboratory X-ray runs was made using a large range of accelerating potential to determine the detecting process efficiency as a function of incident electron energy.

Several other elements of the payloads required calibration. The effects of changes in temperature and supply voltage on the operation of the SUI instrumentation have been discussed in Section III. Similar calibrations were made of the telemetry system by ABMA. In particular the characteristics of the temperature measuring telemetry channels were determined. The results of these calibrations are shown in Figures 155 and 156, which show the subcarrier oscillator frequency as a function of
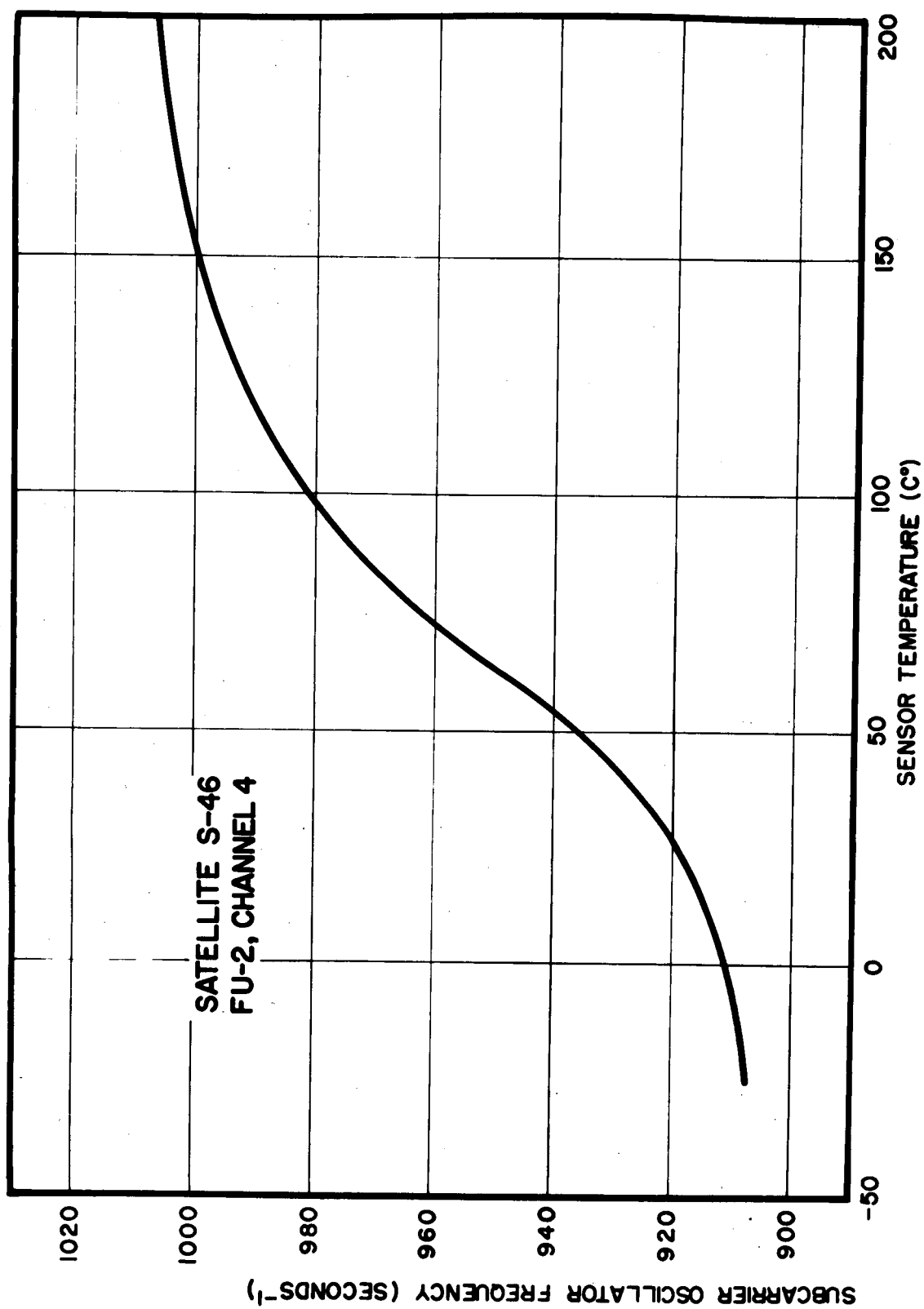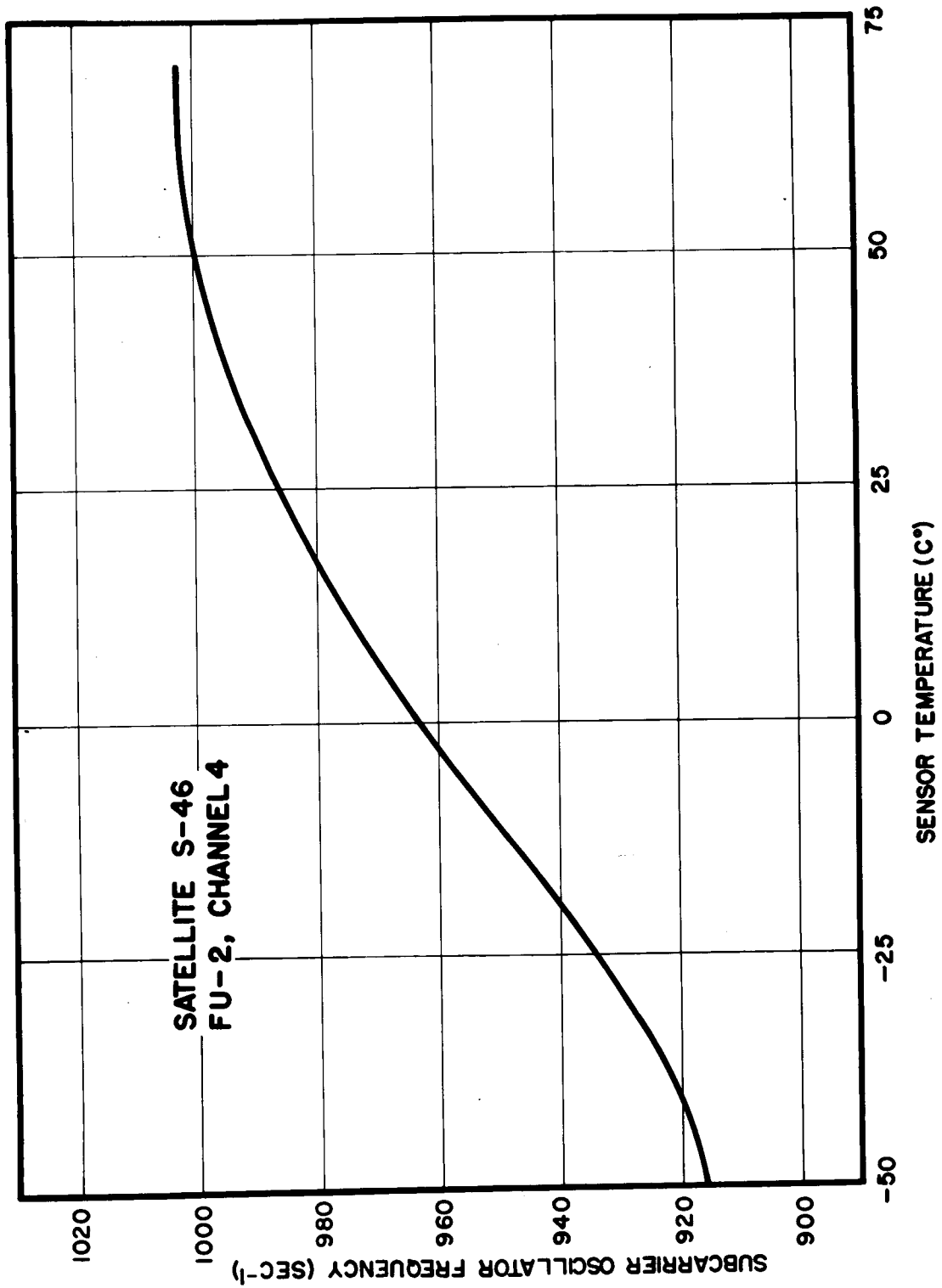
FIG. 155. TABOR SURFACE TEMPERATURE CALIBRATION

FIG. 156. SUI PACKAGE TEMPERATURE CALIBRATION

Tabor surface and SUI thermistor temperature respectively for FU-2. The subcarrier oscillator frequency is a weak function of the temperature of the oscillator circuit. But it is within 0.1 per cent of the room temperature value at all circuit operating temperatures.

SECTION VI. OPERATION DURING THE FLIGHT

It was brought out in Chapter 2, "The S-46 Flight," that the S-46 payload failed to achieve an orbit due to failure of the high speed rocket cluster, and that a conclusive determination of the exact reason for failure was not possible in spite of a complete analysis of all available launch records having been made. Booster rocket performance was normal and the instrument section and high speed stages were in the proper position at the time of second stage ignition. There is evidence that the velocity increments of the high speed stages were low and that there were angular deviations of all three stages.

Payload telemetry signals were received at several stations during the launch operation. The best and most complete record was made by the STL Microlock receiving station at Cape Canaveral. This record extends from the time of liftoff until nearly one minute after programmed injection (a total time of 9.3 minutes). Following the firing of the high speed stages, the signal began a slow fade at about 1343:50 (UT), a more rapid fade at 1344:15, and was below telemetry threshold at 1344:31. No other stations received the signal after this time. Table 11 is included to facilitate reference to important event times in connection with the following discussion of the SUI equipment performance.

Table 11

LAUNCH SEQUENCE

Function	Time (UT)
Lift off	1335:11.2
Beginning of cluster tilt program	1338:41
Shroud ejection	1338:45
Completion of cluster tilt program	1339:30
Second stage ignition	1343:09.1
Third stage ignition	1343:18.6
Fourth stage ignition	1343:28.1
Programmed injection	1343:38
Loss of telemetry	1344:15

The only payload instrumentation abnormality was the loss of the Tabor surface temperature measurement soon after the shroud was installed in place over the payload or flight unit during the prelaunch countdown, apparently due to an open circuit in the thermistor or its wiring.   A decision was made to launch the payload without this measurement after it was ascertained that the abnormality was not a symptom of the failure of some other component (for example a commutator gate) which could have resulted in invalidation of a portion of the primary data.

The operation of all radiation measuring instrumentation, telemetry, and power supply systems appears to have been satisfactory for as long as the signal was received.   The data received during the launch from detectors A and B are contained in Figure 157.   The counting rates observed in these detectors are believed to be proper responses to various stimuli.   It appears likely that the first increase, occurring between 1338:46.7 and 1338:47.3, or about two seconds after shroud separation, was caused by the burning of the shroud lateral-thrust rocket.   This rocket motor, used to push the shroud aside after separation, was programmed to ignite about three seconds after shroud separation and to burn for about one second. Its location at the time of ignition was computed to be about five meters in front of the payload and about 2.4 degrees from the detector axes, or well within their cones of sensitivity. It is also possible that there was some reflection of sunlight from the shroud (and/or some direct light from the sun) incident upon the detectors.   At the time of shroud ejection the angle from the detector axes to the sun was thirteen degrees and increasing at the rate of 0.67 degree per second.   The detector counting rates at sun angles of 15, 20, and 25 degrees were of the order of 0.1, 0.07, and 0.01 counts per second respectively on the basis of the prelaunch calibrations.

There is no obvious explanation for the small increase occurring at 1339:10.

The large increase beginning at 1339:27.1 was probably caused by light from the earth (reflection of sunlight from the sea and from clouds). The angle between the detector axes and the line to the horizon at that time was about 8 degrees.   At the end of the tilt program three seconds later this angle was about 6 degrees, which would have resulted in a high counting rate.   As the cluster continued down-range on its trajectory, with its height continually increasing, the angle between the detector axes and the horizon steadily increased until it reached the value of about 19 degrees at the time of second stage ignition.   The detector counting rate curve during this period declines as the angle increases.   This data can, in fact, be used to obtain realistic plots of detector counting rates as a function of axis-to-light angle for the case of a rapidly spinning payload.   A rough comparison with the values obtained from the calibration before launch shows moderately good agreement.
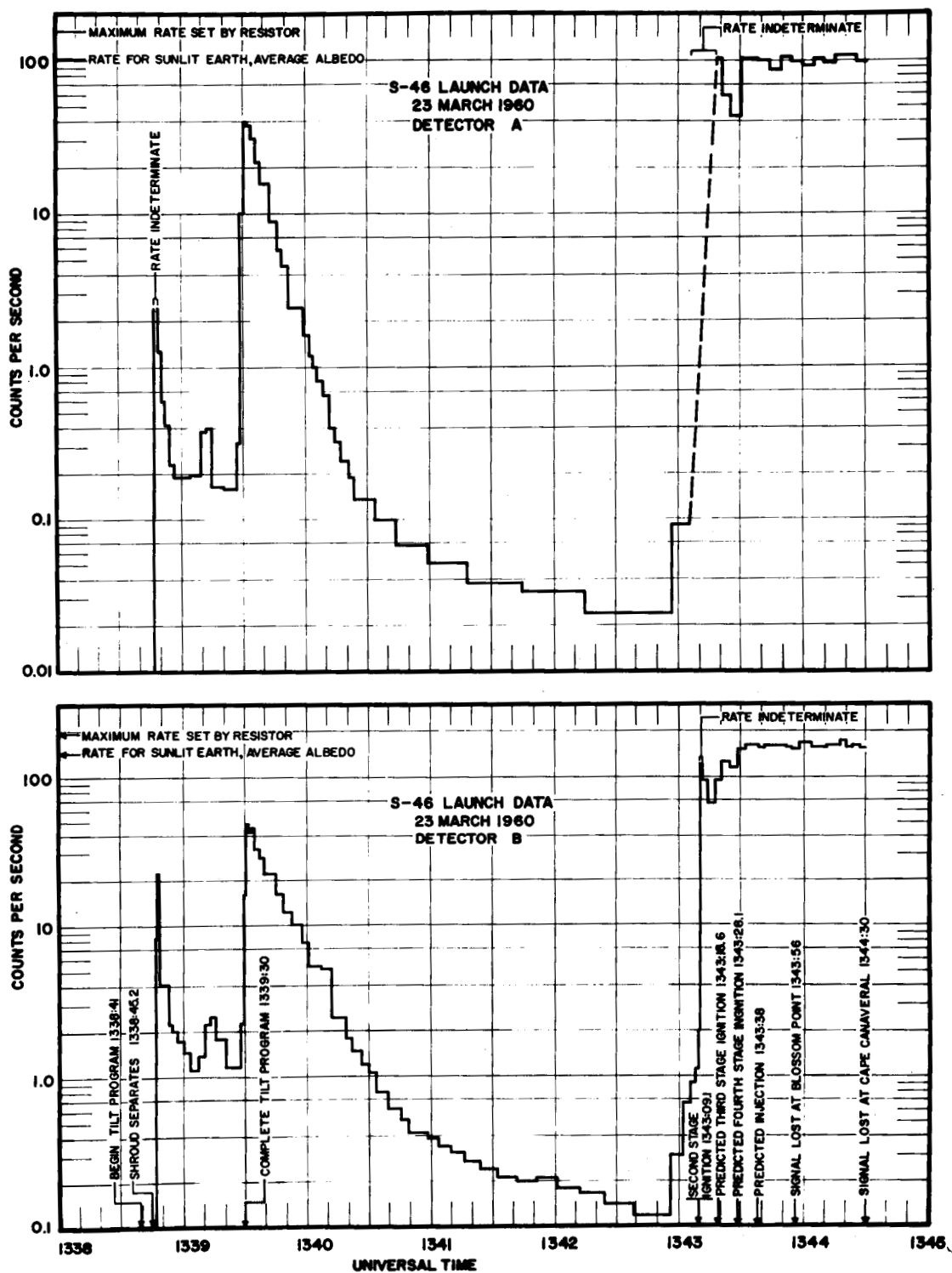
FIG. 157. DETECTOR A AND B LAUNCH DATA

The CdS detector counting rates began to increase again at about 1342:55. The slow increase from this time until the abrupt increase at about 1343:09 is difficult to explain, since the rocket instrumentation telemetry indicated that the cluster orientation was maintained constant until the instant of second stage ignition. C. E. McIlwain, in a private communication, hypothesized that it may have been due to ionic impact directly on the crystals. At the time the increase in counting rate began, the angle between the detector axes and the line of cluster motion was a little less than two degrees and decreasing. The angle to the horizon at that time was nearly 19 degrees and very slowly increasing.

The large, abrupt increase between 1343:08.9 and 1343:09.9 occurs nearly concurrently with the ignition of the second stage. Slightly more than 0.1 second was required for the second stage rocket to leave the launcher, by which its lateral motion was restrained. It is suggested that the second stage rocket was pitched downward by at least 16 degrees for a short time immediately following ignition. The possibility exists that the increase in counting rate may have been caused by increased ionic bombardment of the crystal, due to increased detector velocity, but it is difficult to explain why the rate should have decreased from its peak value while the rocket was still burning and the cluster speed was still increasing, unless a monotonically increasing cluster precession angle was introduced during buring.

The resolution and accuracy of the data are not good enough to permit a discussion of the motion during the third stage burning, other than to state that there seems to have been a slight increase in counting rate at the time of ignition, followed by a decrease. At the time of fourth stage ignition, however, there is a rapid increase in both counting rates to steady values which were maintained until the signal was lost. The rates in both detectors agree, within the possible error, with the predicted counting rates if the detectors were directed toward some portion of the sunlit earth. It seems highly likely, then, that the fourth stage rocket and payload were pitched downward by at least 22 degrees from the intended direction of travel. This finding is compatible with the findings of ABMA, as set forth in Chapter 2, based on a study of the doppler data from a network of receiving stations.

The geometric factors and scaling factors of the G-M counters which were chosen to study the high intensity radiation were such that little geophysically significant data were obtained from them during the short flight. Two switches of the detector C scaler output (scale of 128) occurred at 1339:36 and 1343:51, corresponding to an average rate of 0.25 ± 0.03 counts per second. One switch of the detector E scaler output (scale of 128) occurred at 1337:01. Thus, its average rate could not have been greater than 0.14 counts per second during the period 1337:01

to 1344:30. A number of switches of the detector D scaler output (scale of 8) occurred during the launch trajectory. During the period from 1336:12 to loss of signal, this average rate was 0.20 ± 0.02 counts per second. The differences in the rates of the three G-M counters were probably due to differences in the effective geometric factors. If we consider the average of the detector C and D counting rates as the rate obtained from a counter having a typical geometric factor, then the average omnidirectional cosmic ray intensity in that part of space traversed between shroud ejection (about 150 km height) and loss of signal (about 350 km height) was $J_o \approx 2.0 \ cm^{-2} \ sec^{-1}$. This agrees with the values obtained in other experiments within the accuracy of these measurements.

SECTION VII. CONCLUSION

From the foregoing discussion it can be concluded that the operation of the detectors and associated instruments during the brief launch trajectory was normal, and that the telemetry system operated as anticipated. The flight was not long enough to determine whether the power system would have operated properly, but there is no reason for believing it would not. Since the payload did not go high enough to enter the region of high intensity radiation, the suitability of the cadmium sulfide detectors and the electron spectrometer for investigation of the objectives listed in Chapter I was not ascertained experimentally. However, no evidence to the contrary has been discovered. Similar detectors are being prepared for use in other satellite and space payloads.

In spite of the fact that the S-46 payload configuration may never be utilized due to the lack of a backup launching vehicle, it is felt that this program has resulted in a significant advance in the state of the art of the development of instruments for the investigation of our space environment.